AD_____

Award Number: W81XWH-04-1-0190

TITLE: Magnetic Resonance Spectroscopy: An Objective Technique for the Quantification of Prostate Cancer Pathologies

PRINCIPAL INVESTIGATOR: Leo L. Cheng, Ph.D.

CONTRACTING ORGANIZATION: Massachusetts General Hospital
                          Boston, MA 02114

REPORT DATE: February 2006

TYPE OF REPORT: Annual

PREPARED FOR: U.S. Army Medical Research and Materiel Command
               Fort Detrick, Maryland 21702-5012

DISTRIBUTION STATEMENT: (Check one)

  x ☐ Approved for public release; distribution unlimited

     ☐ Distribution limited to U.S. Government agencies only;
        report contains proprietary information

The views, opinions and/or findings contained in this report are those of the author(s) and should not be construed as an official Department of the Army position, policy or decision unless so designated by other documentation.

REPORT DOCUMENTATION PAGE

Form Approved
OMB No. 0704-0188

1. REPORT DATE	2. REPORT TYPE	3. DATES COVERED
01-02-2006	Annual	12 Jan 2005 – 11Jan 2006

4. TITLE AND SUBTITLE

Magnetic Resonance Spectroscopy: An Objective Technique for the Quantification of Prostate Cancer Pathologies

5a. CONTRACT NUMBER

5b. GRANT NUMBER
W81XWH-04-1-0190

5c. PROGRAM ELEMENT NUMBER

6. AUTHOR(S)

Leo L. Cheng, Ph.D.

5d. PROJECT NUMBER

5e. TASK NUMBER

5f. WORK UNIT NUMBER

7. PERFORMING ORGANIZATION NAME(S) AND ADDRESS(ES)

Massachusetts General Hospital
Boston, MA 02114

8. PERFORMING ORGANIZATION REPORT NUMBER

9. SPONSORING / MONITORING AGENCY NAME(S) AND ADDRESS(ES)
U.S. Army Medical Research and Materiel Command
Fort Detrick, Maryland 21702-5012

10. SPONSOR/MONITOR'S ACRONYM(S)

11. SPONSOR/MONITOR'S REPORT NUMBER(S)

12. DISTRIBUTION / AVAILABILITY STATEMENT
Approved for Public Release; Distribution Unlimited

13. SUPPLEMENTARY NOTES
 Original contains colored plates: ALL DTCI reproductions will be in black and white

14. **ABSTRACT**
In the past year, the second year of the award, according to our proposed Statement of Work, we continued our efforts on the collection of specimens from prostate cancer patients, and spectroscopic and histopathological measurements of these samples for the construction of metabolic markers aimed at tumor diagnosis based on HRMAS 1HMR evaluation. Significant progresses have been achieved. Three peer-reviewed papers from the project have been published, and one new manuscript has been submitted. In addition, two peer-reviewed review articles and one book chapter are currently in pending for publication, and one patent application as the results of the direct funding support from this award. Furthermore, two NIH grants have been submitted as a direct result of researches supported by this award. These advancements will assist us to better understand tumor metabolism observed with MR spectroscopy, and contribute to better patient cares in the future.

15. SUBJECT TERMS
EX VIVO MAGNETIC RESONANCE SPECTROSCOPY, QUANTITATIVE PATHOLOGY CELLULAR METABOLIC MARKERS, PROSTATECTOMY

16. SECURITY CLASSIFICATION OF:			17. LIMITATION OF ABSTRACT	18. NUMBER OF PAGES	19a. NAME OF RESPONSIBLE PERSON USAMRMC
a. REPORT U	b. ABSTRACT U	c. THIS PAGE U	UU	168	19b. TELEPHONE NUMBER *(include area code)*

Standard Form 298 (Rev. 8-98)
Prescribed by ANSI Std. Z39.18

Table of Contents

INTRODUCTION:
In the past year, the second year of the award, in accordance with our proposed time line in the Statement of Work, we continued our efforts on the construction of metabolic markers aimed at tumor diagnosis based on HRMAS 1HMR evaluation by collecting specimens from prostate cancer patients, and obtaining spectroscopic and histopathological measurements of these samples. Significant progress has been achieved in these efforts. These advancements will assist us in better understanding tumor metabolism observed with MR spectroscopy. There is no change in subject, purpose or scope of the research.

BODY:
Summary of Research Accomplishments
We will first summarize our achievements according to an overview of our proposed Statement of Work. In this summary we will use **bold** typeface to indicate a sub-task that has been completed, *italic* typeface will be used to represent on-going efforts, and regular typeface will delineate sub-tasks that have yet to start according to our proposed time line. At the end of the list of each sub-task, our related references published after the application for the award, are given. Among these references, those that acknowledge this award as a grant support source are listed in **bold** typeface.

STATEMENT OF WORK

Task 1 (Completed): Establish Procedures and Protocols.
A.   Comparison of HRMAS 1HMRS spectra and degradation rates of fresh tissue specimen with those obtained from snap-frozen samples from the same cases (20 specimen total). (Appendix 4)
B.   Preparation of detailed protocols for HRMAS 1HMRS examination and establishment of criteria for conducting homo- and heteronuclear correlation examinations. (Appendix 3)
C.   Evaluation of histopathological integrity of specimen after HRMAS measurement by the primary project pathologist (50 cases)
D.   Establishment of detailed protocols for quantitative histopathology and computer-aided histopathological image analysis. (Appendix 1)

Task 2: *Establish Correlations Between MRS and Histopathology. (Specific Aim 1)* **(Appendix 2)**
A.   In Progress & Months 1-30:
Collection of prostate samples from i) 180-200 prostatectomies (among them 80-100 from African-Americans), "pseudo-biopsies" (6 tissue cores) and "permanent section" (20 samples) will be performed on removed prostate, yielding 1200-1600 samples/year), *and ii) normal controls from autopsy subjects (6 cases from each of 3 age groups, 18 cases total).*
B.   In Progress & Months 1-30:
Performance of HRMAS 1HMRS analysis of i) tumor specimen, and ii) autopsy specimen.
C.   Months 3-33:
Histopathological quantification of tissue specimens analyzed with MRS under Task 2B.

Task 3: *Determine Metabolite Markers for Prostate Cancer. (Specific Aim 2)* **(Appendices 2 and 9**)
A.   In Progress & Months 1-18:
Establishment of metabolite profiles for different prostate zones in normal controls. **(Appendix 2)**
B.   Months 6-35:
i). Performance of multivariate analysis on MRS data to identify metabolic markers that correlate with quantitative histopathology (from Task 2C), and with clinical data; **(Appendix 2)**
ii). Evaluation of the sensitivity and specificity of metabolite markers for detecting the presence of cancer cells and predicting the quantity of each pathological component;

iii). Evaluation of the statistical significance of metabolite markers identified by samples from both pseudo-biopsy and permanent section; examination of the sensitivity and specificity of these markers for their ability to suggest the pathologic stage of prostate cancer by using only pseudo-biopsy samples.

C.   Month 36:
Test of the sensitivity of these markers in reflecting the high disease occurrence among African-Americans; conclusion of findings and the clinical implications thereof, and the submission of final report.

Task 4: Develop a Clinically Adaptable MRS Protocol. (Specific Aim 3)

A.   Months 18-30:
Identification of metabolite markers that can divide the Gleason score 5, 6(3+3) and 7(3+4) group into subgroups. (**Appendices 2 and 9**)

B.   Months 31-36:
Preliminary evaluation and modification of the database markers (from Task 4A) in connection with the updated clinical information on patient outcome, and design of a clinical protocol that can be executed, objectively, by a technician without extensive training.

With most technology developments having been accomplished in the first year of the award, as planned in the SOW and reported in the last annual report, in the past year we have concentrated on analyzation of spectroscopy and histopahtology data. Details of our progress and achievements are summarized below.

1. Continued collection of human prostate cancer specimens for the project.
As a translational clinical research project studying human prostate cancer, the success in our proposed tasks is contingent on our achievements in collecting human specimens. Without these samples, none of our proposed tasks can be conducted. In the past year, we have collected **435** samples from **145** cases. Therefore, up till now, the entire project has collected **1077** samples from **392** cases. Among these samples, we have analyzed **450** samples from **180** cases with both NMR spectroscopy and quantitative pathology according to visual estimations provided by project pathologists, and quantitative pathology measurements as reported in the last annual report are currently underway. Results from the first 199 samples from 82 cases have been published in 2005 and are presented below.

2. Publication of the first HRMAS prostate cancer population study (Appendix 2).
In April 2005, we published the first prostate specimen study in Cancer Research (Appendix 2)(1). In that article, we report the first phase of our studies on the correlations between prostate metabolite profiles and tissue pathologies, as well as patient clinical statuses. This study included a large patient population of a total of 199 specimens. We found that metabolite profiles obtained from principle component analysis of MRS were correlated with pathologists' quantitative findings by using linear regression analysis, and evaluated against patient pathological statuses using ANOVA. Paired-t-tests show tissue metabolite profiles can differentiate malignant from benign samples obtained from the same patient ($p<0.005$) (Figure 1), and correlate with patient serum PSA levels ($p<0.006$). Furthermore, metabolite profiles obtained from histologically benign tissue samples of GS6-7 prostates can delineate a subset of less aggressive tumors ($p<0.008$) and predict tumor perineural invasion within the subset ($p<0.03$). These results, obtained under the current award, indicate that MRS metabolite profiles of biopsy tissues may help direct treatment plans by assessing prostate cancer pathological stage and aggressiveness, currently possible to determine histopathologically only after prostatectomy.
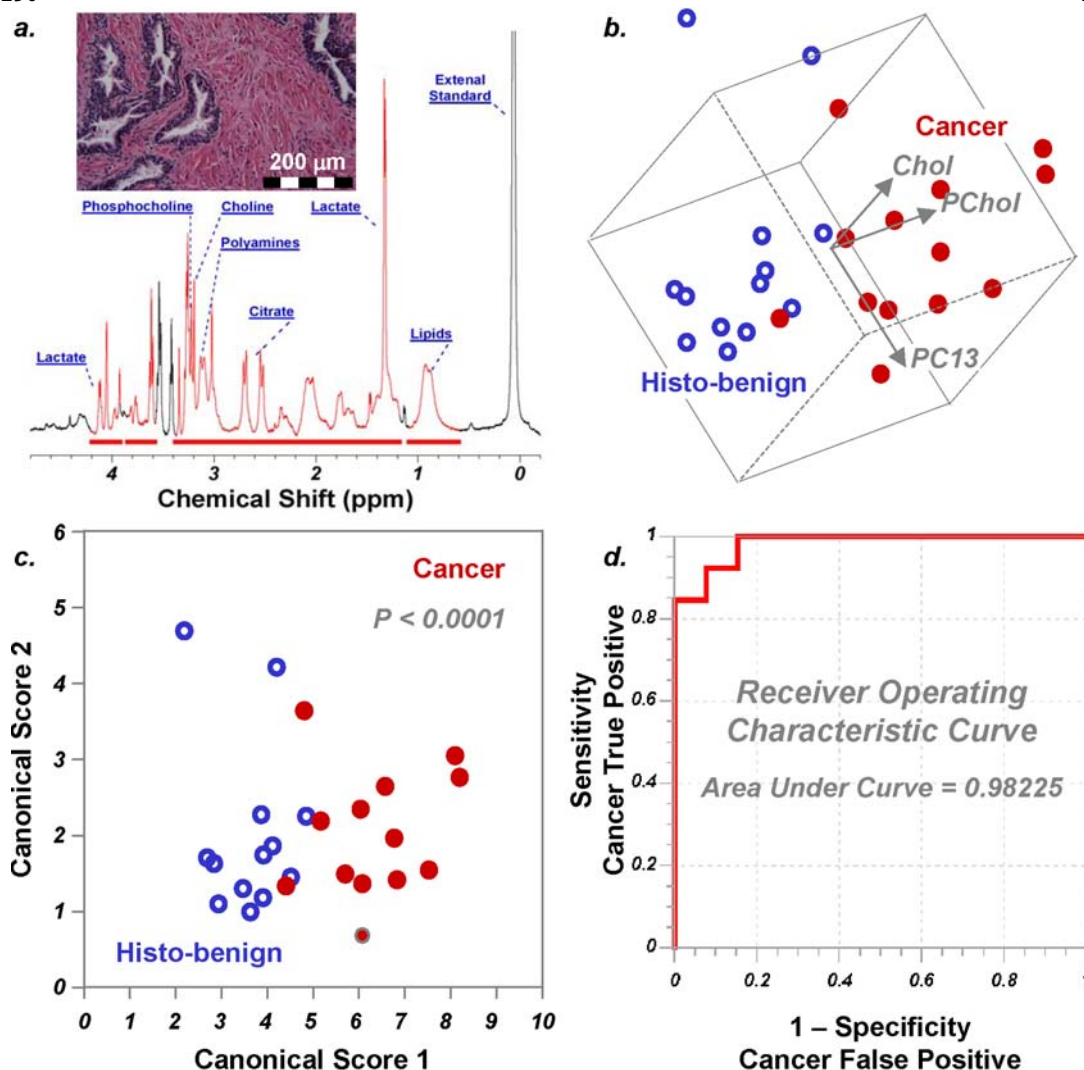
Figure 1. (**a**) High-Resolution Magic Angle Spinning (HRMAS) 1H MR spectrum of intact tissue obtained from the removed prostate of a 61 y.o. patient with Gleason score 6, T2b tumors. Histopathology analysis of the tissue sample (insert) after its spectroscopy measurement revealed that the sample contained 40% histopathologically defined benign epithelium and 60% stromal structures, with no identifiable cancerous glands. Cellular metabolites mentioned in the text are labeled on the spectrum. The 36 most intense resonance peaks or metabolite groups above the horizontal bars were selected for analyses, while the other regions were excluded from calculation, partly due to surgery-related alcohol contamination. (**b**) 3D plot of Principal Component 13 (PC13 correlates linearly with vol% of cancer cells in tissue samples) vs. phosphocholine (Pchol) vs. choline (Chol). Cancerous and histologically benign (histo-benign) tissue samples from 13 patients can be visually separated in observation plane. The paired Student's t-test (cancer vs. histo-benign from the same patients) results for PC13, PChol and Chol are: 0.012, 0.004, and 0.001. Only results from these 13 patients could be evaluated with paired tests, as other cancer positive samples were collected from patients with whom no histo-benign samples were analyzed. (**c**) The canonical plot resulting from discriminant analysis of the three variables in Fig. 1b. presents the maximum separation between the two groups. (**d**) The resulting receiver operating characteristic (ROC) curves indicates the accuracy of using the three variables in Fig. 1b. to positively identify cancer samples.

Results in this article were viewed to be extremely important and novel. Part of the above figure was displayed on the cover of the issue of Cancer Research and the article was featured in the "Cancer Research Highlights"

section (Appendix 2). As a result, the publication was reported by many news medias including ABC news, Forbes, Reuters Health, etc.. Above all we were extremely pleased that our results reported in this article were selected to be included in the Department of Defense, United States Army Medical Research and Materiel Command, Congressionally Directed Medical Research Programs (CDMRP) Annual Report for the fiscal year 2005 (Appendix 10).

3. Establishment of HRMAS spectroscopy protocol for evaluations of clinical prostate biopsies.
Encouraged by the above results, particularly the demonstrated observations suggesting the potential of tissue metabolite profiles to indicate prostate cancer stages, and coinciding with the proposed **Tasks 2** and **4** in "pseudo-biopsies" and in developing a clinically adaptable MRS protocol, respectively, we have tested the feasibility of our HRMAS spectroscopy procedures on prostate biopsy samples, and have designed a project of recruiting prostate biopsies from patients suspected of having prostate cancers. This project has been approved by the IRB of our institution and will be carried out once our NIH grant application for the project is approved.

The current award and its "pseudo-biopsies" component have been critical for our NIH application to continue the HRMAS spectroscopy project on biopsy samples. With supports from this award, we were able to test the feasibility of our entire spectral-pathology procedure, developed thus far only from surgical samples, on delicate thin core prostate biopsies. In principle, HRMAS and quantitative pathology studies of prostate biopsy samples bears no difference from analyses of small surgical samples. However, due to the delicate geometrical shape of the biopsy cores, additional care needs to be exercised during the procedures of tissue transfer. Following the objectives outlined in Task 2, we tested the entire procedure by acquiring biopsy cores from freshly removed prostatectomy specimens. Examples illustrated in **Figure 2** clearly demonstrate our technological feasibility and capability to conduct the tasks proposed in analyses of biopsy samples. Following this demonstrated feasibility, pseudo-biopsy studies proposed in Task 2 are currently underway.

Figure 2. (**A**) "Bench-top pseudo-biopsy" removed a tissue core from a prostate after prostatectomy. (**B**) The Bx core was transferred into a 4mm HRMAS rotor. (**C**) Spectra with 600 and 700 Hz spinning were recorded. The tissue core was (**D**) wisked out from the rotor after HRMAS analyses and (**E**) fixed in formalin. (**F**) An H&E image of the Bx core, with a scale bar denoting 2mm.

4. Developments in heteronuclear MR spectroscopy (Appendix 3).
In the field of MRS measurements of tumor metabolites, no other metabolites have been mentioned more often than choline and the related compounds phosphocholine (PC) and glycerophosphocholine (GPC)(2). They are linked to the development and progression of cancer. In the proposed Task 1, we planned to develop heteronuclear MRS methodology to target these metabolites. Current *in vivo* and tissue *ex vivo* magnetic resonance spectroscopy methods mostly center on measuring the total concentration of these metabolites and have difficulty differentiating between them. Our efforts have led to a proposal of a new scheme that uses ^{31}P edited ^{1}H spectroscopy to quantify the concentrations of choline, PC, and GPC in biological samples (**Figure 3**). This method is particularly well-suited for analytical situations where the PC and GPC resonances are not sufficiently resolved and/or obscured by other metabolites, such as in *ex vivo* tissue studies.
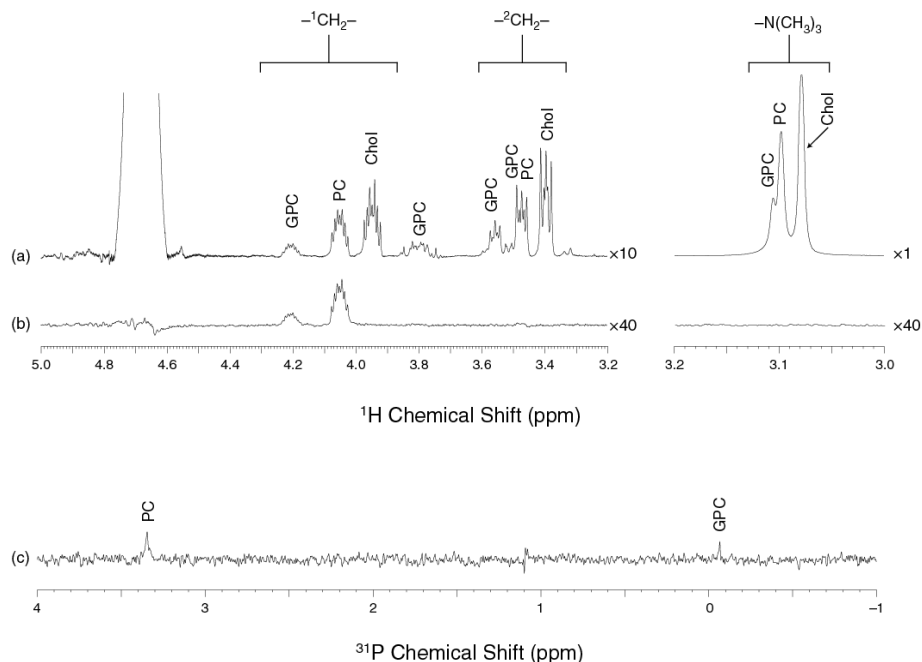
Figure 3. (**a**) ^{1}H, (**b**) ^{31}P filtered ^{1}H, and (**c**) ^{31}P spectra for a standard sample of 3.1 mM choline, 2.0 mM PC, and 1.0 mM GPC in 10% D_2O/90% H_2O. Each spectrum was acquired in 16 scans and with heteronuclear decoupling at 300 MHz for [1]H. In spectrum (**a**), the additional GPC peaks at 3.78 ppm and overlapping the [2]CH_2 resonances at 3.5 ppm arise from the glycerol moiety. The relative scales for spectra (**a**) and (**b**) are indicated at the right of each part. All spectra were processed with 0.5 Hz of line broadening; baseline correction was used for spectrum (**a**) to compensate for the intense water signal at 4.7 ppm.

5. Identification of molecular markers of prostate cancer growth rates.

Task 4 responds to the current situation in the prostate cancer clinic where PSA screening has yielded drastically increased numbers of diagnoses of Gleason score 6 and 7 cancers (>70% of all new cases (3)). Among Gleason score 6 and 7 cancers there is an acknowledged pathological difficulty in subcategorizing these patients to reflect their tumor potential and outcome (4); given such statistics, one critical aim of the current project is to discovery metabolite markers that can sub-categorize these tumors, as proposed in Task 4.

Clinical data indicates that, compared with other malignancies, many primary prostate cancers grow at relatively slow rates, while growth rates of prostate cancer at metastatic sites are similar to other more aggressive malignancies. Thus, it was suspected that there may exist inhibitory mechanisms, and spermine was identified as one such inhibitor(5). Spermine extracts from human prostate tissue were shown in vitro to have down-regulatory effects on the growth of prostate cancer cells and prevented subcutaneous tumor expansion in vivo. Our HRMAS MR spectroscopic analyses of human prostate tissues identified a positive correlation between the level of spermine and the amount of benign prostate epithelia; however, no relationship between spermine level measured from tissue and prostate cancer growth rate determined by PSA velocity (measured from serial PSA tests) was found in further analyses. Thus, we hypothesized that in the in vivo situation it may not be the cellular level of spermine, but rather the increased rate of spermine production, that is indicative of inhibitory activity.

To study spermine production, we assessed the gene expression of ornithine decarboxylase (ODC), the first and rate-limiting enzyme of the spermine metabolic pathway. We used the laser capture microdissection technique to remove benign prostate epithelia from 11 cases of Gleason score 6 and 7 tumors of patients with serial PSA tests prior to their prostatectomies (**Figure 4**). We used semi-quantitative one step RT-PCR to analyze the gene

expression profile of ODC. Five epithelial specimens obtained by LCM from prostatectomies were studied. QuantumRNA 18S Internal Standards and total prostate RNA were used to standardize the reactions.
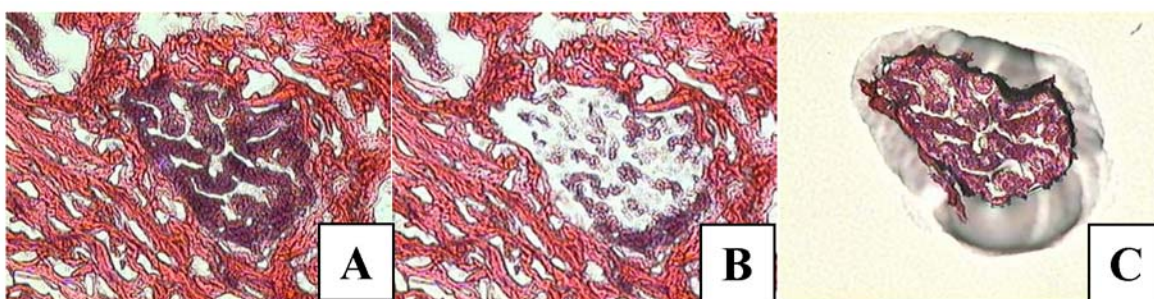

Figure 4. Human prostate epithelia (**A**) before, (**B**) after laser capture microdissection, and (**C**) the captured epithelia.

Among these 11 cases, if we use $R^2 > 0.85$ as a threshold to determine the accuracy of the calculated PSA velocities, five cases satisfied the condition. Within these five cases we observed that the ODC gene expression level linearly correlated to the patient's PSA velocity results ($R^2 = 0.861$; $P < 0.023$), as shown in **Figure 5**. This result, if confirmed, is extremely significant for it suggests that by measuring the ODC gene expression level from a biopsy specimen, the tumor growth rate may be assessed; this extremely relevant information is not currently available with any clinical methodology. These results have been included in a provisional patent application "Method for the diagnosis and prognosis of cancer using ornithine decarboxylase," in which the current award was acknowledged as parts of the funding sources.
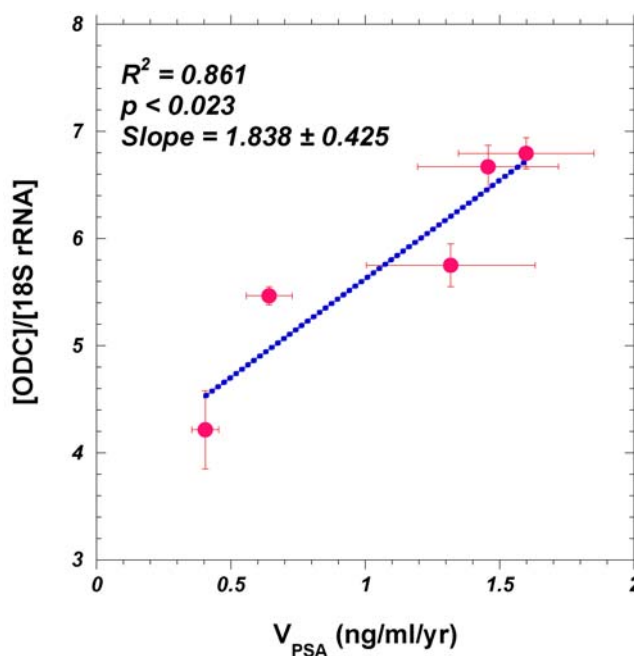
Figure 5. The gene expression levels of ornithine decarboxylase linearly correlated with prostate cancer growth rates determined by PSA velocity.

6. Measurements of possible prostate tissue metabolite degradations.

Evaluation of Tissue Degradation at Different Temperatures.   Metabolic decomposition ensues immediately following tissue excision. Thus, extrapolating the true concentrations of metabolites before tissue excision is of great importance. To study this, degradation rates of various metabolites found in intact prostate tissue were analyzed by continuously recording prostate tissue HRMAS spectra for 18-48 hours at 4°C (n=6) and 37°C

(n=3). These experiments were carried out on specimens that had been previously characterized. Examples of these metabolite degradation spectra are shown in **Figure 6;** measured changes in metabolites, examples of choline and citrate, at both temperatures, are shown in **Figure 7**. The relationships in Figure 7 indicate that different prostate metabolites have different degradation rates at different temperatures, with changes in an hour being less than 2% (within the error margins of an NMR analysis) at 4°C. Tissue degradation curves may allow us to extrapolate the true metabolite concentrations before tissue excision, if such a correction is necessary.
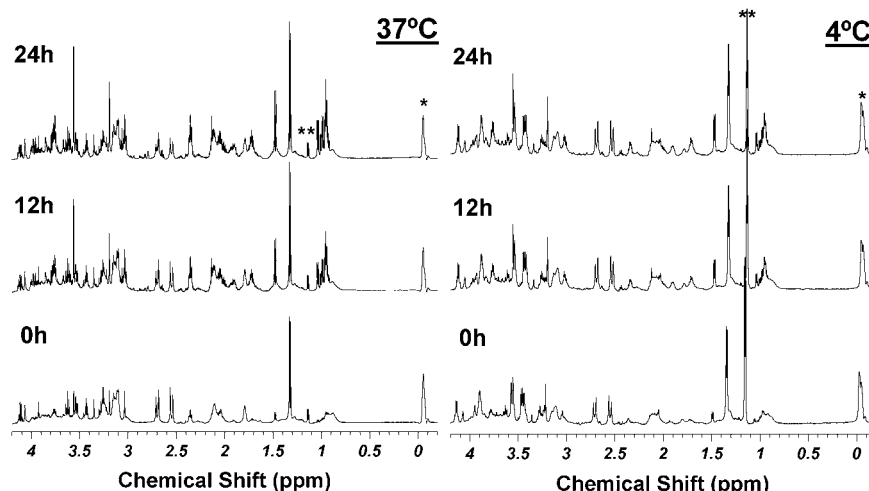

Figure 6. Intact prostate tissue HRMAS spectra measured at 4°C and 37°C at (0, 12, and 24) hours. * denotes an external rubber standard; ** indicates alcohol contaminations.
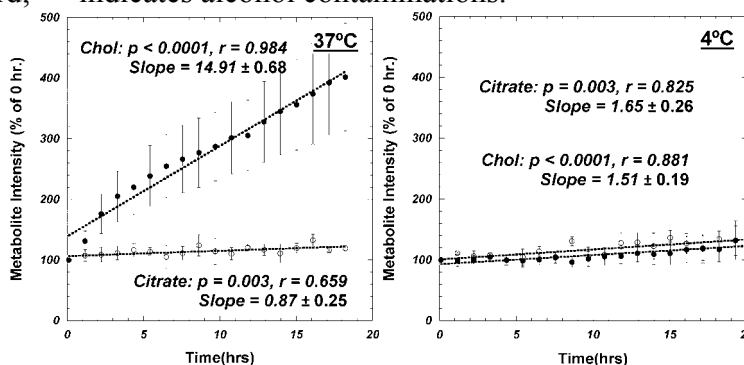

Figure 7. Comparisons of prostate metabolite degradation rates measured at 4°C and 37°C for choline and citrate

Evaluation of Tissue Storage Duration on Prostate Metabolites (Appendix 4)**.** Tissue storage at the –80ºC freezing condition is a common practice employed in biomedical research. The accepted assumption is that such a temperature condition halts biological and biochemical processes and preserves tissue molecular profiles for the duration of the storage. We tested this assumption on a group of previously characterized human prostate samples from our published studies of freeze-thawing effects on tissue metabolites in July 2002(6). These samples have been in storage under –80ºC for 32 months. Fifteen samples from 11 specimens were measured with the same experimental protocol as reported in the 2002 publication. After spectroscopy analysis, quantitative pathology evaluations also confirmed that the pathological compositions of the current samples were similar to those of the same specimens analyzed in 2002. In general, metabolic profiles do not show drastic alteration after storage, an example of such a comparison between metabolic spectra is given in **Figure 8**, where spectra (a) and (b) are the reproduction of Figure 1 in the freeze-thawing report, while spectrum (c) was obtained in March 2005 from tissue samples of the same specimen that resulted in spectra (a) an (b) in July 2002. Quantitative analyses of the ratios over creatine for 12 metabolites suggest that the overall apparent increase, if confirmed, is less than 20% (**Figure 9**). Detailed comparisons are still in the process of analyses.
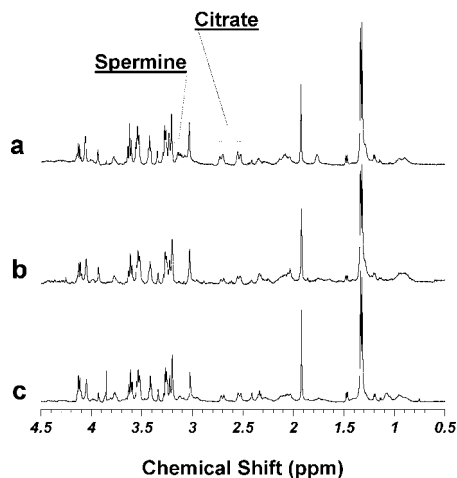
Figure 8. Comparison between metabolite spectra (**a**) and (**b**) reproduced from Fig. 1 in the publication of freeze-thawing studies in July 2002, and spectrum (**c**) obtained in March 2005 from samples of the same specimen that generated (**a**) and (**b**). No drastic changes in metabolite profiles are observed in association with tissue storage.
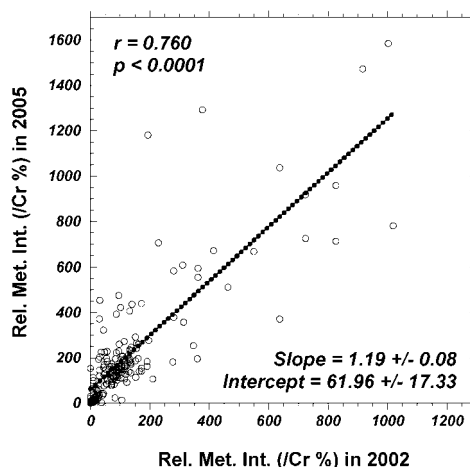

Figure 9. Quantitative analyses of 12 metabolites suggest that the overall apparent increases in metabolite ratios over creatine is less than 20%.

<u>7. Modifications to the proposed searches for metabolite profiles of normal prostates.</u>
In the proposal, we planned to establish a database of normal prostate metabolism based on measurements obtained from human autopsy samples. That was logical as a research project aimed at identification of tumor metabolic markers ought to establish profiles for normal controls before investigating the complexity of tumor profiles. However, during the conduction of the project, particularly in light of new clinical knowledge regarding the specifics of human prostate cancer, we found that there were two obstacles associated with that design, one conceptual and one technical.

First, the conceptual dilemma: how would we define normal prostate, given the new clinical observation stated in the National Cancer Institute's report from the Prostate Cancer Progress Review Group: "[b]ased on autopsy studies it is estimated that as many as 1 in 4 men 30 years of age may harbor a small focus of prostate cancer in their glands " (page 47). The answer seems to rely on what histopathology defines as "normal". Thus, conceptual differences between "normal" from autopsy without knowledge of cancer status and "normal" from cancer-free regions of prostate cancer prostatectomy samples do not exist. Hence, it is very difficult to assure that a subject is indeed a control, having no cancer glands or micro-foci of cancer in his prostate. Furthermore, as suggested by our preliminary results, "normal-looking" glands in a cancerous prostate may possess a metabolic profile predictive of a patient clinical status that would render the subject ineligible as a normal control. The second difficulty lies in the uncontrollable factors associated with autopsy, particularly time and

temperature factors that may cause metabolite degradations and introduce significant errors beyond our current scope of verification for the best use of research resources.

To solve this difficulty, we consider that the seeming impossibility of establishing prostate metabolic profiles for normal controls may be overcome in practice by measuring patient metabolite profiles from biopsy, and following patients closely after their initial biopsy, and using their cancer-free years as conditional controls. For instance, hypothetically, given a patient with elevated PSA, but no cancer-positive detection for n years after the initial biopsy analyzed with MRS, the prostate metabolic profiles of his initial biopsy would be included in a group of profiles that may eventually be used to predict that a patient with such a profile would likely be free of clinically significant cancer within the n years. However, research activities towards this aim, which will require observation periods exceed the duration of this award, are beyond the scope of this award. Nevertheless, our invaluable experience gained from the current project will help us to design and conduct these activities in our upcoming NIH project.

KEY RESEARCH ACCOMPLISHMENTS:

-- Publication of the first population study of prostate cancer metabolite profiles in Cancer Research (April 15, 2005).

-- Identification of the linear relationship between ODC gene expression levels in benign prostate epithelia and prostate cancer growth rates.

-- Verification of the feasibility in conducting HRMAS spectroscopy and histpathology studies on human thin core biopsies.

-- Continuations in sample collections, spectroscopy and quantitative pathology analyses.

REPORTABLE OUTCOME:
Publications:
In the past year, in direct relation to the proposed project, we have published four articles:

1.   Burns MA, Taylor JL, Wu CL, Zepeda AG, Bielecki A, Cory D, Cheng LL. Reduction of spinning sidebands in proton NMR of human prostate tissue with slow high resolution magic angle spinning. *Magn Reson Med* 2005; 54:34-42.

2.   Cheng LL, Burns MA, Taylor JL, He WL, Halpern EF, McDougal WS, Wu, CL. Metabolic characterization of human prostate cancer with tissue magnetic resonance spectroscopy. *Cancer Res.* 2005; I65:3030-3034.

3.   Loening NM, Chamberlin AM, Zepeda AG, Gonzales RG, Cheng LL. Quantification of phosphocholine and glycerophosphocholine with ^{31}P edited ^{1}H NMR spectroscopy. *NMR Biomed.* 2005; 18:413-420.

4.   Lentz MR, Taylor JL, Feldman DA, Cheng LL. Current clinical applications of *in vivo* magnetic resonance spectroscopy and spectroscopic imaging. Curr Med Imag Rev. 2005;1:271-302.

We have three more articles either in press or being submitted for publication:

5.   Jordan KW, He WL, Halpern EF, Wu CL, Cheng LL. Evaluation of tissue metabolites with high resolution magic angle spinning mr spectroscopy human prostate samples after three-year storage at -80ºc. *NMR Biomed.* Submitted.

6.   Cheng LL, Burns MA, Lean CL. High resolution magic angle spinning (HRMAS) proton MRS of surgical specimens. In: Webb G, (ed), Modern Magnetic Resonance, Vol II Medical Uses. Springer. 2006; In press.

7.   Cheng LL, Pohl U. Disease Studies – Cancer. In: Metabolomins. Lindon JC, Nicholson J, Holmes E (eds), Elsevier 2006; In press.

In addition, our work from or partially from this award has been accepted for presentations:

8.   Jordan KW, Cheng LL. Evaluation of Human Prostate Tissue Metabolites with High Resolution Magic Angle Spinning MR Spectrscopy After Three-Year Storage at -80C. Presentation at the 14th Annual Meeting of ISMRM, 2006.

9.   Cortez-Retamozo VF, Jordan KW, He WL, Wu CL, Cheng LL. Evaluating human prostate cancer growth with ornithine decarboxilase. The 97th AACR Annual Meeting, Washington DC, 2006.

Furthermore, one provisional patent application has been filed:

10.   Cheng LL, Pohl U, Wu CL, Cortez-Retamozo VF. Method for the diagnosis and prognosis of cancer using ornithine decarboxylase (odc).

Invited Lectures:

11.   The 5th Bi-Annual 2005 Minnesota Workshop on High Field MR Imaging and Spectroscopy and MR

        Imaging of Brain Function

        October 14-16, 2005

        Department of Radiology

        University of Minnesota
        Minneapolis, Minnesota.

12.   "Metabolomic Profiling of Human Cancer with ex vivo Tissue MR Spectroscopy"

        Frontiers of Metabolomics for Cancer Research

        October 24-25, 2005

        National Cancer Institute

        National Institute of Health

        Rockville, Maryland

Grant Application:

With direct and indirect supports provided by this award, we have submitted one NIH R01 grant titled: Characterizing prostate cancer by ex vivo MRS signatures (R01CA115746-01A1), and one NIH R21 grant titled: Tissue and serum metabolomic profiles of lung cancers (R21CA122478-01). Both are now in the peer-review process.

CONCLUSION:

In the past year we have achieved significant progress with the support of this award. Our results from our work this year further suggest that in the future we are likely to be successful with the direct testing of the hypothesis that prostate metabolic changes measured with HRMAS 1HMRS can correlate well with tumor types and grades, and thus may be used as diagnostic markers for human prostate cancer. With our achievements, we are increasingly confident that our efforts will contribute to the better understanding of prostate tumor biology, its relationship with disease diagnosis, and patient prognostication. Since our efforts and results to date have been in close agreement with our proposed Statement of Work, we do not expect any alterations from it in our research activities in the coming year.

REFERENCES:

1.   Cheng LL, Burns MA, Taylor JL, He W, Halpern EF, McDougal WS, Wu CL. Metabolic characterization of human prostate cancer with tissue magnetic resonance spectroscopy. Cancer Res 2005;65(8):3030-3034.
2.   Podo F. Tumour phospholipid metabolism. NMR Biomed 1999;12(7):413-439.
3.   Carroll P, Lee K, Fuks Z, Kantoff P. Cancer of the Prostate. In: DeVita V, Hellman S, Rosenberg S, editors. Cancer: Principle and Practice of Oncology. 6th ed. Philadelphia: Lippincott Williams & Wilkins; 2001.
4.   Jemal A, Murray T, Ward E, Samuels A, Tiwari RC, Ghafoor A, Feuer EJ, Thun MJ. Cancer statistics, 2005. CA Cancer J Clin 2005;55(1):10-30.
5.   Smith R, Litwin M, Lu Y, Zetter B. Identification of an endogenous inhibitor of prostate carcinoma cell growth. Nature Med 1995;1(10):1040-1045.
6.   Wu CL, Taylor JL, He W, Zepeda AG, Halpern EF, Bielecki A, Gonzalez RG, Cheng LL. Proton High Resolution Magic Angle Spinning NMR Analysis of Fresh and Previously Frozen Tissue of Human Prostate. Magn Reson Med 2003;50:1307-1311.

APPENDICES:

Manuscripts published, pending, and submitted in the past funding period (Jan 2005 - -Jan 2006). *: indicates a manuscript that specifically acknowledge this grant as a funding source.

1*.   Burns MA, Taylor JL, Wu CL, Zepeda AG, Bielecki A, Cory D, Cheng LL. Reduction of spinning sidebands in proton NMR of human prostate tissue with slow high resolution magic angle spinning. *Magn Reson Med* 2005;54:34-42.

2*.   Cheng LL, Burns MA, Taylor JL, He WL, Halpern EF, McDougal WS, Wu, CL. Metabolic characterization of human prostate cancer with tissue magnetic resonance spectroscopy. *Cancer Res.* 2005;I65:3030-3034.

3.   Loening NM, Chamberlin AM, Zepeda AG, Gonzales RG, Cheng LL. Quantification of phosphocholine and glycerophosphocholine with ^{31}P edited ^{1}H NMR spectroscopy. *NMR Biomed*. 2005;18:413-420.

4*.   Jordan KW, He WL, Halpern EF, Wu CL, Cheng LL. Evaluation of Tissue Metabolites with High Resolution Magic Angle Spinning MR Spectroscopy Human Prostate Samples After Three-Year Storage at -80ºC. *NMR Biomed*. Submitted.

5*.   Cheng LL, Burns MA, Lean CL. High resolution magic angle spinning (HRMAS) proton MRS of surgical specimens. In: Webb G, (ed), Modern Magnetic Resonance, Vol II Medical Uses. Springer. 2006; In press.

6*.   Lentz MR, Taylor JL, Feldman DA, Cheng LL. Current clinical applications of *in vivo* magnetic resonance spectroscopy and spectroscopic imaging. Curr Med Imag Rev. 2005;1:271-302.

7*.   Cheng LL, Pohl U. Disease Studies – Cancer. In Metabolomins, Lindon JC, Nicholson J, Holmes E (eds), Elsevier, 2006; In press.

8*.   Jordan KW, Cheng LL. Evaluation of Human Prostate Tissue Metabolites with High Resolution Magic Angle Spinning MR Spectrscopy After Three-Year Storage at -80C. Presentation at the 14th Annual Meeting of ISMRM, 2006.

9*.   Cortez-Retamozo VF, Jordan KW, He WL, Wu CL, Cheng LL. Evaluating human prostate cancer growth with ornithine decarboxilase. The 97th AACR Annual Meeting, Washington DC, 2006.

10.   Copy of email correspondence from Gail Whitehead of Public Affairs Coordinator, Azimuth, Inc for the USAMRMC, CDMRP requesting the use of results in Appendix 2 for the 2005 CDMRP Annual Report.

Reduction of Spinning Sidebands in Proton NMR of Human Prostate Tissue With Slow High-Resolution Magic Angle Spinning

Melissa A. Burns,[1] Jennifer L. Taylor,[1] Chin-Lee Wu,[1] Andrea G. Zepeda,[1] Anthony Bielecki,[3] David Cory,[4] and Leo L. Cheng[1,2]*

High-resolution magic angle spinning (HRMAS) NMR spectroscopy has proven useful for analyzing intact tissue and permitting correlations to be made between tissue metabolites and disease pathologies. Extending these studies to slow-spinning methodologies helps protect tissue pathological structures from HRMAS centrifuging damage and may permit the study of larger objects. Spinning sidebands (SSBs), which are produced by slow spinning, must be suppressed to prevent the complication of metabolic spectral regions. In this study human prostate tissues, as well as gel samples of a metabolite mixture solution, were measured with continuous-wave (CW) water presaturation on a 14.1T spectrometer, with HRMAS spinning rates of 250, 300, 350, 600, and 700 Hz, and 3.0 kHz. Editing the spectra by means of a simple minimum function (Min(A, B, . . ., N) for N spectra acquired at different but close spinning rates) produced SSB-free spectra. Statistically significant linear correlations were observed for metabolite concentrations quantified from the Min(A, B, . . ., N)-edited spectra generated at low spinning rates, with concentrations measured from the 3 kHz spectra, and also with quantitative pathology. These results indicate the empirical utility of this scheme for analyzing intact tissue, which also may be used as an adjunct tool in pathology for diagnosing disease. Magn Reson Med 54:34–42, 2005. © 2005 Wiley-Liss, Inc.

Key words: HRMAS; proton MRS; human prostate; slow spinning; pathology

The utility of high-resolution magic angle spinning (HRMAS) proton NMR spectroscopy for the analyzing intact biological tissues is being demonstrated increasingly by spectroscopic laboratories in the field of medical MR (1–11). Correlations between tissue metabolites measured with this spectroscopic method and tissue pathologies have been identified, demonstrating the potential of this method for supplementing histopathological evaluations. The most significant asset of this method is that it does not jeopardize the structural integrity of the tissue, and therefore makes it possible to evaluate tissue samples histopathologically after they have been studied spectroscopically (12). Therefore, the use of slow-spinning measurements for optimally protecting histopathological tissue structures from possible damage resulting from high-rate spinning has become the subject of research. Studies in this area have also evaluated the possibility of conducting HRMAS measurements on objects larger than surgical specimens (13–15).

MAS, a line-narrowing technique, has the potential to reduce line-broadenings due to both homogeneous and inhomogeneous interactions. Homogeneous line-broadenings, which result from fast spin diffusions (e.g., dipolar couplings) and exchanges, generate the final isotropic lineshape, and obscure the identification of contributions from individual spins. In theory, inhomogeneous line-broadenings can be traced to individual spins that are either oriented differently to the magnetic field (e.g., chemical shift anisotropy), or are experiencing a different field strength (e.g., magnetic susceptibility). With MAS on protons, homogeneous line-broadenings (particularly from dipolar interactions at natural abundance) are too large in scale to be narrowed with the currently achievable spinning rates. As a result, the proton signals from proteins and cell membranes cannot be detected with an HRMAS measurement—even, for instance, at spinning rates of >5 kHz. The enhancement in tissue measurements observed with HRMAS at a spinning rate of a few hundred Hertz is the result of the averaging of inhomogeneous interactions (mostly magnetic susceptibility effects) in cytoplasm and biological fluids. Experimental results have shown that a reduction in spinning rates with HRMAS does not interfere with the ability of HRMAS to reduce spectral line-broadenings due to inhomogeneous interactions (13–16). Furthermore, such reductions in the effects of these inhomogeneous interactions do not happen at a specific, determined spinning rate, but rather occur gradually with the increase of the spinning rate, and are maximized when all of the interactions are experimentally accounted for.

Basic physics suggests that the probability that structural damage will result from the centrifugal stress of spinning greatly decreases as the spinning rate is lowered. Therefore, there seems to be an optimal spinning rate below the maximum rate required for the complete reduc-

[1]Department of Pathology, Massachusetts General Hospital, Harvard Medical School, Boston, Massachusetts, USA.

[2]Department of Radiology, Massachusetts General Hospital, Harvard Medical School, Boston, Massachusetts, USA.

[3]Francis Bitter Magnet Laboratory, Massachusetts Institute of Technology, Cambridge, Massachusetts, USA.

[4]Department of Nuclear Engineering, Massachusetts Institute of Technology, Cambridge, Massachusetts, USA.

*Correspondence to: Leo L. Cheng, Pathology Research, CNY-7, 149 13th Street, Charlestown, MA 02129. E-mail: cheng@nmr.mgh.harvard.edu.

tion of inhomogeneous interactions. At this optimal point, the spinning rate is fast enough to produce a tissue spectral resolution that is adequate for identifying metabolites for pathology, and slow enough to preserve tissue pathology structures. However, to study biological tissues at spinning rates <1 kHz, effective suppression of spinning sidebands (SSBs), particularly those from water signals, is essential in order to eliminate interference with metabolite peaks of interest.

Recently the results of an HRMAS proton NMR study of human prostate tissues obtained under spinning rates of 600 and 700 Hz, with the assistance of a rotor-synchronized delays alternating with nutation for tailored excitation (DANTE) sequence, were reported (16). A robust performance by the technique in terms of the reproducibility of SSB suppression and the simplicity of its concept and execution was observed. With this approach, spectral regions that were free of water SSBs were selected alternately between the 600- and 700-Hz generated spectra. The effectiveness of this approach for biological systems in which SSBs of metabolites other than water are negligible was demonstrated. However, it was acknowledged that the effectiveness of the approach will diminish for systems in which SSBs from tissue metabolites or surgical alcohol contamination are present. In addition, although the empirical selection of spectral regions is effective, it has elicited concerns regarding the objectivity of the procedure.

In the 1980s, S. Patt (personal communication) suggested that SSBs in solid-state NMR could be removed with a novel mathematical scheme by editing two spectra (A, B), obtained at different spinning rates, with the formula: $(A + B - |A - B|)/2$. However, the suggestion received little attention. Upon reviewing this mathematical scheme, it became apparent to us that the proposed formula is equal to the function of Min(A, B), the point-by-point minimum of spectra A and B. This recognition also led to a simple and critical extension of the scheme to Min(A, B,. . ., N). The results obtained from Min(A, B) and/or Min(A, B,. . ., N) on gel samples of a metabolite mixture solution, as well as from human prostate samples, are presented in this report.

MATERIALS AND METHODS

Tissue Protocol

The NMR analysis of human prostate surgical specimens was approved by the Institutional Review Board (IRB) of Massachusetts General Hospital. Tissue samples were snap-frozen in liquid nitrogen and stored at −80°C. Thirty-one prostate samples were used in the study. At the completion of the spectroscopic analysis, tissue samples were fixed in 10% formalin, embedded in paraffin, cut into 5-μm-thick sections at 100-μm intervals, and stained with hematoxylin and eosin. Cross sections of each sample were quantified from pathology slides using an Olympus BX41 Microscope Imaging System (Olympus American, Inc., Melville, NY, USA) equipped with the image analyzer MicroSuite™ (Soft Imaging System Corp., Lakewood, CO, USA). The percentage of the area representing cancer cells, normal epithelial cells, and stroma in each cross section was estimated visually to the nearest 5% by a pathologist who had no knowledge of the spectroscopic results. The reported vol% of each pathological presentation was calculated based on the size of the cross section and the corresponding area percentage of each pathological feature.

Preparation of a Standard Gel Mixture Solution of Common Metabolites

A gel mixture solution of 10 commonly observed cellular metabolites was prepared to test the quantitative capability of HRMAS proton NMRS and, in particular, the examined spectral editing scheme. The following compounds (approximately 1 mM each) were dissolved in 100 ml distilled water: phosphocreatine, L-glutamic acid, sodium citrate, L-glutamine, taurine, myo-Inositol, N-acetylaspartate, phosphorylcholine, glycerophosphorylcholine, and lactic acid. About 1.5 g of agarose was added to the mixture. The pH of the mixture solution was adjusted to ~7.0. The mixture was heated until the agarose dissolved, and then was cooled to form a gel solution. The gel of the mixture solution was kept at 4°C. The measured concentrations determined from the spectroscopy data were between 6.7 and 26.2 mM based on the tested range of spinning rates.

HRMAS Proton NMR

The NMR experiments were carried out on a Bruker (Bruker BioSpin Corp., Billerica, MA, USA) AVANCE spectrometer operating at 600 MHz (14.1T). The HRMAS probe had three frequency channels: ¹H, ¹³C (not used in these experiments), and ²H. The samples were placed into a 4-mm zirconia rotor with Kel-F plastic inserts, which created a spherical sample space of ~10 μl located at the center of the detection coil. A small (~0.1 mg) silicone rubber sample was permanently fixed inside one of the Kel-F spacers, positioned within the detection coil but not in contact with the sample, to function as an external standard (STD) for both frequency (0.06 ppm from TMS) and quantification. Different amounts of the gel-solution sample (6–10 mg) were measured. Prostate tissue samples (8–10 mg) were obtained directly from the freezers without further preparation. The weights of the tissue samples were estimated based on the weight of the empty rotor and the weights of the rotor with the samples, before and after the HRMAS measurements. Because of the weight difference between the rotor and the tissue samples (about 1000 times), and the apparent loss of sample weight after the HRMAS measurements (likely due to water condensation on the outside wall of the rotor, which contained frozen tissue when it was weighed before the HRMAS analysis), the error in weight is generously estimated as 0.5 mg. Approximately 1.0 μl of D_2O was added to each sample for ²H field locking. The sample was introduced into the probe, which was precooled to 3°C for NMR measurements at that temperature. The rotor spinning rate accuracy (±1.0 Hz) was controlled with a MAS controller and was verified with the positions of the SSBs in the spectra.

Spectra were acquired with the spectrometer frequency set exactly on the water resonance. Two types of spectra were acquired: 1) CW water presaturation, followed by a
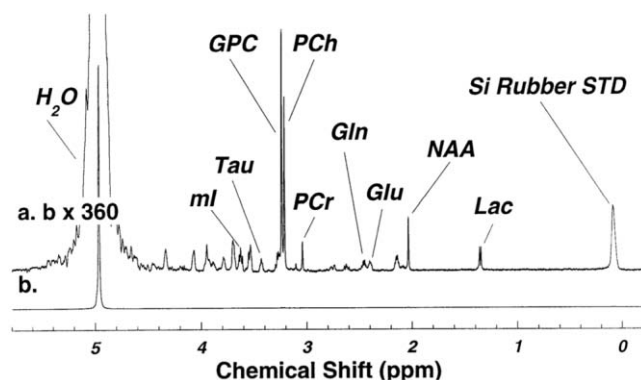
FIG. 1. Proton HRMAS spectrum of the prepared standard gel solution of commonly observed tissue cellular metabolites (as labeled) at 3.0 kHz. The spectrum was measured with a rotor-synchronized CPMG sequence with a total delay time of 20 ms. Spectrum **a** represents a 360-fold vertical expansion of the fully relaxed spectrum (**b**).

single 90° excitation pulse (used for both tissue and gel-solution samples), and 2) rotor-synchronized Carr-Purcell-Meiboom-Gill sequence (CPMG), with a 20-ms delay after the 90° excitation pulse (used only with the gel-solution samples). The CPMG sequence with a very short delay is used to reduce broad resonances caused by the probe background. Metabolite concentrations may be estimated from such a CPMG spectrum by reference to the intensity of water signals, while estimations from water presaturated spectra rely on the simultaneous measurement of the external standard.

Ten gel-solution samples of different weights were measured at spinning rates of 600 and 700 Hz, and 3.0 kHz with both CW water presaturation and rotor-synchronized CPMG pulse sequences. Of these, three were measured at the following additional spinning rates, with only the rotor-synchronized CPMG pulse sequence: 250, 300, 350, 800, and 900 Hz, and 1.0, 1.2, 1.4, 1.6, 1.8, 2.0, 2.4, 2.8, and 3.2 kHz. Of note, when total spectral absolute intensities of different spinning rates were compared, a decreasing trend was observed after 2.4 kHz. This reduction was likely the result of the sample leakage from the center of the rotor to the ends due to the spinning rate increase. Hence, data from 2.8 and 3.2 kHz spectra were not included in further calculations. The CW water presaturation sequence was used to analyze the human prostate tissue samples. Of the reported 31 human prostate samples, two samples were measured at spinning rates of 250, 300, 350, 600, and 700 Hz, and 3.0 kHz. Fourteen samples were measured at spinning rates of 600 and 700 Hz, and 3.0 kHz, and 15 samples were measured at spinning rates of 250, 300, and 350 Hz. Of note, the reported 17 samples measured at 250–350 Hz were the only samples analyzed thus far at those spinning rates, while the 16 samples evaluated at 600 and 700 Hz, and 3.0 kHz were the first samples from a series of studies involving 298 tissue specimens to date measured according to the Min(A, B) scheme. Each spectrum was acquired with 32 transients and a repetition time (TR) of 5 s.

The spectroscopic data were processed using the Nuts software (Acorn NMR Inc., Livermore, CA, USA) accord-

ing to the following procedures: All free induction decays (FIDs) were subjected to 0.5–1 Hz apodization before Fourier transformation, baseline correction, and phase adjustment were performed. Min(A, B, . . ., N) was applied to the data in the frequency domain using Nuts software after all individual spectra had been processed. The resonance intensities reported here represent integrals of curve-fittings with Lorentzian-Gaussian line-shapes, normalized by the STD intensity measured for each sample. All intensities reported here in the context of quantification refer to area integrated intensities. Tissue metabolite concentrations were calculated based on the integrated intensity ratios of metabolites over the STD, as explained in detail in the following section.

RESULTS

Evaluation of the Standard Gel Solution, and Calibration of the Silicone Rubber STD in the Sample Rotor

Figure 1 shows a spectrum of the prepared metabolite gel solution measured at a spinning rate of 3.0 kHz with the CPMG sequence without water presaturation. The spectrum in Fig. 1a, which is a vertical expansion of the entire spectrum (b), clearly shows the resonances of all of the prepared metabolites, although the integrated intensity of citrate appears to be less than its expected concentration. In addition, a prominent $-CH_3$ resonance peak from a piece of silicone rubber STD (~0.1 mg) that was permanently fixed inside the sample rotor was observed. Since the physical nature of the STD is that of a solid, its inte-
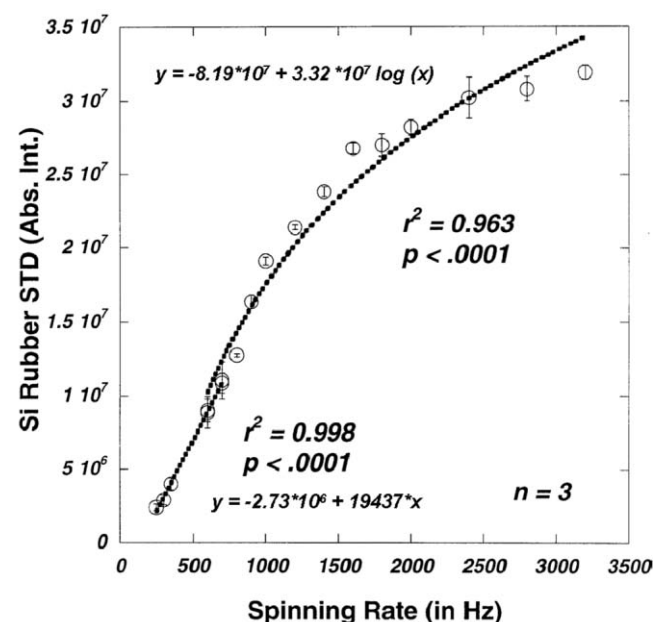
FIG. 2. The center band peak area integrated intensity of a silicone rubber standard (STD) as a function of the rotor spinning rate. The STD (~0.1 mg) was permanently fixed inside one of the Kel-F spacers to function as an external standard for both frequency and metabolite quantification. It appears that the spinning rate and the STD integrated intensity follow a linear relationship in the spinning rate region of 250–700 Hz, and then becomes logarithmic for spinning rates above 700 Hz.
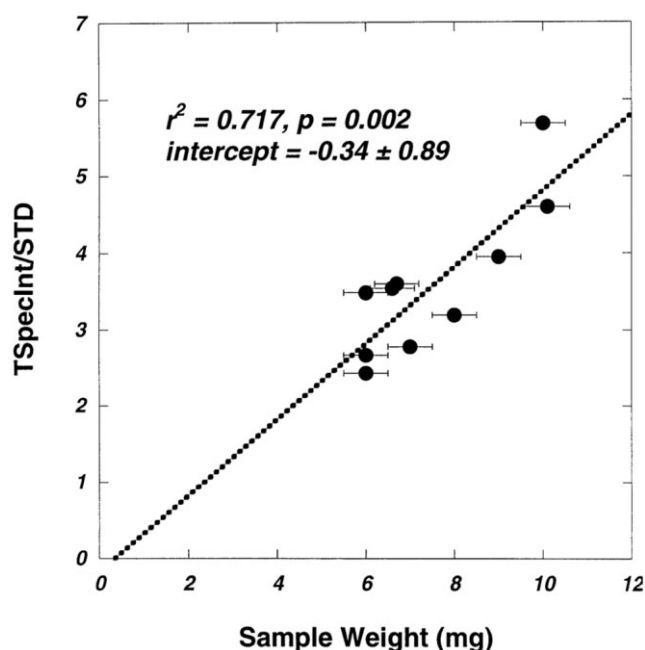
FIG. 3. The observed linear correlation between the sample weight (the mathematical average before and after spinning) and the total proton spectral integrated intensity measured at −0.2 to 4.8 ppm (excluding water signals) under the HRMAS spinning rate of 3.0 kHz from the prepared standard gel solution of metabolites measured with water presaturation.

grated intensity (at ~0 ppm) is heavily dependent on the spinning rate, as shown in Fig. 2. The relationship between the spinning rate and the STD absolute spectral integrated intensity has both linear (for the spinning rate region of 250−700 Hz) and logarithmic (for spinning rates above 700 Hz) components. Of particular interest in the present work, it was found that the STD's integrated intensity at 3.0 kHz was (3.06 ± 0.23) times higher than that measured at 600 Hz (16).

The overall quantitativeness of the HRMAS measurements was tested by varying the sample weights of the metabolite gel solution. A linear relationship was observed between the sample weight and the ratio between the summed spectral integrated intensities of all metabolite peaks and those of the STD measured at 3.0 kHz with the water presaturation sequence, as shown in Fig. 3.

The relationship between the sample spinning rate and the measured metabolite integrated intensities in the gel samples, as represented by both the concentrations (calculated according to the integrated intensity of the water resonance measured from the CPMG sequence) and the relative integrated intensities (Rel. Int., obtained as a ratio over the STD integrated intensity measured with the water presaturation sequence at 600 Hz), was examined. An example of this analysis applied to the lactate data ($N = 3$) is shown in Fig. 4. Both plots in the figure show a very similar logarithmic relationship of statistical significance between the increased spinning rate and the evaluated integrated intensities. The apparent integrated intensities (in both concentration and Rel. Int.) at different spinning rates (e.g., 600 Hz and 3.0 kHz) can be estimated for dif-

ferent metabolites according to these logarithmic curves. The linear relationship between the metabolic Rel. Int. and the metabolic concentration obtained from five measured metabolites at 600 Hz and 3.0 kHz is shown in Fig. 5. This linear relationship is critical for using the STD to estimate metabolite concentrations in intact tissue from spectra for which water presaturation is applied to improve the detectability of endogenous metabolites.

Measurement of Prostate Tissue at Low Spinning Rates

By varying the sample weight and spinning rate, and performing a spectroscopic analysis of the standard gels, we
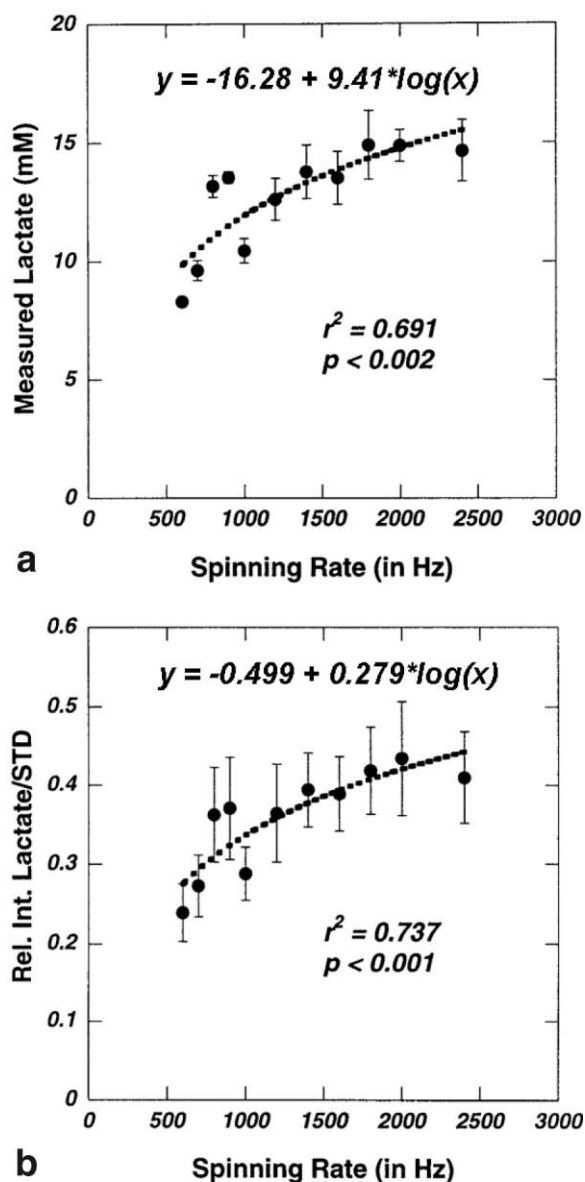
FIG. 4. Comparisons between the measured metabolite (lactate, $N = 3$) integrated intensities in absolute concentrations and relative intensities. (**a**) Absolute concentrations measured from the CPMG sequence and according to the water resonance intensity, and (**b**) relative intensity measured from the water presaturation sequence and according to STD integrated intensity measured at 600 Hz from the standard gel solution as functions of the HRMAS spinning rate.
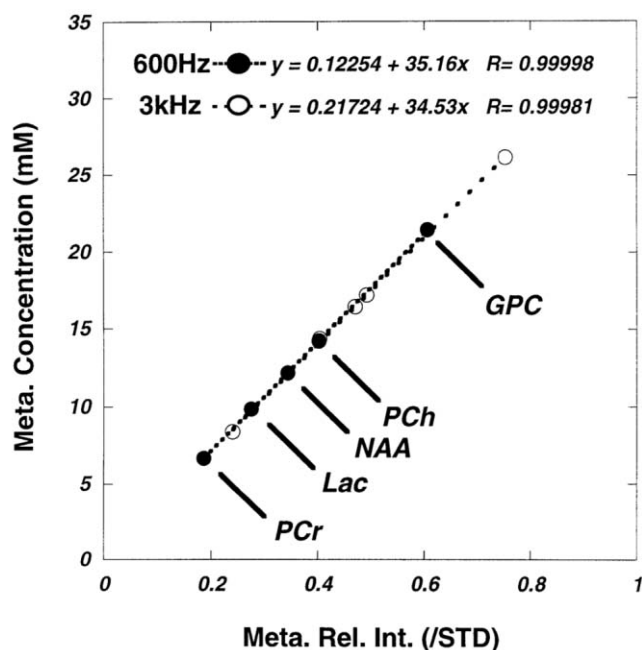
FIG. 5. Linear correlations observed between the relative metabolic integrated intensities as ratios over STD and the metabolite concentration estimated from the observed integrated intensities of water signals. These linear correlations were calculated based on the statistically significant curve-fitting results from the five measured metabolites as exemplified in Fig. 4 for lactate.

were able to identify the relationships necessary to quantify individual metabolites from human prostate tissue spectra edited with the Min(A, B,. . ., N) mathematical scheme. Figure 6 presents the results from the human prostate tissue sample that had the largest residual water SSBs after presaturation. Spectra A (Fig. 6a) and B (Fig. 6b) were measured at spinning rates of 600 and 700 Hz, respectively, where SSBs from water and the external standard were clearly observed. Figure 6d shows a spectrum of the same sample measured at the 3.0 kHz spinning rate, where all of the SSBs were pushed outside the region of interest (ROI; 4.8 ppm – (–)0.2 ppm). However, Fig. 6d was plotted with a different vertical scale to enable a comparison of the overall metabolite profiles with Fig. 6c. A visual inspection reveals no difference between Fig. 6d and c, where c represents the resulting spectrum after Min(A, B) editing. Additionally, Fig. 6e represents the digital inspection of these spectra (c and d). Although the differences between the two spectra are observable, they are minimal and can be neglected without compromising any resulting data. This Min(A, B) editing approach was further applied to three spectra (A, B, and C) (Fig. 7) generated at spinning rates of 250 Hz, 300 Hz, and 350 Hz, respectively. All three spectra showed visible SSBs. However, after the Min(A, B, C) editing scheme was applied to the three spectra, all SSBs were eliminated, as shown in Fig. 7d.

Tissue metabolite concentrations were estimated based on their ratio integrated intensities over the STD, measured both at low spinning rates (600 and 700 Hz) according to Min(A, B), and at 3.0 kHz. The comparison of metabolite concentrations measured with Min(A, B) to those

obtained at 3 kHz is shown for the examples of polyamines and citrate in Fig. 8. Comparisons for other metabolites are presented in Table 1. The results in the table are represented by linear regression analyses performed between the two sets of data collected from the 16 samples. These linear regressions were constructed with the 3.0 kHz data on the horizontal, and the Min(A, B) results on the vertical. Hence, if the Min(A, B) value of a particular metabolite is identical to that measured at 3.0 kHz, the slope of the linear regression will be one and the intercept will be zero. On the other hand, a slope of <1 indicates that the integrated intensity of the metabolite measured at 3 kHz has a higher value than that determined with Min(A, B) at 600–700 Hz. For almost all of the evaluated metabolites, higher apparent concentrations were observed under the 3.0 kHz measurement conditions. This was not surprising because it is widely acknowledged that an increase in spinning rate can potentially increase the observable amount of a metabolite, which is affected by the greater minimization of bulk magnetic susceptibility effects and other physical, environmental effects, such as viscosity.
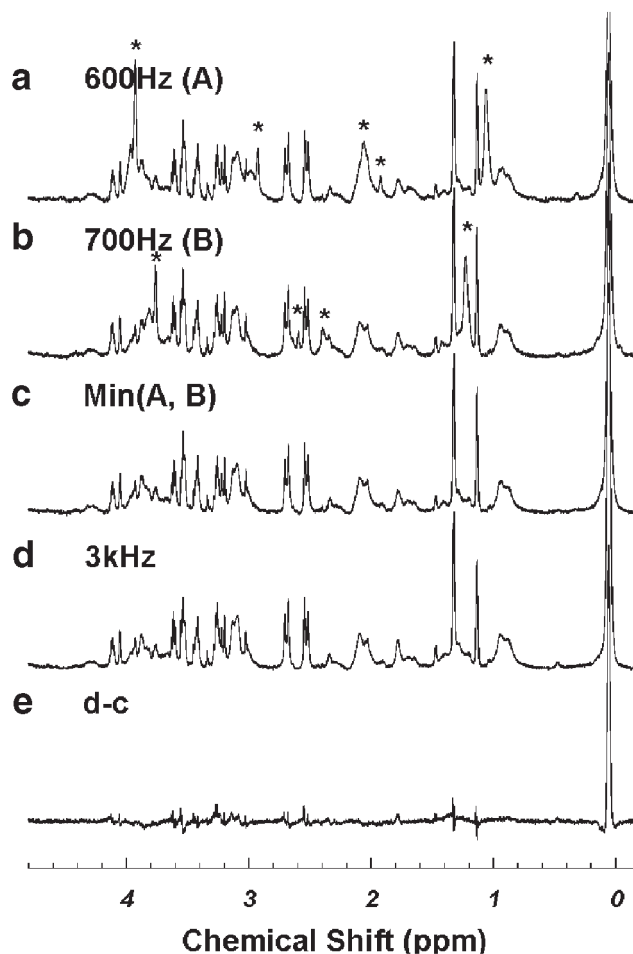
FIG. 6. Human prostate CW water presaturated spectra at spinning rates of (**a**) 600 Hz (A), and (**b**) 700 Hz (B). **c:** A spectrum that was edited, using A and B, with Min(A, B) to be visually compared with **d**, a spectrum obtained at a spinning rate of 3.0 kHz, plotted with a different vertical scale in order to produce **e**, a digital analysis presents the differences between spectra d and c. * SSBs from tissue water and rubber standard signals.
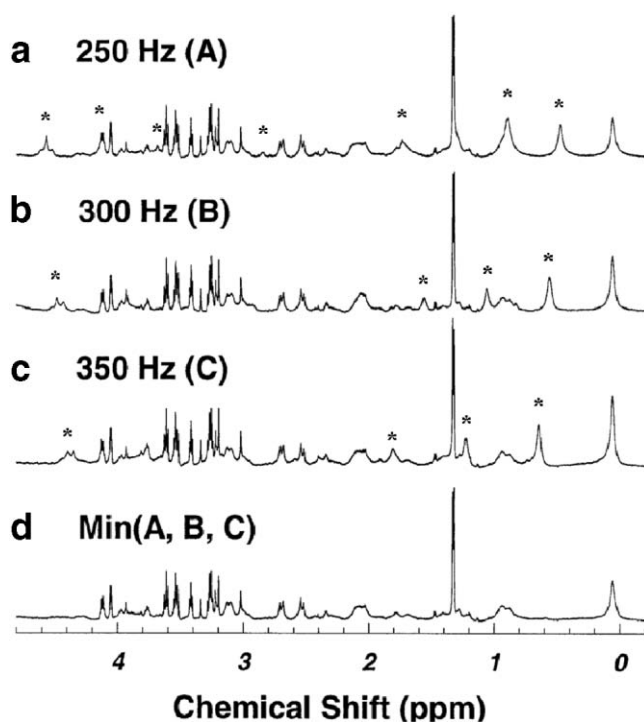
FIG. 7. Human prostate CW water presaturated spectra at spinning rates of (**a**) 250 Hz (A), (**b**) 300 Hz (B), and (**c**) 350 Hz (C). **d:** The resulting spectrum after the Min(A, B, C) editing scheme was applied to A–C. * SSBs from tissue water and rubber standard signals.

The two samples measured at 250, 300, 350, 600, and 700 Hz, and 3.0 kHz demonstrated linear relationships between the metabolic Rel. Int. at 600−700 Hz and 3 kHz, and also between the metabolic Rel. Int. at 250−350 Hz and at 3 kHz obtained with 16 quantified metabolite resonances (32 data points) from the Min(A, B, . . .,N)-edited spectra. Interestingly, while the Rel. Int. at 600−700Hz in Fig. 9 show a overall slope value (0.58) that is similar to those seen in Table 1 (average = 0.79) for concentrations, the Rel. Int. at 250−350 Hz indicates a slope of 0.31, suggesting that the apparent metabolic Rel. Int. measured at 250−350 Hz was much smaller than that measured at 3.0 kHz. Of note, the STD integrated intensities used in the figure were calibrated according to the STD-spinning rate relation curve presented in Fig. 2.

Correlation of Prostate Metabolite Integrated Intensities Measured at Low Spinning Rates With Prostate Pathology

We evaluated the utility of prostate metabolite data obtained with the Min(A, B, C) editing scheme at spinning rates of 250, 300, and 350 Hz by testing the data's correlation with the volume percent of tissue pathological structures. Statistically significant linear correlations between normal epithelium (vol%) and polyamines and citrate are shown in Fig. 10. These are in close agreement with previously reported results obtained at 9.4T (400 MHz) field strength, under a spinning rate of 2.5 kHz (12).

DISCUSSION

The goal of this work was to establish a simple, reproducible, and empirical spectroscopic scheme that can effec-

tively evaluate intact tissue metabolite concentrations measured at slow spinning, which is desirable for protecting tissue pathological structures from the damages of fast mechanical spinning, and for applying spinning to larger objects. This study was conceived because of the need to evaluate pathological tissue after HRMAS analysis to gauge the potential of the metabolite measurements for aiding disease diagnosis. As an empirical approach, the mathematic validity of the scheme from the precise concepts of NMR physics is beyond the scope of the current report.
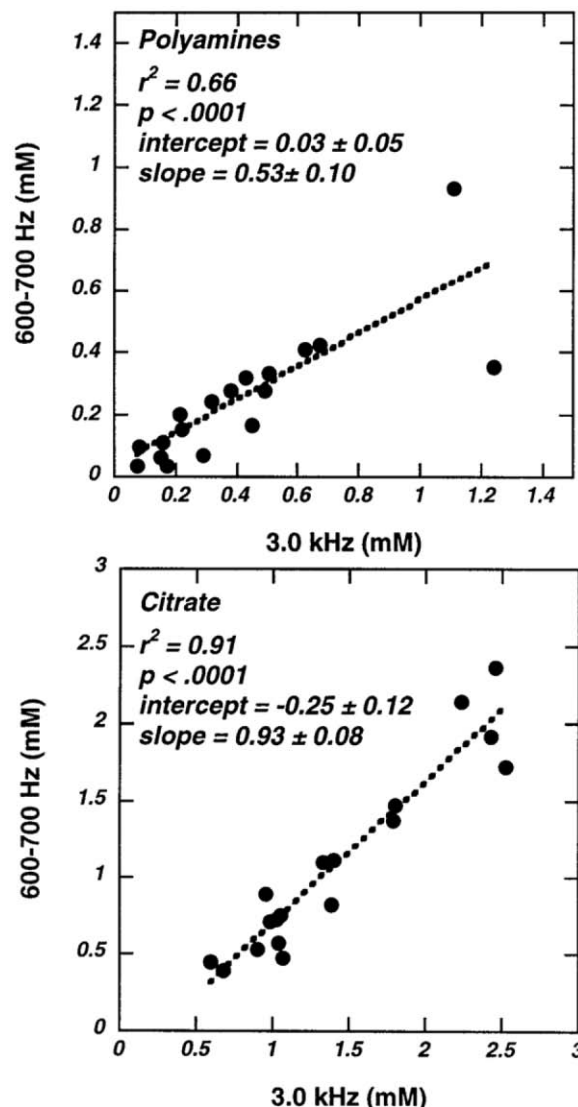
FIG. 8. Comparisons between concentrations of prostate metabolites, polyamines, and citrate measured with sample spinning at 3.0 kHz and those measured at 600 and 700 Hz and determined by Min(A, B) editing. If the Min(A, B) value of a particular metabolite is identical to that measured at 3.0 kHz, the slope of the linear regression would be one and the intercept would be zero. A slope of <1.0 indicates that the measured spectral integrated intensity at a higher (3.0 kHz) spinning rate is greater than that obtained at slower (600–700 Hz) spinning rates. It may be true that the more the slope falls below a value of 1.0, the more "solid-like" is the physical state of the metabolite.

Table 1
Comparison of Linear Regressions (Slow Rates–Vertical, vs. 3.0 kHz Rate–Horizontal) for Selected Metabolites*

Met. reson. (ppm)	P value	R^2	Slope[a]		Intercept[b]	
			Mean	SE	Mean	SE
Lac (4.10–4.14)	<0.0001	0.89	0.91	0.08	−0.24	0.17
ml (4.06)	<0.0001	0.77	1.00	0.14	**−0.18**	**0.18**
3.60–3.63	<0.0001	0.70	0.79	0.13	**−0.07**	**0.34**
3.52–3.54	<0.0001	0.84	0.87	0.10	**−0.09**	**0.32**
Tau (3.41–3.43)	<0.0001	0.80	0.87	0.11	**−0.08**	**0.11**
sl (3.34)	<0.0001	0.84	0.73	0.08	**0.00**	**0.01**
Pch (3.22)	0.0002	0.59	0.83	0.18	**−0.03**	**0.04**
Chol (3.20)	<0.0001	0.81	0.65	0.08	**0.01**	**0.02**
PM (3.09–3.14)	<0.0001	0.66	0.53	0.10	**0.03**	**0.05**
Cr (3.03)	<0.0001	0.87	0.76	0.08	**0.02**	**0.03**
Cit (2.52–2.71)	<0.0001	0.91	0.93	0.08	−0.25	0.12
Glu (2.33–2.36)	<0.0001	0.80	0.86	0.11	**−0.02**	**0.04**
Ala (1.47–1.49)	<0.0001	0.77	0.44	0.06	0.04	0.02
Lac (1.32–1.34)	<0.0001	0.76	0.91	0.13	−0.47	0.32

*The comparisons were made based on the estimated metabolite concentrations.
[a]Statistically significant linear correlations with slopes deviating from unity are observed indicating that the 3.0 kHz spinning rate produces higher metabolite integrated intensities.
[b]Bold faced data in the table indicate the intercepts are indifferent from 0.

Restrictions on Min (A, B,. . ., N)

The principle of Min(A, B,. . ., N) will work only if the following experimental conditions are met: 1) The spectra (A, B,. . .,N) are obtained from the same sample under the same experimental conditions, other than spinning rate. 2) The line-width for an individual resonance is the same (within measurement error) in all spectra, i.e., there is no additional visible narrowing of either homogeneous or inhomogeneous broadenings at higher spinning rates. For instance, in this study the line width at half maximum (LWHM) for creatine at 3.03 ppm in intact tissue was

measured to be 3.73 ± 0.98 Hz at 600 Hz spinning, and 3.83 ± 0.95 Hz at 700 Hz spinning. 3) The spinning rates are decided such that there is no SSB overlap point present in the ROIs in all N spectra. 4) There are no negative resonances in the spectra. Therefore, the spectra should be identical when measured within a reasonable range of spinning rates (e.g., 600 and 700 Hz) if the integrated intensities of SSBs from metabolites can be neglected when compared with the isotropic resonance integrated intensity. The contributions of SSBs from any source (i.e., water, external standard, any metabolites, or even contamination) will result in the increase of local spectral integrated intensity.

Min(A, B,. . ., N) vs. DANTE

In comparison with the previously reported DANTE method, which was optimized mainly for the elimination of SSBs from water and the external standard (STD), the Min(A, B,. . ., N) editing procedure can produce more accurate results for cases in which not only SSBs of water and/or STD, but also SSBs of tissue metabolites or other contaminants are of concern (16). However, the DANTE approach still may prove to be a method of choice for future applications of HRMAS spectroscopy in the clinical setting, where a defined metabolic marker(s) can be quantified with the measurement of one spectrum of an appropriately selected spinning rate. The advantages of the two-spectra Min(A, B) method are apparent, particularly during the research phases of surveying and discovering the marker(s). In addition, the Min(A, B) method can easily be extended to a general scheme of Min(A, B,. . ., N), as was demonstrated in this study using spinning rates of 250, 300, and 350 Hz. Future studies using this method may provide evidence for optimal spinning rates, such that tissue degradation is minimized and metabolic integrated intensity is maximized.

Quantitative evaluations of the relative metabolite integrated intensities (i.e., [metabolite]/[STD]) in the current
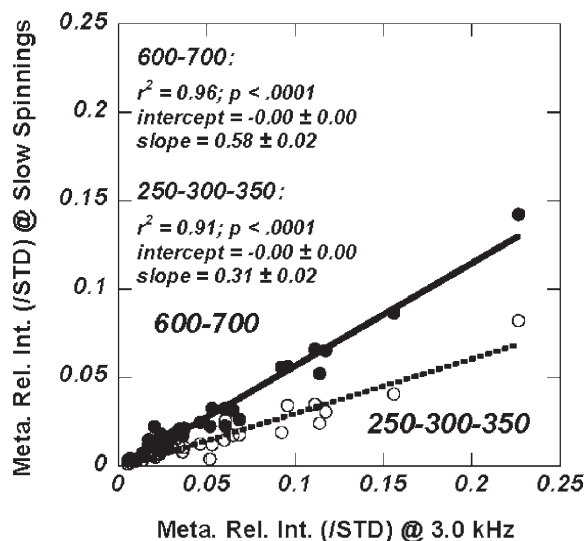

FIG. 9. Linear correlations between relative metabolic integrated intensities determined at an HRMAS spinning rate of 3.0 kHz and those measured at slower spinning rates (as ratios over the STD calibrated according to Fig. 2), i.e., Min(A, B) measured at 600 and 700 Hz, and Min(A, B, C) measured at 250, 300 and 350 Hz, for 16 metabolites from two cases.
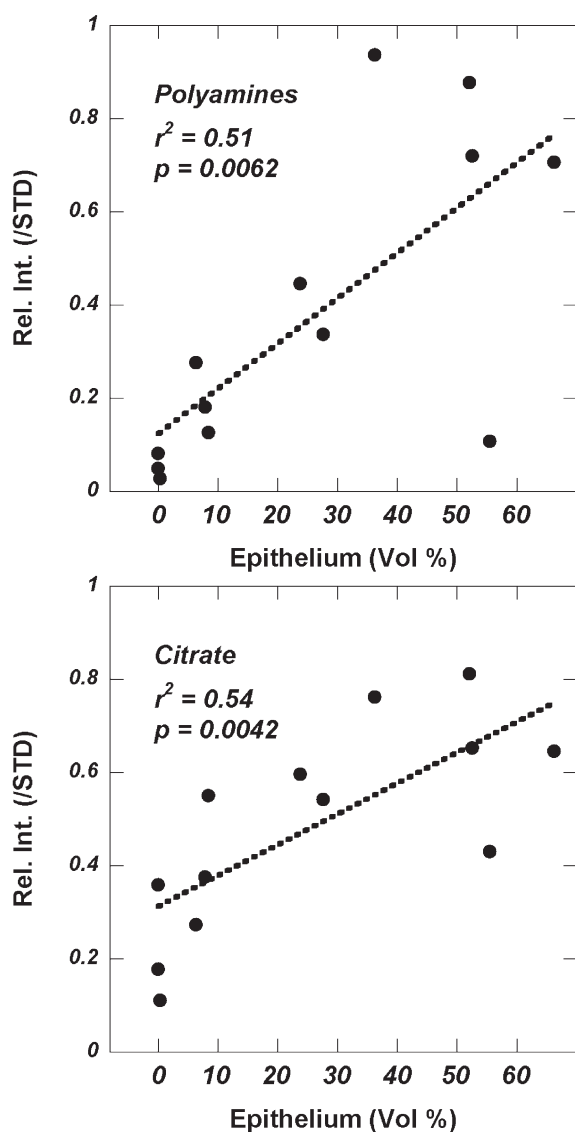
FIG. 10. Linear correlations between relative metabolic integrated intensities of polyamines and citrate with the volume percentage of tissue epithelium measured from the same tissue samples after NMR measurements.

analyses and those presented in the previous report of DANTE-CPMG measurements (16) revealed that the previous method could result in a reduction of metabolite integrated intensities by approximately 43% compared to the current Min(A, B) measurements of a single excitation pulse without CPMG. The reductions were likely the result of T_2 losses due to the rotor-synchronized CPMG of 10 ms.

Metabolite Integrated Intensities

The data presented in Table 1 were collected from the linear regression analysis of metabolite integrated intensities measured at spinning rates of 600–700 Hz with Min(A, B) vs. those obtained at the 3.0 kHz spinning rate. Since the metabolite integrated intensities of both the high and low spinning rates were normalized by the STD integrated intensity from direct measurement or projection, respec-

tively, these integrated intensities represented the concentrations of the measured metabolites. Hence, a slope of <1.0 indicates that the measured spectral integrated intensity at the higher (3.0 kHz) spinning rate was greater than that obtained at the lower (600–700 Hz) spinning rates. In general, it may be expected that the further the slope shrinks from 1.0, the more inhomogeneous the interactions experienced by the metabolite will be (e.g., as in a viscosity-related limitation on molecular mobility). For instance, a recent study of the human prostate indicated that polyamines are secreted in prostatic secretory granules of approximately 1 μm, a degree of spatial constriction that would result in the minimization of metabolite movements (17). If this is true, we may expect that the values of metabolic slopes will vary with different tissue types. Studies in this direction may have the potential to increase our understanding of the physical nature of these endogenous cellular metabolites; however, this is beyond the scope of the current evaluation. Nevertheless, this difference in the measured metabolite integrated intensities at different spinning rates is expected, and should not affect the accuracy of the HRMAS method for diagnosing disease as long as the metabolite data are acquired at the same spinning rate.

Correlation of Metabolite Integrated Intensity to Tissue Pathologies

Since the Min(A, B, . . ., N) editing approach minimizes tissue degradation caused by high spinning rates, the same tissue samples can undergo pathological assessment, thus allowing for the study of any correlations between individual metabolite Rel. Int. and vol% of a specific tissue component, such as glandular epithelium or cancer cells. Expanding on this concept, the use of more detailed pathological assessments than the vol% of a tissue component (such as immunohistochemical stainings) for comparison with metabolite integrated intensities may aid in disease diagnosis and patient prognosis.

Nonlinearity of Min(A, B,. . ., N) and Fitting of Min(A, B,. . ., N) Spectra With Lorentzian-Gaussian Functions

Careful consideration must be given to the nonlinear nature of the minimum function, Min(A, B,. . ., N), as it relates to measurement accuracy and statistical treatment of metabolite concentration. The validity of the Min(A, B,. . ., N) function relies heavily on the assumption that the component spectra differ only in the SSB frequencies. It is easy to conceptualize that various instrument errors (e.g., baseline or phasing errors) and spectroscopic effects (e.g., changes in peak amplitude or line-width associated with MAS rate changes) may, after processing with Min(A, B,. . ., N), introduce errors in spectral integrated intensities, leading to errors in metabolite concentration estimates. Furthermore, the Min(A, B,. . ., N) function is not appropriate for processing spectra with negative peaks unless additional nonlinear treatment (e.g., taking absolute value spectra) is executed.

The effects of the nonlinearity of Min(A, B,. . ., N) on spectral noise deserve special attention. In the presence of noise, spectra that are run at different spinning rates but
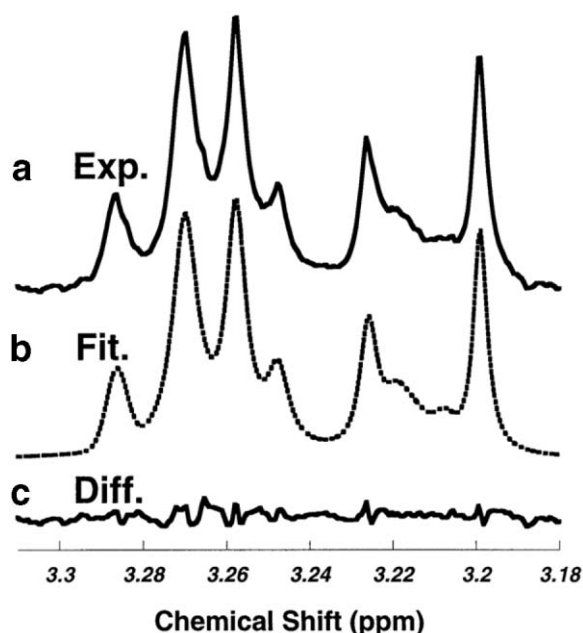
FIG. 11. Example of Lorentzian-Gaussian curve-fitting results for a Min(A, B,. . ., N)-edited spectrum. **a:** The 3.31–3.18 ppm spectral region from Fig. 7d. **b:** The Lorentzian-Gaussian curve-fitting results of a. **c:** Spectrum representing the difference between a and b. These differences are minimal and are typically observed with any curve-fitting process.

are otherwise identical will differ on a point-by-point basis. As Min(A, B,. . ., N) selects the lowest point, it introduces a negative bias that is uniform across the spectrum. If uncorrected, this will result in a negative bias in the metabolite measurement, with a magnitude that depends on the width and shape of the metabolite peak. The nonlinearity of the minimum function changes the noise statistics as well. A spectrum with normal (Gaussian) background noise, processed with Min(A, B,. . ., N), yields a spectrum with a non-Gaussian noise distribution, making statistical analysis more difficult but not impossible (given certain treatments of numerical methods). However, these theoretical concerns may not impair the empirical utility of the scheme in biological tissue analysis. Figure 11 illustrates that while there is some difference between the resulting Min(A, B,. . ., N) spectra (a region of Fig. 7d) obtained from a sample (Fig. 11a), and that obtained through curve-fitting (Fig. 11b) of the spectra, it is minimal and typical of any curve-fitting process (Fig. 11c). Thus, the production of spectra with non-Gaussian noise distribution resulting from the application of Min(A, B,. . ., N) should not remarkably affect metabolite integrated intensities. Therefore, since the interests and the purpose of this report are focused on the application of this empirical spectroscopic method in medical pathology, any further discussion of the nonlinearity of Min(A, B,. . ., N) and its correction may exceed the intended scope of this study.

CONCLUSIONS

The reported results indicate that by editing two or three slow-spinning tissue HRMAS spectra with a simple math-ematical function Min(A, B, . . ., N), the SSBs can be eliminated to produce an SSB-free tissue NMR spectrum that may be sensitive enough for the purpose of disease diagnosis. Tests of the proposed scheme on both a standard gel solution of commonly observed tissue metabolites and intact human prostate tissue samples revealed the empirical usefulness of the scheme. The results further suggest that the metabolite integrated intensities thus observed can be correlated with quantitative histopathological data obtained from the same tissue after NMR measurement.

REFERENCES

1. Coen M, Lenz EM, Nicholson JK, Wilson ID, Pognan F, Lindon JC. An integrated metabonomic investigation of acetaminophen toxicity in the mouse using NMR spectroscopy. Chem Res Toxicol 2003;16:295–303.
2. Huster D, Schiller J, Arnold K. Comparison of collagen dynamics in articular cartilage and isolated fibrils by solid-state NMR spectroscopy. Magn Reson Med 2002;48:624–632.
3. Kurhanewicz J, Swanson MG, Nelson SJ, Vigneron DB. Combined magnetic resonance imaging and spectroscopic imaging approach to molecular imaging of prostate cancer. J Magn Reson Imaging 2002;16:451–463.
4. Sitter B, Sonnewald U, Spraul M, Fjosne HE, Gribbestad IS. High-resolution magic angle spinning MRS of breast cancer tissue. NMR Biomed 2002;15:327–337.
5. Waters NJ, Holmes E, Waterfield CJ, Farrant RD, Nicholson JK. NMR and pattern recognition studies on liver extracts and intact livers from rats treated with alpha-naphthylisothiocyanate. Biochem Pharmacol 2002;64:67–77.
6. Tzika AA, Cheng LL, Goumnerova L, Madsen JR, Zurakowski D, Astrakas LG, Zarifi MK, Scott RM, Anthony DC, Gonzalez RG, Black PM. Biochemical characterization of pediatric brain tumors by using in vivo and ex vivo magnetic resonance spectroscopy. J Neurosurg 2002;96:1023–1031.
7. Morvan D, Demidem A, Papon J, De Latour M, Madelmont JC. Melanoma tumors acquire a new phospholipid metabolism phenotype under cystemustine as revealed by high-resolution magic angle spinning proton nuclear magnetic resonance spectroscopy of intact tumor samples. Cancer Res 2002;62:1890–1897.
8. Chen JH, Enloe BM, Fletcher CD, Cory DG, Singer S. Biochemical analysis using high-resolution magic angle spinning NMR spectroscopy distinguishes lipoma-like well-differentiated liposarcoma from normal fat. J Am Chem Soc 2001;123:9200–9201.
9. Griffin JL, Walker L, Shore RF, Nicholson JK. High-resolution magic angle spinning 1H-NMR spectroscopy studies on the renal biochemistry in the bank vole (*Clethrionomys glareolus*) and the effects of arsenic (As3+) toxicity. Xenobiotica 2001;31:377–385.
10. Schiller J, Naji L, Huster D, Kaufmann J, Arnold K. 1H and 13C HR-MAS NMR investigations on native and enzymatically digested bovine nasal cartilage. MAGMA 2001;13:19–27.
11. Barton SJ, Howe FA, Tomlins AM, Cudlip SA, Nicholson JK, Bell BA, Griffiths JR. Comparison of in vivo 1H MRS of human brain tumours with 1H HR-MAS spectroscopy of intact biopsy samples in vitro. MAGMA 1999;8:121–128.
12. Cheng LL, Wu C, Smith MR, Gonzalez RG. Non-destructive quantitation of spermine in human prostate tissue samples using HRMAS 1H NMR spectroscopy at 9.4 T. FEBS Lett 2001;494:112–116.
13. Wind RA, Hu JZ, Rommereim DN. High-resolution (^{1})H NMR spectroscopy in organs and tissues using slow magic angle spinning. Magn Reson Med 2001;46:213–218.
14. Hu JZ, Rommereim DN, Wind RA. High-resolution 1H NMR spectroscopy in rat liver using magic angle turning at a 1 Hz spinning rate. Magn Reson Med 2002;47:829–836.
15. Hu JZ, Wind RA. Sensitivity-enhanced phase-corrected ultra-slow magic angle turning using multiple-echo data acquisition. J Magn Reson 2003;163:149–162.
16. Taylor JL, Wu CL, Cory D, Gonzalez RG, Bielecki A, Cheng LL. High-resolution magic angle spinning proton NMR analysis of human prostate tissue with slow spinning rates. Magn Reson Med 2003;50:627–632.
17. Cohen RJ, Fujiwara K, Holland JW, McNeal JE. Polyamines in prostatic epithelial cells and adenocarcinoma; the effects of androgen blockade. Prostate 2001;49:278–284.

Cancer Research Highlights

Metabolite Profiles Depict Prostate Cancer Status

Cheng *et al.*   **Page 3030**

At present, the cancer pathological stage obtained from prostatectomy is the only way to evaluate the appropriateness and effectiveness of the surgery for the patient and to direct adjuvant therapies. To explore the utility of tumor metabolism, Cheng *et al.* analyzed prostatectomy samples with tissue MR spectroscopy. Tissue metabolite profiles were found to be extremely sensitive in differentiate cancer *versus* histologically benign samples obtained from the same patients. Furthermore, metabolite profiles measured from histologically benign samples differentiate tumor pathological stages. Tissue metabolite profiles show promise as a clinically relevant tool in screening biopsy of cancer patients and directing effective treatments.

Spontaneously Transformed Stem Cells Support Cancer Origin Thesis

**Rubio** *et al.*   **Page 3035**

Human adult stem cells are being evaluated widely for various therapeutic approaches and are thought to be highly resistant to transformation. It was, nonetheless, recently proposed that altered stem cells can give rise to cancer stem cells. Rubio *et al.* show that human mesenchymal stem cells (MSC) can undergo spontaneous transformation following long-term *in vitro* culture. This is the first report of spontaneous transformation of human adult stem cells, supporting the hypothesis of cancer stem cell origin. These findings indicate the importance of biosafety studies of MSC biology to efficiently exploit their full clinical therapeutic potential.

MPSS and ICAT Systematically Define Prostate Cancer Progression Pathways

Lin *et al.*   **Page 3081**

Prostate cancer is initially responsive to androgen-ablation therapy and progresses to androgen-unresponsive states that are refractory to treatment. The mechanism of this transition is unknown. Lin *et al.* employed two high-throughput technologies, massively
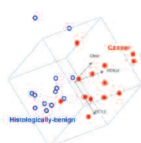
parallel signature sequencing (MPSS) and isotope-coded affinity tag (ICAT), to gain a system-wide understanding of this transition in LNCaP and CL1 cell line models. They found that 37 BioCarta and 14 KEGG pathways are up-regulated and 23 BioCarta and 22 KEGG pathways down-regulated during this transition. Their efforts represent a significant step towards a systems approach to understanding prostate cancer progression.

Stripped-Down Mini-HIV Maintains Killer Function Specific to Leukemic T Cells

Jeeninga *et al.*   **Page 3347**

Virotherapy of cancer is based on the selective replication of modified viruses in malignant cells. Jeeninga *et al.* tested whether the human immunodeficiency virus (HIV-1) can be transformed such that it replicates exclusively in leukemic T cells. When the HIV-1 genome was stripped from all accessory functions, the resulting mini-HIV variant was totally replication-impaired in normal T cells. Interestingly, this mini-HIV can still replicate in leukemic T cells and is able to selectively kill these cells in a mixed culture with untransformed control cells.

Stromal Cell Chemokine Receptor 5 Promotes Pulmonary Metastasis

van Deventer *et al.*   **Page 3374**
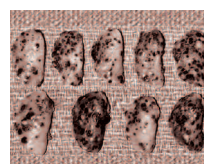
Inflammatory C-C chemokines are thought to facilitate cancer progression by binding to chemokine receptors on leukocytes or tumor cells. van Deventer *et al.* show that absence of one of these receptors, chemokine receptor 5 (CCR5), decreases tumor metastases. However, experiments with CCR5-/- and wild type bone marrow chimeric mice imply this effect is not mediated by CCR5 on white blood cells. The importance of CCR5+ stromal cells was confirmed by the transfer of these cells into CCR5-/- mice. This data provide an understanding of how CCR5 inhibitors that have been developed for HIV patients can benefit patients with cancer.

Metabolic Characterization of Human Prostate Cancer with Tissue Magnetic Resonance Spectroscopy

Leo L. Cheng,[1,2] Melissa A. Burns,[1] Jennifer L. Taylor,[1] Wenlei He,[1,3] Elkan F. Halpern,[2] W. Scott McDougal,[3] and Chin-Lee Wu[1,3]

Departments of [1]Pathology, [2]Radiology, and [3]Urology, Massachusetts General Hospital, Harvard Medical School, Boston, Massachusetts

Abstract

Diagnostic advancements for prostate cancer have so greatly increased early detections that hope abounds for improved patient outcomes. However, histopathology, which guides treatment, often subcategorizes aggressiveness insufficiently among moderately differentiated Gleason score (6 and 7) tumors (>70% of new cases). Here, we test the diagnostic capability of prostate metabolite profiles measured with intact tissue magnetic resonance spectroscopy and the sensitivity of local prostate metabolites in predicting prostate cancer status. Prostate tissue samples (n = 199) obtained from 82 prostate cancer patients after prostatectomy were analyzed with high-resolution magic angle spinning proton magnetic resonance spectroscopy, and afterwards with quantitative pathology. Metabolite profiles obtained from principal component analysis of magnetic resonance spectroscopy were correlated with pathologic quantitative findings by using linear regression analysis and evaluated against patient pathologic statuses by using ANOVA. Paired t tests show that tissue metabolite profiles can differentiate malignant from benign samples obtained from the same patient ($P < 0.005$) and correlate with patient serum prostate-specific antigen levels ($P < 0.006$). Furthermore, metabolite profiles obtained from histologically benign tissue samples of Gleason score 6 and 7 prostates can delineate a subset of less aggressive tumors ($P < 0.008$) and predict tumor perineural invasion within the subset ($P < 0.03$). These results indicate that magnetic resonance spectroscopy metabolite profiles of biopsy tissues may help direct treatment plans by assessing prostate cancer pathologic stage and aggressiveness, which at present can be histopathologically determined only after prostatectomy. (Cancer Res 2005; 65(8): 3030-4)

Introduction

Prostate-specific antigen screening has effectively increased detection of prostate cancer at early stages. However, histopathology cannot reliably direct treatment in the prostate-specific antigen testing era: more than 70% of the newly diagnosed tumors receive a Gleason score (GS) of 6 or 7, yet clinical outcomes for these patients differ markedly (1). The limited prognostic insight of such clinical measures as prostate-specific antigen, Gleason score, and digital rectal exams often occasions either unnecessarily aggressive or dangerously conservative interventions (2–7). Prostate tumor heterogeneity further compromises histopathology in comprehen-

sive evaluations as prostate cancer cells often elude biopsy, producing false negatives (8–10). More reliable and informative prognostic tools are needed. Changes in tumor metabolism, downstream from genomic and proteomic transformations, are thought to reflect disease-related biochemical reactivity, to precede histologically observable changes in cell morphology, and thus to offer an early means for predicting tumor behaviors (11).

Recently, high-resolution magic angle spinning proton magnetic resonance spectroscopy was developed for intact tissue analysis (12, 13). Magic angle spinning, originally used to reduce resonance line width in solid-state nuclear magnetic resonance, subjects samples to mechanical rotations (approximately in kilohertz) at the magic angle (54 degrees 44 minutes) away from the direction of the static magnetic field of the spectrometer while spectroscopy is recorded. Applied to intact tissues, high-resolution magic angle spinning can produce highly resolved spectra, allowing identification of individual metabolites while preserving tissue pathologic morphology.

We evaluated the diagnostic utility of prostate tissue metabolite profiles measured with high-field (14.1 T), high-resolution magic angle spinning proton magnetic resonance spectroscopy. Unaltered prostatectomy samples were analyzed spectroscopically, then histopathologically. Prostate metabolite profiles obtained from principal component analysis of tissue spectra were correlated with pathology quantities and with patient serum prostate-specific antigen levels. Finally, the diagnostic potentials of tissue metabolite profiles in predicting pathologic stage and tumor perineural invasion were investigated.

Materials and Methods

Sample collection. This study of human prostate tissue with magnetic resonance spectroscopy was reviewed and approved by the Institutional Review Board at Massachusetts General Hospital. Samples (n = 199, from 82 cancer prostatectomies) were collected from different prostate zones of the following patient population: (A) Gleason score: 5 [2 cases, 5 samples]; 6 [51, 126]; 7 [21, 53]; 8 [4, 9]; and 9 [4, 6]; and (B) American Joint Committee on Cancer/Tumor-Node-Metastasis (AJCC/TNM) stages (6th ed.): T_{2ab} [24 cases, 59 samples], T_{2c} [44, 112], T_{3a} [10, 17], T_{3b} [3, 5], and T_{3ab} [1, 6]. The few T_{3a}, T_{3b}, and T_{3ab} cases identified were combined and regarded in the study as T_3. Surgical tissue samples were snap frozen in liquid nitrogen and stored at $-80°C$ until magnetic resonance spectroscopy. Patient clinical statuses were obtained from pathology reports.

High-resolution magic angle spinning proton magnetic resonance spectroscopy. A Bruker (Billerica, MA) AVANCE spectrometer operating at 600 MHz (14.1 T) was used for all magnetic resonance experiments. Tissue samples were placed into a 4-mm rotor with 10-μL plastic inserts. One-microliter D_2O was added for field locking. Spectra were recorded at 3°C with the spectrometer frequency set on the water resonance and a rotor-synchronized DANTE experimental protocol was applied with spinning at 600 and 700 Hz (± 1.0 Hz; ref. 14). Thirty-two transients were averaged at a repetition time of 5 seconds.

Spectra were processed with AcornNMR-Nuts (Livermore, CA) according to the following procedures: 0.5-Hz apodization before Fourier

transformation, baseline correction, and phase adjustment. Resonance intensities used in the study were integrals of curve fittings with Lorentzian-Gaussian line shapes measured from either 600- or 700-Hz high-resolution magic angle spinning spectrum (14).

Quantitative histopathology. Following spectroscopy, samples were fixed in 10% formalin, embedded in paraffin, cut into 5-µm sections at 100-µm intervals throughout the entire sample, and stained with H&E.

An Olympus BX41 Microscope Imaging System (Melville, NY), in conjunction with the image analyzer SoftImaging-MicroSuite (Lakewood, CO), was used to quantify sample cross sections. A pathologist with no knowledge of the spectroscopic results visually estimated to the nearest 5% the percent area representing cancer cells, normal epithelial cells, and stroma in each cross section. The percent volume of these features was calculated from the sizes of the cross sections and the corresponding percent area of each pathologic feature.

Statistical analysis. The aim of the present work was to correlate spectral metabolite profiles with tissue pathologies and patient clinical statuses. Prior to investigating such correlations, the metabolite matrix was subjected to statistical data treatment—principal component analysis—to reduce the complexity of spectral data.

Because certain pathologic processes can manifest simultaneous changes in multiple measurable metabolites, a change in a single metabolite may not represent the underlying process. Principal component analysis attempts to identify combinations (principal components) of the measured concentrations that may reflect distinct pathologic processes if they exist in the set of the samples. A positive contribution of a certain metabolite indicates the elevation of the metabolite within the component (process), and a negative contribution suggests suppression.

The components are ordered by the extent to which they are associated with variability in the observed cases. The more metabolites affected by a process (the more associated with a principal component), the greater the association. The stronger the change in the metabolites caused by a process, the greater the association. Additionally, the incidence of the process is a factor in the associated variability: extremely rare and extremely common processes cause little variability whereas processes that are seen in 50% of the cases have the greatest associated variability.

Principal components may differ from the actual underlying processes in one important respect. Principal components are required to be independent. Actual processes may affect some metabolites in common. For instance, one process might elevate metabolites A, B, C, and D, while suppressing E and F. A second process might elevate A and B, while suppressing C, D, E, and F. As both affect A, B, E and F in the same way, it is likely that the principal component analysis results identify a strong component, expressing an elevation of A and B with the simultaneous suppression of E and F. Another, possibly weaker, component might express metabolites C and D and would distinguish the first process from the second.

The hypothesis that different prostate pathologic features (percent volume epithelia, cancer cells, stroma) possess different metabolite profiles can thus be tested by using linear regression analysis against these principal components. Paired Student's *t* tests were used to evaluate the ability of cancer-related principal component 13 and its major contributing metabolites (phosphocholine and choline) from histologically benign samples obtained from the same patient, whereas discriminant analyses were used to generate a canonical plot to achieve the maximum separation between the two groups, with accuracy being analyzed by receiver operating characteristic curves (15). Student's *t* tests were used

Figure 1. *A*, high-resolution magic angle spinning ¹H MR spectrum of intact tissue obtained from the removed prostate of a 61-year-old patient with GS 6 T$_{2b}$ tumors. Histopathology analysis of the tissue sample (*insert*) after its spectroscopy measurement revealed that the sample contained 40% histopathologically defined benign epithelium and 60% stromal structures, with no identifiable cancerous glands. Cellular metabolites mentioned in the text are labeled on the spectrum. The 36 most intense resonance peaks or metabolite groups above the horizontal bars were selected for analyses, whereas the other regions were excluded from calculation, partly due to surgery-related alcohol contamination. *B*, three-dimensional plot of principal component 13 (PC13 correlates linearly with percent volume of cancer cells in tissue samples) versus phosphocholine versus choline. Cancerous and histologically benign (histo-benign) tissue samples from 13 patients can be visually separated in observation plane. The paired Student's *t* test results (cancer versus histo-benign from the same patients) for principal component 13, phosphocholine, and choline are 0.012, 0.004, and 0.001. Only results from these 13 patients could be evaluated with paired tests for other cancer positive samples were collected from patients from whom no histo-benign samples were analyzed. *C*, the canonical plot resulting from discriminant analysis of the three variables in *B* presents the maximum separation between the two groups. *D*, the resulting receiver operating characteristic curves indicates the accuracy of using the three variables in *B* to positively identify cancer samples.
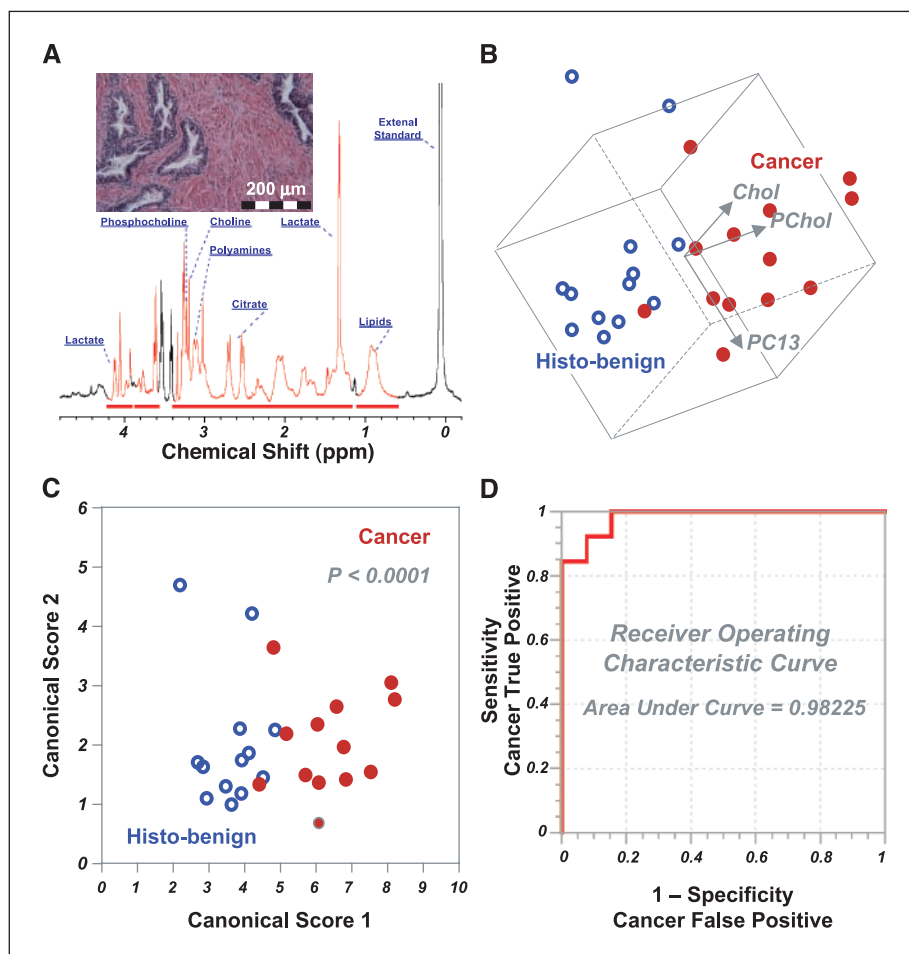
to investigate the relationship between cancer-related principal component 14 and tumor perineural invasion. The abilities of principal components 2 and 5 to differentiate between pathologic stages were tested using ANOVA. Statistical analyses were carried out using SAS-JMP (Cary, NC).

Results and Discussion

High-resolution tissue proton magnetic resonance spectroscopy and principal component analysis. High-resolution magic angle spinning magnetic resonance spectroscopy permits the acquisition of high-resolution proton spectra from intact tissue, while preserving tissue architectures for subsequent histopathologic analysis (Fig. 1*A*). To achieve high resolution before high-resolution magic angle spinning, tissue metabolites were analyzed in solutions of chemical extraction so that results depended on the applied procedures and their completeness. Furthermore, tumor heterogeneity limits the usefulness of extraction approaches.

Histomorphologic evaluations proved critical for the correct interpretation of spectroscopic data obtained from the same samples. In this study, 20 of 199 analyzed samples from prostate cancer patients contained cancerous glands, whereas the rest ($n = 179$) represented histologically benign tissue obtained from cancerous prostates. This frequency reflects the infiltrative, heterogeneous nature of prostate cancer; producing no visible mass, its architecture precludes cancer-selective tissue removal and thus accounts for the clinical complexity of prostate biopsy (8–10).

Principal component analysis was carried out on the concentrations of the 36 most intense resonance peaks or groups assigned to specific metabolites to generate principal components representing different variations of tissue metabolite profiles. Because of the existence of pathologic variations among the samples, certain principal components may capture these variations. For instance, principal component 2, reflecting changes in polyamines, citrate, etc., was found to differentiate epithelia from stroma with statistical significance (16.5% of variance; epithelia: $r = 0.381$, $P < 0.0001$; stroma: $r = -0.303$, $P < 0.0001$), in agreement with previous observation (16). Moreover, both principal component 13 and principal component 14 differentiate cancer from stroma (cf. principal component 14 represents 1.54% of variance; cancer: $r = -0.160$, $P = 0.0243$; stroma: $r = 0.217$, $P = 0.0021$). The difference of variance representation (16.5% versus 1.54% of the total variability of the standardized 36 metabolites for principal components 2 and 14, respectively) agrees with the fact that only 10% of the samples were identified as cancer positive, whereas >90% of them were designated epithelium positive. Of note, not all principal components are related with the evaluated pathologies. Many of them may indicate intrinsic differences that are not evaluated or variables, such as spectrometer instabilities, that are not the subjects of interest.

Differentiating cancer from histologically benign samples. By using histologically defined noncancer (histo-benign) samples from 13 of 20 patients from whom histologically cancer-positive samples were also analyzed, we observed a separation between the cancerous and histo-benign groups on a plane of a three-dimensional plot (Fig. 1*B*) of principal component 13 versus phosphocholine and choline. Both metabolites were found to be the major contributors to principal components 13 and 14, in agreement with descriptions by the current *in vivo* and *ex vivo* magnetic resonance spectroscopy literature of their relationship with malignancy (18). Further, both principal components were
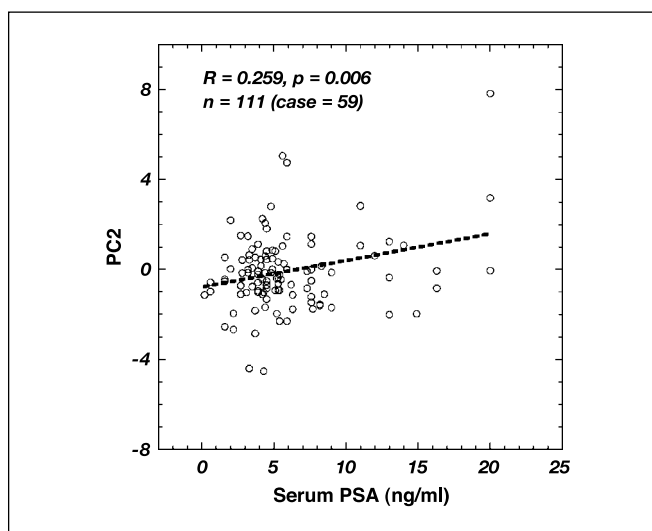

Figure 2. Statistically significant correlation between the patient serum prostate-specific antigen levels before prostatectomy and the metabolite profiles represented by principal component 2 (*PC2*), as measured from 111 histo-benign prostate tissue samples obtained from 59 prostatectomy cases for prostate cancer. Plotted principal component 2 values represent the linear combinations of metabolite concentrations according to the principal component 2 formula obtained from principal component analysis.

linearly correlated (*P*: 0.04, 0.02) with percent volume of cancer cells. Application of discriminant analysis to the three variables indicated a classification accuracy of 92.3% (Fig. 1*C*). An overall accuracy of 98.2% for the identification of cancer samples was obtained from a receiver operating characteristic curve generated from the three variables (Fig. 1*D*).

Correlating with patient serum prostate-specific antigen levels. From the 82 prostatectomy cases studied, we identified 59 cases for which the serum prostate-specific antigen levels of patients before surgery were available. Among these, 111 histo-benign tissue samples from different prostate zones (central, transitional, and peripheral) were identified. We evaluated the relationship between prostate-specific antigen levels and tissue metabolite profiles, and found that principal component 2 was linearly correlated, with statistical significance, to prostate-specific antigen results (Fig. 2). Because principal component 2 is linearly correlated with the percent volume of histo-benign epithelial cells, as previously presented, we verified that no coincidental correlation occurred between prostate-specific antigen levels and epithelial percent volume among these measured samples.

Identifying tumor pathologic stages and predicting tumor perineural invasion. We examined the correlation between principal components and tumor pathologic stage (AJCC/TNM staging system). With all 199 samples, we observed that principal component 2 differentiated T_{2c} cancer (prostate-confined; both lobes) from T_3 (invading extraprostatic tissue, $P < 0.03$) and T_{2ab} cancer (prostate confined; one lobe, $P < 0.005$). Principal component 5 also differentiated T_{2ab} cancer from T_{2c} ($P < 0.003$) and T_3 cancer ($P < 0.00005$). Again, we verified that the observed principal component 2 differentiation among tumor stages was independent of epithelial content (e.g., T_{2ab}, 21.88 $\pm$ 2.59%; T_{2c}, 20.21 $\pm$ 1.91%).

More interestingly, on analysis of the histo-benign samples ($n = 179$), similar differentiations persisted for both principal

Figure 3. Principal components 2 and 5 as predictors of tumor stage. Principal component 2 (*A*) can differentiate T_{2c} stage tumors from T_{2ab} and T_3 tumors, whereas principal component 5 (*B*) can differentiate T_{2ab} from T_{2c} and T_3 stages, as defined by AJCC/TNM staging system with histo-benign samples, and with histo-benign GS 6 and 7 samples (*C* and *D*). In the latter, principal components 2 and 5 can differentiate among three tumor groups: GS 6 T_{2ab}, GS 6 T_{2c}, and GS 6 T_3 plus GS 7 tumors.
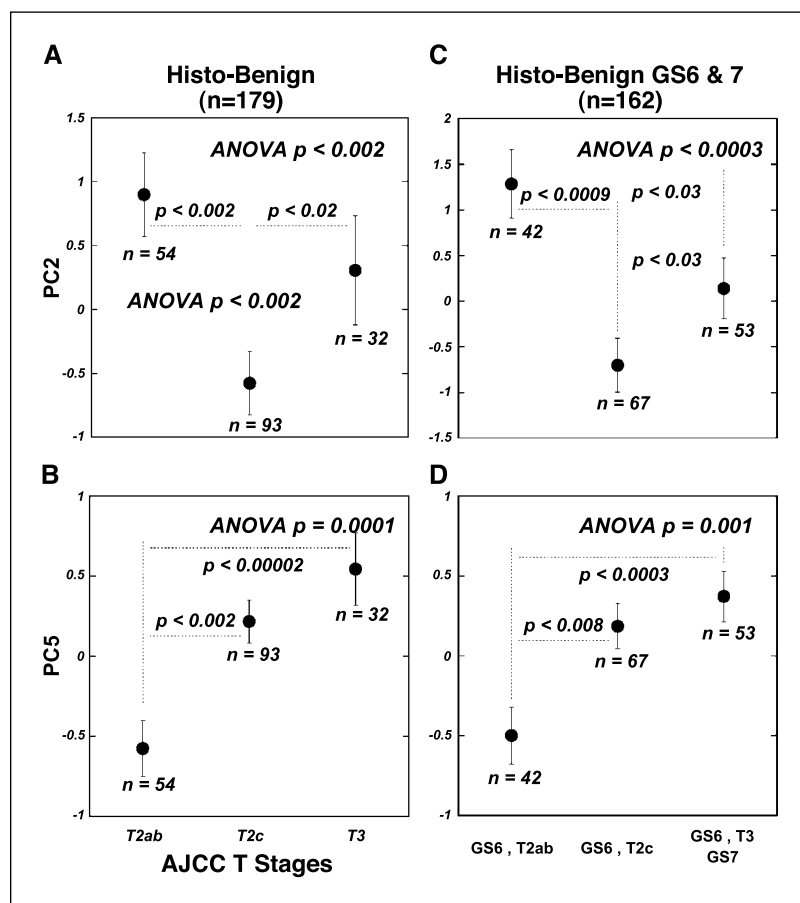
components (Fig. 3*A* and *B*). Furthermore, when the same principal components were applied to histo-benign samples of GS 6 and 7 tumors (*n* = 162), both principal components identified the least aggressive tumor (i.e., GS 6 T_{2ab} tumors, *n* = 42) from those of the more aggressive groups (GS 6 T_{2c}, GS 6 T_3, and GS 7 tumors; Fig. 3*C* and *D*).

Tumor perineural invasion status, although not yet incorporated in AJCC/TMN staging, indicates prostate tumor aggressiveness and aids treatment planning (17). Unfortunately, tumor heterogeneity prevents the visualization of invasion in biopsy samples. Our evaluation yielded a statistically significant correlation between principal component 14 levels and invasion status for all 199 samples (126 "+" and 73 "−"; *P* < 0.01), for 179 histo-benign samples (103 "+" and 71 "−"; *P* < 0.035), and more interestingly, for 42 histo-benign samples from GS 6 T_{2ab} tumors (13 "+" and 29 "−"; *P* < 0.028). This last observation, combined with results shown in Fig. 3*E* and *F*, may have great clinical significance in identifying and managing the less aggressive tumor group within the >70% newly diagnosed moderately differentiated tumors.

Our findings, with respect to tumor pathologic stages and perineural invasion, present an important indication of the technique's potential to improve current pathology in prostate cancer diagnosis. Despite its significance in treatment planning, tumor pathologic stage can now only be assessed from resected prostate. Our observations indicate that metabolite profiles may provide a "second opinion" for prostate biopsy evaluation. They further suggest that an additional biopsy core, obtained to generate

metabolite profiles, could help predict tumor stage for cancer-positive patients, even if the core itself is histo-benign.

In this report, we emphasize the phrase "histo-benign" to introduce the fact that the noncancer status of these tissue samples was based on histologic examination. We also emphasize that currently our metabolite results are analyzed according to histopathology, which remains the "gold standard" for cancer diagnosis and treatment planning. However, evaluation of the metabolite paradigm presented, and its usefulness in the oncology clinic, may require reconsideration of the boundaries of histopathology and metabolites. Current wisdom concerning the development and progression of malignancy, such as the widely proposed stroma effects, may assist this transformation (19, 20).

Our data leave unanswered questions. First, we cannot be certain from where, in proximity to cancer glands, our histo-benign samples were obtained. Therefore, we cannot predict whether observed metabolite alterations are global or focal. Additionally, comparisons between cancer-positive and histo-benign samples rely entirely on tissue from prostate cancer patients due to the lack of normal controls and the disqualifying metabolic degradation of tissue upon death. Our limited number of cancer-positive samples has also prevented determination of prostate pathologic stage based exclusively on cancer-positive samples.

We have nevertheless shown that metabolites measured with tissue magnetic resonance spectroscopy correlate with histopathology findings and that metabolite profiles reveal overall tumor clinicopathologic status and aggressiveness before either is

visible to histopathology. We believe the data presented here show the diagnostic and prognostic potential of the metabolite protocol. However, its clinical utility can be assessed only through longitudinal patient follow-up. Only correlations between tumor metabolites and patient outcome will allow us to establish the sensitivity and specificity of diagnostic and prognostic values for tumor metabolites, independent of current pathology.

References

1. Pound CR, Partin AW, Eisenberger MA, Chan DW, Pearson JD, Walsh PC. Natural history of progression after PSA elevation following radical prostatectomy. Jama 1999;281:1591–7.
2. Carter HB, Isaacs WB. Improved biomarkers for prostate cancer: a definite need. J Natl Cancer Inst 2004;96:813–5.
3. Incrocci L, Slob AK. Incidence, etiology, and therapy for erectile dysfunction after external beam radiotherapy for prostate cancer. Urology 2002;60:1–7.
4. Eton DT, Lepore SJ. Prostate cancer and health-related quality of life: a review of the literature. Psychooncology 2002;11:307–26.
5. Ko YJ, Bubley GJ. Prostate cancer in the older man. Oncology (Huntingt) 2001;15:1113–9, 23–4; discussion 24–6, 31.
6. Ransohoff DF, McNaughton Collins M, Fowler FJ. Why is prostate cancer screening so common when the evidence is so uncertain? A system without negative feedback. Am J Med 2002;113:663–7.
7. Smith RA, Cokkinides V, Eyre HJ. American Cancer Society guidelines for the early detection of cancer, 2003. CA Cancer J Clin 2003;53:27–43.
8. Zackrisson B, Aus G, Lilja H, Lodding P, Pihl CG, Hugosson J. Follow-up of men with elevated prostate-specific antigen and one set of benign biopsies at prostate cancer screening. Eur Urol 2003;43:327–32.
9. Mazal PR, Haitel A, Windischberger C, et al. Spatial distribution of prostate cancers undetected on initial needle biopsies. Eur Urol 2001;39:662–8.
10. Steiner H, Moser P, Hager M, et al. Clinical and pathologic features of prostate cancer detected after repeat false-negative biopsy in a screening population. Prostate 2004;58:277–82.
11. Mountford C, Doran S, Lean C, Russell P. Cancer pathology in the year 2000. Biophys Chem 1997;68:127–35.
12. Cheng LL, Lean CL, Bogdanova A, et al. Enhanced resolution of proton NMR spectra of malignant lymph nodes using magic-angle spinning. Magn Reson Med 1996;36:653–8.
13. Cheng LL, Ma MJ, Becerra L, et al. Quantitative neuropathology by high resolution magic angle spinning proton magnetic resonance spectroscopy. Proc Natl Acad Sci U S A 1997;94:6408–13.
14. Taylor JL, Wu CL, Cory D, Gonzalez RG, Bielecki A, Cheng LL. High-resolution magic angle spinning proton NMR analysis of human prostate tissue with slow spinning rates. Magn Reson Med 2003;50:627–32.
15. McNeil BJ, Keller E, Adelstein SJ. Primer on certain elements of medical decision making. N Engl J Med 1975;293:211–5.
16. Cheng LL, Wu C, Smith MR, Gonzalez RG. Non-destructive quantitation of spermine in human prostate tissue samples using HRMAS ^{1}H NMR spectroscopy at 9.4 T. FEBS Lett 2001;494:112–6.
17. Beard CJ, Chen MH, Cote K, et al. Perineural invasion is associated with increased relapse after external beam radiotherapy for men with low-risk prostate cancer and may be a marker for occult, high-grade cancer. Int J Radiat Oncol Biol Phys 2004;58:19–24.
18. Podo F. Tumour phospholipid metabolism. NMR Biomed 1999;12:413–39.
19. Wong YC, Wang XH, Ling MT. Prostate development and carcinogenesis. Int Rev Cytol 2003;227:65–130.
20. Cooper CR, Chay CH, Gendernalik JD, et al. Stromal factors involved in prostate carcinoma metastasis to bone. Cancer 2003;97:739–47.

Quantification of phosphocholine and glycerophosphocholine with ^{31}P edited ^{1}H NMR spectroscopy

Nikolaus M. Loening,[1]* Anne M. Chamberlin,[1] Andrea G. Zepeda,[2] R. Gilberto Gonzalez[3], and Leo L. Cheng[2,3]

[1]Department of Chemistry, Lewis & Clark College, 0615 SW Palatine Hill Road, Portland, OR 97219, USA
[2]Department of Pathology, Massachusetts General Hospital, Harvard Medical School, Boston, MA 02129, USA
[3]Department of Radiology, Massachusetts General Hospital, Harvard Medical School, Boston, MA 02129, USA

ABSTRACT: Choline and the related compounds phosphocholine (PC) and glycerophosphocholine (GPC) are considered to be important metabolites in oncology. Past studies have demonstrated correlations linking the relative ratios and concentrations of these metabolites with the development and progression of cancer. Currently, *in vivo* and tissue *ex vivo* magnetic resonance spectroscopy methods have mostly centered on measuring the total concentration of these metabolites and have difficulty in differentiating between them. Here, a new scheme that uses ^{31}P edited ^{1}H spectroscopy to quantify the concentrations of choline, PC and GPC in biological samples is reported and its applicability is demonstrated using samples of human brain tumor extracts. This method is particularly well-suited for analytical situations where the PC and GPC resonances are not sufficiently resolved and/or are obscured by other metabolites. Consequently, this scheme has the potential to be used for the analysis of choline compounds in *ex vivo* tissue samples. Copyright © 2005 John Wiley & Sons, Ltd.

KEYWORDS: ^{31}P edited ^{1}H NMR; INEPT; choline compounds; human brain tumor extracts

INTRODUCTION

Choline and the related compounds phosphocholine (PC) and glycerophosphocholine (GPC) are essential nutrients that function as substrates in many major bio-metabolic pathways. These choline-compounds participate in a number of biological processes ranging from the normal development of the brain and liver in infants[1] to various pathological conditions such as the progression of neoplasm.[2] Although the biochemical functions of these compounds have been studied for decades, their unique importance has only come to light over the past 20 years with the application of NMR spectroscopy to medical science.

The relationship between the concentrations of choline-compounds and pathology has been measured and documented for many medical conditions, such as HIV infections,[3] traumatic brain injuries,[4] schizophrenia,[5] neuro-degenerative[6] and neuro-genetic[7] disorders, chronic fatigue[8] and multiple sclerosis,[9] as well as for the processes of normal development[10] and aging.[11] However, one of the most studied connections has been with cancer.[12–18] In general, the concentrations of choline-compounds are elevated in cancer and, more importantly, *ex vivo* studies of tissue extract samples suggest that the ratio of the phosphoryl derivatives indicates the status of the disease.[19–21] The signals of the methyl [–N(CH$_3$)$_3$] protons has been used to differentiate choline (3.185 ppm) from PC (3.208 ppm) and GPC (3.212 ppm) in *ex vivo* analyses.[22] Unfortunately, present NMR-based *in vivo* techniques cannot differentiate the methyl protons of choline from those of PC and GPC as their signals are separated by less than 0.03 ppm. For *ex vivo* samples of intact tissue the methyl protons of choline can be differentiated from those of the other choline compounds using high-resolution magic angle spinning proton NMR spectroscopy. Differentiating between the methyl protons of PC and GPC is a great challenge because of their very small chemical shift separation (0.007 ppm, see Results section).[23,24] Therefore, even at moderate field strengths (e.g. 300 MHz), the resonances are difficult to resolve. This means that it is currently almost impossible to quantify these metabolites simultaneously *in vivo*. Although *ex vivo* quantification of all three compounds

Abbreviations used: GPC, glycerophosphocholine; INEPT, insensitive nuclei enhanced by polarization transfer; PC, phosphocholine.

Choline

$$(CH_3)_3\overset{+}{N} - {}^2CH_2 - {}^1CH_2 - OH$$

Phosphocholine (PC)

$$(CH_3)_3\overset{+}{N} - {}^2CH_2 - {}^1CH_2 - O - \overset{\overset{O}{\|}}{\underset{\underset{O^-}{|}}{P}} - O$$

Glycerophosphocholine (GPC)

$$(CH_3)_3\overset{+}{N} - {}^2CH_2 - {}^1CH_2 - O - \overset{\overset{O}{\|}}{\underset{\underset{O^-}{|}}{P}} - O - \overset{\overset{CH_2OH}{\underset{|}{CHOH}}}{\underset{|}{CH_2}}$$

Figure 1. Molecular structures of choline, PC, and GPC. The ^{31}P edited ^{1}H experiment discussed in the text uses INEPT steps to transfer magnetization from the [1]CH_2 protons to the phosphorous nuclei and back, and selectively refocuses the scalar couplings between the [1]CH_2 and [2]CH_2 protons during the transfers

is possible using the methyl proton signals, it is difficult and requires techniques such as post-processing peak deconvolution or two-dimensional spectroscopy.[25–28]

Here, we introduce a scheme that can efficiently differentiate and quantify PC and GPC, and we demonstrate its applicability to both model compounds and extracts of human brain tissue. The crux of this method is the use of phosphorous (^{31}P) edited proton (^{1}H) NMR spectroscopy to measure signals from the [1]CH_2 protons (see Fig. 1) of PC and GPC. These protons have a spectral separation that is about 20 times greater than that between the methyl protons (0.13 vs 0.007 ppm). The ^{31}P editing is accomplished using the scalar couplings between the ^{31}P nucleus and the [1]CH_2 protons in PC and GPC. Although the sensitivity of this technique suffers compared with the direct analysis of the methyl protons, the better resolution of the [1]CH_2 protons allows for analysis in situations where the individual methyl proton resonances from the three choline compounds are not sufficiently resolved. Consequently, we believe this ap-

proach may be helpful in the future for *ex vivo* analyses of intact tissue samples and, if sensitivity issues can be resolved, has the potential to be incorporated into *in vivo* examinations.

EXPERIMENTAL

The experiments were carried out using vertical standard-bore Bruker Avance NMR spectrometers. The standard samples were studied using a 300 MHz (7.05 T) system equipped with a Bruker broadband inverse-geometry *z*-axis gradient probe. The brain tissue extract samples were studied using a 600 MHz (14.1 T) system equipped with a Bruker ^{31}P/^{13}C/[15]N–[1]H inverse-geometry *z*-axis gradient probe. The pulse sequence developed for the experiment is shown in Fig. 2. It consists of two INEPT steps[29] that transfer the initial ^{1}H magnetization to ^{31}P and then back to [1]H. Inserted into these INEPT steps are selective 180° pulses that only affect the [2]CH_2 protons and, consequently, refocus the homonuclear scalar couplings between the [1]CH_2 and [2]CH_2 protons. These selective pulses are essential because the [1]H–[1]H couplings are similar in size to the [31]P–[1]H couplings. Without the selective pulses the effect of the [1]H–[1]H couplings during the INEPT delays would be to transform the single quantum coherences arising from the [1]CH_2 protons into multiple quantum coherences. Pulsed field gradients are used in conjunction with phase cycling to eliminate unwanted signals in the ^{31}P edited ^{1}H spe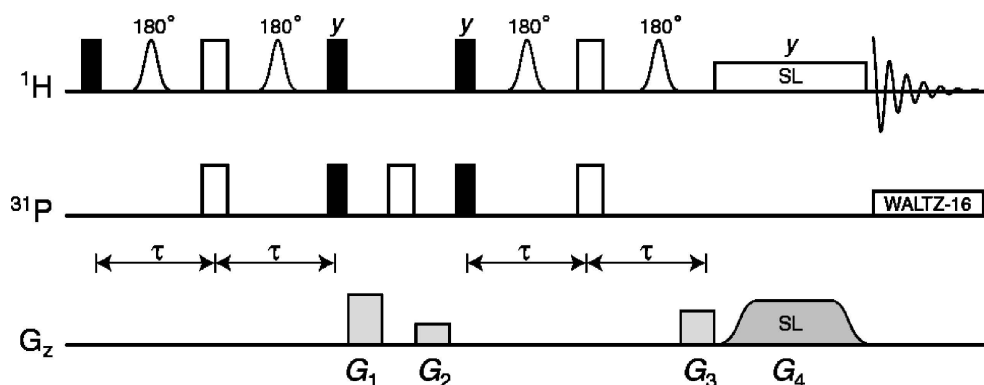ctra. The gradients G_1 and G_2 impart a phase label to the ^{31}P magnetization that is later refocused after the magnetization has been transferred to ^{1}H by the final coherence selection gradient, G_3. Finally, a zero-quantum filter is included at the end of the sequence to further attenuate contributions from undesired coherence transfer pathways.[30]

A recycle time of 10 s was used for both the regular and ^{31}P edited experiments to ensure that the sample magnetization was at equilibrium before every scan. During the

Figure 2. The pulse sequence used to acquire the ^{31}P edited ^{1}H spectra. For the ^{1}H and ^{31}P channels, solid rectangles correspond to 90° radiofrequency pulses, open rectangles correspond to 180° pulses, and Gaussian shapes represent selective 180° pulses. The spin-lock pulse is denoted by 'SL'. The phase of all pulses is *x* unless indicated otherwise

recycle delay, the water resonance was saturated with a weak radio frequency field ($\gamma B_1/2\pi = 50$ Hz). Low power Waltz-16 decoupling[31] ($\gamma B_1/2\pi = 625$ Hz) was used on the ^{31}P channel during ^{1}H acquisition to narrow the lines of the PC and GPC ^{1}CH$_2$ resonances; this resulted in an increase (20%) in the sensitivity of the experiment. For the high-power pulses, the radiofrequency field strength ($\gamma B_1/2\pi$) was 40 kHz for ^{1}H and 10 kHz for ^{31}P on the 14 T instrument, and 35 kHz for ^{1}H and 20 kHz for ^{31}P on the 7 T instrument. For the ^{31}P experiments, Waltz-16 decoupling ($\gamma B_1/2\pi = 2500$ Hz) was used on the ^{1}H channel.

In the ^{31}P edited ^{1}H experiment, Gaussian 180° pulses were used to selectively decouple the ^{1}H homonuclear scalar couplings during the INEPT steps. The selective pulses were 5 ms on the 14 T system and 10 ms on the 7 T system; for both systems the pulses were applied at 3.3 ppm. Consequently, these pulses refocused the ^{2}CH$_2$ protons of choline, PC, and GPC, but left the ^{1}CH$_2$ protons of these molecules unperturbed. The gradients G_1, G_2, G_3 and G_4 were set to 35, 15, 20, and 1 G cm^{-1} and were 2.47, 2.47, 1, and 10 ms in length, respectively. The first three gradients were shaped to a half-sine bell; the shape of the fourth gradient was constant over the central 80% of the pulse and was smoothly ramped on and off at the ends of the pulse.

The sample temperature was maintained at 10 °C with a cooling gas flow rate of 535 l h^{-1} for the experiments at 14 T to minimize any potential problems owing to sample degradation. The experiments at 7 T were performed at 25 °C. The temperature was controlled to better than ± 0.2 °C during the experiments; temperature stability is important for quantitation as the efficiency of the heteronuclear transfer steps varies with temperature.

Standards

The standard samples consisted of between 0 and 5 mM PC, between 0 and 5 mM GPC, and 3.1 mM choline in 10% D$_2$O–90% H$_2$O. D$_2$O was included in the sample for the purpose of locking the magnet field. All spectra for the standards were acquired with 16 scans (each spectrum required just under 3 min to complete). The pH of each sample was adjusted to be in the range 6–7.5 by the addition of small amounts of HCl or NaOH.

Solutions of human brain tumor metabolites

Eleven samples of human glioma (malignant brain tumor) extracts were prepared using the FastPrep^{TM} and Speed Vac$^{®}$ systems (Thermo Savant, Holbrook, NY, USA) according to the following procedure. Between 100 and 200 mg of frozen tissue samples from surgeries or autopsies were transferred into Lysing Matrix D tubes (Qbiogene, Carlsbad, CA, USA) along with 1.2 ml

methanol. The sample tubes were then placed in the FastPrep^{TM} system and processed for 35 s on speed dial 4.0. This was repeated at least three times until no visible tissue pieces remained. Next, a modified methanol–chloroform extraction was carried out.[32] The resulting aqueous layer of brain metabolites was dried with the Speed Vac$^{®}$ system and redissolved in D$_2$O. The pH of these samples was adjusted to be in the range 7–8. Since this preparation method is not a calibrated protocol for metabolite quantification, we observed a decrease in the absolute metabolite concentrations. For instance, the mean concentration for total choline was determined to be 0.31 ± 0.07 mM, which is only 25% of the literature values (1.24 ± 0.10 mM) for extracts of tumor tissues of similar type.[33–35] Although this reduction in concentration resulted in much longer experiment times, it did not interfere with the aim of this work, which was to test the capability of the ^{31}P edited ^{1}H spectral protocol to quantify PC and GPC concentrations of tissue extract samples. ^{1}H spectra for the brain extracts were acquired using 1024 scans, resulting in an experiment time of 3.2 h. ^{31}P edited ^{1}H spectra were acquired using between 3096 and 5192 scans, resulting in experiment times ranging from 9.8 to 16.3 h.

RESULTS

^{31}P edited spectra of the standards

The method described in this report concentrates on the measurement of signals from the ^{1}CH$_2$ protons instead of the more intense signals that arise from the methyl protons. Focusing on the ^{1}CH$_2$ protons has two main advantages. First, as seen in the regular ^{1}H spectrum shown in Fig. 3(a), the signals from the ^{1}CH$_2$ protons are dispersed over a range of 0.13 ppm instead of the 0.007 ppm range of the methyl protons. This suggests that the measurement of the ^{1}CH$_2$ protons is better suited for situations, such as *ex vivo* tissue analyses, where the spectral resolution is limited to the point that the individual methyl resonances cannot be resolved. The second advantage is that the ^{1}CH$_2$ protons for PC and GPC have observable (~6.1 and 6.3 Hz, respectively [22]) couplings to the ^{31}P nucleus, which allows for the use of ^{31}P editing. This fact is important as, without ^{31}P editing, the ^{1}H signals of the choline-compounds (especially those from the ^{1}CH$_2$ resonances but also the methyl resonances) are mingled with signals from other metabolites, making quantification more difficult and less reliable.

The main disadvantage of our method is that the integral of the ^{1}CH$_2$ protons is 4.5 times smaller than the integral of the methyl protons [note the separate intensity scale used for the methyl region in Fig. 3(a)]. Nevertheless, the quality of the ^{31}P editing allows the relatively weak ^{1}CH$_2$ peaks to be easily resolved and measured in a ^{31}P edited ^{1}H spectrum. With ^{31}P editing,
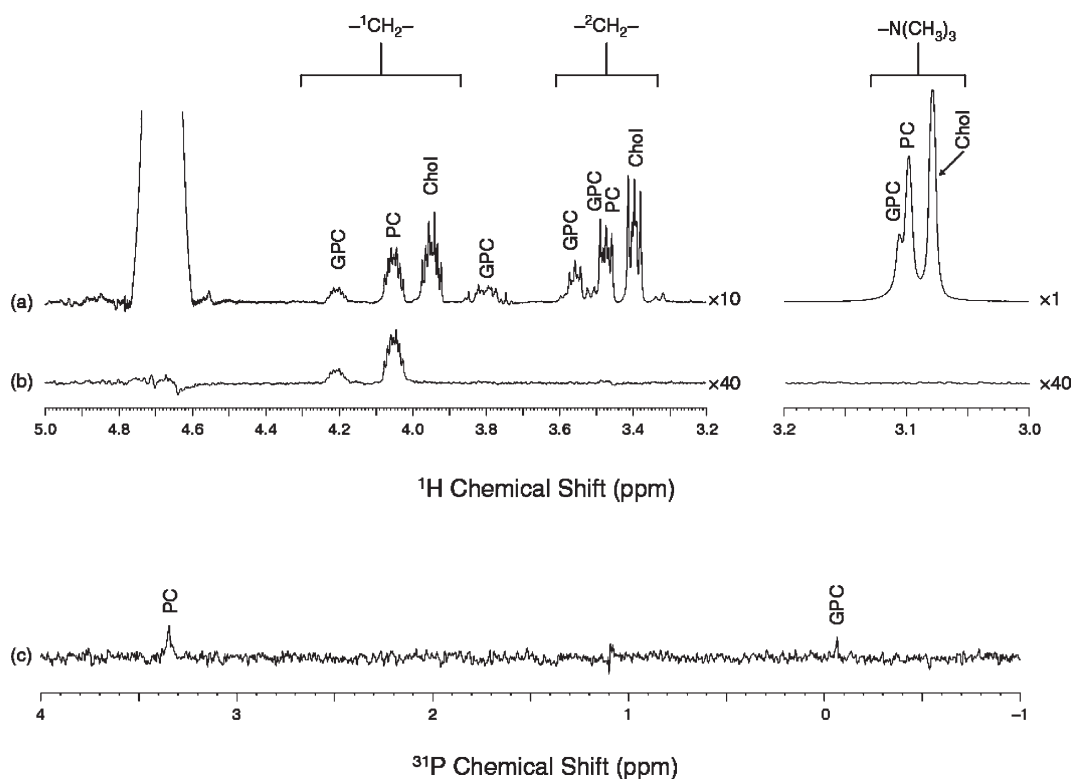
Figure 3. (a) ^{1}H, (b) ^{31}P filtered ^{1}H, and (c) ^{31}P spectra for a standard sample of 3.1 mM choline, 2.0 mM PC, and 1.0 mM GPC in 10% D_2O–90% H_2O. Each spectrum was acquired in 16 scans and with heteronuclear decoupling at 300 MHz for ^{1}H. The lack of resolution in the methyl region (3.12–3.06 ppm) is what makes it hard to use the methyl peaks to quantify the concentrations of choline, PC, and GPC in tissue samples. In spectrum (a), the additional GPC peaks at 3.78 ppm and overlapping the ^{2}CH$_2$ resonances at 3.5 ppm arise from the glycerol moiety. The relative scales for spectra (a) and (b) are indicated at the right of each part. All spectra were processed with 0.5 Hz of line broadening; baseline correction was used for spectrum (a) to compensate for the intense water signal at 4.7 ppm

the only peaks that remain in the ^{1}H spectrum are those from the ^{1}CH$_2$ protons of PC and GPC. The signal from the ^{1}CH$_2$ protons of choline, which would have appeared at 3.95 ppm, is completely removed, as are the intense methyl signals at ∼3.1 ppm from all three choline compounds. The small artifact at 4.7 ppm in the ^{31}P edited ^{1}H spectrum is all that remains of the water signal after suppression by presaturation and coherence transfer pathway selection. This artifact has an integral close to zero and is 0.5 ppm downfield from the signals of interest, so it does not affect the integration of the GPC and PC signals.

Signals from choline are removed in the ^{31}P editing step, so it is not possible to determine its concentration directly from the ^{31}P edited ^{1}H spectrum. However, the quantitative relationship between the ^{31}P edited and the regular ^{1}H spectra can be exploited to determine the choline concentration. This can be accomplished by determining the PC and GPC concentrations from the edited spectrum, and then using this information to subtract their contributions from the total integrated intensity of the methyl protons in the regular ^{1}H spectrum. The remaining intensity corresponds to the concentration of

choline. As a result, it is possible to determine the relative concentrations of all three species in cases where the individual methyl signals are not resolved.

Quantification of the amount of choline, PC, and GPC in a sample using ^{31}P edited ^{1}H spectra depends on the transfer efficiency of the INEPT steps. This transfer efficiency, in turn, depends on the ^{31}P–^{1}H coupling constants, pulse imperfections, and the transverse and longitudinal relaxation rates. The coupling constants are largely insensitive to sample conditions and the INEPT steps are reasonably tolerant of variations in pulse calibration, so the main difficulty with establishing the transfer efficiency stems from variations in the relaxation rates. For the range of concentrations used in our samples we found that the transfer efficiencies were independent of the relative concentrations of choline, PC, and GPC. However, relaxation rates (and therefore the transfer efficiency) depend on temperature so it is important to establish the transfer efficiency for whatever temperature is used for the experiment. For our experiments with brain tissue samples, which were kept at 10 °C, we observed signal intensities in the ^{31}P edited spectra that were 13.4 and 18.5% of the unedited signal intensities for
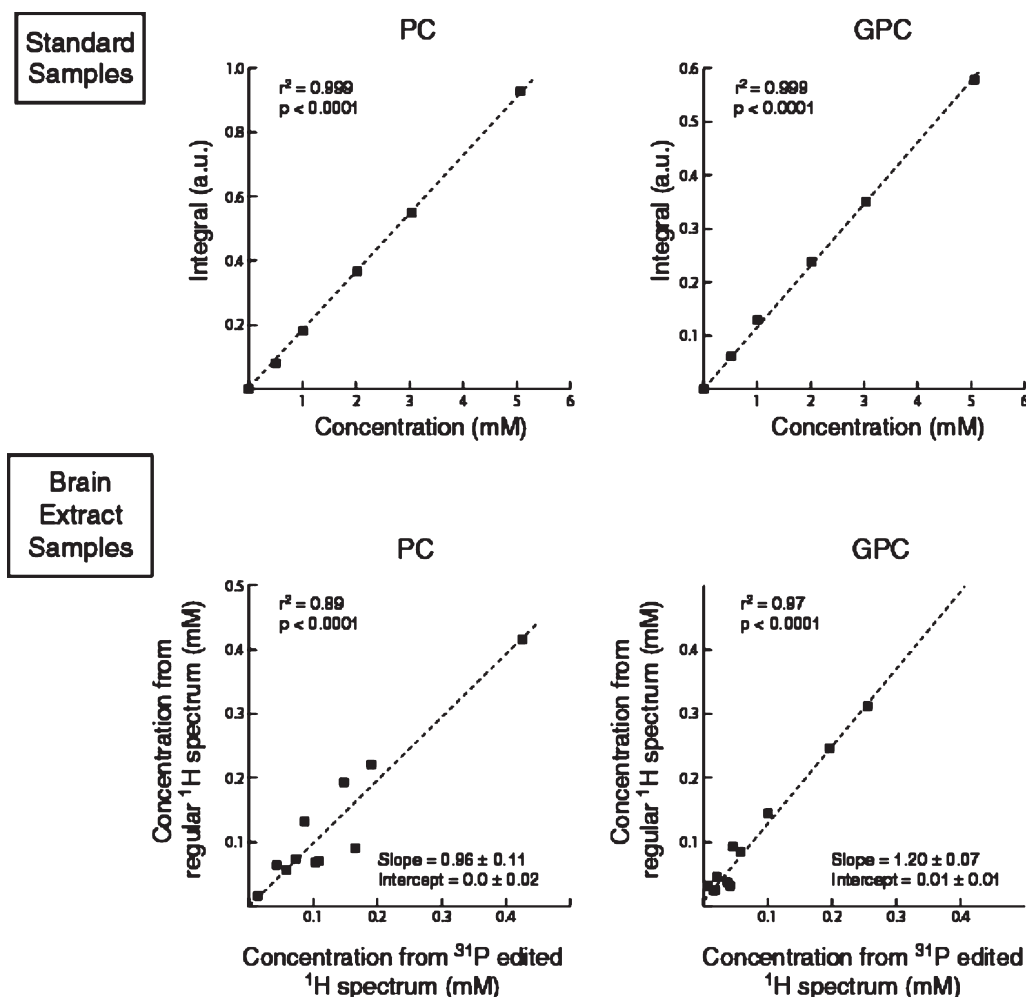
Figure 4. At the top are graphs demonstrating the linear response of the integrals from $^{1}CH_2$ peaks in the ^{31}P edited H spectra for the standard samples (0–5 mM PC, 0–5 mM GPC and 3.1 mM choline in 10% D_2O–90% H_2O) at 300 MHz. At the bottom are graphs showing how the concentrations of PC and GPC, determined by fitting the methyl peaks in regular ^{1}H spectra, compare with the concentrations determined using the integrals of the $^{1}CH_2$ peaks in the ^{31}P edited ^{1}H spectra. These results were determined from spectra acquired at 600 MHz for ^{1}H for the brain extract samples described in the text. The dotted lines indicate the results from linear regression analyses of the data; the result of each analysis is shown with the relevant graph

PC and GPC, respectively. These results are 54 and 74% of the theoretical maximum transfer efficiency of 25% (see Discussion section). At 25 °C, the transfer efficiencies (PC = 24.1% and GPC = 20.1%) were much closer to the theoretical value, as would be expected based on the connection between temperature and relaxation rates for small molecules in solution.

The top half of Fig. 4 demonstrates the linear relationship between the PC and GPC peak integrals in the ^{31}P edited ^{1}H spectra and the PC and GPC concentrations for a series of standard samples.

Analyses of human brain extracts

We tested the applicability of ^{31}P editing for the quantification of PC and GPC in biological systems using a series of 11 human glioma extract samples. Representa-

tive 600 MHz ^{1}H spectra for one of these samples are shown in Fig. 5. From the subspectrum shown in Fig. 5(b), it is clear that the $^{1}CH_2$ resonances are overlapped by peaks from other metabolites in the regular ^{1}H spectrum; this problem also affects the methyl resonances, although to a smaller extent. The complexity of the spectrum makes it difficult to quantify the relative amounts of the choline compounds using just the regular ^{1}H spectrum.

In the ^{31}P edited ^{1}H spectrum [Fig. 5(c)], the $^{1}CH_2$ resonances are clearly resolved and the relative amounts of PC and GPC can be easily quantified. The additional peaks at 4.095 and 3.96 ppm arise from other phosphorous containing brain metabolites such as, possibly, phosphoethanolamine (PE) and glycerophosphoethanolamine (GPE). [22] If these additional peaks prove to be due to PE and GPE, then the use of ^{31}P editing for quantification is even better justified. This is because the methyl signals of

Figure 5. The 600 MHz regular (a) and ^{31}P edited ^{1}H (c) spectra obtained for a human glioma extract sample. Spectrum (b) highlights two regions of the regular spectrum with the scale increased by a factor of 4. The scale of the ^{31}P edited ^{1}H sp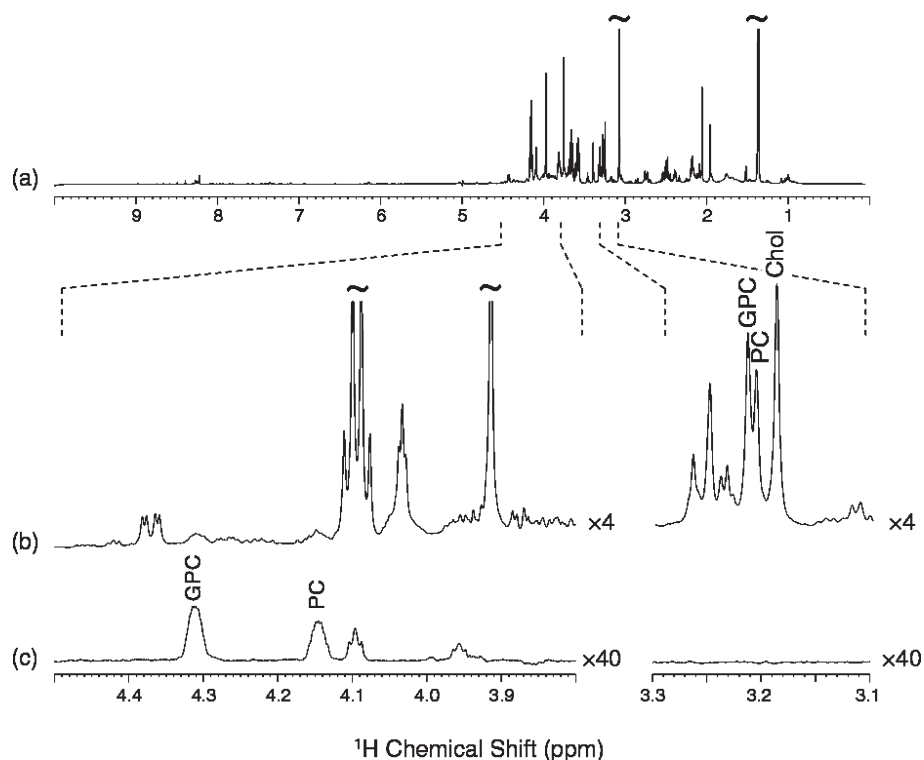ectrum shown as spectrum (c) is increased by a factor of 40 relative to spectrum (a). Peaks other than those from PC and GPC in the ^{31}P edited ^{1}H spectrum arise from other phosphorous-containing brain metabolites in the sample

PE and GPE interfere with the quantification of the PC, GPC, and choline methyl peaks in regular ^{1}H spectra.[22] In contrast, the PE and GPE peaks that appear in the ^{31}P edited ^{1}H spectrum are well-resolved and, consequently, do not affect the quantification of the ^{1}CH$_2$ resonances from PC and GPC.

The graphs shown in the bottom half of Fig. 4 demonstrate the correlation between the results of fitting the methyl peaks in the regular ^{1}H spectra (as has been done in the past) vs the results from the ^{31}P edited ^{1}H experiment. The variation seen in these graphs is not surprising owing to difficulties in quantifying the methyl peaks in the regular ^{1}H spectra. These difficulties are due to: (1) the lack of baseline resolution between the methyl peaks, and (2) the presence of other components that overlap the methyl peaks. These difficulties can be expected to be greatly exacerbated when using an instrument at lower field or in the analysis of *ex vivo* tissue samples.

DISCUSSION

^{31}P spectroscopy vs ^{31}P edited ^{1}H spectroscopy

As the ^{31}P resonances of PC and GPC differ from one another by $\sim$3.5 ppm, it could be argued that a better approach for the quantification of PC and GPC would be

to directly observe the ^{31}P signal.[2,36–39] In fact, with the development and availability of high field MR imagers, it has been demonstrated recently that PC and GPC can be observed in *in vivo* ^{31}P spectroscopy at 7 T from a voxel size of 27 ml.[40] However, it may be better to utilize the improved sensitivity of ^{1}H nuclei for detection due to the higher magnetogyric ratio of ^{1}H, especially if an inverse geometry probehead is in use (as is often the case for *ex vivo* studies). This is clearly demonstrated in Fig. 3. The signal-to-noise ratio for the peaks in the ^{31}P edited ^{1}H spectrum [Fig. 3(b)] is roughly 10 times greater than the signal-to-noise ratio of the resonances in the ^{31}P spectrum [Fig. 3(c)] when the line broadening is optimized. The signal-to-noise ratio was calculated as the ratio of the PC or GPC peak intensity to the root-mean-square noise of a signal-less spectral region. As quantitative work usually makes use of integrals instead of intensities, the comparison of these techniques based on their signal-to-noise ratios underestimates the advantages of the ^{31}P-filtered ^{1}H experiment because the peaks in the ^{31}P spectrum are approximately 10 times narrower than the ^{1}CH$_2$ peaks in the ^{31}P filtered ^{1}H spectrum. In addition, ^{31}P nuclei typically relax more slowly than ^{1}H nuclei, so ^{31}P edited ^{1}H spectra will have a further signal-to-noise advantage compared with ^{31}P spectra when comparing data acquired with the same amount of experiment time instead of the same number of scans.

Signal intensities in ^{31}P edited ^{1}H spectra

The use of a ^{31}P filter for editing in these experiments reduces the signal intensity due to the added restrictions to the coherence transfer pathway. In theory, the edited spectrum should have 50% of the intensity of the unedited spectrum if only phase cycling is used for selecting the coherence transfer pathway. However, we found that it was useful to supplement the phase cycling with pulsed field gradients to further attenuate artifacts in the spectrum. However, this comes at the price of an additional two-fold reduction in signal intensity, resulting in a total theoretical transfer efficiency of 25%.

INEPT transfer vs Hartman–Hahn mixing

We note that we also attempted to use heteronuclear Hartman–Hahn mixing[41] for the heteronuclear transfer steps. However, the measured transfer efficiency was around 3%, much lower than the efficiency of INEPT transfers. The inefficiency of heteronuclear Hartman–Hahn mixing compared with INEPT is attributable to the longer periods required to complete the heteronuclear magnetization transfer as well as to interference from homonuclear Hartman–Hahn mixing.

Realistic experiment times

The use of a non-quantitative extraction procedure for the preparation of the human glioma samples used in this study led to relatively low metabolite concentrations. Consequently, the ^{1}H spectra for the brain extracts were acquired using 1024 scans, resulting in an experiment time of 3.2 h, and the ^{31}P edited ^{1}H spectra were acquired using between 3096 and 5192 scans, resulting in quite lengthy experiment times of between 9.8 and 16.3 h. Owing to the low metabolite concentrations, as well as other factors, the measurement times used for these experiments are much longer than what will typically be needed. If samples were used with metabolite concentrations similar to those reported in the literature (which are about four times higher than the concentrations of the brain extract samples used for this study), then a spectrum equivalent to the results shown in Fig. 5 could be achieved while reducing the experiment time by a factor of 16. In addition, the signal-to-noise ratio (SNR) shown in Fig. 5 is greater than what is actually needed for quantification. If half the SNR were deemed acceptable for quantification, than the experiment time could be reduced by a factor of 4. Combined, these two changes would reduce the experiment time by a factor of 64, shortening a 9.8 h experiment to a much more reasonable 9.5 min experiment. In addition, experiment times can be further reduced by using shorter recycle delays as long as all samples are analyzed using the same conditions.

CONCLUSION

We have demonstrated a scheme that uses ^{31}P edited ^{1}H NMR spectroscopy to quantify the concentrations of phosphocholine and glycerophosphocholine in biological samples. In addition, the concentration of choline can be indirectly determined using this method. This method is particularly well-suited for analytical situations in which the ^{1}CH$_2$ resonances are obscured by other metabolites and/or the methyl resonances are not sufficiently resolved. We believe this method will be applicable for the analysis of choline compounds in *ex vivo* tissue samples. In addition, if problems of sensitivity are resolved, this method may have potential for the *in vivo* non-destructive quantification of choline, PC and GPC.

REFERENCES

1. Holmes HC, Snodgrass GJ, Iles RA. Changes in the choline content of human breast milk in the first 3 weeks after birth. *Eur. J. Pediatr.* 2000; **159**(3): 198–204.
2. Podo F. Tumour phospholipid metabolism. *NMR Biomed.* 1999; **12**(7): 413–439.
3. Chang L, Ernst T, Witt MD, Ames N, Walot I, Jovicich J, DeSilva M, Trivedi N, Speck O, Miller EN. Persistent brain abnormalities in antiretroviral-naive HIV patients 3 months after HAART. *Antivir. Ther.* 2003; **8**(1): 17–26.
4. Brenner T, Freier MC, Holshouser BA, Burley T, Ashwal S. Predicting neuropsychologic outcome after traumatic brain injury in children. *Pediatr. Neurol.* 2003; **28**(2): 104–114.
5. Delamillieure P, Constans JM, Fernandez J, Brazo P, Benali K, Courtheoux P, Thibaut F, Petit M, Dollfus S. Proton magnetic resonance spectroscopy (^{1}H MRS) in schizophrenia: investigation of the right and left hippocampus, thalamus, and prefrontal cortex. *Schizophr. Bull.* 2002; **28**(2): 329–339.
6. Firbank MJ, Harrison RM, O'Brien JT. A comprehensive review of proton magnetic resonance spectroscopy studies in dementia and Parkinson's disease. *Dement. Geriatr. Cogn. Disord.* 2002; **14**(2): 64–76.
7. Brockmann K, Dechent P, Meins M, Haupt M, Sperner J, Stephani U, Frahm J, Hanefeld F. Cerebral proton magnetic resonance spectroscopy in infantile Alexander disease. *J. Neurol.* 2003; **250**(3): 300–306.
8. Chaudhuri A, Condon BR, Gow JW, Brennan D, Hadley DM. Proton magnetic resonance spectroscopy of basal ganglia in chronic fatigue syndrome. *Neuroreport* 2003; **14**(2): 225–228.
9. Arnold DL, De Stefano N, Narayanan S, Matthews PM. Proton MR spectroscopy in multiple sclerosis. *Neuroimag. Clin. N. Am.* 2000; **10**(4): 789–798, ix–x.

10. Filippi CG, Ulug AM, Deck MD, Zimmerman RD, Heier LA. Developmental delay in children: assessment with proton MR spectroscopy. *AJNR Am. J. Neuroradiol.* 2002; **23**(5): 882–888.

11. Sijens PE, den Heijer T, Origgi D, Vermeer SE, Breteler MM, Hofman A, Oudkerk M. Brain changes with aging: MR spectroscopy at supraventricular plane shows differences between women and men. *Radiology* 2003; **226**(3): 889–896.

12. Galanaud D, Chinot O, Nicoli F, Confort-Gouny S, Le Fur Y, Barrie-Attarian M, Ranjeva JP, Fuentes S, Viout P, Figarella-Branger D, Cozzone PJ. Use of proton magnetic resonance spectroscopy of the brain to differentiate gliomatosis cerebri from low-grade glioma. *J. Neurosurg.* 2003; **98**(2): 269–276.

13. Rijpkema M, Schuuring J, Van Der Meulen Y, Van Der Graaf M, Bernsen H, Boerman R, Van Der Kogel A, Heerschap A. Characterization of oligodendrogliomas using short echo time ^{1}H MR spectroscopic imaging. *NMR Biomed.* 2003; **16**(1): 12–18.

14. Lindskog M, Kogner P, Ponthan F, Schweinhardt P, Sandstedt B, Heiden T, Helms G, Spenger C. Noninvasive estimation of tumour viability in a xenograft model of human neuroblastoma with proton magnetic resonance spectroscopy (^{1}H MRS). *Br. J. Cancer* 2003; **88**(3): 478–485.

15. Howe FA, Barton SJ, Cudlip SA, Stubbs M, Saunders DE, Murphy M, Wilkins P, Opstad KS, Doyle VL, McLean MA, Bell BA, Griffiths JR. Metabolic profiles of human brain tumors using quantitative *in vivo* [1]H magnetic resonance spectroscopy. *Magn. Reson. Med.* 2003; **49**(2): 223–232.

16. El-Sayed S, Bezabeh T, Odlum O, Patel R, Ahing S, MacDonald K, Somorjai RL, Smith IC. An *ex vivo* study exploring the diagnostic potential of ^{1}H magnetic resonance spectroscopy in squamous cell carcinoma of the head and neck region. *Head Neck* 2002; **24**(8): 766–772.

17. Katz-Brull R, Lavin PT, Lenkinski RE. Clinical utility of proton magnetic resonance spectroscopy in characterizing breast lesions. *J. Natl. Cancer Inst.* 2002; **94**(16): 1197–1203.

18. Nakagami K, Uchida T, Ohwada S, Koibuchi Y, Suda Y, Sekine T, Morishita Y. Increased choline kinase activity and elevated phosphocholine levels in human colon cancer. *Jpn. J. Cancer Res.* 1999; **90**(4): 419–424.

19. Sabatier J, Gilard V, Malet-Martino M, Ranjeva JP, Terral C, Breil S, Delisle MB, Manelfe C, Tremoulet M, Berry I. Characterization of choline compounds with *in vitro* [1]H magnetic resonance spectroscopy for the discrimination of primary brain tumors. *Invest. Radiol.* 1999; **34**(3): 230–235.

20. Morvan D, Demidem A, Papon J, De Latour M, Madelmont JC. Melanoma tumors acquire a new phospholipid metabolism phenotype under cystemustine as revealed by high-resolution magic angle spinning proton nuclear magnetic resonance spectroscopy of intact tumor samples. *Cancer Res.* 2002; **62**(6): 1890–1897.

21. Katz-Brull R, Margalit R, Degani H. Differential routing of choline in implanted breast cancer and normal organs. *Magn. Reson. Med.* 2001; **46**(1): 31–38.

22. Govindaraju V, Young K, Maudsley AA. Proton NMR chemical shifts and coupling constants for brain metabolites. *NMR Biomed.* 2000; **13**(3): 129–153.

23. Cheng LL, Ma MJ, Becerra L, Ptak T, Tracey I, Lackner A, Gonzalez RG. Quantitative neuropathology by high resolution magic angle spinning proton magnetic resonance spectroscopy. *Proc. Natl. Acad. Sci. USA* 1997; **94**(12): 6408–6413.

24. Sitter B, Sonnewald U, Spraul M, Fjosne HE, Gribbestad IS. High-resolution magic angle spinning MRS of breast cancer tissue. *NMR Biomed.* 2002; **15**(5): 327–337.

25. Ala-Korpela M, Posio P, Mattila S, Korhonen A, Williams SR. Absolute quantification of phospholipid metabolites in brain-tissue extracts by ^{1}H NMR spectroscopy. *J. Magn. Reson. B* 1996; **113**(2): 184–189.

26. Moreno A, Lopez LA, Fabra A, Arus C. ^{1}H MRS markers of tumour growth in intrasplenic tumours and liver metastasis induced by injection of HT-29 cells in nude mice spleen. *NMR Biomed.* 1998; **11**(3): 93–106.

27. Morvan D, Demidem A, Papon J, De Latour M, Madelmont JC. Melanoma tumors acquire a new phospholipid metabolism phenotype under cystemustine as revealed by high-resolution magic angle spinning proton nuclear magnetic resonance spectroscopy of intact tumor samples. *Cancer Res.* 2002; **62**(6): 1890–1897.

28. Morvan D, Demidem A, Papon J, Madelmont JC. Quantitative HRMAS proton total correlation spectroscopy applied to cultured melanoma cells treated by chloroethyl nitrosourea: demonstration of phospholipid metabolism alterations. *Magn. Reson. Med.* 2003; **49**(2): 241–248.

29. Morris GA, Freeman R. Enhancement of nuclear magnetic-resonance signals by polarization transfer. *J. Am. Chem. Soc.* 1979; **101**: 760–762.

30. Davis AL, Estcourt G, Keeler J, Laue ED, Titman JJ. Improvement of z filters and purging pulses by the use of zero-quantum dephasing in inhomogenous B_1 and B_0 fields. *J. Magn. Reson.* 1993; **A105**: 167–183.

31. Shaka AJ, Keeler J, Freeman R. Evaluation of a new broad-band decoupling sequence—Waltz-16. *J. Magn. Reson.* 1983; **53**: 313–340.

32. Le Belle JE, Harris NG, Williams SR, Bhakoo KK. A comparison of cell and tissue extraction techniques using high-resolution ^{1}H-NMR spectroscopy. *NMR Biomed.* 2002; **15**(1): 37–44.

33. Peeling J, Sutherland G. High-resolution ^{1}H NMR spectroscopy studies of extracts of human cerebral neoplasms. *Magn. Reson. Med.* 1992; **24**(1): 123–136.

34. Sutton L, Wehrli S, Gennarelli L, Wang Z, Zimmerman R, Bonner K, Rorke L. High-resolution [1]H-magnetic resonance spectroscopy of pediatric posterior fossa tumors *in vitro*. *J. Neurosurg.* 1994; **81**(3): 443–448.

35. Kinoshita Y, Yokota A. Absolute concentrations of metabolites in human brain tumors using *in vitro* proton magnetic resonance spectroscopy. *NMR Biomed.* 1997; **10**(1): 2–12.

36. Ronen SM, Leach MO. Imaging biochemistry: applications to breast cancer. *Breast. Cancer Res.* 2001; **3**(1): 36–40.

37. Leach MO, Verrill M, Glaholm J, Smith TA, Collins DJ, Payne GS, Sharp JC, Ronen SM, McCready VR, Powles TJ, Smith IE. Measurements of human breast cancer using magnetic resonance spectroscopy: a review of clinical measurements and a report of localized ^{31}P measurements of response to treatment. *NMR Biomed.* 1998; **11**(7): 314–340.

38. Bhujwalla ZM, Aboagye EO, Gillies RJ, Chacko VP, Mendola CE, Backer JM. Nm23-transfected MDA-MB-435 human breast carcinoma cells form tumors with altered phospholipid metabolism and pH: a ^{31}P nuclear magnetic resonance study *in vivo* and *in vitro*. *Magn. Reson. Med.* 1999; **41**(5): 897–903.

39. Lehtimaki KK, Valonen PK, Griffin JL, Vaisanen TH, Grohn OH, Kettunen MI, Vepsalainen J, Yla-Herttuala S, Nicholson J, Kauppinen RA. Metabolite changes in BT4C rat gliomas undergoing ganciclovir-thymidine kinase gene therapy-induced programmed cell death as studied by ^{1}H NMR spectroscopy *in vivo*, *ex vivo*, and *in vitro*. *J. Biol. Chem.* 2003; **278**(46): 45915–45923.

40. Lei H, Zhu XH, Zhang XL, Ugurbil K, Chen W. *In vivo* [31]P magnetic resonance spectroscopy of human brain at 7 T: an initial experience. *Magn. Reson. Med.* 2003; **49**(2): 199–205.

41. Ernst M, Griesinger C, Ernst RR. Optimized heteronuclear cross polarization in liquid. *Mol. Phys.* 1991; **74**: 219–252.

Evaluation of Tissue Metabolites with High Resolution Magic Angle Spinning

MR Spectroscopy

Human Prostate Samples After Three-Year Storage at -80ºC

Kate W. Jordan[1], Wenlei He[1], Elkan F. Halpern[2] Chin-Lee Wu[1], Leo L. Cheng[1,2,*]

Departments of [1]Pathology and [2]Radiology

Massachusetts General Hospital, Harvard Medical School

Boston, Massachusetts;

Running Title: Prostate tissue HRMAS ^{1}HNMR After 3-year -80ºC Storage.

[*]**Correspondence to:** Leo L. Cheng, Pathology Research, CNY-7, 149 13th Street, Charlestown, MA 02129; 617-724-6593 (Phone); 617-726-5684 (Fax); E-mail: cheng@nmr.mgh.harvard.edu.

Total Words: <u>2,998</u>.

Abstract

Accurate interpretation and correlation of tissue spectroscopy results with pathological conditions requires research efforts to establish disease specific tissue metabolite databases; these research specimens are often found in frozen storage for various lengths that can potentially cause alterations in the measured metabolites. In this study, human prostate tissues from specimens that had been stored at -80°C for 32 months were analyzed with high resolution magic angle spinning (HRMAS) MR spectroscopy, and compared with the initial measurements of the same specimens when snap frozen for less than 24 hours. Results of the study have led to the conclusion that the possible frozen storage induced metabolite alterations are as minimal as tissue MR spectroscopy can disseminate. Furthermore, such alterations, even if in existence, are much less critical in the interpretation of tissue HRMAS spectroscopy for pathological purposes than the contributions from the variations in pathology heterogeneities to the observed metabolite profiles.

Introduction

Since our introduction of the magic angle spinning methodology in studies of biological tissue samples(1), particularly after our demonstration of the compatibleness of tissue histopathology evaluations after their ex vivo spectroscopy measurements for human pathological samples(2), a question frequently posed to us has been the possible effect of sample storage duration on the measured metabolite concentrations.

This inquiry is scientifically logical and clinically relevant because of the increasing tests and evaluations of the spectroscopy methodology for its biomedical utilities, and the observed correlations between the measured tissue metabolite changes and their underlying pathological alterations. A large body of research has suggested the seeming utility of using tissue metabolic profiles thus obtained to indicate and predict the existence of certain pathological conditions(3-10). Therefore, the promising and practical utilities of this methodology in disease diagnosis, patient prognostication, and therapy monitoring have been increasingly recognized.

We realize that as interest in disease related HRMAS MR spectroscopy grows the HRMAS methodology is being tests at a research stage. As such, more often then not, human specimens of interest from surgeries and/or biopsies, or even from autopsies, cannot be analyzed immediately without frozen storage durations due to various technical, administrative, or logistical reasons. Very often research projects, particularly of retrospective studies, also use frozen human samples, such as those collected by various tumor banks, stored in either liquid nitrogen (-196ºC) or -80ºC freezers for months or even years. At present there is no data to either support or contradict the rationale for using these samples, as the existence or non-existence of frozen storage induced metabolic alternations has not been demonstrated.

Here, we report a study that we designed to investigate prostate tissue metabolite profile changes (or lack of changes) for samples kept at −80ºCduring a storage period of three years. In this study we used our advantage of possessing of a set of well-characterized human prostate tissue specimens from prostatectomies of cancer patients. In 2002, in order to evaluate tissue freeze-thawing processes in the presentations of the measured metabolite concentrations, we collected and analyzed 12 fresh human prostate specimens from five patients and reported those results in an article in 2003(11). After that study we stored excessive specimens at −80ºC from 2002 to 2005.

Methods.

Tissue Protocol. MR spectroscopy analysis of surgical specimens from human prostates was approved by the Institutional Review Board (IRB) at Massachusetts General Hospital. Twelve human prostate specimens were collected in 2002 in the operating room from five cases of prostatectomies representing different prostate zones (central, transitional and peripheral). Among these 12 specimens there were 11 specimens that left remaining tissue samples after our 2002 study(11). These samples have been stored at −80ºC from July 2002 to March 2005. A total of 15 samples cut from these 11 specimens were analyzed with spectroscopy, duplicates were measures from four samples with extra material.

HRMAS Proton NMR. The spectroscopy experimental protocol is exactly the same as used in the 2002 freeze-thawing study. Briefly, MR experiments were carried out on a Bruker (Billerica, MA) AVANCE spectrometer operating at 600 MHz (14.1T). A 4 mm zirconia rotor was used with Kel-F plastic inserts which created a spherical sample space of ~10 µl located at the center of the detection coil. A small (~0.1 mg) silicone rubber sample was permanently fixed inside one of the Kel-F spacers, positioned within the detection coil but not in contact with the sample,

which functioned as an external standard for both frequency reference (0.06 ppm from TMS) and quantification. Approximately 1.0 µl of D_2O was added into the rotor with the tissue sample for ^2H field locking. All spectroscopy measurements were carried out at 3ºC for better tissue preservation. The rotor-spinning rate was regulated by a MAS controller (Bruker), and verified by the measurement of inter-SSB distances from spectra, with an accuracy of ±1.0 Hz. A repetition time of five seconds and 32 transients were used to acquire each spectrum.

Spectra were collected with spinning rates of 600 and 700 Hz, with or without a rotor synchronized DANTE sequence of 1000 DANTE pulses of 1.5 µs (8.4º flip angle)(12). A rotor-synchronized CPMG filter (10 ms) was included in the pulse sequence after the execution of the DANTE frequency-selective pulses to reduce broad resonances associated with probe background, rotor, and/or macromolecules. Spectra measured at 600 Hz spinning without DANTE were used to quantify the total metabolite signal intensity including tissue water, its sidebands, and all the metabolites.

Spectroscopic data were processed with Nuts software (Acorn NMR Inc. Livermore, CA) according to the following procedures. All free induction decays were subjected to 1Hz apodization before Fourier transformation, baseline correction, and phase adjustment. Resonance intensities reported here represent integrals of curve-fittings with Lorentzian-Gaussian line-shapes. As previously reported, resonance intensities, depending on the particular spectral regions, were analyzed from one of the two spectra where there was no effect of water spinning sidebands (SSB) and DANTE suppression(12). The absolute concentration for a metabolite was estimated according to the metabolite intensity measured in DANTE spectra, the total MR spectral signal intensity from the single pulse measurement, and the intensities of the rubber standard measured under both conditions, as previously formulated.

Histopathology. After spectroscopy analyses all 15 samples were fixed in formalin for histopathology evaluations. Fixed tissue samples were embedded in paraffin, cut into 5 μm sections, and stained with Hematoxylin and Eosin. Sets of serial-section cuts at 100 μm apart were obtained from each sample. Volume percentages of histologically benign epithelia and stromal cells were quantified from these histopathological images(13), as within these research specimens from prostate cancer patients no cancerous gland was detected.

Results and Discussions.

Figure 1 compares two proton HRMAS spectra acquired from the same prostate specimen after tissue samples were frozen at −80ºC either for less than 24 hours in July 2002 (Fig. 1b), or over 32 months until March 2005 (Fig. 1a). Examining the two almost identical tissue metabolite profiles revealed by two spectra suggests that the possible metabolite degradations over a tissue – 80ºC storage period up to 32 months are as minimal as visual evaluations can dissimilate. However, this seeming preservation of prostate metabolite profiles over such a period of 32 months of tissue freezing was contradicted by observations of other test specimens. Another example is shown in **Figure 2**, where metabolite intensities, such as in the spermine and citrate regions particularly visible in the inserted spectra of vertical enlargement, from spectra obtained in 2005 (Fig 2a and 2b) were clearly different from those in the spectrum of the same specimen measured in 2002 (Fig. 2c). Of further note, the two spectra acquired from adjacent samples in 2005 (Fig. 2a and 2b) also revealed differences in metabolite intensities to a certain degree.

The advantage of HRMAS is that it permits tissue samples to be histopathologically evaluated after spectroscopy measurements. This advantage assisted us in the interpretation of the observed spectral differences. Histopathological examinations of serial sections created from these tissue samples after their spectroscopy analyses indicated that among all the tested samples

6

there was no cancerous gland detected. Hence, the major quantifiable histopathological differences among them were the variations in the volume percentage ratios between histopathologically benign prostate epithelial glands and stromal cells. Quantitative histopathology results showed that while the amounts of benign epithelia were (a) 46.09 and (b) 33.75 %(vol) in Figure 1 for the two samples measured for in 2005 and 2002, respectively, the volume percentages for samples acquired in Figure 2 were (a) 32.60 % and (b) 23.28 % in 2005 and were very different from (c) 3.49 % experienced in 2002. It is, therefore, likely that the observed spectroscopic differences were the reflection of the alterations in tissue pathological compositions, rather than of storage effects. Heterogeneity in pathological compositions between adjacent prostate tissues is known and is documented for the 15 pairs of samples reported in this study by **Table 1**. In this table we summarize all 15 tested samples and their counter measurements evaluated in 2002, together with the calculated pathological absolute differences represented by benign epithelial percentages (Diff. Epith. %), and the relative differences in terms of the absolute differences normalized by the sum of the values of the both years.

We test the hypothesis of pathological composition effects in **Table 2** by evaluating paired t-tests results of the 13 most intensive resonance peaks measured from the HRMAS spectra for all 15 sample pairs, 12 sample pairs of absolute epithelial volume percentage differences smaller than 20%, eight pairs with epithelial differences <10%, and seven pairs with relative percentage differences less than 20%. A paired t-test can be used to examine the existence of a statistically significant difference for a particular metabolite between the two tested groups, in this study groups measured in 2002 vs. in 2005. A resulting p value of greater than 0.05 (after a Bonferroni correction for multiple comparisons) indicates that there is no

statistically significant difference between the two groups of interest. Examining Table 2, we notice that while some metabolite, such as creatine (Cr, 303), displayed seemingly significant differences (after Bonferroni corrections) between the two groups when considering all 15 sample pairs and the 12 pairs of absolute epithelial differences of less than 20%. These significances do not persist when more rigorous controls on pathological compositions are applied by including only sample pairs of absolute differences <10%, or the relative differences < 20%.

Following the analytic pathologies used for the 2002 report(11), in **Table 3**, we examine concentrations of 21 prostate metabolites summarized in the 2002 report for seven sample pairs with relative differences of epithelial volume percentages less than 20% within each pair. Metabolite concentrations obtained in 2002 are compared with those measured in 2005 together with their respective p values (without Bonferroni corrections) of paired t-tests included. Data in this table further and more conclusively demonstrate that no HRMAS-visible statistically significant prostate metabolite differences can be contributed to sample storage at −80ºC for 32 months as tested in this study.

However, we wish to emphasize that the above conclusion regarding a lack of significant measurable metabolite changes over long term frozen storage can only be utilized within the current experimental conditions. For instance, since the tested prostate specimens contained no histologically visible cancer glands, theoretically, we cannot simply extend the experimental observations directly to cancer cells. However, based on observations here reported, we may suggest that quantification of prostate pathologies may be more critical for the correct interpretation of tissue spectroscopy results than any possible storage effects. Furthermore, although the concept that storage of tissue samples at −80ºC halts the processes of metabolite

pathways may be applicable to other types of tissues, the universal applicability is not self-evident and cannot be directly extend from the current results measured on prostate tissues. Separate studies on the types of tissues of interest are necessary to verify the concept.

Conclusion.

Analyzing and comparing human prostate tissue spectra from specimens that have been stored at −80ºC for 32 months after their initial spectroscopy measurements when snap frozen for less than 24 hours has led us to conclude that the possible frozen storage induced metabolite alterations are as minimal as tissue MR spectroscopy can distinguish. Such alterations, even if in existence, are much less critical to the interpretation of tissue HRMAS spectroscopy for pathological purposes than the influence of innate pathological heterogeneities.

References.

1. Cheng LL, Lean CL, Bogdanova A, Wright SC, Jr., Ackerman JL, Brady TJ, Garrido L. Enhanced resolution of proton NMR spectra of malignant lymph nodes using magic-angle spinning. Magn Reson Med 1996;36(5):653-658.

2. Cheng LL, Anthony DC, Comite AR, Black PM, Tzika AA, Gonzalez RG. Quantification of microheterogeneity in glioblastoma multiforme with ex vivo high-resolution magic-angle spinning (HRMAS) proton magnetic resonance spectroscopy. Neuro-oncol 2000;2(2):87-95.

3. Duarte IF, Stanley EG, Holmes E, Lindon JC, Gil AM, Tang H, Ferdinand R, McKee CG, Nicholson JK, Vilca-Melendez H, Heaton N, Murphy GM. Metabolic assessment of human liver transplants from biopsy samples at the donor and recipient stages using high-resolution magic angle spinning 1H NMR spectroscopy. Anal Chem 2005;77(17):5570-5578.

4. Sitter B, Lundgren S, Bathen TF, Halgunset J, Fjosne HE, Gribbestad IS. Comparison of HR MAS MR spectroscopic profiles of breast cancer tissue with clinical parameters. NMR Biomed 2005.

5. Keshari KR, Zektzer AS, Swanson MG, Majumdar S, Lotz JC, Kurhanewicz J. Characterization of intervertebral disc degeneration by high-resolution magic angle spinning (HR-MAS) spectroscopy. Magn Reson Med 2005;53(3):519-527.

6. Tugnoli V, Schenetti L, Mucci A, Nocetti L, Toraci C, Mavilla L, Basso G, Rovati R, Tavani F, Zunarelli E, Righi V, Tosi MR. A comparison between in vivo and ex vivo HR-MAS 1H MR spectra of a pediatric posterior fossa lesion. Int J Mol Med 2005;16(2):301-307.

7. Cheng LL, Burns MA, Taylor JL, He W, Halpern EF, McDougal WS, Wu CL. Metabolic characterization of human prostate cancer with tissue magnetic resonance spectroscopy. Cancer Res 2005;65(8):3030-3034.

8. Tugnoli V, Mucci A, Schenetti L, Calabrese C, Di Febo G, Rossi MC, Tosi MR. Molecular characterization of human gastric mucosa by HR-MAS magnetic resonance spectroscopy. Int J Mol Med 2004;14(6):1065-1071.

9. Sitter B, Bathen T, Hagen B, Arentz C, Skjeldestad FE, Gribbestad IS. Cervical cancer tissue characterized by high-resolution magic angle spinning MR spectroscopy. MAGMA 2004;16(4):174-181.

10. Swanson MG, Vigneron DB, Tabatabai ZL, Males RG, Schmitt L, Carroll PR, James JK, Hurd RE, Kurhanewicz J. Proton HR-MAS spectroscopy and quantitative pathologic analysis of MRI/3D-MRSI-targeted postsurgical prostate tissues. Magn Reson Med 2003;50(5):944-954.

11. Wu CL, Taylor JL, He W, Zepeda AG, Halpern EF, Bielecki A, Gonzalez RG, Cheng LL. Proton High Resolution Magic Angle Spinning NMR Analysis of Fresh and Previously Frozen Tissue of Human Prostate. Magn Reson Med 2003;50:1307-1311.

12. Taylor JL, Wu CL, Cory D, Gonzalez RG, Bielecki A, Cheng LL. High-resolution magic angle spinning proton NMR analysis of human prostate tissue with slow spinning rates. Magn Reson Med 2003;50(3):627-632.

13. Burns MA, He W, Wu CL, Cheng LL. Quantitative pathology in tissue MR spectroscopy based human prostate metabolomics. Technol Cancer Res Treat 2004;3(6):591-598.

Figure Legends

Figure 1. Visually undifferentiated human prostate tissue HRMAS proton spectra from two cuts of the same surgical specimen of a cancerous prostate measured (a) in 2005 after being stored at −80ºC for 32 months, and (b) in 2002 when the sample was thawed after being frozen overnight. Quantitative pathology detected no histopathologically identifiable cancerous glands in either sample; other than stromal cells, the majority of prostate pathology in both samples was histopathologically benign epithelia, which comprised 46.1 and 33.8 %, for (a) and (b), respectively. Figure 1 (b) was adopted from Fig. 1 (b) of Ref.(11).

Figure 2. Human prostate tissue HRMAS proton spectra from three cuts of the same surgical specimen of a cancerous prostate measured (a, b) in 2005 after stored at −80ºC for 32 months, and (c) in 2002 when the sample was thawed after being frozen overnight. Quantitative pathology detected no histopathologically identifiable cancerous glands in all samples; other than stromal cells, the majority of prostate pathology in both samples was histopathologically benign epithelia, which comprised (a) 32.6 %, (b) 23.3 % and (c) 3.5 %. Apparent spectroscopy differences are visible by comparing these spectra, particularly in the spermine and citrate regions, as demonstrated in the inserted vertically expanded spectra.

Table Legends.

Table 1. Quantitative pathology results of prostate samples pairs measured in 2002 and 2005. Since no histopahtologically identifiable cancer gland was detected in these samples, and the major pathological components were histologically benign epithelia and stromas, the quantitative results are presented as the percentage of benign epithelia as Epith. 2002 (% Vol) and Epith. 2005 (%Vol), respectively. Diff. Epith. %: the absolute values of the epithelial difference between each sample pair. The relative difference is presented as the ratio of the absolute difference over the sum of epithelial percentages for each pair; (a) two values indicate specimens were analyzed twice in 2005; (b) ***Bold*** identifies samples with Diff. Epith. % < 10%; (c) **Bold** identifies samples with values < 20% for both absolute and relative epithelial differences.

Table 2. The p values of paired t-tests for the 13 most intensive resonance peaks measured from the HRMAS spectra.

Table 3. The concentrations of 21 prostate metabolites for seven sample pairs with relative differences of epithelial volume percentages less than 20% within each pair. Metabolite concentrations (means and standard deviations) obtained in 2002 are compared with those measured in 2005 together with their respective p values (without Bonferroni corrections) of paired t-tests. These 21 metabolites included all the reported metabolites in Ref.(11).

Table 1.

Specimen No.	Epith. 2002 (% Vol)	Epith. 2005 (% Vol)	Diff. Epith. %	$\dfrac{\lvert\text{Epith. 2002 – Epith. 2005}\rvert}{(\text{Epith. 2002 + Epith. 2005})}$ %
1	4.01	46.98, 11.69 [a]	42.97, *7.68* [b]	84.27, 48.92
2	3.49	32.60, 23.28	29.11, **19.79** [c]	80.66, 73.93
3	3.84	14.88	**11.04**	58.97
4	26.64	24.61	*2.03*	**3.96**
5	38.31	40.00	*1.69*	**2.16**
6	0.00	16.11, 4.74	**16.11, *4.74***	100.00, 100.00
7	27.76	33.12	*5.36*	**8.80**
8	23.67	18.89, 18.30	*4.78, 5.37*	**11.23, 12.79**
9	8.69	8.49	*0.20*	**1.164**
10	33.75	46.09	**12.34**	**15.46**
11	10.00	41.19	31.19	60.93

Table 2.

	All Samples (n = 15)	Diff. Epith. < 20% (n = 12)	Diff. Epith. < 10% (n = 8)	|Epith. 2002 – Epith. 2005| / (Epith. 2002 + Epith. 2005) < 20% (n = 7)
Lac(4.10-4.14)	0.841	0.300	0.739	0.375
MI(4.05)	0.080	0.041	0.326	0.307
3.29	0.030	0.019	0.110	0.132
3.27	0.084	0.033	0.260	0.298
3.25-3.26	0.008	0.008	0.095	0.263
Pch(3.22)	0.016	0.014	0.219	0.376
Chol(3.20)	0.186	0.095	0.514	0.637
Spm(3.05-3.14)	0.516	0.492	0.825	0.517
Cr(3.03)	0.002	0.002	0.010	0.075
Cit(2.70-2.73)	0.020	0.097	0.018	0.170
Acet(1.92)	0.310	0.700	0.924	0.439
Ala(1.47-1.49)	0.083	0.019	0.124	0.183
Lac(1.32-1.34)	0.057	0.065	0.277	0.368
Minimum	0.002	0.002	0.010	0.075
Maximum	0.841	0.700	0.924	0.637
Mean	0.1716	0.1451	0.3415	0.3199
Std Deviation	0.2495	0.2188	0.3113	0.1573
Std Error	0.0692	0.0607	0.0863	0.0436

Table 3.

|	2005		2002		Paired
	Mean	**SD**	**Mean**	**SD**	**t-Test**
Lac(4.10-4.14) [a]	14.29	3.98	12.87	6.68	0.38
MI(4.05)	10.30	2.77	12.57	5.39	0.31
3.60-3.63 [b]	16.98	6.78	20.17	13.57	0.56
3.34	5.18	2.08	5.49	1.95	0.82
3.29	1.11	0.63	2.53	2.13	0.13
3.27	8.79	2.38	11.17	5.60	0.30
3.25-3.26	12.22	3.32	13.95	5.85	0.26
Pch(3.22)	1.05	0.28	1.44	1.05	0.38
Chol(3.20)	1.53	0.22	1.70	0.91	0.64
Spm(3.05-3.14)	1.75	2.69	2.21	1.72	0.52
Cr(3.03)	2.66	0.92	5.19	3.69	0.08
Cit(2.70-2.73)	4.87	1.86	3.44	1.66	0.19
2.31-2.37	5.60	2.13	10.17	3.32	0.06
2.01-2.14	29.67	14.92	42.51	6.99	0.13
Acet(1.92)	1.36	3.02	1.19	2.54	0.44
1.68-1.78	10.89	7.11	10.98	7.34	0.98
Ala(1.47-1.49)	1.00	0.42	1.52	1.13	0.18
Lac(1.32-1.34)	17.45	4.18	20.53	9.80	0.37
1.19-1.20	2.70	2.30	2.13	2.67	0.35
1.04-1.05	0.51	0.32	1.59	2.21	0.25
Lipid(0.90) [c]	22.87	5.11	14.65	6.55	0.03

Figure 1.
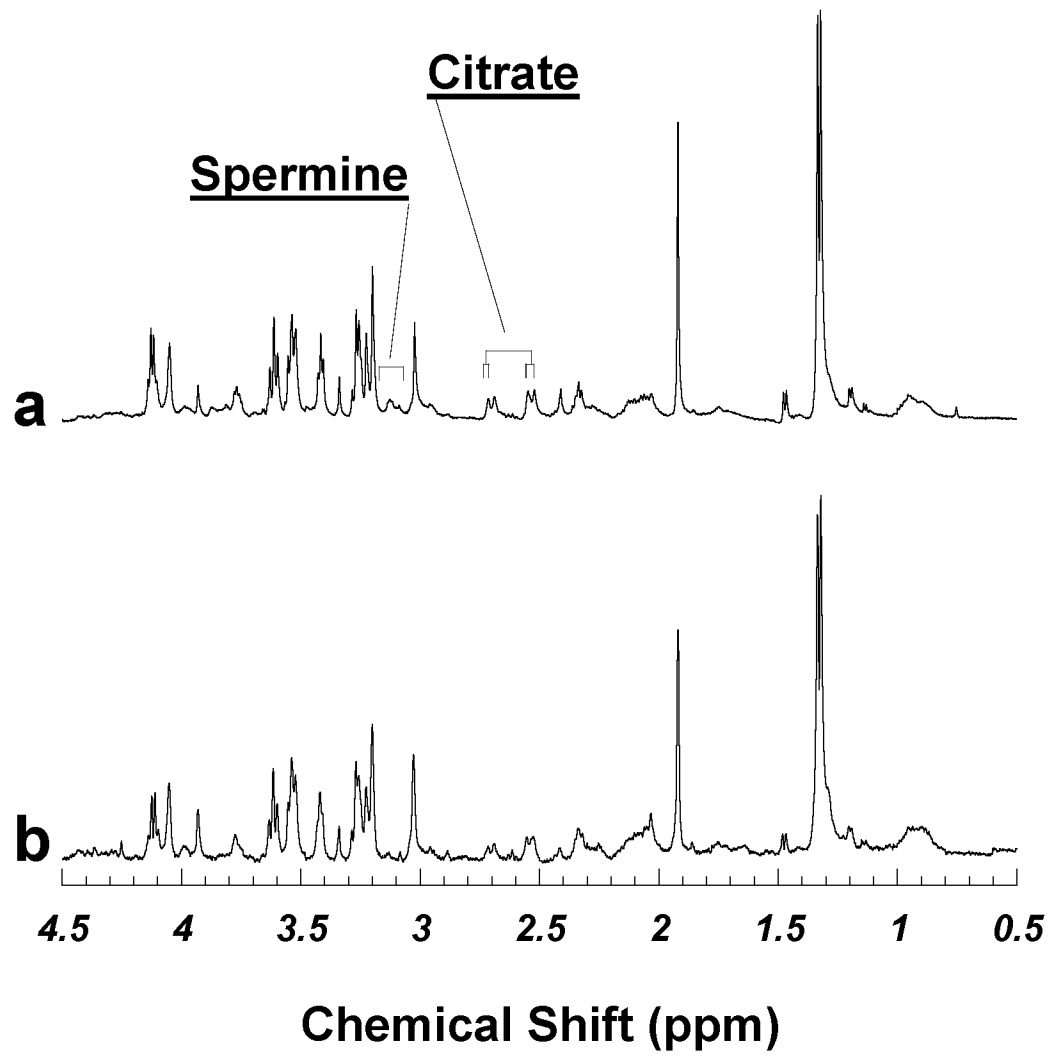
Figure 2.
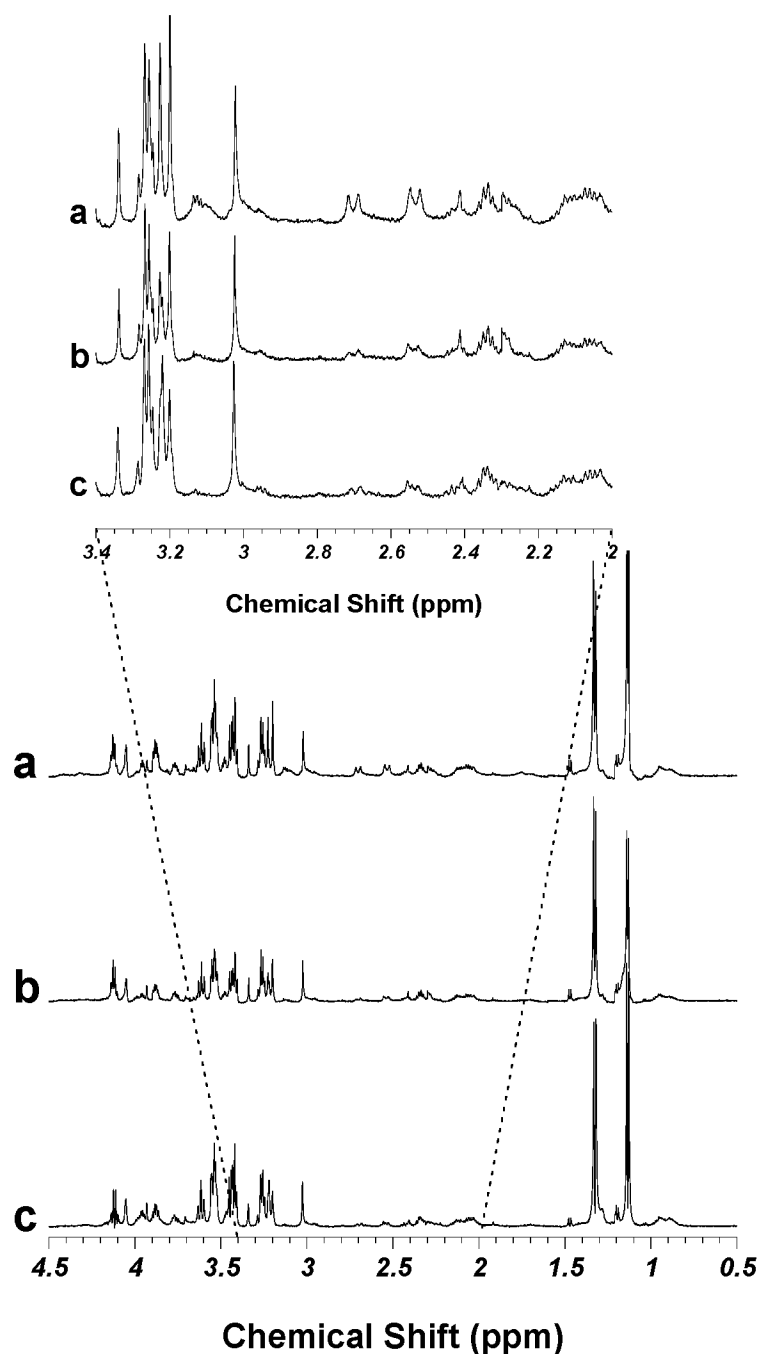
High Resolution Magic Angle Spinning (HRMAS) Proton MRS of Surgical Specimens

Leo L. Cheng[1,2], Melissa A. Burns[1] and Cynthia L. Lean[3,4]

[1]Departments of Pathology;
[2]Departments of Radiology Massachusetts General Hospital, Harvard Medical School Boston, Massachusetts 02114, USA;
[3]Institute for Magnetic Resonance Research, NSW 1590, Australia; and
[4]Department of Magnetic Resonance in Medicine, University of Sydney, NSW 2006, Australia

List of Abbreviations

BPH	Benign prostatic hyperplasis
DCIS	Ductal carcinoma *in situ*
FNAB	Fine needle aspiration biopsy
GBM	Glioblastoma multiforme
HCA	Hierarchical cluster analysis
^{1}H MRS	Proton magnetic resonance spectroscopy
HPLC	High pressure liquid chromatography
(HR)MAS	(High resolution) Magic angle spinning
NAA	N-acetyl aspartate
PA	Polyamines
PC	Phosphocholine
PCA	Principal component analysis
PTC	Phosphatidylcholine
SCS	Statistical classification strategy
SSB	Spinning side bands

Introduction

Over the last two decades, a large body of *ex vivo* work and some *in vivo* work has demonstrated the utility of proton magnetic resonance spectroscopy (^{1}H MRS) in detecting and monitoring cellular chemical alterations associated with the development and progression of human malignant diseases [1–3]. Reports of conventional *ex vivo* ^{1}H MRS studies of human tissues, i.e. analysis of intact tissues with liquid-state MRS probes, have demonstrated that diagnosis, and for some organs, prognosis of malignant disease using metabolite ratios measured from spectra may reach 95% for both sensitivity and specificity. The accuracy can further be improved using an objective pattern recognition technique, statistical classification strategy (SCS) [2]. While tissue conventional MRS is fast and has shown the ability to diagnose accurately various human malignancies, it is limited by poor spectral resolution caused by the magnetic susceptibility effects of heterogeneous structures of the sample, and therefore detailed identification of individual metabolites is difficult. Metabolite profiling involving the measurement and quantification of tissue metabolites [4], is of increasing interest in the era of genomics and proteomics due to the direct involvement of tissue metabolites in tumor development and progression. High-resolution magic angle spinning (HRMAS) was developed to improve the spectral resolution of MR spectra of intact tissue by the reduction of susceptibility induced broadening such that individual metabolites may be identified and correlated with disease states.

Characterization of Human Malignancies

A malignant lesion exhibits unregulated growth characteristics both at primary and secondary (metastatic) sites. Initial attempts to characterize and understand tumor development and progression hinged therefore on lesion morphology and, as such, on histopathology using the light microscope, which has been the medical diagnostic "gold standard" for much of the 20th century. With the discovery of DNA and the advent of molecular genetics it became evident that tumor morphology represented only a single variable in the characterization of malignancies and could not report on risk factors or on the biological potential of a lesion. Predicting tumor behavior is essential for determining optimal disease management protocols and it is proteomics and spectroscopic metabolite profiling that have the potential to provide the information necessary for this endeavor. Metabolite profiling data, thus far, has been generated predominantly by studies involving MR spectroscopy and mass-spectrometry.

Specific Limitations of Histopathology

The principal limitation of histopathology is the restricted range of morphological changes that tissues can express. Pathologists attempt to extract a sophisticated pattern specific for an individual disease process from a continuum of morphological changes. These patterns overlap

are susceptible to subjective assessment and may be altered by sampling error. Patient assessment involves histological grading and clinicopathological staging. Tumor grading attempts to establish the aggressiveness of the tumor based on the degree of differentiation, or anaplasia, of tumor cells. However, such a distinction is subjective and often inconclusive. Staging of cancer determines the extent and spread of the disease, but it is unable to distinguish between recent but aggressive primary tumors and older but more slowly growing ones since clinical presentation of patients does not usually reveal how long a neoplasm has been present. Adequate staging of disease is often problematic. For instance, histopathological assessment of lymph nodes is subject to observer and sampling errors due to the large volumes of tissue to be assessed and the time and resource constraints that prevent thorough and complete examination. A retrospective study revealed that: "Serial sectioning of lymph nodes judged to be disease-free after routine examination revealed micrometastases in an additional 83 (9%) of 921 breast cancer subjects" [5].

Current histopathology has shown both conceptual and procedural inadequacies in providing optimal medical diagnosis. The development of new modalities capable of improving the accuracy of disease diagnosis is needed.

Cancer Pathology Determined by Conventional ^{1}H MRS

Conventional MRS measures cellular chemicals that are mobile on the MR time scale and their variations with changes in physiological or pathological function [6]. Although restricted by achievable spectral resolutions due to susceptibility induced broadening of resonances, many promising results have been obtained from conventional proton MRS studies of human malignant tissue and fine needle aspiration biopsies. The potential for diagnoses of malignant diseases in many organs has been demonstrated and more importantly, metabolic changes have been reported that were not morphologically manifest [7,8]. A study of aspiration biopsies from primary breast tumors not only determined diagnosis, but also reported on nodal involvement and tumor vascularization [9]. The sensitivity of MRS was demonstrated in a study using a rat model for lymph node metastasis where malignant cells in lymph nodes were detected with a greater sensitivity than histology. Micrometastases were detected that were not apparent even when the entire node was serially sectioned for examination by histology. The MR diagnoses were confirmed to be correct by xenografting nodal tissue into nude mice [10].

Historically, the limitation in spectral resolution of conventional proton MRS of tissue samples was realized as an obstacle to the identification of detailed cellular

metabolism. A number of procedures, including sample packing and chemical extraction of tissue were investigated as ways to improve spectral resolution [11]. While solutions of tissue extracts did produce high-resolution spectra, the process was destructive and was found to alter the spectroscopic results to an unknown degree, depending on the procedure used and the thoroughness of extraction. Therefore, neither broad-line tissue analyses nor high-resolution measurements of extracts have been able to successfully evaluate malignant disease or exemplify the advantages of proton MRS in metabolite identification.

Methodology

Limited spectral resolution is a common problem in solid-state MRS for which many techniques have been proposed and tested. Among these magic angle spinning (MAS), a line-narrowing technique, was invented after the realization of the angle-dependent characteristics of the so-called "solid effects" that broaden the resonance lines [12,13]. These "effects" classically include dipolar coupling and chemical shift anisotropy, which always exist in solids. It was later shown that MAS could also reduce resonance line-broadenings caused by bulk magnetic susceptibility [14]. Specifically, in solids, spectral broadening due to these effects follows $(3\cos^2\theta - 1)$, where θ is the angle between the static magnetic field and the internuclear vector. Therefore, if a sample is spun mechanically at the "magic angle $(54°44'$, i.e. $3\cos^2(54°44') - 1 = 0)$," and at a rate faster than the broadening originating from these effects, the contribution of these effects to the spectral broadening can be reduced [15].

The HRMAS Method

The term HRMAS is currently used to refer to proton MRS of non-solution samples, such as biological tissues and cells, obtained with the application of MAS. It is important to note, however, that there are conceptual differences between classical MAS, and tissue HRMAS used with proton spectroscopy [16]. The targets of MAS in classical proton solid-state studies are chemical shift anisotropies and dipolar couplings that are in ordinary solids >50 kHz. The application of MAS in solid-state studies has involved the use of high spinning rates and strong radio-frequency pulses in an attempt to decouple these homonuclear interactions. This is not the case, however, for the MAS study of cellular metabolites in biological tissues. Here, water-soluble molecules reside in the cytoplasm wherein their motion is restricted by magnetic susceptibilities caused by various interfaces with other cell structures and by inherent viscosity. Although classical "solid-effects" exist, for instance within cell membranes, they would

contribute only to an almost invisible spectral background that is too broad (∼50 kHz) to be measurable in a typical HRMAS spectrum of metabolites (∼5 kHz, or 10 ppm on a 500 MHz spectrometer). Overall, the magnitude of line-broadenings due to magnetic susceptibility is approximately 10^3 less than that caused by "solid-effects," and can be greatly reduced by MAS.

Experimental

Sample Preparation

Fresh and previously frozen samples may be measured directly with HRMAS MRS [17–21]. For the purpose of preserving the metabolite concentrations within tissues, samples should not be collected or stored in any liquid medium. In cases where the size of frozen tissue exceeds the sample size required for HRMAS MRS analysis, samples must be cut on a frozen surface to avoid multiple freezing and thawing. Such a surface can be made with a thin metal plate, covered with gauze and placed on top of dry ice.

Tissue samples may be washed briefly with D_2O prior to spectroscopy if they contain visible amounts of blood. However, exposure to D_2O should be brief to minimize the possible loss of cellular metabolites [22]. We have observed complete depletion of metabolites for human prostate samples (∼10 mg blocks) submerged in ∼2 ml D_2O for approximately 10 min.

As always, when working with human materials of potential biohazard, universal precautions need to be practiced at all times. In particular, tissue samples will undergo spinning and even at "slow spinning speeds" of less than 1 kHz, tissue fluid can leak from the rotor cap if the cap is not in tight-fit with the rotor (Figure 1). Thus the compatibility and seal between rotor and cap should be tested

Fig. 1. Photograph of the rotor and a typical biopsy tissue sample that will be placed in the rotor using the tweezers for HRMAS MRS analysis.

using a D_2O solution prior to tissue analysis. The test can be done by comparing the weights of the rotor with solution before and after HRMAS using the same experimental conditions (temperature and spinning speed) used for tissue analysis.

To maximize spectral resolution, tissue samples should be limited to the physical boundaries of the receiving coils; for example by using Kel-F inserts to create a spherical sample when measuring samples on a Bruker spectrometer (Bruker BioSpin Corp., Billerica, MA). The use of a spherical sample is recommended for it minimizes shimming efforts as well as reduces the effect of the magnetic field inhomogeneity on the broadening of spectral lines.

Spectrometer Settings

Before tissue measurements, the HRMAS probe should be adjusted for its magic angle with potassium bromine (KBr) following the manufacturer's protocol for solid-state MRS. Ideally, measurements should be made at a low temperature (e.g. 4 °C) to reduce tissue degradation during acquisition.

The optimal spinning rate should be decided after consideration of several factors, including tissue type, metabolites of interest, and the plan for the tissue after HRMAS MRS analysis. Generally, the higher the spinning rate, up to 10 KHz as reported in the literature, the better the spectral resolution [23]. However, since high spinning rates can function as a centrifuge that can potentially disrupt tissue structures, if subsequent histopathological evaluation of the tissue is critical to the study, spinning rates must be reduced to limit any structural damage of the tissue that may interfere with histopathology. It is important to note that different tissue types endure different levels of stress. For instance, for the same spinning rate, skin tissue may be perfectly preserved in structure, while brain tissue can be completely destroyed. On the other hand, if less mobile metabolites such as lipids are the focus of HRMAS MRS evaluation, faster spinning rates may be necessary. The preservation of tissue architectures during HRMAS MRS is often critical and, as such, a number of studies have explored HRMAS MRS tissue analysis using moderate to slow spinning conditions [24–27]. These studies aimed to suppress spinning side bands (SSB) that overlapped with metabolite spectral regions of interest, using spinning rates that were not fast enough to "push" the 1st SSB beyond these regions. Interested readers should test these reported techniques for applicability to their specific tissue systems.

Optimal probe shimming is another critical factor that directly affects achievable spectral resolution. We have found that shimming on the lock or tissue water signal was not as sensitive as shimming on the splitting of the lactate doublet at 1.33 ppm, which fortunately presents in most excised biological tissues. However, in order to shim

interactively on the degree of splitting, it is necessary to work with the frequency domain. This should not present a challenge to most current spectrometers. Furthermore, it should be possible to establish autoshimming protocols based on this criterion.

It is now accepted that malignancy related cellular marker metabolites may not present simply as present or absent, but rather as continuous changes in intensity throughout disease development and progression. Quantification of these metabolites can be extremely important if they are to accurately diagnose and characterize stages of disease. Metabolite concentrations may be estimated from HRMAS MR spectra by using either the intensity of tissue water signals or an external standard (e.g. a small piece of silicone rubber) permanently attached to the inside of the rotor or attached to the rotor inserts. Such an external standard can be calibrated with known compounds of known concentrations. Interested readers can make such compounds by dissolving known amounts of relevant metabolites in agarose gel.

HRMAS MR spectra may be acquired with or without water suppression, depending on whether water intensities are required for the estimation of metabolite concentrations. A rotor-synchronized CPMG sequence may be applied to achieve a flat spectral baseline if there are undesired broad resonances from the probe background.

Histopathology

The clinical utility of high-resolution tissue metabolite profiles obtained with HRMAS MRS needs to be investigated and validated by means of accurate and detailed correlation with serial-section tissue pathologies. Such correlations are particularly important for studies of human malignancies due to the heterogeneity that may be inherent in the disease. Tissue pathology can vary greatly from region to region within a single tumor, and intertumor differences may be even more pronounced. An obvious advantage of HRMAS MRS is its preservation of tissue for subsequent histopathological analyses, allowing the establishment of correlations between metabolite profiles and quantitative pathologies [28–30].

Routine clinical histopathology data is most often inadequate. Routine histopathology, in particular 5 micron slices of the tissue biopsy, provides information about the presence or absence of certain features. These features may vary from slice to slice and therefore information from a small percentage of the tissue may not correlate with the spectral profile, which consists of the weighted sum of the profiles from all tissue slices or indeed the entire piece of tissue. Hence, for certain types of tissues, particularly neoplasm samples with known heterogeneities, histopathology needs to be evaluated quantitatively. This can be achieved laboriously by the histopathologist's

examining serially sectioned tissue slices or possibly with the assistance of computer image analysis of these same sections. The sectioning frequency differs with tissue type and should be determined in consultation with the pathologist. For instance, the optimal sectioning frequency for human prostate was found to be between $200 \sim 400$ μm.

Data Analysis

Histopathological analysis in cancer diagnosis relies on the observation of variations in colors and shapes using a light microscope. Importantly, to suspect disease the pathologist must observe widespread rather than isolated changes in color and/or shape, a process requiring keen pattern recognition. Similarly, pattern recognition methods are most often required to allow the diagnosis of malignancy from MRS tissue metabolite profiles. Development and progression of malignant disease involves the simultaneous evolution of many metabolic processes. Therefore, although some individual metabolites have been reported to correlate with disease types and stages [1,2] it is more likely that the overall metabolite profile rather than changes in single metabolites will be sensitive and specific for disease diagnosis [31,32]. Sophisticated statistical classification strategies (SCS) have been developed and applied to the analysis of conventional MRS of malignant tissues [33]. To date, however, principal component analysis (PCA) using readily available statistical programs has been sufficient for revealing accurate diagnostic information from HRMAS MRS data [34,35]. However, the application of SCS may further improve these accuracies.

HRMAS MRS of Human Surgical Specimens

Over recent years, HRMAS MRS has been applied biomedically to the analysis of human surgical samples, research animal tissues and cultured cells. The scope of the methodology presented in this section will be limited to HRMAS MRS studies of human tissues and will be presented where possible in context with preceding studies of the same tissues using conventional MRS. Although presented in this context comparison of the sensitivities and specificities obtained using conventional and HRMAS MRS are not at this stage warranted as unlike the mature discipline of conventional MRS, HRMAS MRS is still in its infancy and has reported only studies with restricted patient numbers. Although the capability of HRMAS has been clearly demonstrated in generating high-resolution spectra from which individual metabolites can be measured and such measurements were impossible with conventional methods, studies of large patient populations, as with conventional MRS studies, that allow evaluation of the sensitivity and specificity of the method have not

yet appeared in literature. Similarly, it is not as yet possible to provide the reader with one concise and optimal method for undertaking HRMAS MRS. Detailed methods are provided for each of the studies presented and these methods discussed in terms of the study aims. In an emerging discipline such as HRMAS MRS care must be taken to rigorously address methodological variables with respect to the type of tissue being analyzed and the specific information required. Increased spectral quality will most often be obtained with higher spinning speeds but this will be at the expense of tissue preservation allowing subsequent histopathological assessment of the tissue. Some tissues are less easily destroyed than others by high spinning speeds and thus preliminary experiments need to be undertaken to determine optimal parameters.

MRS analyses on tissue extracts have been studied for many years on many diseases, and have formed a large body of literature. Results from these studies are worthy of close examination and review but will not, however, be included in this review due to the following: the pathology of the tissue samples most often remains incomplete and/or the degree of extraction cannot be certain.

Brain

Human brain was the first study reported using proton HRMAS MRS to determine tissue pathology. Due to the relative motion stability and homogeneity compared to other organs, brain has dominated the development of *in vivo* MRS, and accordingly has inspired many *ex vivo* studies, primarily including neurodegenerative diseases and tumors, aimed at understanding metabolism and defining brain tissue chemistry.

The first HRMAS MRS human studies on brain tissues from autopsies described semi-quantitative evaluation of the pathology of a neurodegenerative disease, specifically Pick disease [36]. Through MRS measurements and traditional neurohistopathology, direct and semi-quantitative correlations were found to exist between the levels of N-acetyl aspartate (NAA) and the amount of surviving neurons in varying regions of examined brain as seen in Figure 2. The study also, for the first time, demonstrated that the spectral resolution of HRMAS proton MRS was comparable with that measurable with conventional proton MRS of tissue
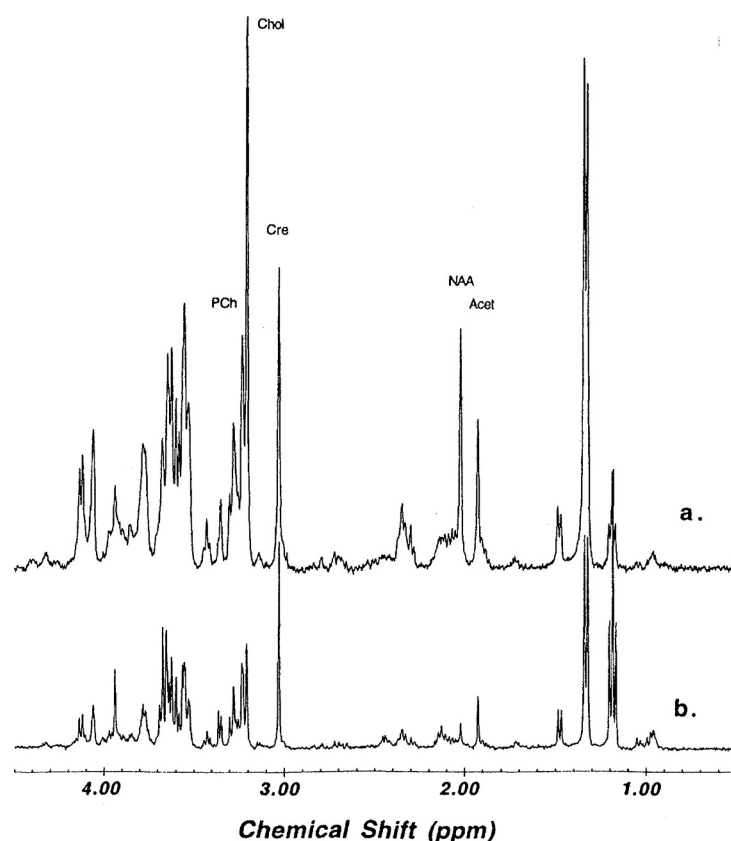
Fig. 2. Comparison of HRMAS MR spectra of brain tissue from the relatively unaffected primary visual cortex region (a) and the severely Pick disease affected rostral inferior temporal gyrus region (b), showing a marked decrease in NAA concentration, 8.48 μmol/g for spectrum a and 4.96 μmol/g for spectrum b. This decrease in NAA was found to correlate with an average neuronal count decrease of 33 neurons per 0.454 mm^2. The spectra were acquired at 2 °C, and were scaled according to concentration of creatine at 3.03 ppm for enhanced visualization. *Figure 4 from ref. [36]*

Fig. 3. Comparison of human brain proton MRS acquired with (a) HRMAS on intact tissue and (b) conventional method on extract solution. The spectral resolution was comparable while relative intensities for certain metabolites varied.
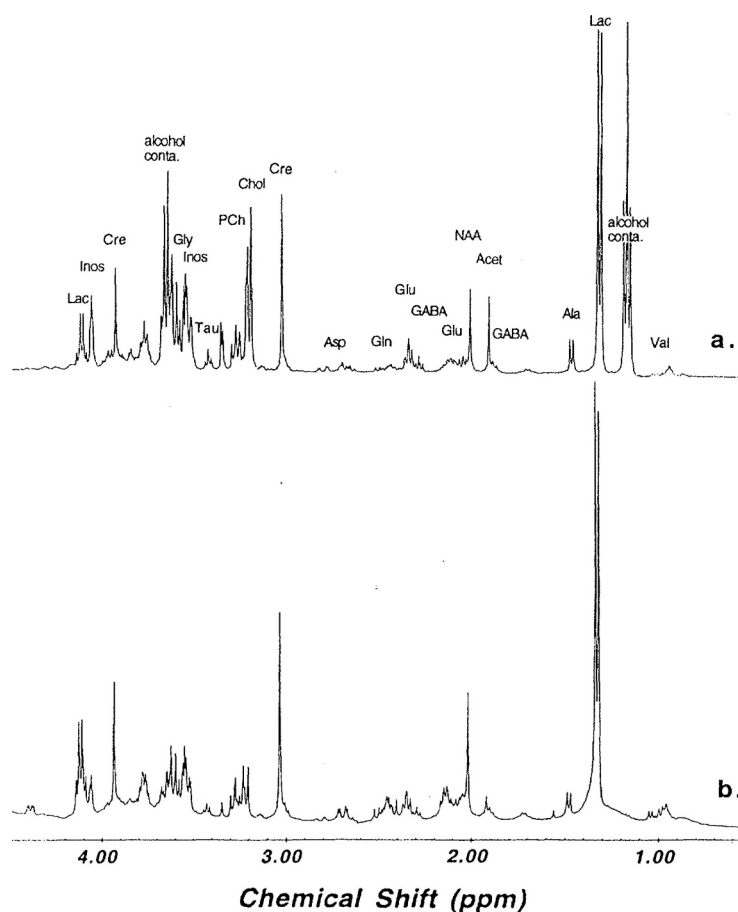
extracts (Figure 3), and superior to that obtained using conventional MRS of intact tissue (Figure 4). Another early study also on autopsy brain tissues correlated MRS data and stereological pathology for Alzheimer's disease and confirmed NAA concentration to be proportional to neuronal density (Figure 5). In this study, 7 human brains were examined, 3 of which were Alzheimer diseased and 4 which presented as normal human control brains. Figure 5 demonstrates the quantitative nature of the NAA and neuronal count relationship, as the correlation intercepted at zero (−0.29 ± 1.15 μmol/g) [37].

The MRS study of brain tumor intact tissues using conventional MRS suggested the diagnostic importance of lipid and lipid metabolites. Kuesel and colleagues reported correlations between MR lipid signal intensities and the amount of necrosis in astrocytomas [38]. With 42 cases, they showed that the intensity of the mobile

fatty acyl –CH=CH- resonance at 5.3 ppm, differentiated 0, 1–5 and 10–40% of necrosis with statistical significance [39]. These results represented a great potential use for *ex vivo* MRS for astrocytoma diagnosis, in particular for differentiating Grade III and Grade IV tumors, which have radically different prognoses. The technique also ensured that necrotic foci often missed by clinical pathology were identified. Working with conventional MR spectra of brain tumor tissues, Rutter *et al.* attempted to categorize tumors according to 1D peak ratios (3.1–3.4 vs. 1.1–1.5 ppm), T_2 values of peaks at 1.3 ppm and cross-peaks on 2D COSY spectra (0.9 ppm with 1.35 ppm, representing methyl-methylene couplings; and 1.3 ppm with 2.05 ppm for couplings between methylene groups in fatty acids) [40]. With 38 samples studied from 33 subjects (including normal tissue, astrocytoma, GBM, meningiomas, and metastases), they were able to use peak ratios to
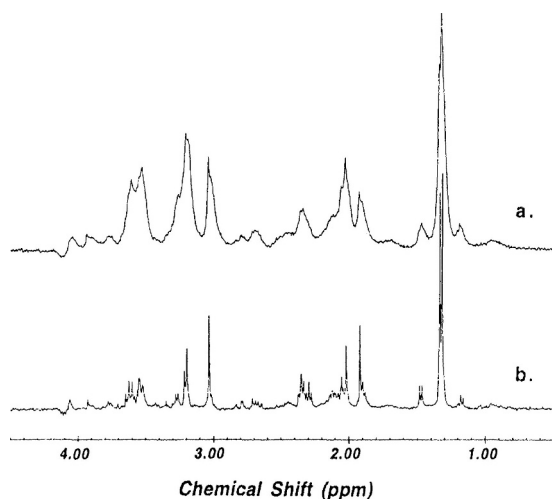
Fig. 4. Comparison of human brain proton MRS acquired with (a) conventional MRS and (b) HRMAS MRS. *Figure 2 from ref. [36].*

differentiate GBM from astrocytomas and normal tissues. They also found that the T_2 of the 1.3 ppm peak could be fitted by a double exponential function and that the long fraction of T_2 values could be used to group both GBM and metastasis from normal tissue. However, tissue spectra measured with conventional method of low resolution

Fig. 5. A statistically significant linear correlation was found to exist between the number of neurons and the concentration of NAA_{total}, measured from 3 Alzheimer diseased and 4 normal control brains (the dotted line, $r = 0.828$, $P = 0.021$). The solid line represents the linear correlation obtained when only normal control brains were included ($r = 0.989$, $P = 0.011$). *Figure 3 from ref. [37].*

prevented these studies from observation of individual brain metabolites other than identification of broad lipid peaks.

HRMAS MRS of brain tumors allowed for the first-time detailed profiles of water-soluble metabolites and lipids to be obtained from the same spectra [31]. In a study of 19 brain tumors, including astrocytomas, GBM, meningiomas, Schwannomas, and normal brain, metabolite concentrations both in absolute units and relative ratios normalized to the creatine resonance at 3.03 ppm were reported and T_2 values for these metabolites were measured *ex vivo* for the first time (Table 1). Metabolite concentrations from intact tissues and tissue extracts from the same tumors were compared to each other and to the literature values. While the concentrations for some metabolites, measured by HRMAS MRS, were similar to those in extracts, others showed much higher concentrations in tissue than in extracts. Metabolite concentrations and T_2 values accurately differentiated tumor types based on clinical data, but detailed histopathology of the tissue samples was not performed due to the false belief at the time that HRMAS MRS damaged tissue such that subsequent histopathological analysis was not possible.

The important fact that accurate histopathological evaluation of tissue samples after HRMAS MRS is possible and the necessity of performing quantitative pathology on the same tissues after MRS was reported by Dr. Anthony and colleagues [28]. Tissue pathologies from both HRMAS MRS analyzed tissue and adjacent tissue that had not undergone HRMAS MRS before histopathological evaluation were analyzed semi-quantitatively for each region of the brain tumor. The quantitative histopathological data obtained from the study showed that adjacent specimens from the same tumor region shared similar histopathological features. Although quantitative differences were noted, these differences were most likely due to extensive tumor microheterogeity and not the result of the HRMAS MRS procedure. Futhermore, correlations between the amount of tumor necrosis and the concentrations of mobile lipids ($R^2 = 0.961$, $p < 0.020$) and lactate ($R^2 = 0.939$, $p < 0.032$), as well as between the numbers of glioma cells and the ratio of phosphocholine (PC) to choline resonances ($R^2 = 0.936$, $p < 0.033$) were observed. The strong linear correlation between tissue necrosis (%area) and lipids (mM) indicated that the amount of tissue necrosis can be estimated using the measured concentration of lipids from HRMAS MRS, and that according to the long T_2s these lipids are relatively mobile consistent with them being products of cell membrane degradation. Additionally, the results of the correlation obtained between the number of glioma cells and the phospocholine to choline resonances suggested the importance of measuring and quantifying these two resonances separately, which is difficult with both *in vivo* and *ex vivo*
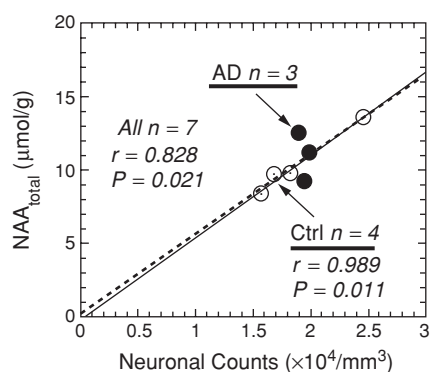
Table 1: Matrix of selected brain metabolite concentrations measured with HRMAS MRS for differentiation between different pathological specimens NAA, in the table, includes both measured resonances of NAA at 2.01ppm and acetate at 1.92 ppm (see text for details); Numbers in parentheses represent resonance chemical shift in ppm. The resonance at 3.93 is tentatively assigned to the Cr metabolite. As an example of the use of this matrix, the Chol resonance can be used to differentiate low-grade/anaplastic astrocytomas from GBMs with a significance of $p < 0.05$. Similarly, the glycine resonance (Gly) can be used to distinguish GBMs from Schwannomas with a $p < 0.005$

	Normal	LG and AA[a]	GBMs	Schwannomas	Meningiomas
Normal		NAA[b] Lac (1.33)[c]	Cr (?, 3.93)[c] Gly (3.55)[d] Chol (3.20)[b] Cr (3.03)[b] NAAf Lac (1.33)[b]	Chol (3.20)[b] NAA[b] Lac (1.33)[d]	Cr (?, 3.93)[b] Chol (3.20)[e] Glu (2.35)[d] Ala (1.48)[b]
LG&AA			Chol (3.20)[e]		Glu (2.35)[b]
GBMs				Gly (3.55)[d]	Gly (3.55)[b]
Schwannomas					
Meningiomas					

[a]LG and AA, low-grade/anaplastic astrocytomas
[b] $p < 0.05$, two-tailed student's t test.
[c] $p < 0.0005$, two-tailed student's t test.
[d] $p < 0.005$, two-tailed student's t test.
[e] $p < 0.05$, calculated according to one-tailed student's t test, based on the hypothesis that chol increases in tumors.
[f] $p < 0.00005$, two-tailed student's t test.

conventional MRS methods, but readily achievable with MAS.

It is expected that HRMAS MR spectra of tissue rather than MRS of tissue extracts will provide metabolite information more closely related to that in the *in vivo* brain. However, cautions should be exercised when comparing *in vivo* MRS and HRMAS MRS data, as *in vivo* MRS will always be broad-line in nature. Nevertheless, a number of studies, both in adult [41] and pediatric [42] brain tumors, have concluded that there is good agreement between *in vivo* and *ex vivo* tissue MR spectra with high-resolution *ex vivo* results providing both insight into which metabolites reside within the broad resonances observed *in vivo* and a link between *in vivo* MRS evaluations and neuropathologies.

Prostate

The search for marker metabolites of prostate cancer has been inspired by the current state of prostate cancer pathology, wherein more than 70% of newly diagnosed cases are categorized with similar Gleason scores (6 or 7), but for which individual patient outcomes within these tumors are drastically different and unpredictable.

Hahn and colleagues reported the first intact prostate tissue conventional MRS study of 66 benign prostatic hyperplasia (BPH) and 21 prostate cancer samples from

50 patients [43]. They divided the proton spectral region between 0.5 and 3.55 ppm into 50 equal subregions, and applied multivariate linear-discriminant analysis to the point-reduced spectra. The study found six spectral regions including those containing citrate, glutamate, and taurine to be sensitive in differentiating BPH from cancer with an overall accuracy of 96.6%. This algorithm was tested by the same research group on another group of 140 samples from 35 patients after radiotherapy to test for the sensitivity of spectroscopy analysis in differentiating cancer positive vs. cancer negative samples [44]. After eliminating 24 samples that did not have sufficient signal-to-noise ratios, they reported, with the remaining 116 spectra, the sensitivity and specificity of tissue spectra in identifying cancer samples to be 88.9 and 92%, respectively.

Van der Graaf and colleagues presented another interesting study of intact prostate tissue combining conventional MRS and high-pressure liquid chromatography (HPLC) analysis to measure the relationship between polyamines (PA) and prostate cancer [45]. Although they observed PA in the proton spectra and measured statistically significant drops of PA in cancer samples with HPLC, no correlation between PA levels measured by MRS and those determined by HPLC were presented for the same cases due to very limited number of samples analyzed. Nevertheless, the study suggested the existence
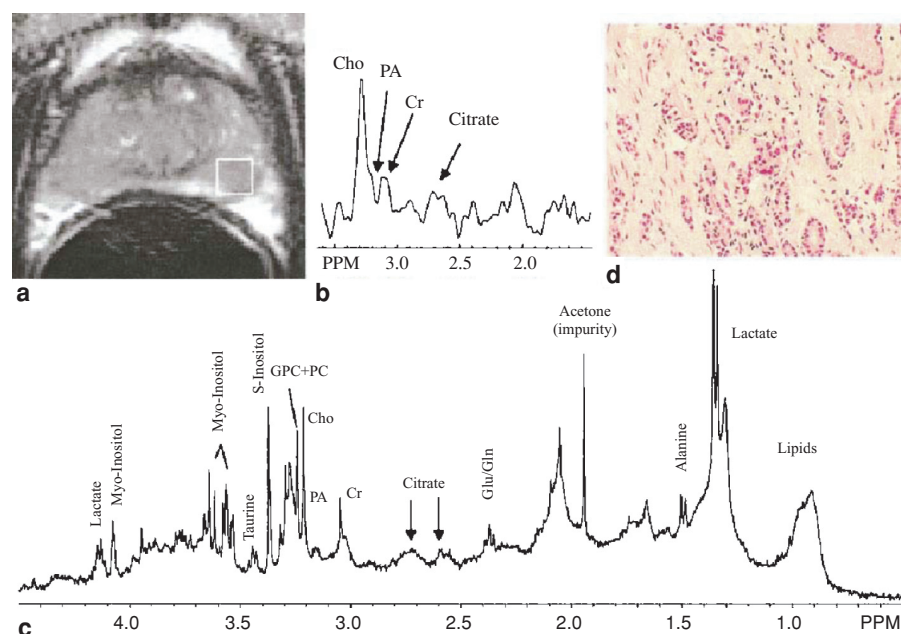
Fig. 6. Results from a presurgical 3D-MRSI of a 56-year-old prostate cancer patient were concordant with histopathologically classified malignancy of H and E stained tissue samples of excised tissue with Gleason 3 + 4 prostate cancer, **d**. Spectrum **b**, shows elevated levels of choline and low levels of citrate and polyamines relative to creatine in the 0.24 cm3 voxel of **a**. The postsurgical HRMAS MR spectrum (c) confirms the 3D-MRSI results with enhanced resolution that also identifies elevated levels of GPC + PC relative to choline. *Figure 2 from ref. [30].*

of a potential prostate biomarker that MRS may be able to quantify, as well as a direction for future studies. More recently, Mountford *et al.* reported a conventional MRS study of 71 prostate samples from 41 patients who underwent both cancer and non-cancer prostate surgeries [46]. By using peak ratios 3.2/3.0 ppm (choline-to-creatine) and 1.3/1.7 ppm (lipid-to-lysine), they were able to differentiate malignant from benign tissues with 97% sensitivity and 88% specificity.

Tomlins and colleagues experimented with proton HRMAS MRS analysis on human prostate tissues with both 1D and 2D MR spectroscopy. In their qualitative report, they confirmed the usefulness of HRMAS MRS in producing high-resolution spectra from intact human prostate tissues [47]. A second HRMAS MRS study of human prostate tissues from 16 patients was the first to include quantitative pathology on the MRS specimens and to include multiple subjects [29]. The results of the study proved the validity of HRMAS MRS for the accurate determination of tissue histopathology. Both citrate and spermine were quantified from the tissue HRMAS MR spectra and shown to be linearly correlated with the amounts of prostate normal epithelium. In 2003, Swanson and colleagues reported an interesting study of HRMAS

MRS of tissues from 26 patients harvested post surgically under the guidance of 3D-MRSI from lesions that had been analyzed using *in vivo* MRS prior to prostatectomy. Figure 6 shows the resulting spectra from a 56-year-old prostate cancer patient [30]. By combining the MRS results with quantitative pathology of the same tissue after spectroscopy, metabolite discriminators (i.e. ratios of citrate, polyamine, and choline compounds to creatine) were found to differentiate normal prostate epithelial tissue from cancer and stromal tissue. Furthermore, a correlation between the intensity of MIB-1 immunohistochemical staining and the ratio of choline to creatine resonances was reported, supporting their findings *in vivo*. These results were dependent on the assumption that the creatine concentration did not alter during the disease process, which awaits verification.

Breast

Human breast tissue was difficult to analyze using conventional proton MRS due to high lipid content. As pioneers of this work, Mountford and colleagues noted that to acquire a spectrum that was diagnostically meaningful,

fine-needle aspiration biopsy (FNAB) instead of regular tissue samples had to be utilized [48]. In a study of 218 FNAB samples from 191 patients with benign lesions, ductal carcinoma *in situ* (DCIS), and invasive carcinoma, they found that by using the resonance peak height ratio threshold of 1.7 (3.25 vs. 3.05 ppm; or choline-compounds vs. creatine), benign lesions could be differentiated from carcinoma with 95% sensitivity and 96% specificity. However, this single ratio identifier only worked if the signal-to-noise ratio, particularly for choline peaks at 3.25 ppm, was above 10. To extend the MRS differentiation capability below this limit, and more importantly to search for a more robust diagnostic protocol of computerized spectral analysis, Mountford *et al.* ,along with Smith *et al.* at the NRC, Canada, used a pattern recognition method, SCS, developed to utilize the entire MR spectrum instead of only the aforementioned two peaks for the purpose of analysis [9]. From measurements conducted on 140 samples, they reported an overall accuracy of 93% in distinguishing benign from malignant tumors using SCS. Furthermore, they reported that using SCS classifiers, lymph node involvement and tumor vascular invasion could be predicted with 95 and 94% overall accuracies, respectively. The advantage of SCS in relating proton FNAB spectra with breast cancer diagnosis and possibly prognosis is evident and its potential in clinical usage is apparent. However, the more advanced the SCS, the less evident were the direct connections with individual metabolites.

HRMAS MRS overcame many of the limitations of conventional MRS32. Even with such lipid-rich tissue, HRMAS MRS successfully produced high-resolution proton spectra. Results from a study at 400 MHz of 19 cases of ductal carcinomas showed that both the high fat contents and individual cellular metabolites could be measured from the same spectrum. Particularly, from these spectra, PC could be quantified separately from choline; and the ratio between PC and choline was found to correlate with tumor grades, as shown in Figure 7.

A more recent detailed HRMAS MRS study at 600 MHz of 10 ductal carcinomas by Sitter *et al.* compared HRMAS MR spectra with those obtained using conventional MRS of perchloric acid tissue extracts [20]. The study concluded that for breast tissue, HRMAS MRS was able to achieve spectral resolutions approaching those obtained using conventional MRS of extracts. 2D J-resolved and COSY MRS was used to accurately assign metabolites.

Cervix

Mountford and colleagues began analysis of human cervical biopsies with conventional proton MRS in the early 1990s [49]. Broad-line resonances at 0.9 ppm (CH3), 1.3 ppm (CH2), and 3.8–4.2 ppm (CH) were found to
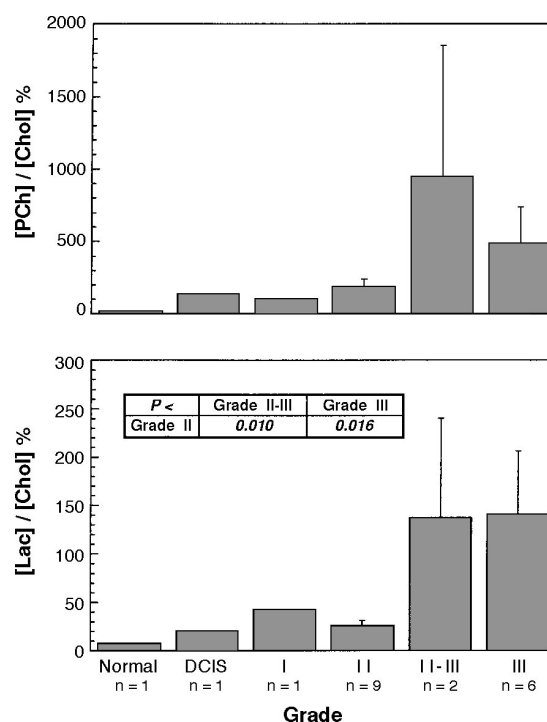
Fig. 7. Examples of observed correlations between histopathological grades of breast ductal carcinomas and the means for metabolic intensities, particularly PC over choline (A) and lactate over choline (B) measured with HRMAS MRS. Of note, the HRMAS method provided a means to differentiate PC from choline in the such a lipid-rich tissue. *Figure 4 from ref. [32].*

distinguish invasive from pre-invasive epithelial malignancy [50].

More recently, Sitter and colleagues reported the use of HRMAS MRS of cervical tissue from eight cancer and eight non-cancer patients [.35]. In addition to their presentation of detailed resonance assignments for cervical metabolites, they were able to use PCA to separate cancer from non-cancer samples with the first principal component (PC1). This principal component was comprised primarily of lactate, the methyl, and methylene groups of lipids, and, to a lesser extent, the choline-containing compounds. This component represented 63% of the variations in the spectra.

Kidney

HRMAS MRS analysis of kidney tissue has been shown to diagnose renal cell carcinoma based on an increased intensity of lipid resonances in malignant compared to
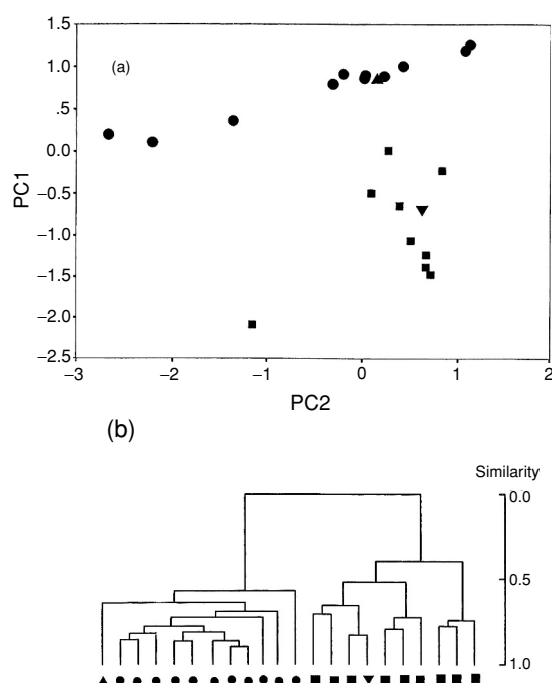
Fig. 8. Using PCA (a) and HCA (b), tumor samples can be differentiated from non-tumor samples. Key: (•) normal tissue; (■) renal cell carcinoma; (▲) sample from bladder metastasis in renal collecting duct; and (▼) lung metastasis in renal cortex. *Figure 3 from ref. [.35].*

control tissues [51,52]. These studies were not designed to test the utility of HRMAS MRS in the diagnosis of renal cell carcinoma, but rather to illustrate the feasibility of HRMAS MRS for assignment of resonances and identification of metabolites as well as to develop two-dimensional HRMAS MRS techniques for the assessment of intact tissues.

Later, a study of 22 paired control and tumor samples of human renal cortex used computer-based pattern recognition techniques to show that using PCA and hierarchical cluster analysis (HCA), tumor samples were differentiated from non-tumor samples, as shown in Figure 8 [34].

Sarcoma

HRMAS MRS has been shown to be a useful technique in the analysis of human sarcoma tissue. Singer and colleagues reported a comparison of 2D TOCSY spectra with and without HRMAS MRS, which demonstrated the superior resolution of the MAS technique by revealing less intense cross peaks that were not observed when the

sample was not spun [53,54]. For this initial study, spectra of liposarcoma and lipoma were dominated by signals from lipids, interfering with the ability to observe resonances from other metabolites. More recently, Chen and colleagues have developed a double pulsed field gradient selective echo (DPFGSE) technique in combination with HRMAS MRS to selectively excite spectral regions that contain less abundant non-lipid metabolites [23]. With their new technique they were able to observe and quantify phosphatidylcholine (PTC), PC and choline, and found, using six paired samples from six patients, that the ratio of PTC/PC differentiated normal fat from lipoma-like well-differentiated liposarcoma with statistical significance ($p < 0.001$).

Lymph Nodes

Accurate detection of metastatic deposits in lymph nodes is often the most important predictor of cancer patient prognosis. Histopathology is subject to sampling and observer error and thus there is a real need for a new, rapid, and cost-effective method with high accuracy for this purpose.

An early study identifying malignant cells in lymph node tissue using 1D ^{1}H MRS was limited by high fat content of the tissue and the low spectral resolution obtained. Two-dimensional (2D) techniques successfully resolved resonances and allowed the complex spectra from lymph nodes to be assigned and correlated with detailed histopathology [.10]. Choline and lactate were found to be key metabolites diagnostic of the presence of metastases in lymph nodes using the 2D method. However, these 2D MR experiments require long acquisition times (4–5 h) during which sample degradation may occur, potentially compromising the outcome of the measurement. In addition, conventional 1D and 2D techniques cannot address the problem of resonance broadening directly and thus useful diagnostic information may be missed.

Alternatively, MRS of FNAB of lymph node tissues has been used to diagnose the presence of metastases in lymph nodes from melanoma patients [55]. Spectra of node tissue containing metastatic melanoma were characterized by the presence of a distinct resonance from choline-containing metabolites at 3.2 ppm. The ratio of the integrals of resonances from lipid and metabolites (1.8–2.5 ppm region) and "choline" (3.1–3.3 ppm region) distinguished benign nodes (38.8 ± 34.3) from melanoma containing nodes (7.2 ± 6.8) with $p < 0.012$ (separate *t*-test) [55]. This method assumes the chemistry of the node detectable by MRS changes immediately upon the node being infiltrated by metastatic cells. This is supported by studies in a rat lymph node metastasis model where MRS detected the presence of malignant cells prior to clusters of metastatic cells being identified by histopathology.

Instead, single malignant cells were observed unclustered throughout the node, the presence of which was confirmed by growing these nodes in nude mice, which subsequently developed tumors. Datasets in the study of MRS on FNAB as a method of diagnosing lymph node metastases remain, however, small and until larger databases confirm these findings the possibility that the method introduces a sampling error cannot be excluded.

The application of HRMAS MRS to intact tissue analysis was in fact initiated from the proton MR detection of lymph node metastases in a rat model for breast cancer metastasis. Since then, HRMAS MRS has also been successfully applied to the proton MR analyses of human lymph nodes from breast cancer patients. Malignant nodes were distinguished from reactive nodes based on the peak height ratio of the smallest to largest peaks resolved in the 0.9 ppm resonance multiplied by the peak height ratio of the choline and creatine resonances at 3.2 and 3.0 ppm, respectively (Figure 9). Three of four axillary nodes from breast cancer patients that were clinically suspicious but diagnosed cancer free on routine histopathology had an HRMAS MRS ratio consistent with reactive nodes. The fourth node in this category was, by HRMAS MRS criteria, malignant. Review of the histology of these nodes using increased magnification and immunohistochemical staining identified malignancy in the fourth node missed during routine examination.
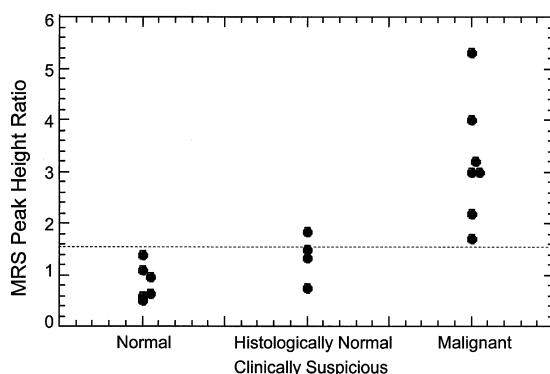

Fig. 9. HRMAS MRS of Human Lymph Nodes: Malignant nodes were distinguished from normal (reactive) nodes based on the MRS Peak Height Ratio (ratio of the smallest to largest peaks resolved in the 0.9 ppm resonance multiplied by the ratio of the choline and creatine resonances at 3.2 and 3.0 ppm). One of four axillary nodes that were clinically suspicious but cancer free on routine histopathology had an HRMAS MRS ratio consistent with malignancy. Review of the histology for all four nodes identified malignancy in this one node missed by routine histopathology.

Future Developments and Conclusions

The development of proton HRMAS MRS for tissue analysis has not only drastically simplified the procedure of obtaining high resolution cellular metabolite spectra directly from intact tissue, but more importantly allows quantitative pathology to be conducted on the same tissue after MRS measurements for correlation with individual metabolite concentrations or collective alterations in overall metabolite profiles. The high-resolution spectra generated by HRMAS MRS contain many more resonance peaks for analysis than conventional MRS. This greatly improves the likelihood that sophisticated data analysis methods can accurately distinguish between differing pathologies. However, the increased discriminatory power of the method relies on precise histopatholgical information about the tissue assessed by HRMAS MRS being available. This is only possible when detailed serial section histopathological methods are undertaken to substantially increase the precision of the information currently obtained from clinical pathology.

Glossary of Terms

Astrocytoma—The most common type of brain tumor in adults; astrocytomas, known for their marked potential for malignant progression and infiltrative nature, can be classified histopathologically into three grade of malignancy: WHO Grade II astrocytoma, WHO Grade III anaplastic astrocytoma, and WHO Grade IV GBM.

Benign Prostatic Hyperplasia—Enlargement of the prostate and more specifically, overgrowth of the epithelium and fibromuscular tissue of the transition zone and periurethral area.

Ductal Carcinoma *In Situ*—Noninfiltrative lesions composed of malignant epithelial cells that are confined to the mammary ducts and lobules.

Glioblastoma Multiforme—The most malignant grade of astrocytoma (WHO Grade IV), which has an overall survival time of less than 2 years for most patients. These tumors are histopathologically characterized according to their dense cellularity, high proliferative indices, endothelial proliferation, and most importantly the presence of focal tissue necrosis.

Lipoma—Commonly diagnosed benign tumors of adipose tissue that can develop anywhere in the body where fat is normally found.

Liposarcoma—A commonly diagnosed soft tissue sarcoma in adults which be found anywhere in the body and for which there exists several types with varying clinical outcomes.

Meningioma—Intracranial tumors that arise in the meninges and compress the underlying brain. In general, many of these tumors are benign, however, others are

malignant with the capability to metastasize, both locally and distally.

Metabolite Profiling—The study of small molecules, such as lipids, peptides, amino acids, and carbohydrates, which represent steady-state concentrations of intermediate products or end products of cellular processes and as a result can be thought of as the ultimate response to genetic and environmental stimuli.

Necrosis—Tissue and/or cell death.

Neoplasm—Literally meaning "new growth." An abnormal growth of tissue which may be benign or malignant.

Oncogenomics—The study of genes, gene sequences, and the underlying genetic alterations that appear to be involved in oncological pathways.

Reactive Nodes—Lymph nodes that have been immunologically challenged.

Schwannoma—Benign tumors that arise on peripheral nerves in general and on cranial nerves in particular, especially on the vestibular portion of the eighth cranial nerve.

Sensitivity—The term relating to the percentage of people with disease who test positive for the disease, i.e. the percentage of patients with cancer who have positive biopsy results.

Specificity—The term referring to the percentage of people without disease who test negative for the disease, i.e. patients without cancer with cancer negative biopsy results.

Acknowledgments

References

Author: Please provide publisher place and location for ref. [2].

1. Mountford C, Doran S, Lean C, Russell P. Chem. Rev. 2004;104:3677.
2. Lean C, Somorja R, Smith I, Russell P, Mountford C. In: AG Webb (Ed). Accurate Diagnosis and Prognosis of Human Cancers by Proton MRS and A Three Stage Classification Strategy, 2002.
3. Pomper MG. In VT DeVita Jr, S Hellman, SA Rosenberg (Ed). Functional and Metabolic Imaging. Philadelphia, 2001.
4. Nicholson JK, Lindon JC, Holmes E. Xenobiotica 1999;29: 1181.
5. Bettelheim R. Price K, Gelber R, Davis B, Castiglione M, Goldhirsch A, Neville A, Lancet 1990;335:1565.
6. Mountford C, Lean CL, Mackinnon W, Russell P. In G Webb (Ed). The Use of Proton MR in Cancer Pathology. London, 1993.
7. Russell P, Lean C, Delbridge L, May G, Dowd S, CE M. Am. J. Med. 1994;96:383.
8. Doran ST, Falk GL, Somorjai RL, Lean CL, Himmelreich U, Philips J, Russell P, Dolenko B, Nikulin AE, Mountford CE. Am. J. Surg. 2003;185:232.
9. Mountford CE, Somorjai RL, Malycha P, Gluch L, Lean C, Russell P, Barraclough B, Gillett D, Himmelreich U, Dolenko B, Nikulin AE, Smith IC. Br. J. Surg. 2001;88:1234.
10. Mountford C, Lean C, Hancock R, Dowd S, Mackinnon W, Tattersall M, Russell P. Invasion and Metastasis, 1993; 13:57.
11. Kuesel A, Kroft T, Saunders J, Prefontaine M, Mikhael N, Smith I. Magn. Reson. Med. 1992;27:340.
12. Andrew E, Bradbury A, Eades R. Nature 1958;182:1695.
13. Lowe I. Phy. Rev. Lett. 1959;2:285.
14. VanderHart D, Earl W, Garroway A. J. Magn. Reson. 1981;44:361.
15. Maricq M, Waugh J. J. Chem. Phys. 1979;70:3300.
16. Cheng LL, Lean CL, Bogdanova A, Wright SC Jr, Ackerman JL, Brady TJ, Garrido L. Magn Reson Med. 1996;36: 653.
17. Middleton DA, Bradley DP, Connor SC, Mullins PG, Reid DG, Magn. Reson. Med. 1998;40:166.
18. Garrod S, Humpfer E, Spraul M, Connor SC, Polley S, Connelly J, Lindon JC, Nicholson JK, Holmes E. Magn. Reson. Med. 1999;41:1108.
19. Waters NJ, Garrod S, Farrant RD, Haselden JN, Connor SC, Connelly J, Lindon JC, Holmes E, Nicholson JK. Anal. Biochem. 2000;282:16.
20. Sitter B, Sonnewald U, Spraul M, Fjosne HE, Gribbestad IS. NMR Biomed. 2002;15:327.
21. Wu CL, Taylor JL, He W, Zepeda AG, Halpern EF, Bielecki A, Gonzalez RG, Cheng LL. Magn. Reson. Med. In Press (2003)
22. Bourne R, Dzendrowskyj T, Mountford C. NMR Biomed. 2003;16:96.
23. Chen JH, Enloe BM, Fletcher CD, Cory DG, Singer S. J. Am. Chem. Soc. 2001;123:9200.
24. Wind RA, Hu JZ, Rommereim DN. Magn. Reson. Med. 2001;46:213.
25. Hu JZ, Rommereim DN, Wind RA. Magn. Reson. Med. 2002;47:829.
26. Hu JZ, Wind RA. J. Magn. Reson. 2003;163:149.
27. Taylor JL, Wu CL, Cory D, Gonzalez RG, Bielecki A, Cheng LL. Magn. Reson. Med. 2003;50:627.
28. Cheng LL, Anthony DC, Comite AR, Black PM, Tzika AA, Gonzalez RG, Neuro-oncol. 2000;2:87.
29. Cheng LL, Wu C, Smith MR, Gonzalez RG. FEBS Lett. 2001;494:112.
30. Swanson MG, Vigneron DB, Tabatabai ZL, Males RG, Schmitt L, Carroll PR, James JK, Hurd RE, Kurhanewicz J. Magn. Reson. Med. 2003;50:944.

Author: Please provide publisher name for ref. [6].

Author: Please provide full name for "CE M." in ref. [7].

Author: Please update ref. [21].

31. Cheng LL, Chang IW, Louis DN, Gonzalez RG. Cancer Res. 1998;58:1825.

32. Cheng LL, Chang IW, Smith BL, Gonzalez RG. J. Magn. Reson. 1998;135:194.

33. Somorjai R, Dolenko B, Nikulin A, Pizzi N, Scarth G, Zhilkin P, Halliday W, Fewer D, Hill N, Ross I, West M, Smith I, Donnelly S, Kuesel A, Briere K. J. Magn. Reson. Imaging. 1996;6:437.

34. Tate AR, Foxall PJ, Holmes E, Moka D, Spraul M, Nicholson JK, Lindon JC. NMR Biomed. 2000;13:64.

35. Sitter B, Bathen T, Hagen B, Arentz C, Skjeldestad FE, Gribbestad IS. MAGMA. 2004;16:174.

36. Cheng LL, Ma MJ, Becerra L, Ptak T, Tracey I, Lackner A, Gonzalez RG. Proc. Natl. Acad. Sci. U.S.A. 1997;94:6408.

37. Cheng LL, Newell K, Mallory AE, Hyman BT, Gonzalez RG. Magn. Reson. Imag. 2002;20:527.

38. Kuesel A, Donnelly S, Halliday W, Sutherland G, Smith I. NMR Biomed. 1994;7:172.

39. Kuesel AC, Briere KM, Halliday WC, Sutherland GR, Donnelly SM, Smith ICP. Anticancer Res. 1996;16:1485.

40. Rutter A, Hugenholtz H, Saunders J, Smith I. J. Neurochem. 1995;64:1655.

41. Barton SJ, Howe FA, Tomlins AM, Cudlip SA, Nicholson JK, Bell BA, Griffiths JR. Magma 1999;8:121.

42. Tzika AA, Cheng LL, Goumnerova L, Madsen JR, Zurakowski D, Astrakas LG, Zarifi MK, Scott RM, Anthony DC, Gonzalez RG, Black PM. J. Neurosurg. 2002;96:1023.

43. Hahn P, Smith I, Leboldus L, Littman C, Somorjai R, Bezabeh T. Cancer Res. 1997;57:3398.

44. Menard C, Smith IC, Somorjai RL, Leboldus L, Patel R, Littman C, Robertson SJ, Bezabeh T. Int. J. Radia. Oncol. Biol. Phys. 2001;50:317.

45. van der Graaf M, Schipper RG, Oosterhof GO, Schalken JA, Verhofstad AA, Heerschap A. Magma 2000;10:153.

46. Swindle P, McCredie S, Russell P, Himmelreich U, Khadra M, Lean C, Mountford C. Radiology 2003;228:144.

47. Tomlins A, Foxall P, Lindon J, Lynch M, Spraul M, Everett J, Nicholson J. Analy. Common. 1998;35:113.

48. Mackinnon WB, Barry PA, Malycha PL, Gillett DJ, Russell P, Lean CL, Doran ST, Barraclough BH, Bilous M, Mountford CE. Radiology, 1997;204:661.

49. Mountford CE, Delikatny EJ, Dyne M, Holmes KT, Mackinnon WB, Ford R, Hunter JC, Truskett ID, Russell P. Magn. Reson. Med. 1990;13:324.

50. Delikatny E, Russell P, Hunter J, Hancock R, Atkinson K, van Haaften-Day C, Mountford C. Radiology, 1993;188:791.

51. Moka D, Vorreuther R, Schicha H, Spraul M, Humpfer E, Lipinski M, Foxall P, Nicholson J, Lindon J. Analy. Common. 1997;34:107.

52. Moka D, Vorreuther R, Schicha H, Spraul M, Humpfer E, Lipinski M, Foxall PJ, Nicholson JK, Lindon JC. J. Pharm. Biomed. Anal. 1998;17:125.

53. Millis KK, Maas WE, Cory DG, Singer S. Magn. Reson. Med. 1997;38:399.

54. Millis K, Weybright P, Campbell N, Fletcher JA, Fletcher CD, Cory DG, Singer S. Magn. Reson. Med. 1999;41:257.

55. Lean CL, Bourne R, Thompson JF, Scolyer RA, Stretch J, Li LX, Russell P, Mountford C. Melanoma Res. 2003;13:259.

Current Clinical Applications of *In Vivo* Magnetic Resonance Spectroscopy and Spectroscopic Imaging

Margaret R. Lentz[1], Jennifer L. Taylor[2], D. Ashley Feldman[3] and Leo L. Cheng[1, 3, *]

Departments of [1]Radiology, [3]Pathology, Massachusetts General Hospital, Harvard University, Boston, Massachusetts, [2]Department of Cancer Biology and Pritzker School of Medicine, The University of Chicago, Chicago, Illinois

Abstract: Magnetic resonance imaging (MRI) infused Radiology with rejuvenating vigor in the 1980s, owing credit to a couple of magnetic resonance spectroscopy (MRS) experiments performed in 1973. MRI has since been embraced by the radiology and medical communities. If the goal of MRS is to measure many chemicals in a homogeneous magnetic field, then the function of MRI is, in general, to measure one chemical – water – in an artificially created inhomogeneous field.

Combining spectroscopy principles with technologies developed over the past two decades for MRI presented the philosophical appeal of non-invasively measuring metabolic molecules in living tissue, and led to the explosive developments in the last decade of *in vivo* MRS, and more recently MRSI, in the settings of diagnostic radiology.

This review is intended to discuss the basic technologies of the current trends in the field of *in vivo* MRS and MRSI, especially the inherent predilections of individual techniques to the study of certain disease states. Following a historical introduction, individual techniques and their clinical applications, found in publications between January 2000 and October 2004, are reviewed in connection with related *ex vivo* results, after which the practical aspects of *in vivo* MRS and MRSI in clinical settings are discussed.

1. INTRODUCTION

1.1. Time Before Magnetic Resonance

If we adopt arbitrarily that human civilization has a 5,000-year history, then consider the recent and rapid progress of medicine in reference even to our own lifetimes, we are left straining to imagine what medical feats were performed before the birth of a "little" trick now known as radiology. The Renaissance curiosity of human anatomy and desire to depict it accurately was historically unique, and many believe that the scientific, and therefore modern notion of medicine was born with Leonardo Da Vinci's anatomical maps. However, if for medicine, to penetrate the skin was to see, then for 400 years after Da Vinci's suggestive drawings, the scalpel remained medicine's only way to see.

Light streamed in at the dawn of the 20th century first with Roentgen's breakthrough mass-density (absorption) based X-ray[1], and subsequently with the Becquerel[2] and Curies[3]' discovery of radioactivity. X-ray dominated medical diagnostics for the first eight decades of the 20th century. Particularly, the invention of computers in the 1970s led to the development of the x-ray based computed tomography (CT)[4], which emerged as a powerful tool, bringing a third dimension to the classical two-dimensional x-ray films.

Radiology, from the 2nd half of the 20th century, has become a substitute word for non-invasive diagnosis. Although excessive exposure to x-rays causes irreversible damage to living organisms, the benefits of examining, without surgery, the internal structure of the body outweigh the risks. This newly broad definition of radiology exceeded the parameters of its simple and direct reference of association to radioactivity. In fact, every technology developed to render "non-invasive" diagnoses has been embraced by radiology and enlisted into its service. These umbrella-crowders include ultrasound, positron emission tomography (PET), and most notably, MRI. Of these new technologies, MRI is regarded as the most versatile, sharing not only the historical idealism of non-invasive diagnosis, but also having in common with x-ray the electromagnetic spectrum. However, in opposition to x-ray, MRI resides at the low energy end of the spectrum, in the range of the radio

*Address correspondence to this author at the Pathology Research CNY-7, 149 13th Street, Charlestown, MA 02129, USA; Tel: 617-724-6593; Fax: 617-726-5684; E-mail: cheng@nmr.mgh.harvard.edu

---

[1] **Wilhelm Conrad Röntgen** (1845-1923), The Nobel Prize in Physics 1901 "in recognition of the extraordinary services he has rendered by the discovery of the remarkable rays subsequently named after him."(http://nobelprize.org/physics/laureates/1901/index.html)

[2] **Antoine Henri Becquerel** (1852-1908), The Nobel Prize in Physics 1903 "in recognition of the extraordinary services he has rendered by his discovery of spontaneous radioactivity." (http://nobelprize.org/physics/laureates/1903/index.html)

[3] **Pierre Curie** (1859-1906), **Marie Curie** (1867-1934), The Nobel Prize in Physics 1903 "in recognition of the extraordinary services they have rendered by their joint researches on the radiation phenomena discovered by Professor Henri Becquerel."(http://nobelprize.org/physics/laureates/1903/index.html)

[4] **Allan M. Cormack** (1924-1998), **Godfrey N. Hounsfield** (1919-2004), The Nobel Prize in Physiology or Medicine 1979 "for the development of computer assisted tomography." (http://nobelprize.org/medicine/laureates/1979/index.html)

frequency. Accordingly, one might claim that it was MRI which assisted radiology in becoming truly non-invasive.

The underlying technology of MRI is fundamentally different from that of x-ray. Since x-ray is mass-density based, when the mass within a particular region of an object is more dense, less ray penetrates this region, resulting in its appearing light in the eventual image. MRI is based on the quantum mechanic properties of the nucleus, which govern its behavior (orientation profile) when it is placed in an externally applied magnetic field. Acquisition of an image using MRI is not as straightforward as it is for x-ray. To understand MRI, particularly the topics of this review, MRS and MRSI, it is necessary to discuss very briefly the related physical principles. Expert readers may wish to proceed directly to the second section: The Current Clinical Usage of MRS and MRSI, while more determined learners may wish to read dedicated monographs on the principles of MRS.

1.2. A Few Principles of Magnetic Resonance

To physicists and chemists, MRS has been known as nuclear magnetic resonance (NMR) since its development in the 1940s. It is based on the quantum mechanic properties of nuclei, first predicted by theory and later observed experimentally in 1946 with technologies developed during World War II[5]. As NMR became clinically relevant, the word "nuclear" was abandoned to prevent misguided apprehensions arising from the common association, after WWII, of "nuclear" with nuclear fission. Thus, NMR became MRS both in the public arena and in certain scientific circles. MRI, discovered in the early 1970s[6], is an extension of NMR and is now commonly used for clinical diagnosis.

For a nucleus that possesses angular momentum (a.k.a. spin), quantum mechanics predicts that the energy levels of this nucleus will degenerate in a magnetic field. The splitting of these energy levels depends on the strength of the applied magnetic field (B_o), as well as the intrinsic properties of the nucleus, such as the gyromagnetic ratio. If a nucleus is unperturbed in the field, it will tend to stay at the lowest energy level, which is said to be in alignment with the field. Fortunately for biological investigations, most biologically relevant elements have isotopes (such as ^1H, ^{13}C, ^{31}P, ^{17}O, and ^{15}N) that possess this property (spin). To accomplish a transition between the degenerate energy levels, energy, in the range of radiofrequencies (rf), needs to be supplied.

The introduction of Fourier Transform (FT) to spectral acquisition has proved critical to the fundamental developments of modern MRS and MRI[7]. With FT, energy (in the form of the so-called "rf pulses") of different levels is supplied simultaneously and perpendicular to B_o, to the object of interest. The nucleus will resonate when the energy

of this pulse equals the energy difference between these levels. The applied rf pulse, which is composed of a broad range of frequencies, will cause all nuclei of interest (e.g. ^1H) to resonate simultaneously. When the rf pulse is turned off, the spins of the resonating nuclei immediately begin to realign with B_o, and dephase due to field inhomogeneities. The rate at which the spins realign with B_o is termed T1 relaxation, or the longitudinal relaxation rate. The dephasing process that these spins undergo is termed T2 relaxation or transverse relaxation. The relaxation rates for a given nucleus depend on the surrounding physical and chemical environments.

The paramount importance of relaxation in terms of MR imaging was the discovery that relaxation rates vary with tissue type and disease [1]. Of particular interest for clinical evaluation was the observed increase in relaxation rates in the malignant cells. A large amount of work has been devoted to developing rf pulse sequences for MRS and MRI, based on the exploitation of these relaxation rates. The decay of the object or region's net magnetization due to these relaxation effects is called the free induction decay (FID), which is obtained in the time domain. Using FT techniques, the FID is converted into the frequency domain, generating the peaks which one sees in an MR spectrum. The effective magnetic field strength experienced by a particular nucleus is the sum of B_o and the induced fields resulting from the motions of electrons surrounding the nucleus. Therefore, the chemical environment has a perceptible influence on the field experienced by a particular nucleus and hence, the same nucleus may experience slightly different fields in different chemical environments. The end result is a slight difference in the energy level splitting. This phenomenon is known as chemical shift. Chemical shifts are very useful in MRS because they allow for the identification of different nuclei and functional groups within a molecule. With *in vivo* MRS, several molecules or metabolites are measured, many of which have overlapping resonances. A typical ^1H MRS measured at 1.5T with a clinical scanner is shown in (Fig. **1**).

In order to obtain a narrow linewidth in a MR spectrum, the object of interest must experience a homogeneous magnetic field. The extent to which the applied magnetic field is inhomogeneous will be reflected in the degree of broadening of the linewidth of each peak in the spectrum. To obtain the most homogeneous field in the volume of interest (VOI), a technique called shimming is used in both MRS and MRI, which uses many channels of electrical currents to generate induced fields in different directions in order to compensate for the inhomogeneities of B_o.

MR images are generated by applying a linearly varying magnetic field, known as a gradient, to the uniform field, B_o. Nuclei are localized by spatial encoding of the frequency of nucleus rotation in the FID signal. To obtain an axial MR image, one gradient in the z-direction is used for slice selection, while a gradient in the x-direction is used for frequency encoding, and a gradient in the y-direction is used for phase encoding. The phase encoding gradient is applied for a short period of time, and is turned off prior to data acquisition. This allows spatial localization of the nuclei, and thus, following a two-dimensional FT, an image of the object is digitally generated. A more detailed description of MRI

---

[5] Felix Bloch (1905-1983), Edward Mills Purcell (1912-1997), The Nobel Prize in Physics 1952 "for their development of new methods for nuclear magnetic precision measurements and discoveries in connection therewith. " (http://nobelprize.org/physics/laureates/1952/index.html)

[6] Paul C. Lauterbur (1929-), Sir Peter Mansfield (1933-), The Nobel Prize in Physiology or Medicine 2003 "for their discoveries concerning magnetic resonance imaging." (http://nobelprize.org/medicine/laureates/2003/index.html)

[7] Richard R. Ernst (1933-), The Nobel Prize in Chemistry 1991 "for his contributions to the development of the methodology of high resolution nuclear magnetic resonance (NMR) spectroscopy." (http://nobelprize.org/chemistry/laureates/1991/index.html)
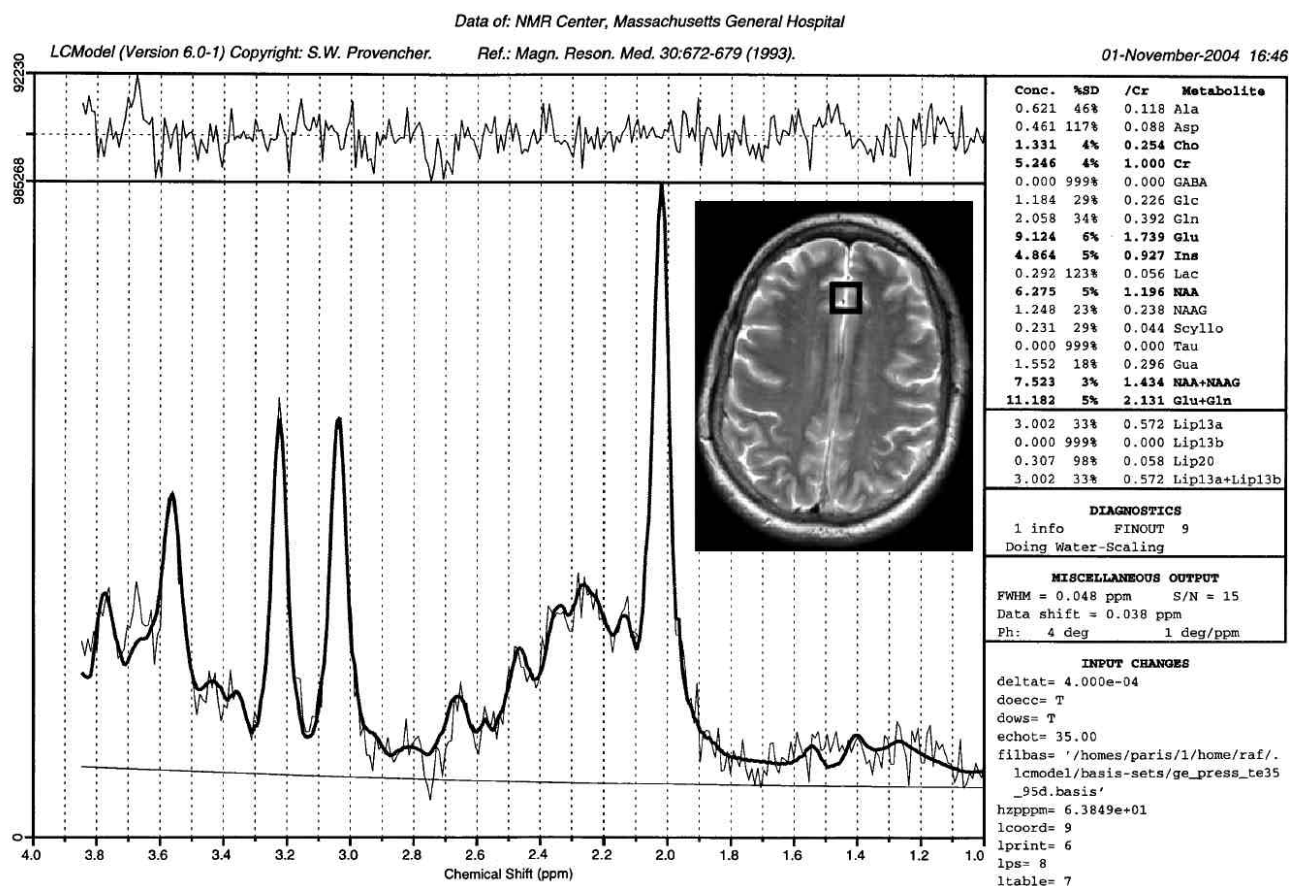
Fig. (1). A typical single-voxel ^{1}H MR spectrum measured from the frontal cortex of a healthy volunteer in a clinical GE 1.5T scanner. The brain region from where the spectrum was acquired is labeled with a square voxel, along with the caluclated metabolite concentrations from curve fittings using computer software LCModel [89, 90].

can be found in a variety of MR textbooks [2-4]. Readers with interest in the quantum mechanic principles of MR theory can find discussions in classical MR monographs [5, 6].

MRS has opened many frontiers in chemical investigation, while, ironically, the tremendous success of MRI in medicine reduced such investigations to a single chemical: water. In any biological object, such as a human body, there are many other interesting and potentially important chemicals than water. Therefore, built on the successes of MRI, progress in the past decade has brought *in vivo* MRS and spectroscopic imaging (MRSI) onto the radiology stage.

In radiology, MRS is employed to study cellular chemistry. MRS may be able to supply a chemical fingerprint of the biochemical state of the sample studied. The implications for the understanding of cellular metabolism and physiology are staggering. MRS has the potential to help define mechanistic details of disease progression and function as a non-invasive means of monitoring the effectiveness of treatments and therapies. What better non-invasive means exist to help unite the study of anatomic structure with function than the use of *in vivo* MRS and MR imaging?

1.3. Towards a Working Knowledge of MRS/MRSI

Reviewing the literature of MRS can be confusing even to readers familiar with it, particularly because of the non-standardized terminology used by researchers to describe experiments during the rapid development of the field. For a clinician interested in translating results "from bench to bedside", the task of understanding the utility of MR technologies from a literature search can be daunting. In this review, we intend to demystify the acronyms of these techniques, and focus on areas where current research is being translated to clinical practice.

Most magnets currently used for clinical MRI are also equipped with the hardware and software necessary for acquiring MRS, as would be performed on a vertical magnet spectrometer found in the basement of a chemistry department at any university.

The majority of MRSI currently performed is the so-called metabolic imaging. Several variations of this technique exist, and some confusion is present in the terminology. However, the general approach is to use a multi-voxel spectroscopy sequence in which the VOI is localized from the MR images and selective saturation bands are used for outer voxel suppression. Other than additional

complexity due to its multi-voxel nature, MRSI is not fundamentally different from single-voxel MRS. MRSI is often referred to in the literature as chemical shift imaging (CSI), or occasionally as *in vivo* MRS, making it easily mistaken for single-voxel MRS experiments. MRSI has found its most important clinical applications in neurological and oncological evaluations, because of its ability to distinguish between normal and abnormal metabolic profiles at high spectral resolutions. In this review, we will use MRSI to refer only to multi-voxel techniques, and "*in vivo* MRS" or simply "MRS" to refer to single-voxel evaluations if the latter is clearly distinushable from *ex vivo* MRS beased on the context.

In addition to MRSI, there have been developments in other types of metabolic imaging that are gaining popularity, among them, the most noteable echo planar spectroscopic imaging (EPSI). EPSI is based on Mansfield's technique which allows the simultaneous and rapid acquisition of spatial and spectral data. Furthermore, availability of high field strengths and an interest in measuring low gyromagnetic nuclei of biological importance, such as ^{31}P and ^{13}C, have also shown promise for advancing the clinical utility of *in vivo* MRS and spectroscopic imaging.

While the focus of this review is ^{1}H on *in vivo* MRS and MRSI, it is important to note that MRS experiments have been carried out both on solutions of purified chemical extracts from excised tissue samples, and on intact tissue specimens for more than 20 years, yielding a wealth of results. These experiments are typically described as "*ex vivo* MRS" or "MRS on extracted metabolites". Interested readers are encouraged to examine the many excellent reviews of these topics. Because of the limited scope of this review, we do not intend to cover these results, except for those observed with intact tissue specimens that may have direct benefits for the discussion of *in vivo* observations.

The following sections will outline details of *in vivo* MRS and MRSI techniques, their clinical utility, and our comments regarding clinical applications of these techniques. Because of the enormous volume of published clinical results and because of our limits, we will focus in this review on clinical concerns and the applications of *in vivo* MRS and MRSI, with particular consideration to many of the results published between January 2000 and October 2004. Reviews of clinical work prior to 2000 can be found in a large number of excellent, already published reviews.

2. THE CURRENT CLINICAL USAGE OF MRS AND MRSI

Experimentation with *in vivo* proton (^{1}H) MRS was initiated after the development of ^{1}H MRI, roughly 20 to 30 years ago. It is difficult to determine specifically when and by whom the first, single-voxel *in vivo* (human) MRS was observed. However, it most certainly predated the observations of MRSI in the early 1980s both on ^{1}H and ^{31}P [7, 8]. Many reasons can be cited for presence of ^{31}P in the sequence of developments of MRS, including the importance of phosphorus in biological processes, and limits of several techniques essential for ^{1}H measurements, such as water suppression, automated shim routines and development of localization methods in the early age of surface coil

techniques [9-11]. The massive physiological concentration of hydrogen within living organisms, and the large natural abundance of its MR active isotope, ^{1}H, with its high gyromagnetic ratio makes it remarkably suitable for MRS studies. In the mid 1980's, many of the techniques essential for proton measurements were developed, making the clinical use of ^{1}H MRS and MRSI a testable concept [12-14]. By 1983, the first *in vivo* ^{1}H MRSI was reported on a human forearm [7]. This technique was based on a simple modification of the three-dimensional fourier zeugmatography method outlined in 1979 [15, 16], and latter described in a theoretical paper in 1982 [17].

The reports discussed in this review, if not otherwise specified, were measured at the magnetic field strength of 1.5T (T – Tesla, the unit for magnetic field strength, named after Nikola Tesla 1856-1943). To give context to this magnitude, the average Earth field strength is on the order of 0.00005T. For readers who still remember the details of their experience with NMR in organic chemistry lab, 1.5T is equivant to 64 MHz, for it is the resonance frequency of ^{1}H at this field strength.

2.1. Proton Single Voxel Spectroscopy – *In Vivo* MRS

Diseases that cause a functional disturbance at the cellular level are potential systems for *in vivo* MRS evaluations. The need for non-invasive diagnostic tools is the driving force for much of *in vivo* MRS investigation. Currently, the widest clinical application of MRS is to the study of neurological conditions ranging from stroke, ischemic brain injury, HIV and infectious diseases, Central nervous system (CNS) degenerative brain diseases, and peripheral nervous system diseases like multiple sclerosis. Another area to which MRS is already widely applied is human oncological evaluations, for instance, of brain tumors and prostate cancer for which treatment options are limited and non-invasive diagnostic methods are greatly appreciated. Recently, MRS reports have been seen in studies of human breast and cervical cancers.

2.1.1 Techniques

In vivo MRS is performed using clinical imaging systems, or scanners, and more often than not results are combined with imaging studies. The major, and perhaps only difference between *in vivo* MRS of a human and MRS measurements in a chemistry department with a sample tube is the necessity to localize a VOI within the body for *in vivo* MRS. In contrast, MRS of a chemical is performed on the entire volume of the sample. The same whole-sample approach is also practiced occasionally in biomedicine when a global value is desired, for instance in measuring and monitoring the total brain n-acetyl aspartate (NAA) level in volunteers [18], and in multiple sclerosispatients [19]. However, generally, *in vivo* MRS obtains a FID of a single-voxel VOI that is defined by the user from a previously acquired scout image, using one of two localization pulse sequences: point-resolved spectroscopy (PRESS), or stimulated echo acquisition mode (STEAM). These pulse sequences were developed in the 1980s for the purpose of exciting nuclei only in the assigned VOI [20, 21]. When reviewing reports of measurements with these methods, readers inevitably will encounter the abbreviations TR, TE

and sometimes TM, which mean recycle time, echo time, and mixing time, respectively. These terms refer to the delays in the pulse sequences used to record the localized FIDs. There is another localization approach, (ISIS for image selective *in vivo* spectroscopy) which excites an entire region, and subsequently subtracts signals originating from beyond the VOI, but this approach has been applied less frequently in recent years.

After the identification of the VOI, and before the acquisition of the FID, the user needs to perform magnet shimming, most likely, in a modern imager, by invoking the automatic shimming procedure to ensure that the applied field in the VOI is maximally homogenous. Another technical point that merits emphasis is that since MRS is not a technique of high signal-to-noise ratios (SNR), most often, signal averaging is necessary, which understandably requires the VOI, in other words the subject, to be motionless during the period of data acquisition.

As previously indicated, where *ex vivo* data is available, we will review clinical results of *in vivo* MRS (as well as of MRSI in Section 2.2) for a particular disease in the context of its *ex vivo* measurements. However, we will restrict our discussions to intact tissue studies either with conventional MRS or with the recently developed high resolution magic angle spinning (HRMAS) MRS approach, and exclude measurements on tissue chemical extracts. Solutions of tissue extracts can produce high-resolution spectra, allowing for the identification of individual metabolites which is unachievable from the broad-line spectra of conventional MRS. However, the extraction process is destructive and has been found to alter the spectroscopic results to an unknown degree [22], depending on the procedure used and the thoroughness of extraction. The tested benefit of the HRMAS MRS approach is that it allows for the identification of individual metabolites from intact tissue studies, as with extract solutions, while also preserving the tissue structure, making possible subsequent pathological studies of the same tissue.

2.1.2. Clinical Applications

Because the ability to detect a chemical depends directly on its abundance in a sample, single-voxel techniques, which acquire data from a relatively large area, are ideally suited for examining less prevalent metabolites, and for detecting other non-proton nuclei of low natural abundance. The primary function of *in vivo* MRS has been to identify metabolic markers of diseases, and to distinguish pathological from normal tissue. Because of the complex pathophysiology of human disease, it is not surprising that the search has met with only limited success.

With the amount of information that can be obtained using *in vivo* MRS, it may be difficult for a person interested in a particular disease to know where to begin an MRS experiment. In the next several sections we will look at the most relevant ways MRS contributes to the clinical setting, and discuss the particular metabolites that are most interesting to study in some of the systems in which MRS is most commonly used. Here, we wish to emphasize that in most cases or in general, there is not a single metabolite whose presence or absence alone directly corresponds to the presence or absence of a particular disease condition. However, there seem to be exceptions.

2.1.2.1. Neurological Disorders

In the brain, for example, the amino acid NAA is interpreted as a marker of neuronal cell health, and its changes have been recorded in both neuronal injury and death. Although tissue contains many cell types, the finding that NAA in the adult brain is detectable only in neurons and not in glial cells, the two major components of brain tissue, provided excellent support for the use of NAA to study pathologies targeting neurons [23, 24]. Other metabolites of importance in brain MRS include myo-inositol (MI, a sugar present only in glia), choline-compounds (Cho), and creatine (Cr) as well as lactate (Lac), which although are not specific to neural cells, are often elevated in the pathological processes of inflammation and necrosis, respectively [25].

The substantial clinical contribution of ^{1}H MRS of the brain is due in part to the difficulty of obtaining brain biopsy specimens, which has driven researchers to find a means to investigate neurological disorders non-invasively. Other reasons explaining the large number of neurological studies using MRS are the brain's homogeneous nature (relative to other organs) and its lack of major physiological motions. Having these requirements and advantages, brain studies provided the impetus for technological improvements and innovations in many areas of MRS including developments of pulse sequences, outer volume suppression methods for better suppression of lipids from nearby tissue, functional imaging, and the use of high field magnets (e.g. 3T or higher). In general, high field experiments improve not only image quality by increasing SNR, but also spectral quality by resolving spectral components that normally overlap at 1.5T.

In vivo MRS studies of brain have penetrated almost every subject of neurology and neuropathology. *In vivo* MRS may be particularly well suited for studies of neurological conditions that affect a large volume of tissue somewhat uniformly. However, even our limited survey of this body of work has presented us with a rich coverage of MRS clinical investigations of various neurological diseases. The topics include neuro-anatomy, vascular, infectious, demyelination, degenerative diseases, metabolic disorders, trauma, epilepsy, psychiatry, and the impact on the brain of non-neurological diseases such as pulmonary, liver, and cardiac conditions.

Neuro-Anatomy Studies

The rationale of employing the single-voxel procedure is very well illustrated by a number of neuro-anatomy studies, including those which have measured metabolite levels of human fetal brains at 30 to 40+ weeks gestational age [26-29], of healthy elderly subjects in two VOIs [30], and of the cervical spinal cord [31].

The single-voxel approach is best suited for investigations in which either a large sample size is preferred for achieving an optimal SNR, as in fetal brain studies, or the structure of the experimental object is irregular and small in certain dimensions, exemplified by the spinal cord. It was found that with the cervical spinal cord, because of the susceptibility effects of the surrounding tissue, the optimal result could be obtained with the elongated voxel (9x7x35

mm^3) placed at the inferior end of vertebral C2. The study used PRESS and demonstrated that the concentration of NAA in the cord is lower than that in the brainstem, but higher than that in the cortex and cerebellum. Cr in the cord was lower than in the cerebellum, but no statistical differences were observed with cortex and brainstem [31].

In fetuses, the underdeveloped brains are known to be have a high concentration of water, and measurable metabolite concentrations are expected to be lower than in adult brains, hence the largest possible voxel sizes are desirable. Larger voxel size would also translate into high SNR and would require less measurement time. Shorter measuring time was also critical in reducing the effects of motion by the fetus. A number of commonly observed brain metabolites, including MI, Cho, Cr, and NAA, were quantified and expressed as functions of fetal gestational age for 35 normally developing fetuses, with VOI between 15 and 40cc, which to some degree reflected the growth of the brain during the third trimester. The most interesting result was that among these quantified metabolites, only the increase with age of neuron-specific NAA was determined statistically significant. In this study, both STEAM (TR/TE/TM: 2500/20/30ms) and PRESS (TR/TE: 2500/15ms) were used. No observable difference between the two methods was noticed [28].

Vascular Disease

Single-voxel MRS can be used to detect sensitively the Lac signal to observe the recovery of brain tissue following a stroke from the acute stage through the subacute and chronic stages of neuronal recovery [32]. MRS has also been used, with a double-blind, placebo-controlled study, to assess the effect of a sodium dichloroacetate infusion on the Lac level of the lesion. Reductions were seen with high doses, and with patients treated within the first two days following infarction [33]. However, MRS results so far have shown that with ischemic stroke, the level of Lac never returns to normal. Here, the advantage of employing single-voxel measurements is evident because the interest is localized on the lesion and the study's question is focused on the measurement and interpretation of the temporal changes. To improve the sensitivity of MRS evaluation of stroke, diffusion weighted imaging (DWI) has been introduced to identify regions of ischemia for the placement of MRS VOI. DWI is the most sensitive test for detecting the occurrence of an ischemic stroke within a few hours of a cerebrovascular event. The sensitivity of DWI to stroke can be utilized in the selection of VOI for metabolic MRS studies, in order that they may find more sensitive predictors of neurological deficits resulting from stroke injury [34].

MRS can be used also to probe the pathogenesis of stroke [35]. Like NAA to neurons, MI is proposed to be a metabolite specific to the glial cells. However, declaring MI a marker of cell density can be problematic. Glial cells increase the production of MI in response to osmolarity changes, which often accompany brain injury. In addition, glial cells proliferate in response to neuron damage in a process known as reactive gliosis. In many studies, the proposed role of the metabolite measured in MRS is an indicator of pathology, but when the metabolite's synthesis is altered or degraded in response to cellular injury, as may

be the case in stroke, the relationship of the metabolite to the pathogenic process is obscured. Understanding the physiology of the pathogenic process aids in the interpretation of metabolite ratios, or "markers", in terms of their relationship to the disease. The role of a measured metabolite is not only to be an empirical statistic associated with the disease, but also to provide possible directions toward therapy design and patient follow-up.

Trauma

While Lac can be used as a marker for brain recovery from stroke, it also appears to have predictive value in determining the outcome of patients who have suffered from perinatal asphyxia and pediatric closed head injury [36-40]. However, this predictive power was found lacking in cases of adult traumatic brain injury. While some reports indicate changes in Lac in this group, others reported conflicting observations [41-45].

Infectious Disease

The most publicized infectious disease MRS has been utilized to understand is HIV infection and the dementia it causes (NeuroAIDS) [46-48]. The selection of the single-voxel MRS approach in these studies was motivated by the aim of measuring possible correlations between cerebral metabolites in well hypothesized brain regions (frontal lobe and basal ganglia) with cognitive function and clinical variables, such as CD4 counts, plasma and CSF viral loads [46, 47].

In a correlation study, 45 antiretroviral-naïve HIV patients were recruited. The study was designed to test, and later confirmed the hypothesis that MI and Cho, suspected glial markers, should be elevated due to glial proliferation caused by virus infection. Measuring patients before antiretroviral treatments avoided possibly confounding factors introduced by treatment agents. The authors warned that future MRS studies of HIV patients should consider using metabolite concentrations rather than the ratios over Cr, since Cr may also change during the course of the disease [46].

A MRS study involving a consortium of eight medical centers throughout the U.S has been reported. It was designed to evaluate the effect of an AIDS Clinical Trials Group (ACTG) phase II trial of memantine, a N-methyl D-aspartate (NMDA) receptor antagonist, as treatment of neuroAIDS. The first consortium's report on 58 patients indicated that neuroAIDS might correlate with significantly elevated Cho/Cr and MI/Cr levels in the basal ganglia, and NAA/Cr reduction and MI/Cr elevation in the frontal white matter. Although these results of the study were useful confirmations of the predictions based on previous measurements, the valuable contribution of this multi-center report reached beyond its tabularized results, presenting a quality control paradigm that may be adopted by future multi-center MRS studies or clinical trials of other diseases [47].

Brain abscesses, another form of infectious disease, have also been evaluated by MRS. With brain abscesses, the benefit of a single-voxel is evident by the presence of lesions, easily identifiable by imaging [49, 50]. Unlike

HIV/AIDS studies, abscess studies often have the opportunity to obtain pus samples for *ex vivo* analyses. *Ex vivo* analysis of these pus samples using high field MRS methods (for instance at 4.7T) can produce high resolution spectra, from which metabolites can be identified, even verified with two-dimensional correlation spectroscopy. In combining the applications of *in vivo* and *ex vivo* MRS, it was possible to differentiate anaerobic and aerobic sterile brain abscesses based on their metabolite patterns [50].

Demyelinating Disease

Multiple sclerosis (MS) is perhaps the best-known demyelination disease. Since MS is a global white matter disease, it is best suited for multi-voxel analysis, as will be discussed in the later sections. Nevertheless, single-voxel approaches have been employed to study identifiable lesions caused by the disease. It has been shown with measurements of NAA, Cho and Cr in the parieto-occipital region, that NAA/Cr, Cho/Cr, and NAA can differentiate primary from secondary progressive lesions, and NAA/Cr as well as the absolute concentration of NAA can differentiate normal-appearing white matter (NAWM) from both primary and secondary progressive lesions [51]. Another interesting study reported the relationship between NAA levels and the major CNS myelin protein, proteolipid protein (PLP1), and concluded that axonal degeneration might occur due to the lack of PLP1. By using an animal model of PLP1 deficiency, they concluded that the degeneration process is length-dependent, but not associated with significant demyelination [52]. However, a reported measurement of the whole-brain NAA level did not find correlation with MS clinical status scale scores for 49 relapsing-remitting MS patients [19].

Neuro-degenerative Disease

The class of diseases described as neuro-degenerative presents a number of familiar names, Alzheimer [53-58], Parkinson [59, 60], ALS [61-66], etc., all of which have been actively pursued by single-voxel MRS.

Among the Alzheimer (AD) reports, we noticed a longitudinal (a one-year gap between studies of the same subject) quantitative study of hippocampus of nine probable AD patients with 14 age-matched control subjects. Lower hippocampal NAA levels for the cognitively impaired patients were observed relative to controls, however the changes within the one-year period were not significant [56]. An interesting report of 18 AD patients and 12 healthy controls dealt with glutamate and glutamine measurements at 0.5T [53]. Glutamate is an energy metabolite and the most abundant neurotransmitter in the brain, while glutamine, a product of the glutamate cycle, is transferred from glial cells to neurons after exocytotic release of glutamate into the synaptic space. Both metabolites are critical for a number of neuronal functions, and are expected to play important roles in AD. In the report, the authors clearly demonstrated that while the sum of glutamate and glutamine (Glx) could be seen in the 0.5 T spectrum of cingulated cortex, and a significant reduction in Glx was found with AD patients. However, the same Glx signal was not observed with the same subjects in a 1.5 T spectrum. Including Glx, in addition to NAA and MI, for the metabolite diagnosis of AD resulted in an increase in sensitivity from 78% to 89%.

NAA is a proposed neuronal marker of injury, damage, and death, and nearly all MRS studies of AD seem to measure changes in NAA and discuss its changes. However, a study comparing elderly subjects with chronic hypertension, early AD and healthy controls (ten in each group) revealed significantly elevated MI/Cr ratios in both disease groups, but no differences in either NAA or Cho ratios between the three groups [55]. The lack of NAA reduction in early stages of AD may suggest that neuronal injury at the tested stage is not MRS apparent, or that neuronal death at the later AD stages is responsible for the commonly reported NAA decrease with AD. The latter conclusion is supported by autopsy studies of AD brain tissues. For instance, an *ex vivo* HRMAS study showed correlations between MRS data and stereological pathology for AD brains (n=7), and confirmed the proportionality of NAA concentration to neuronal density. This study also demonstrated the quantitative nature of the NAA and neuronal count relationship, as the linear correlation intercepted at zero (–0.29±1.15 _mol/g) [67].

It is not surprising to see NAA levels affected in Parkinson disease (PD), as it is also a neuro-degenerative disease. For example, a study comparing PD patients with (n=14) and without (n=12) dementia to healthy controls (n=13) suggested that NAA in the occipital region could identify PD patients with dementia, while no differences in MI levels were seen between the groups. The study suggested that by combining measurements of NAA with MI, PD might be differentiated from AD, where MI increases have been frequently observed [60]. The indicative value of NAA/Cho in the evaluation of PD after thalamotomy was reported in a study of 15 patients who underwent surgeries for control of Parkinsonian tremor, and the results were compared with 15 age-matched control subjects. It was indicated that patients who improved after stereotactic thalamotomy had significantly reduced post-surgical NAA/Cho values compared to levels measured prior to the procedure in both substantia nigra and thalamus, but not in putamen. However, the changes were not significant if evaluated by ratios of NAA/Cr and Cho/Cr [59]. Without the opportunity to evaluate brain tissues of PD patients (which is a general difficulty with studies of neurological disease), a recent report compared metabolite levels in cerebrospinal fluid (CSF) for PD patients and controls. However, this approach yielled no significant results [68].

Amyotrophic lateral sclerosis (ALS) is a neuro-degenerative disorder with unknown cause which has also been measured extensively by *in vivo* MRS [61-64, 66]. The hallmark of these studies is the observation of a decrease in NAA, or NAA/Cr, occasionally accompanied by observations of MI and Cho increases, particularly in motor cortices, and its correlations with clinically evaluated neurological functions [63, 64]. A recently reported longitudinal study evaluated the motor cortices of 70 ALS patients and 48 healthy controls [66]. These patients were divided according to the EL Escorial Criteria into subgroups of suspected, possible, probable, and definite ALS. The concentration results showed that both NAA and Cr were reduced in patients compared with controls, while no Cho differences were detected. When the results were arranged by metabolite ratios, they showed reductions of NAA/Cho

and NAA/Cr with all subgroups, while an increase in Cho/Cr was detected only with definite ALS patients. Sixteen of these patients were followed for an average of one year (12.1±8.7 months), and showed a further reduction in NAA/Cho of 9.1%. A 7.0% increase in Cho/Cr was found to correlate with disease progression [66]. The study indicated that *in vivo* MRS might eventually be used clinically as a means of non-invasively monitoring neuro-degeneration and the effects of therapy strategies, at least for ALS.

Metabolic Diseases

A number of *in vivo* MRS studies on metabolic diseases were found, including a study of adrenoleukodystrophy for the evaluation and prediction of patient outcomes with hematopoietic stem cell transplantation therapy [69], and the searches for the mechanism of cerebrotendinous xanthomatosis with NAA/Cr and Lac/Cr levels [70]. Studies were also seen in diabetes mellitus [71], and most interestingly, after the lengthy discussion of NAA, Cho, MI, and Cr, in phenylketonuria by measuring phenylalanine (Phe) signals resonating at the opposite spectral side of water signals from the other metabolites [72]. In this study, brain Phe levels presented as Phe/Cr ratios were measured from ten patients, four in earlier stages and six in later stages, each whose disease was detected and treated. The Phe/Cr ratios were correlated with clinical, biochemical, and MRI findings. The study showed that in both groups brain Phe/Cr levels correlated with plasma Phe concentrations, and with clinical phenotype for patients whose disease were detected in later stages.

Changes in brain metabolites due to non-neurological diseases have been investigated and measured extensively. These studies cover a wide spectrum of conditions represented by inflammatory diseases such as systemic lupus erythematosis with reduction in NAA and increases in MI and Cho [73, 74], chronic pain with reduction in NAA and glucose [75], chronic fatigue syndrome with increases in Cho/Cr [76], chronic obstructive pulmonary disease [77], liver cirrhosis with decreases in Cho and MI and increases in Glx [78-80], and dilated idiopathic cardiomyopathy with decreased Cr and lipid levels [81].

Psychiatry

The psychiatric topics addressed by *in vivo* MRS cover an array of conditions, although our inclusion of certain topics may be somewhat liberal, such as the observations in panic disorder of disorder-related reduction of -aminobutyric acid (GABA) in the occipital cortices for 14 patient-control pairs [82], and decreases of Cr in the right medial temporal lobe in patients (measured from 11 patient-control pairs) [83], or the evaluation of mood in terms of the Positive and Negative Affect Scale by the levels of Cho in the left frontal lobe [84], .

Studies of classical psychiatry also tested the utility and reproducibilty of MRS. NAA, Cho and Cr were evaluated in the left frontal white matter and caudate nucleus for schizophrenic patients, but no significant metabolite differences were observed between scans of a one-week gap for 12 patients. While NAA was found to have a small coefficient of variance in all brain regions examined, Cr and Cho measured in the left caudate nucleus were found to have

larger variance (16-18%) [85]. Evaluations of NAA in the dorsolateral frontal lobe for children with attention-deficit/hyperactivity disorder (ADHD) have also been reported. 23 patients and 24 controls were enrolled in the study, but no significant difference between them was recorded [86].

As a prominent category of neurological disorders, epilepsies present a clinical phenotype that may be caused by a variety of neurological conditions. This presents epilepsy as a fundamentally global disease of the CNS, which is therefore best suited for MRSI examinations, rather than a local disorder of certain brain structures for which the single-voxel approach would have many advantages. We noticed that most often epilepsy is reported in the temporal lobe (TLE), according to clinical observations, and there have been single-voxel studies of TLE reported, for instance the study of the complementary roles of MRS and diffusion-weighted MRI [87], and the comparison between MRS and PET [88]. However, a large volume of epilepsy studies have utilized the MRSI approach, and we will defer our detailed epilepsy discussion to the later MRSI section.

In conclusion, in single-voxel MRS applications to neurological conditions, other than for a few specific diseases, the majority of measurements are centered on the analyses of NAA, Cho, Cr, and MI, which most of time are the only resolved signals in an *in vivo* brain spectrum. Nevertheless, efforts have been employed to identify other brain metabolites, for instance, those in brain tumors, using automated spectral analysis programs based on model compound measurements. One of the most popular and commonly used spectral analysis programs for MRS is the linear combination (LC)Model [89, 90]. To conduct an analysis of this type, a basis-set specific to each scanner should be constructed using *in vivo* phantom measurements on the scanner for every expected metabolites. The knowledge of the chemical shift values for these model compounds is necessary, and interested readers are encouraged to start the pursuit from reviewing the existing data reported for *in vitro* measurements of brain metabolites [91].

With the status of current MRS techniques, it is impossible to definitively diagnose a neurological disease based purely on the changes observed in a limited number of metabolites. However, as discussed, the reported changes in different brain regions even for a single metabolite may be meaningfully indicative of the underlying disease. Therefore, to achieve disease diagnosis, or to test the ability of MRS in disease detection, the simultaneous mapping of different metabolites in different brain regions may be necessary, which is the strength of MRSI.

2.1.2.2. Oncological Diseases

The brain has more restricted physiological motion, and a more homogeneous structure compared to other organs, which is why it has been the subject of a large number of MRS studies. This fact, combined with the ability to visualize easily a lesion on the brain and to prescribe a VOI through MR images, encouraged the extensive pursuits of MRS studies of brain tumors. If the heterogeneity within a single tumor is the focus of the examination, MRSI tends to

be the more desirable evaluation method. The main advantage of single-voxel measurement in tumors is that it leads to a spectrum with a higher SNR than that usually achievable with MRSI.

Single-voxel MRS is not a screening tool. Mostly, it is used to further investigate suspicious lesions identified in brain images. Therefore, the primary utility of MRS is to differentiate a tumor lesion from other brain mass presented in an image. There are two other main functions of MRS: to achieve non-invasive diagnosis of the tumor, and to monitor both the response of the tumor and other changes in the brain resulting from therapy. It warrants emphasis that until now all studies had either the nature of feasibility evaluations, or the status of clinical trials. To the best of our knowledge, there exists no clinically approved MRS protocol in oncological clinics. Therefore, in most of the reported studies, the accuracy of MRS results was determined at final biopsy conclusion.

Brain Tumors

MRS covers the entire spectrum of functions that a radiology tool is expected to contribute to the oncological clinic. These functions include: detection of neoplasm, characterization of tumors, and monitoring the effectiveness of therapy. Since the most commonly encountered brain tumors are gliomas, the majority of MRS studies on brain tumors are centered on this type of tumors, although we noticed that the approach developed for them has been applied to the evaluations of non-malignant brain lesions, such as neurofibromatoses [92] and epileptogenic hypothalamic hamartomas [93].

The detection of tumors from metabolite measurements has been reported in the context of differentiating lesions of tumors from those of other origins, such as large inflammatory lesions [94] and inflammatory demyelinating disease [95] that mimic tumors in both CT and MR images. It has been reported that in order to differentiate cerebral ischemia lesions from tumors, the apparent diffusion coefficients (ADC) of NAA and Cr must be taken into consideration [96]. The technique of measuring brain metabolites with single-voxel MRS has also been applied to the detection and identification of pediatric brain tumors. However, because of the developing status of brain metabolism in children, a study of this nature must include age-matched control subjects [97].

Many recent reports on the diagnosis or characterization of brain tumors by their types and grades have included large patient numbers, on the order of more than 100 [98-100]. The different types of tumors studied were astrocytomas (WHO II), anaplastic astrocytomas (WHO III), glioblastomas (GBM, WHO IV), medulloblastomas, meningiomas (MNG), and metastases (MET). The evaluated brain metabolites included Cho, Cr, NAA, Lac, lipids, and in some studies alanine and Glx. When metabolite results were included in the diagnostic parameters obtained from MRI, it was reported that the number of correct diagnoses increased (15.4%), while the number of incorrect and equivocal diagnoses decreased (6.2% and 16%, respectively), from diagnoses using MRI parameters alone [100].

An elaborate algorithm for discrimination of the most common brain tumors has been proposed based on the measured values of metabolites [99]. Another study, although with a smaller number of patients (n=42), also reached a diagnostic scheme by involving a 2D plot of (alanine+lactate+lipids) vs. MI/Cho. The resulting 2D field was divided into four areas: WHO II, III, MNG, and a mixture of GBM and MET, where GBM and MET were the worst possible conditions [101]. Furthermore, the specific ability of MRS to identify lipid signals for both the diagnosis of GBM and the possible transformation of low-grade tumors to GBM, was reported [102].

These *in vivo* observations were in close agreement with *ex vivo* MRS analyses of human brain tissue performed in the past ten years. For instance, examination of brain tumor tissues by MR spectrometers similar to those used for chemical analyses, suggested the diagnostic importance of lipid metabolites. Correlations between the MR lipid signal intensities and the amount of necrosis in astrocytomas were reported in 42 cases, where the intensity of the mobile fatty acyl –(CH=CH)– resonance differentiated with statistical significance three tumor groups with varying amounts (0%, 1-5% and 10-40%) of necrosis [103].

Recently, with the development of HRMAS, ^{1}H MRS for intact tissue analysis[8], high resolution brain tumor spectra can be measured, for the first time, with detailed profiles of both water-soluble metabolites, as can be obtained from extract solutions, and lipids. A study of 19 brain tumors, including astrocytomas, GBM, MNG, schwannomas, and normal brain, reported that metabolite concentrations both in absolute units and relative ratios normalized to the Cr (3.03 ppm). Metabolite concentrations from intact tissues, and from tissue extracts of the same tumors were compared to each other and to the literature values. While the concentrations of some metabolites measured by HRMAS MRS were similar to those measured from extracts, concentrations of others were much higher in tissue than they were in extracts. However, it should be noticed that the capability for metabolite concentrations to differentiate tumor types was reported based on clinical data, rather than on detailed histopathology of the tissue samples examined by *ex vivo* MRS [104]. Because of tumor histopathological heterogeneities, the reported correlations might be considered only as a proof of concept, in light of a later report which analyzed quantitative histopathological data obtained from the same brain tumor specimen after the *ex vivo* MRS study. Quantitative histopathological evaluation accounted for the observed spectral differences measured between different regions of a single tumor as consequences of extensive tumor microheterogeity. Particularly, correlations were observed between the amount of tumor necrosis and the concentrations of mobile lipids (R^2=0.961, p<0.020) and Lac (R^2=0.939, p<0.032), and between the numbers of glioma cells and the ratio of the phosphocholine to choline resonances (R^2=0.936, p<0.033) [105]. The strong

---

[8] Magic-angle spinning, originally used to reduce resonance line-width in solid-state NMR, subjects samples to fast mechanical rotations (~kHz) at the magic-angle, (54°44') away from the direction of the spectrometer's static magnetic field while spectroscopy is recorded. When applied to intact tissues, HRMAS can produce high spectral resolution metabolite spectra that allow identification of individual metabolites, while leaving tissue pathological structures intact.

linear correlation between tissue necrosis (%area) and lipids (mM) indicates that the amount of tissue necrosis can be estimated using the measured concentration of lipids from MRS, which agrees well with *in vivo* results.

The diagnostic value of automated pattern recognition analysis of brain tumor single-voxel MRS has been tested and reported by a study involving three clinical centers [106]. This study included 144 patients of four different tumor types: WHO II, GBM, MNG, and MET, and reported an accuracy of over 92.3% in characterizing individual cases according to the automated pattern recognition.

Of special interest in tumor detection and diagnosis is the elevation of Cho observed *in vivo*. These compounds are associated with cellular proliferations, although the exact biochemical events underlying these experimental observations are still unknown. However, with brain tumor studies, the correlation between Cho and cellular proliferation seems strong as a number of studies have shown the linkage between elevated Cho levels and proliferative activity, measured by the immunohistochemical marker Ki-67 (MIB-1) [107, 108]. However, one must exhibit caution in examining reported results of this nature because of the heterogeneity of the disease, and the lager (>1000) differences in scale between the measured volumes of MRS (>1 cm^3) and immunohistochemistry (~1 mm^2).

The elevation of a unique metabolite, glutathione, observed in *in vivo* MRS, has been associated with the diagnosis of meningiomas, a finding reported by a study of a small number of cases (n=6). Although the presence of the compound was not obvious upon visual evaluation, it was revealed and quantified by curve fits of the LCModel. The MRS results on glutathione were shown to be in agreement with the published data obtained with other chemical methods [109].

In addition to using sophisticated spectral analysis software, such as the LCModel, to achieve diagnostic conclusions, investigators may need to consider the experimental conditions upon which the spectral data are obtained. These considerations have a fundamental importance to any conclusions that one may hope to reach. Since almost all *in vivo* MRS are measured with a certain echo time, the relaxations that occur during those echoes reduce the measured concentrations from their intrinsic levels. Hence, corrections may be necessary. However, since such corrections can only be achieved with time-consuming calibrations, they are not feasible to conduct experimentally for each individual case. Instead, corrections according to tissue types may be measured and used [110] to validate the diagnostic values of tissue metabolite levels for certain diseases. These tissue-type specfic correlations permit the comparison of results, where the values are recorded under the same experimental conditions with the same amounts of relaxation time.

Another commonly encountered possible experimental artifact relates to the measurement sequence of MR examinations. As previously discussed, the advantage of MRS is to further investigate the chemical composition of a lesion identified by MRI. Nowadays, most MRIs are measured with the assistance of agents that enhance the contrast of the diseased lesion for interpretation of disease anatomy. The possible influence of these administered contrast agents to the resulting spectral data needs to be carefully evaluated before the data is employed for the dissemination of information about the disease. In reference to the commonly used Gd-DTPA agent, it was found that although it broadened the linewidth of Cho in gliomas, the changes in the peak areas of Cho were not significant [111]. Similar evaluation needs to be undertaken for other agents before there is any attempt to correlate MRS chemical data with diseases.

In vivo MRS measurable brain tumor metabolic profiles have been tested as a non-invasive means, both for children and adults, of monitoring tumors and their responses to therapies, including radiation effects [112-114], and chemotherapy differences [115, 116]. The potential contribution of MRS non-invasive monitoring towards the design of brain tumor treatments is apparent in its alleviation of the requirement of invasive biopsies. However, compared with diagnostic studies, these reports of monitoring trials included relatively small patient numbers. Hence, the potential influence of MRS in the brain tumor clinic still needs to be evaluated with large patient populations.

Breast Cancer

Breast cancer is another oncological area in which MRS reports on primary lesions and lymph nodes have been frequently published [117-119]. However, MRS technologies for breast examinations are not as mature as those utilized in brain studies because of the challenge introduced by the abundance of mobile lipids found in the breast. A new spectral strategy has been proposed to reduce the confounding effects of lipids to other metabolites in breast lesion MRS [120].

Fortunately, or perhaps unfortunately from the MR technique point of view, the *in vivo* MR spectrum of breast cancer is often very simple consisting only of lipids and Cho, and therefore although data evaluations present a somewhat simple task, the options to correlate these evaluations with clinical data are limited. A study of 38 patients showed that by using the elevated Cho levels, the sensitivity and specificity in differentiating breast malignancy from benign lesions were 83 and 87%, respectively [118]. Another study of 105 subjects, examined at a field strength of 4T (a higher field strength can produce better resolved MRS for better observation of different resonance peaks), confirmed these observations. It showed that Cho levels were significantly more elevated in the malignant breast lesions than in the benign abnormalities and normal breast tissues [117]. Elevated Cho levels were also reported with lymph nodes in the evaluations performed in breast cancer patients. Combining *in vivo* Cho data with the fine-needle aspiration biopsy (FNAB) results, the report concluded that the overall accuracy of *in vivo* MRS detection of malignancy was 90% [119].

The diagnostic function of Cho measured from *in vivo* MRS of breast cancer has been corroborated by *ex vivo* studies. Since the high lipid content of human breast tissue also complicates *ex vivo* analysis, FNAB needed to be obtained in order to acquire a breast tissue spectrum that was

diagnostically meaningful [121]. In a study of 218 FNAB samples from 191 patients with benign lesions, ductal carcinoma in situ (DCIS), and invasive carcinoma found that the resonance peak height ratio threshold of 1.7 (3.25 ppm vs. 3.05 ppm; or Cho vs. Cr), could be used to differentiate benign lesions from carcinoma with 95% sensitivity and 96% specificity. However, this single ratio identifier only worked if the SNR, particularly for Cho peaks at 3.25 ppm, was above 10. To extend the MRS differentiation capability below this limit, and more importantly, to search for a more robust diagnostic protocol for computer spectrum analysis, a more elaborated three-stage statistical classification strategy (SCS) that utilizes the entire MR spectrum rather than just two peaks is necessary. The advantages of SCS for relating broad line ^{1}H FNAB MR spectra to breast cancer diagnosis and possibly prognosis are discussed [121]. However, the more advanced the SCS is, the less evident were the direct connections with individual metabolites.

Similar conclusions of the role of Cho on breast cancer may be more clearly presented with HRMAS MRS studies. Even with lipid-rich tissue, HRMAS MRS has successfully produced high-resolution ^{1}H spectra. Results from a study at 9.4T of 19 cases of ductal carcinomas showed that both the high fat contents and the individual cellular metabolites could be measured from the same spectrum. In particular, phosphocholine could be quantified separately from choline; the ratio between phosphocholine and choline was found to correlate with tumor grades [122].

A more recent detailed HRMAS MRS study at 14.1T of 10 ductal carcinomas compared HRMAS MR spectra with those obtained using conventional MRS of perchloric acid tissue extracts. The study concluded that for breast tissue, HRMAS MRS was able to achieve spectral resolutions approaching those obtained using conventional MRS of extracts. 2D J-resolved and correlation (COSY) MRS were used to accurately assign metabolites [123].

Other Solid Tumors

In addition to brain tumors and breast cancer, single-voxel MRS studies of many other solid tumors have been reported over the past years, including cervical cancers [124-126], bone and soft tissue tumors [127], lymphomas [128], head and neck lymph node metastases [129], female intrapelvic tumors [130], and rectal adenocarcinomas [131]. Generally, these studies are more challenging than brain tumor MRS, because the regions of interest are located physically near the centers of physiological motions, and the SNR limitations of MRS require more signal averaging. To address complicationsarising from these motions, a breathhold (20 seconds) MRS scheme was proposed for 3T investigations, and was tested on patients with abdominal and thoracic metastatic lesions due to renal cell carcinomas [132].

Human cervical cancer specimens have been analyzed with *ex vivo* MRS since 1990 [133]. Broad-line resonances corresponding to lipid contribution at 0.9 ppm (-CH$_3$), 1.3 ppm (-CH$_2$-), and 3.8-4.2 ppm (CH) were found to distinguish invasive from preinvasive epithelial malignancy [134].

An interesting recent study combined both *in vivo* MRS and *ex vivo* HRMAS MRS analyses of human invasive and preinvasive cervical cancer of 51 subjects (nine normal controls, 10 preinvasive, and 32 invasive) (Fig. **2**). The study reported that by measuring triglyceride-CH$_2$ (1.3 ppm) *in vivo* with endovaginal coils, the presence of cancer could be predicted with sensitivity and specificity of 77.4 and 93.8%, respectively. *Ex vivo* measurements of the same resonance from biopsy samples presented 100% sensitivity, while the specificity of this marker was only 69% [125].

In addition to the discussed *ex vivo* MRS studies of cervical biopsies examined with the HRMAS technique, there are a number of recent *ex vivo*reports on HRMAS studies with statistically significant results [135, 136]. Of particular interest is a study that advanced from evaluations of a single (or a small number of) metabolite(s), to the use of principal component analysis (PCA) to analyze the entire spectrum. The loading profile of the principal component (PC) that can differentiate cancer from non-cancer samples is comprised primarily of Lac, the methyl and methylene groups of lipids, and, to a lesser extent, the choline-containing compounds, representing 63% of the variations in the spectra. In cervical cancer cases, this PC evaluation had higher scores, implying that the diagnostic compounds are present in elevated levels in the cancerous samples.

2.1.2.3. Other Clinical Conditions

In addition to its neurological and oncological applications, single-voxel MRS has been used for other medical evaluations, including the measuring of total body fat and muscle contents [137-141], and the composition of gallbladder bile [142, 143]. As a non-invasive procedure, MRS provided a platform with which Cho and lipids in bile were quantified.

2.1.3. Comments on Advantages and Limitations

Not surprisingly, some of the first 1H MRS experiments were tested on the brain, and the brain continues to be a good system for study with single-voxel MRS, despite the popularity of multivoxel methods. Because of the importance of the potential ability to perform "virtual", non-invasive biopsies, high resolution single-voxel methods will continue to be appropriate in brain.

It should be cautioned that relying on MRS alone for the oncological evaluation of malignancies other than brain tumors may not be necessary, since biopsy or surgical samples are relatively easy to access, and pathology studies can be done for evaluation. Hence, *in vivo* MRS criteria can be evaluated and verified with *ex vivo* analyses. But, with neurological conditions, even brain tumors, tissue sampling for *ex vivo* analyses is often not an option; hence, the ensuthssism towards the metabolic characterization of brain disease with *in vivo* MRS techniques is rational.

2.2. Proton Multi-Voxel Metabolite Imaging – MRSI

Although single-voxel MRS yields relatively high resolution spectra with clearly resolved metabolite peaks, multivoxel approaches have gained popularity due to their surveying ability. Currently multivoxel approaches represent the most common application of MR spectroscopy to the evaluation of clinical disease.
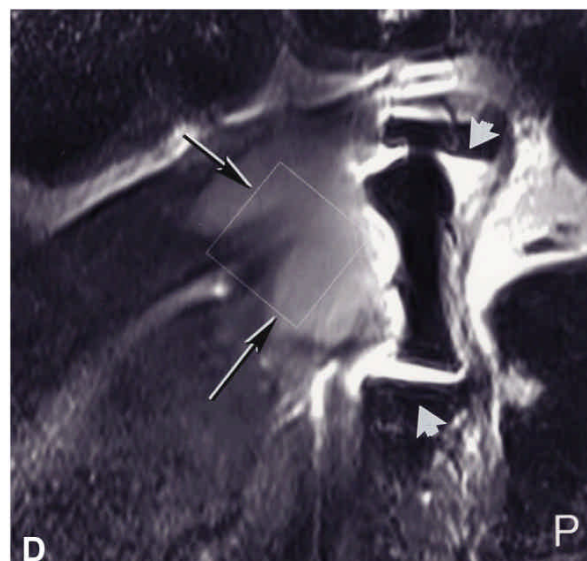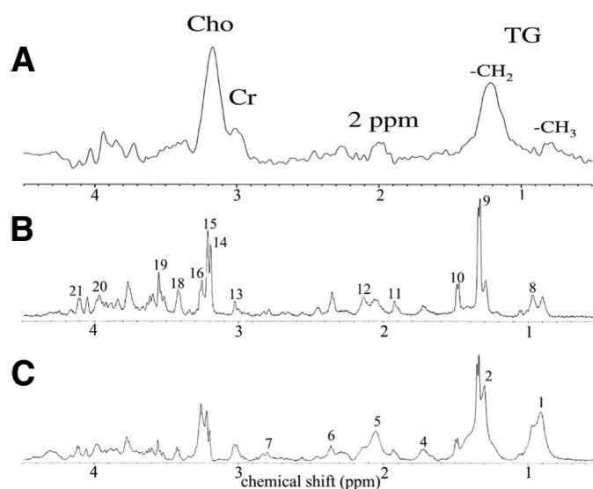
Fig. (2). [1]H MR spectra of cervical cancer. A). *in vivo* PRESS (TR=1600ms, TE=135ms); B) *ex vivo* CPMG at TE=135ms; C). *ex vivo* single pulse; D). A T2-weighted fast spin echo image (TR=4000ms, effective TE=88ms) used a 37mm diameter endovaginal coil (arrowheads) showed an irregular mass of tumor centrally within the cervix (arrors) filling 70% of the *in vivo* MRS VOI (marked square). (From Figure 3 in Mahon MM *et al*. [125]).

Despite the ability to correlate high resolution *in vivo* MRS acquired from large voxels with *ex vivo* tissue MRS metabolite profiles and with pathological evaluations, researchers recognized limitations of these methods for many pathologies in which there was heterogeneity of the lesion contained in the single large voxel. In brain, for instance, inflammation and edema often complicate stroke. Inflammatory cells, as well as normal tissue still present in the ischemic area contaminate the spectra from stroke voxels. Metabolite concentrations obtained from these spectra could be difficult to interpret because the individual contributions of normal and ischemic neural tissue, as well as inflammatory infiltrate, are impossible to deduce without histopathological investigation. In addition to problems of metabolite concentration, metabolite location is also problematic in studies using large voxels; that is, when one detects the presence of a particular metabolite, one cannot determine with any certainty from which cells, or even from which part of the voxel, the particular signal arises.

In addition to its surveying character, multivoxel studies can also take into account lesion heterogeneity by obtaining spectra from many relatively smaller voxels, often arranged in a two-dimensional grid. This technique, known as metabolic imaging or chemical shift imaging has the added advantage of being able to generate maps of metabolites of interest by specialized processing methods. The intensities of metabolite peaks in each spectrum can be mapped onto an image of the sampled region, similar to the activation maps familiar from the now-popular functional (f)MRI. For instance, one can acquire a 4x4 grid of 16 spectra, with a spatial resolution on the order of a cubic centimeter, approximately an order of magnitude lower than that attained with single-voxel techniques. By observing the change in metabolite peaks across the entire VOI, one can begin to correlate more clearly lesion pathogenesis with spectral findings. Since the SNRs of MRS spectra are directly related to the amount of the analyzed sample, by sacrificing in SNR with measurements of smaller volumes, one can approach the tangible goal of performing "virtual biopsy" of multiple regions with metabolic imaging, or MRSI. However, readers should be aware that this improved spatial resolution is at the expense of spectral resolution of the spectrum of each voxel.

2.2.1. Techniques

The general technique of MRSI is similar to the single-voxel MRS applications. A VOI is localized using either PRESS or STEAM sequences, modified to obtain spectra from the multiple small voxels of the matrix placed onto the VOI. As in single-voxel MRS, outer volume suppression techniques can be applied to avoid partial volume artifacts from the region outside the defined VOI. Upon detection of a VOL from a scout MRI, the user can visualize and place a grid onto the VOI. Some specialized techniques allow shaping of the region (to circles or free-form areas, rather than rectangular regions) or tilting of the grid over the VOI. The pulse sequence typically consists of 8-10 phase-encoding steps that generate an 8x8 to 10x10 array of rectangular voxels positioned over the defined VOI. One spectrum will be obtained from each voxel to achieve a spatial resolution on the order of a cubic centimeter, or smaller. The arrangement of the voxels in a grid-pattern has led to the term 2D-MRSI to distinguish single-voxel *in vivo* MRS from multi-voxel MRSI. Three-dimensional (3D) MRSI methods are also possible on some research scanner systems at this moment. In this review, we will consider both 2D and 3D phase-encoding techniques together.

With a single pulse sequence, multiple spectra are acquired simultaneously from the VOI indicated by the grid. Improvements in methods have allowed increasingly shorter acquisition times, enabling higher spectral resolution from

the ability to average over a larger number of acquisitions in a clinically tolerable time window. Ideally, combined MRI and MRSI evaluations can be conducted in less than one hour to minimize patient discomfort during data acquisition.

2.2.2. Clinical Applications

The same theme present in the use of single-voxel methods applies to multivoxel MRSI applications as well, in that MRSI studies are predominantely applied to investigations of brain pathology and solid cancers. This technique has particular relevance in cancers where single-voxel studies are clearly insufficient to address lesion heterogeneity and to survey the surroundings of solid tumors. Because of its sensitivity and higher spatial-spectral resolution, the technique has shown promise in aiding diagnosis, staging and even grading of malignant disease, as well as treatment planning, MR guided biopsy, and the monitoring of treatment response.

We will continue our clinical review on the path laid out in the presentation of single-voxel applications, beginning with neurological disorders, then proceeding to oncological diseases and finally, other clinical conditions. However, though we will attempt to categorize studies according to disease type, our review efforts will focus on the new insights of biomedical processes and new knowledge about diseases revealed by MRSI, which were not available with single-voxel MRS. When reviewing MRSI reports, the most important concept of which readers may wish to constantly remind themselves is that MRSI is a "mapping" approach targeted at evaluations of global changes of multiple regions, which should be familiar to radiologists who are used to image examinations.

2.2.2.1 Neurological Disorders

Neuro-Anatomy Studies

Before we discuss evaluations of various disorders, we wish to mention that we noticed a large number of neuro-anatomy studies that used MRSI to measure metabolite concentrations [144, 145] or ratios [146] in different brain regions simultaneously. Metabolite differences for NAA, Cho, Cr, Glx and MI were observed in these studies with healthy subjects. Documenting these regional differences is very important since these normal levels and their variations are the basis upon which detection and determination of abnormalities may be possible. A further level of complication is the changes of brain neurochemistry with age. This simple concept is readily acceptable to anyone, however documentation of these changes demands great efforts. Again, as a mapping task, many MRSI reports have been devoted to the topic, with subjects ranging from premature neonates (30-34 weeks of postconceptional age) to senior citizens of 89 y.o. [147-151]. In these studies, NAA, Cho, Cr, and occasionally MI are measured and their changes, correlated with age. However, from the existing data, even though some of these studies by the standard of a single project are extensive, for instance, with inclusion of 68 subjects covering three adult age groups [150], or 90 subjects of ages 4 to 88 years [148], we are compelled to comment that more studies may be needed to generate complete human brain metabolic maps for different age groups. The existing data is composed of measurements from different brain regions, and was analyzed and reported non-uniformly, with either metabolite ratios or concentrations.

Vascular Diseases and Traumas

Studies of vascular diseases and traumas have been reported. All of these studies shared the common theme of evaluation of the overall brain response to these conditions and attacks, rather than only a focus on lesions or the affected regions. For instance, in a study of nine patients with intracerebral hemorrhages, MRSI in combination with diffusion-weighted MRI revealed that the secondary neuronal injury after the onset may not follow the proposed mechanism of ischemia, for instead of observing the expected reduction in ADCs and the presence of Lac, as demonstrated with only one patient (Fig. **3**), the measurements of the areas surrounding the hemorrhages in eight others revealed the opposite [152]. A Lac increase was observed in 11 patients suffering from chronic cerebral infarction, and was found in correlation with the decrease of vascular reactivity quantified by PET [153]. A stroke MRSI study assisted by regional cerebral blood flow (rCBF) measured with SPECT (single-proton emission computer tomography) showed that a perfusion defect in the region of cortical diaschisis correlates with the NAA/Cr decrease in the white matter in the region [154]. Trauma effects on brain metabolites were surveyed for as many as 25 brain regions with MRSI after mild closed head injuries [155]. With Lac/NAA mappings before and after surgery, it was concluded that the often observed neurodevelopmental impairment following surgical repair of congenital heart disease might be attributable to conditions preexistent to the heart surgeries [156].

Demyelinating Disease

As we previously explained, since multiple sclerosis (MS) could be a global demyelination disorder, MRSI should be more suitable than single-voxel evaluations in assessing the brains of patients with this disease. MRSI has been tested in almost every aspect of the MS clinic, including: 1). investigations of MS metabolite patterns for diagnosis of primary progressive (PPMS), relapsing-remitting (RRMS), and secondary progressive (SPMS); 2). analyses of patients at early stages; 3). predictions of disease progression; and 4). evaluations of therapy efficacy. In all these studies, since MS is a white matter disorder, most often the measurements were centered on the so call "normal-appearing white matter (NAWM), " as defined from MR images.

Primary progressive disease is characterized by a gradual progression of the disease from its onset with no superimposed relapse and remission. A 3D MRSI study of 34 PPMS patients and ten controls of the central brain region (a total VOI 160 cc) at the middle of the corpus callosum presented a statistically significant 12% NAA/Cr decrease in the examined area of patients compared with controls. This total VOI in patients consists mostly of NAWM, gray matter (GM) and CSF, with less than 2% T2 MRI identified lesions [157]. Of note, this study measured patients both with 3D MRSI and 3D EPSI, which will be discussed latter, however there was no difference in the calculated NAA/Cr results
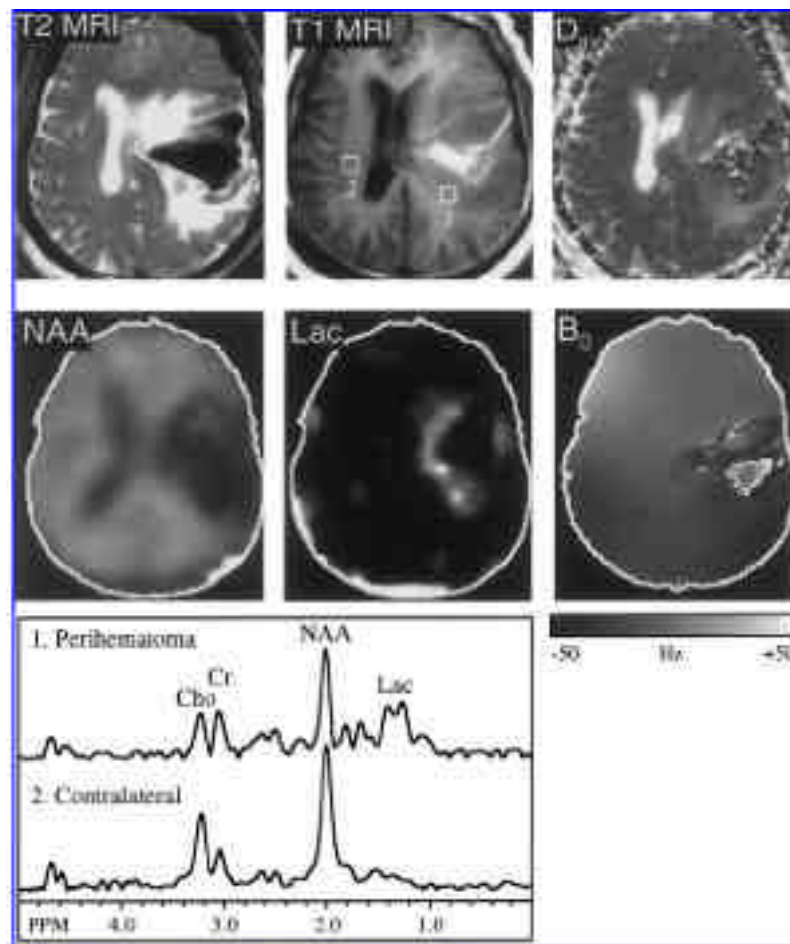
Fig. (3). T2-, T1-weighted, Dav (a.k.a. ADC) images; proton MRSI (NAA, lactate); B_0 field map; and selected proton spectra from perihematoma and contralateral VOI in a patient four days after symptom onset. Hematoma is dark on T 2-weighted images and shows a large local disturbance of field homogeneity (presumably due to the presence of paramagnetic deoxyhemoglobin). Dav or proton spectra could not be evaluated in the hematoma because of focal-field inhomogeneity. However, perihematoma regions show increased signal on T 2-weighted images, increased Dav, and increased lactate. Lactate is definitively assigned on the basis of a chemical shift of 1.33 ppm and 7-Hz J coupling. (From Figure 2 in Carhuapoma JR *et al*. [152]).

between the two approaches. When NAA and Cr were analyzed separately, the observed increase in NAWM Cr with PPMS patients (n=15) when compared with RRMS patients (n=13) and 20 control subjects supported the hypothesis that gliosis increases during this phase of the disease, whereas reduction in NAA in the lesions of both patient groups reflects the axonal loss that results in progressive disability [158].

Representing a more easily identifiable patient group, RRMS patients are the focus of many studies, either alone [159-163] or in comparisons with secondary progressive SPMS subjects [164-168]. RRMS is different from SPMS by its characteristic of relapse with appearance of new symptoms or worsening of preexisting ones, followed by periods of remission during which time the person fully or partially recovers from the deficits acquired during the relapse. However, SPMS is characterized by a steady progression of clinical neurological damage with most of these patients having previously experienced RRMS for a number of years.

Using 3D MRSI measurements of a total of 480cc, the overall reduction of NAA was 9%, with increases in Cr (22%) and Cho (32%), when NAWM from 11 RRMS patients were compared with measurements from nine control subjects. Observations of the study suggested that changes of Cho in NAWM preceded those of NAA and atrophy, and that Cho was the only metabolite among the three analyzed to have the power to differentiate RRMS from controls (100% specificity and 90% sensitivity) [160]. Another 2D MRSI analysis of voxels immediately superior to the roof of the lateral ventricles, confirmed the reduction of NAA in NAWM, while reporting that no statistical significances in Cr and Cho were observed. On the other hand, an increase of MI in NAWM was reported, as were reductions of Cho, NAA, and Glx in the cortical GM. In addition, Cr and Glx in GM, and MI in NAWM were found to significantly correlate with functional composite scores [161].

3D MRSI was attempted to evaluate lesions of RRMS patients during high-dose methylprednisolone therapy. With

MS, methylprednisolone is used because of its capacity to close the damaged blood-brain barrier and reduce inflammation. In this study of 14 RRMS patients, 29 contrast-enhancing and 24 non-enhancing lesions were analyzed along with NAWM. The study measured NAA, Cho, Cr, and Lac. Although, NAA/Cr did display lower values in both types of lesions than NAWM, and Cho/Cr had higher values in the enhanced lesions than in both the non-enhanced ones and NAWM, no treatment related metabolite change was recorded [163]. The differences between RRMS and SPMS were reported in the study of normal-appearing corpus callosum (NACC), and NAWM outside of the corpus callosum for 12 RRMS and 12 SPMS patients, and 15 healthy controls. For SPMS patients, NAA/Cr levels were lower in both measured regions compared with the controls, however the same reduction was only detected in NACC for the RRMS patients (p<0.001) along with decreased levels of Cho/Cr (p=0.003) [168].

In a study with a larger population of patients (88 RRMS and SPMS), reductions in NAA/Cr were detected before patients experienced significant disabilities, and in particular, the ratio was found to be linearly correlated with mild disabilities, represented by values of below 5 in the Expanded Disability Status Scale (EDSS) [165]. The predictive value of MRSI for the population of RRMS and SPMS was demonstrated by a study of the corpus callosum and the adjacent periventricular NAWM of 12 patients. It showed that NAWM voxels with significant higher Cho/Cr values presented MRI visible lesions in the following scans after six months than the unchanged voxels (p<0.001), and higher Cho/Cr values in voxels with lesions also resulted in lesion volume increases after 6 months (p<0.009) [167]. These results indicate the better sensitivity of MRSI than conventional MRI towards pathological changes in tissue, and were in agreement with the knowledge of the focal pre-lesion myelin membrane pathology.

A MRSI and fMRI study of nine RRMS and SPMS patients without impaired hand functions reported an interesting observation [166]. It was found that fMRI activation of the ipsilateral sensorimotor cortex with simple hand movements of patients was increased fivefold from controls (20.0±24.3 vs. 3.8±4.2), and was negatively correlated with the decreases in NAA (p=0.0001). This observation suggest the existence of a compensatory cortical adaptive response, and the authors further hypothesized that such responses may explain the discrepancy between the observation of MRI lesions and the clinical measures of disability.

Neuro-Degenerative Diseases

Applications of MRSI evaluations in neuro-degenerative disorders have been seen in AD [169-172] and ALS patients [65, 173-175]. When comparing large numbers of AD patients (n=56) and controls (n=54), it was apparent that NAA reductions in AD were region selective and concentrated in the medial temporal lobes and GM in the parietal lobes with no effect to WM and no changes in the frontal lobes. It was reported that by inclusion of NAA reduction to the volume measurements of the hippocampus, the accuracy of the classification of AD patients from controls improved from 89% to 95% [169]. When MRSI

measurements were combined with FDG (18F-2-fluoro-2-deoxy-D-glucose) PET analysis, significant correlations between metabolite ratios (Cho/Cr and NAA/Cho) and regional cerebral glucose metabolism quantified from PET were observed [172].

The advantage of global evaluation with MRSI was also demonstrated in ALS studies. For instance, NAA/(Cho+Cr) ratios were found to be significantly reduced in the motor cortex of ALS patients when compared with those in controls [173, 174], and furthermore, with longitudinal evaluations, decreases in all three metabolites were detected in motor cortex, but not in the non-motor regions [174].

Of particular interest, a study compared results obtained with single-voxel to those obtained with MRSI for 12 patients and ten controls. The single-voxels were placed bilaterally in the precentral gyrus, from which NAA/Cho, NAA/Cr, and Cr/Cho were determined. While no statistically significant differences were observed with these ratios between the ALS patients and the controls, MRSI measurements found that patients with clinically pronounced upper motoneuron signs had significantly lower (P = 0.037) NAA/Cr ratios in the more affected hemisphere [65].

MRSI has also been used in the evaluation of a proposed ALS therapy [176]. The therapy study was designed based on the hypothesis that ALS might be the result of excessive glutamate-mediated excitotoxicity. Gabapentin (GBP), a structural analog of the neurotransmitter GABA, was shown to modulate the GABA and glutamate neurotransmitter systems by reducing the synthesis of glutamate and hastening its degradation, thereby reducing fasciculation and muscular cramps for ALS patients. However, MRSI analysis of eight patients placed on this drug and 14 controls concluded that the difference in NAA/Cr between patients and controls observed before and after treatment did not change. It also noted that no improvement in patient clinical condition was seen [176].

Metabolic Diseases

An interesting MRSI study of metabolic disorder was reported on the evaluations of 76 women heterozygous for x-linked adrenoleukodystrophy (X-ALD). Although in general, x-linked disorders transmitted by female carriers affect only males, the study showed the reduction of NAA levels in the corticospinal projection fibers of these subjects who had normal MRI examinations [177]. In addition, the utility of MRSI in the evaluation of X-ALD patients (mostly men) has been tested [178, 179], and it was found that NAA/Cr can be used to measure disease progression [178].

A report of MRSI study on phenylketonuria concluded that in order to detect phenylalanine, the sum of all 256 MRSI voxels was necessary to achieve a sufficient SNR [180]. This presented the best illustration of the limitation of MRSI, when low metabolic concentrations in each voxel prevent the production of a visible MRSI map.

Psychiatry

Metabolite variations in schizophrenic patients have been probed with MRSI. In adults, NAA reductions were seen in hippocampus and thalamus, and in the latter, Cho was also reduced [181]. In children, however, the most prominent

changes were increases in Cr and Cho. It was measured that Cr increased 14.3% in superior anterior cingulated and Cho increased 30.3% in superior anterior cingulated, 13.3% in frontal cortex, and 13.5% in caudate head[182]. The increase in Cr was explained by the abnormal local cellular energy demands, while Cho results were in agreement with the hypothesis that children with early schizophrenia experience phospholipid membrane disturbances. MRSI has been used to evaluate brain responses to psychiatric treatments for schizophrenia patients [183, 184]. Higher NAA levels in dorsolateral prefrontal cortex were measured when patients were on antipsychotic treatments for more than four weeks [183]. This observation supports the belief that reduction in NAA may represent not only neuronal damage and death, but neuronal injuries that could be reversed with treatment.

Studies of other psychiatric conditions have also been reported, including the evaluation of a panic treatment [185], the measurement of Cr in autism where it was observed to be higher (21.1%) in the head of the right caudate nucleus and lower in the body of the left caudate nucleus (17.9%) and right occipital cortex (16.6%) [186], the increased Cho in medial thalamus with child obsessive-compulsive disorders [187], and investigations of unipolar and bipolar disorders [188-191]. With bipolar disorders, it was shown that Cho/Cr levels measured in the left cingulated cortex correlated with depression ratings, and the levels on Cho/Cr in the right cingulated cortex were higher in patients not on medication than in those on medications. Both patient cohorts had higher Cho/Cr levels than controls [190].

Although this psychiatry section may not be entirely appropriate to contain the following result, we cannot find a better-suited part of the review in which to discuss it. A hippocampus study of five ecstasy users showed that there was no measurable brain metabolic change with the users when compared with controls [192]. Perhaps, neuronal damage had not yet caught up with these particular subjects, at least in the tested brain region.

Epilepsy

Epilepsy presented as a neurological condition can be the result of many different neurological diseases. The survey of brain metabolite alterations for epilepsy patients may be the first step in understanding the causes of the condition, which may lead to the design of treatment plans. Hence, it is not surprising to see that a large number of MRSI studies have been devoted to the mapping of different types of epilepsies [193-200], to the investigation of metabolite correlations with brain neuro-electrical currents measured by EEG [201, 202], and to the development of metabolite prediction markers for surgical planning [203-207].

MRSI metabolite patterns were observed with epilepsy patients that verified clinical observations and confirmed hypothesis. Idiopathic generalized epilepsy (IGE) is considered to be related to the thalamo-cortical circuitry. A MRSI study of 20 IGE patients revealed the reduction of NAA/Cr in thalamus compared with controls, while no significant NAA/Cr difference was found with other examined brain regions [194]. Temporal lobe epilepsy (TLE) is the most frequent cause of focal and refractory seizures. The pathology of TLE frequently finds mesial temporal

sclerosis in temporal lobectomy specimens. Mesial temporal sclerosis displays neuronal loss in the hippocampal formation. A study of 15 patients with mesial temporal lobe epilepsy (mTLE) found that in the ipsilateral hippocampus, NAA concentration was 27.3% lower in patients compared with its concentration in controls (P < 0.001), and 18.5% lower compared with that in the contralateral side (P < 0.01). Using only hippocampal data, 60% of the cases of mTLE were correctly lateralized. Lateralization, determined using whole temporal lobe data, had 87% sensitivity and 92% specificity. Of note, in addition to hippocampus, NAA was bilaterally reduced in the frontal, parietal, and occipital lobes of patients with mTLE compared with that in controls (P < 0.01) [198]. The importance of lateralization in epilepsy evaluation has encouraged investigations in accurate analysis of MRSI data. A study of 9 patients and an equal number of controls compared visual inspections by three radiologists with computer quantification of NAA/(Cho+Cr) ratios for each voxel. The result showed that visual inspection correlated with the measured ratios, and thus concluded that while visual inspection can be preformed routinely by experienced radiologists with high accuracy, metabolite ratios from MRSI may provide more quantifiable assessments of the spatial distribution of the disease [200].

Another study intended to investigate the cause of TLE either as the result of an early injury or due to ongoing neuronal damage from seizures. With 82 consecutive patients of medically intractable, non-foreign-tissue TLE, the study was able to conclude that ipsilateral and contralateral NAA/Cr was negatively correlated with duration of epilepsy. Furthermore, it was found that patients with frequent seizures presented lower NAA/Cr than patients with no or rare seizures. The results suggest that although an early injury may cause asymmetric temporal lobe damage that is present at the onset of epilepsy, generalized seizures may induce additional neuronal damage, marking progression over the course of the disease [193].

Since EEG is used clinically to provide measures of epilepsy, the relationship between clinical EEG results and MRSI evaluation of brain areas is of great interest. A study of temporal and frontocentroparietal regions for 51 patients of TLE, extra-TLE and multilobar epilepsy reported that 38% of TLE and 50% of extra-TLE presented low NAA/Cr areas outside of the EEG defined disease areas [201]. However, the clinical implication of this observed discrepancy for treatment planning still needs more detailed investigation.

A number of reports have suggested the value of MRSI measured metabolites in predicting patient surgical outcomes. A comparative study of 32 patients undergoing epilepsy surgeries divided these patients in two groups: seizure-free or not seizure-free, with 16 patients in each group. The results showed that after surgeries, NAA/Cr in temporal lobe is significantly higher with the seizure-free group than with the non-seizure-free group, and in the seizure-free group the post-surgical NAA/Cr levels were higher than their pre-surgical values [205]. Patients (n=6) who underwent Gamma Knife radiosurgery on amygdale and hippocampus for mTLE were followed by MRSI for three years. The most significant spectroscopic changes were

reported to be in the first year after the irradiation, with the formation of edema and strong lipid signals in the spectra. Then, the subsequent changes presented were decreases in NAA, Cr, and Cho in the ipsilateral region of the brain to the irradiation. However, the most unexpected observation was the increases of NAA in the contralateral side after irradiation. The author explained this phenomenon as possible evidence that chronic seizure might cause secondary contralateral dysfunction. Irradiation eliminated seizures and allowed contralateral neurons to return to normal functioning [207]. Once again, a relationship between NAA and neuronal injury/recovery was proposed.

2.2.2.2. Oncological Diseases

Brain Tumors

MRSI has been extensively applied in human brain tumor studies. Our inexhaustive literature search produced more than three dozen reports since January, 2000. This clearly indicates the very large research efforts in the area, considering brain tumors represent only less than 1.4% of malignancy and less than 2.3% malignancy related deaths, for instance in the US [208]. But, as previously explained, brain, and particularly brain tumor, provided us with an almost ideal living phantom that allows the MRSI technique to be tested, developed and implemented.

Brain tumor MRSI studies have covered many clinical aspects. However, analyses of tumor metabolites still have fundamental importance in characterization of the diseases. For example, pediatric pilomyxiod astrocytomas were found to have less Cho, NAA, and Cr than pilocytic astrocytomas [209]. In addition to the expected NAA reduction and Cho increase in oligodendrogliomas, these tumors were found with increased Glx. The levels of Glx in the low grade oligodendrogliomas were higher than those in the low grade astrocytomas [210]. Gliomatosis cerebri were found to be differentiable from low grade gliomas [211]. However, evaluated from the current reports, it is apparent that the investigations of brain tumor MRSI have turned more directly towards clinical applicationss in the last couple of years.

The concept of trading single-voxel spectral resolution for MRSI spatial resolution was appreciated in brain tumor evaluations with detailed correlations of tumor metabolites with histopathological examinations of tissue samples obtained from MRSI voxels. For better correlations, MRSI compatible stereotactic biopsy approaches have been developed and applied [212, 213]. Furthermore, to account for tumor heterogeneity (may be determined macro-heterogeneity according to the histopathology scale), three dimensional MRSI techniques have been tested with voxel sizes between 0.2-1.0 cc [147, 214-216]. In order to achieve diagnosis or to be able to label different voxels for different pathological conditions, such as tumor, normal brain, or necrosis, MRSI data need to be processed with accuracy and reproducibility, from which numerical threshold values for tumor detection can be empirically determined [217], such as the Cho/NAA Index (CNI) proposed to identify tumor voxels. It was reported that by using the CNI threshold value, 2.5, on 68 newly diagnosed tumors, MRSI had 90% sensitivity and 86% specificity [216]. Another study of 18

glioma patients showed correlations between an increase in Cho, and the increased expression of proliferative index MIB-1 [218].

Applications of knowledge acquired through tumor metabolite pattern analyses, and from observed correlations with tumor pathology extended logically into evaluations of their capacity to predict patient outcomes and to monitor therapy response. However, before treatment planning, accurate assessment of tumor size and its extensions into the surrounding tissue is necessary. There are studies that have directly utilized the advantage of high spatial resolution, the distinguishing feature of MRSI. These studies aimed to improve tumor volume assessments based on MRSI quantified metabolite abnormalities, either for the planning of primary tumor treatments [219-222] or for the detection of residual disease after surgery [223].

While most of these works measured MRSI against conventional MRI, an interesting study compared MRSI with MEG (magnetoencephalography, measuring brain activities in terms of slow, fast waves and spike) for measurements of astrocytomas and meningiomas. It showed that brain pathological activities observed in MEG were localized in surrounding regions of the bulk of tumors, where mild reduction of NAA and slight accumulation of Lac were measured. The study suggested these areas might be considered as border zones between normal tissue and tumor tissues [220].

It was demonstrated with evaluations of pathologies of 247 tissue samples from 31 glioma patients, that with voxel sizes of 0.8 cc, MRSI data can better identify tumor boundaries than results from conventional MRI alone, and Cho signals can be used to detect the presence of tumor infiltrations into the surrounding tissues [219]. Another study of glioma patients (n=34, 22 WHO III and 12 GBM) concluded that although T2-weighted MRI presented tumor risk regions more than 50% larger than those proposed by MRSI, in 88% patients MRSI regions extended outside of the T2 regions by as much as 28 mm [221]. Similarly, discrepancies between MRI and MRSI were reported for the identification of residual tumors after surgeries [223]. Therefore, these two methodologies clearly report different cellular populations. However, pathological evaluations to determine which assessment is more meaningful and important to patient survival can be difficult to conduct even with primary tumor cases in which imaging results are known prior to surgery. This is due to special surgical procedures involving brain tumors. Except for the removal of the not so frequently observed solid lesions, the most useful tool to a neurosurgeon is not a scalpel, but rather a suction tip. Furthermore, the critical and mystical importance of the brain does not always allow us to plan surgeries according to the combined maximal area. Nevertheless, with low grade gliomas, the MRSI-defined, metabolically (e.g. high CNI) active tumors were restricted mainly to the T2 enhanced lesions with less then 2 cm extensions to the outside. This led the proposal to construct a clinical target volume by including both areas of T2 enhancing and metabolically active extensions. It was rationalized that this proposed volume would result in a reduction in the size and a change in the shape of the currently used standard clinical

target volumes, generated by adding uniform margins of 2-3 cm to the T2 lesions [224].

The proposed CNI measured before and after surgery has been tested for its value in predicting survival for glioma patients. The CNI maps generated for patients undergoing either regular or gamma knife surgeries, and in some studies combining with ADC and rCBV measurements, were evaluated against patient survival data [225-227]. In addition to Cho, the resonance peak representing the combination of Lac and lipid has also shown sensitivity in prognostics of glioma patients [226, 228].

More often than not, even for operable gliomas, patients are treated with radiation therapy after surgery because of the understandable neurooncological conflict between the concept of "clean margins" emphasized with other oncological surgeries, and the preservation of brain functions. However, radiation therapy delivers the same fatal effects to both cancer cells and normal tissues. Therefore, a major task in the neurooncological clinic is to differentiate recurrent tumors from lesions caused by radiation. Unfortunately, conventional imaging methods such as CT, MRI, PET, etc. cannot distinguish between the two types of lesions. This is a very active area for MRSI to contribute in clinical decision making. Both resonance peaks of Cho and Lac-lipids have shown ability to differentiate between the two types, with a Cho increase indicating tumor, and a Lac-lipid increase suggesting necrosis, in the latter cases there most likely to be radiation necroses [229-232]. In addition to evaluating radiation therapy effects on glioma patients, MRSI was also tested for monitoring chemotherapy of high grade gliomas with high-dose orally administered tamoxifen. Clinically, it was observed that there were no differences between responders and nonresponders in terms of age, sex, tumor type, mean tumor volume, mean Karnofsky scale score, mean number of weeks postradiotherapy, or mean amount of prior radiation exposure. However, metabolites measured with MRSI differed significantly between the two groups before and during treatment. Furthermore, the study indicated that linear discriminant analyses, based on patients' MRSI results, could accurately predict individual response to tamoxifen both before treatment, and at very early treatment stages (2 and 4 weeks) [233].

Pediatric brain tumors as a distinct group have also been investigated by MRSI studies. These studies included measurements of their metabolite patterns [234, 235], analyses of tumor progression [236], evaluations of therapies [237], and prediction of survival [238].

Prostate Cancer

Another major focus of MRSI in clinical oncology has been in the area of prostate cancer. Since prostate cancer presents the major male malignancy in many areas of the world, extensive MRS studies, both *in vivo* and *ex vivo*, have been reported.

Ex vivo studies are aimed at establishing metabolite markers of prostate cancer. An interesting study of intact prostate tissue, combining conventional MRS and high-pressure liquid chromatography (HPLC) analysis, aimed to measure the relationship between polyamines (PA) and prostate cancer [239]. Although PA were observed in the *ex*

vivo MRS and measured to have statistically significant drops in cancer samples with HPLC. However, no correlation between PA levels measured by MRS and those determined by HPLC was presented for the same cases due to the limited number of samples analyzed. Nevertheless, the study suggested the existence of a potential prostate biomarker, as well as a direction for future studies.

A recent conventional MRS study measured 71 prostate samples from 41 patients who underwent both cancer and non-cancer prostate surgeries [240]. Using peak ratios Cho/Cr and lipid/lysine, they were able to differentiate malignant from benign tissues with 97% sensitivity and 88% specificity.

Experiments of HRMAS *ex vivo* MRS analysis on human prostate tissues were reported in a qualitative study that also measured two dimensional correlation spectroscopy [241]. Another HRMAS MRS study of human prostate tissues from 16 patients was the first to perform quantitative pathology on the MRS specimens and to include multiple subjects [242]. The results of the study proved the validity of HRMAS MRS for the accurate determination of tissue histopathology. Both citrate (Cit) and PA were quantified from the tissue HRMAS MR spectra and were shown to be linearly correlated with the amounts of prostate normal epithelium. Recently, an interesting study of HRMAS MRS of tissues from 26 patients was published. In this study, prostate tissues were harvested post surgically under the guidance of 3D-MRSI from lesions that had been analyzed using *in vivo* MRS prior to prostatectomy. By combining the MRS results with quantitative pathology of the same tissue after spectroscopy, metabolite discriminators (i.e. ratios of Cit, PA, and Cho to Cr) were found to differentiate normal prostate epithelial tissue from cancer and stromal tissue. Furthermore, a correlation between the intensity of MIB-1 immunohistochemical staining and the ratio of Cho/Cr resonances was reported, supporting their findings *in vivo*. These conclusions were dependent on the assumption that the Cr concentration did not change during the disease process, which awaits verification [243].

With knowledge of prostate metabolites, obtained from *ex vivo* analyses and the identification of *in vivo* visible prostate metabolites: Cho, Cr, Cit and PA, in the past years the MRSI efforts have been seen in the further development of technology for more accurate tumor detection; in the attempt to establish a consultation role in patient treatment planning; and in tests of efficacy for the monitoring of treatments.

Technology developments cover a wide array of topics, including data acquisition methods, such as water and fat suppression and localizations [244, 245], MRSI reader accuracy [246], and tests of surface pelvic phase array vs. endorectal signal receiving coils [247]. Of particular interest, the coil test study showed that at 1.5T with measurements of 35 prostate cancer patients and five controls, there was no measurable difference between the two types of coils in terms of detection accuracy. A study testing dynamic contrast-enhanced (DCE) MRI and 2D MRSI was performed on 23 cancer patients, with cancer regions histopathologically quantified by whole-mount sections after radical prostatectomy. It concluded that by combining high-

resolution spatio-vascular information from DCE MRI, with a (Cho+Cr)/Cit threshold of 0.68, an indicator of tumor presence, cancer voxels could be reliably located and characterized [248].

Detection of prostate cancer from biopsy with patients considered to be at risk who have elevated PSA levels is challenging due to the extremely heterogeneous characteristics of the disease. Such tissue heterogeneity results in both high rates of false negative biopsies and for many patients, repeated biopsies. MRSI's non-invasive "biopsy" ability was tested with 24 consecutive patients who had at least one prior negative prostate biopsy, and presented with PSA levels between 4 and 40 ng/ml. Based on the MRSI finding, 10-core biopsies were carried out. By combining MRSI and MRI, the final analysis showed 100% sensitivity, 70.6% specificity, 58.3% positive and 100% negative predictive values, and the accuracy was determined to be 79.2% [249].

The utilization of prostate MRSI in patient treatment planning has been seen in the contribution of prostate metabolite information to the placement of radiation seeds in brachytherapy. Optimization procedures were developed that incorporated MRSI with ultrasound or CT images by coregistrations [250-252]. Furthermore, MRSI results have impacted brachytherapy directly by defining areas in the cancerous prostate in which boost doses should be introduced [253].

Patients undergoing a variety of prostate cancer treatments have been monitored by MRSI evaluations. A very recent study of 21 patients treated with an external radiation beam concluded that, in one hemiprostate, three or more voxels (size: 0.32 cc/ea) suspicious of containing cancer has 89% sensitivity and 82% specificity for the diagnosis of local tumor recurrence [254]. Another recent report presented the conclusion that MRSI examinations might provide an earlier indication of tumor response to brachytherapy than PSA response (28.9 months vs. 42.5 months) [255]. With hormone-deprivation therapy, comparisons between 65 treated, and 30 untreated patients showed that treatments resulted in time-dependent metabolite loss of all *in vivo* visible metabolites. While healthy and malignant tissues showed different time courses in the losses, Cit displayed more rapid reduction than the rates for Cho and Cr because of the known hormonal effects on Cit production, and the loss of its secluded prostate glandular ducts due to therapy [256].

Breast Cancer

The feasibility of MRSI has been tested in the diagnoses of other malignancies. A recent report on breast cancer showed that Cho was significantly more elevated in the malignant tissue than in benign tissue with measurements of 15 patients. However, the challenges for MRSI utilization in breast cancer were clearly illustrated by the study, with three out of 18 examined patients (~16.6%) not able to produce sufficient MRSI data, and with reporting Cho in terms of SNR, rather than in concentrations [257].

2.2.2.3. Other Clinical Conditions

Besides the above reviewed MRSI applications in the clinic, we also notice its attempts in the evaluation of many

other anatomic structures and conditions, such as knee joints for suspected internal derangement measured on an open magnet of 0.35T [258], bone marrow [259], spinal vertebra [260], muscles [261-264], and intramyocellular lipid levels [265]. However, other than the knee joint report, all the other reports dealt with the development and implementation of various MRSI methodologies, and were too early for actual clinical measurements for disease detection and diagnosis.

2.2.3. Echo Planer Spectroscopic Imaging – EPSI

The ability to localize metabolite concentrations to small voxels in an image represents a great technological advantage in the ability to generate maps of metabolite concentrations in the VOI. Spatial resolution of spectra (or spatial-spectral resolution) becomes a limiting factor in the ability to specifically localize a metabolite within a voxel. To address this limitation of MRSI, other forms of metabolite imaging have been developed and attempted to be employed in the clinic.

The most promising, recently developed metabolite imaging method is EPSI. EPSI, based on Mansfield's technique [266], is able to simultaneously and rapidly acquire spatial and spectral data at high resolutions, because all phase-encoding information is obtained in a single excitation. Because EPSI generates a frequency spectrum at each pixel in an image, with resulting voxel sizes on the order of 1 mm^3, maps of spectral components are created with extremely high spatial resolution to aid in the evaluation of metabolite changes.

Traditional MRSI relies on conventional MR imaging to locate a VOI for spectroscopic investigation, and to handle the post-spectral acquisition alignment of spectra with the original image to represent data and generate metabolite maps. EPSI however has the advantage of simultaneously acquiring spatial and spectral data from a single excitation. Following excitation, a readout gradient is applied in one spatial direction, and a series of phase encoding steps generates a train of spin echo images. By sampling along the echo images, a change of the signal over time is generated. Thus, following three dimensional FT, a frequency spectrum is generated at every pixel in an image with resulting voxel sizes on the order of 1 mm^3 depending on the field of view.

Recently, technical developments of EPSI have been witnessed in a number of research groups [267-270], with preliminary applications in brain imaging [271, 272] and in breast cancer detection [273-275]. Particularly, in the breast cancer study, eight patients having suspicious lesions were compared with six healthy female volunteers. The result showed that with high spatial-spectral resolutions achievable with EPSI, observation of tumor anatomic details was greatly improved [273]. An example of an infiltrating ductal carcinoma is shown in (Fig. **4**). In the figure, EPSI is compared with T1-weighted fat saturated MRI, illustrating the superior ability of EPSI to present clearly the cancer lesion. It is apparent that with the inclusion of spectral information that eliminates the chemical shift effect, which causes blurring at the fat-water interfaces, the resulting resolution and anatomical detail are better displayed in EPSI. Another reason for the observation of high-resolution EPSI is that the magnetic susceptibility gradients minimized for
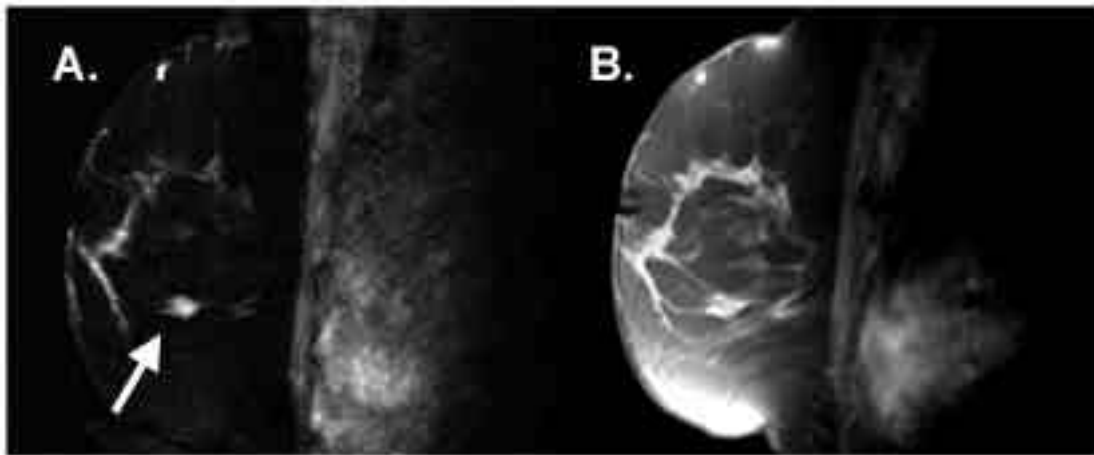
Fig. (4). A comparison between A). EPSI, and B). the standard clinical post-contrast, T1-weighted fat saturated images obtained from an infiltrating ductal carcinoma (arrow) (The images were kindly provided by Drs. Milica Medved and Gregory S. Karczmar at The University of Chicago).

EPSI images are synthesized from only one frequency component, rather than from the whole water resonance, which may be significantly broadened. With the demonstrated EPSI advantage, researchers at the University of Chicago, have begun integrating EPSI into clinical evaluations of patients with suspicious breast lesions identified with mammography.

EPSI has its own set of unique challenges and limitations. The bandwidth of the spectral acquisitions is sufficiently wide, for example, to separate the ^{1}H containing components of water and fat. The sensitivity, however, is low as for any other kind of metabolite imaging because of the low abundance of other materials. The gain in high spatial resolution still results in the sacrifice of spectral SNR and sensitivity. However EPSI shows great promise in its ability to clearly resolve anatomical structures from variations in water and fat chemical shift, and intensity across an image. Additionally, images generated from EPSI acquisitions do not require contrast agent injection or fat suppression. Images of water peak height or integrals can be made equal in spatial resolution to the T1-weighted image obtained from the first echo method, with fat and other metabolites now removed. This is especially useful as a conventional imaging technique, eliminating the need for tedious and frustratingly inconsistent fat saturation methods.

3. ISSUES REGARDING CLINICAL MRSI USE

3.1 A Few Practical Guidelines

MRS Training and Education

The development of MRS as a clinical diagnostic tool for radiology is currently in its infancy, despite its continuing success in researche. Spectroscopists, clinicians and scientists who have dedicated much effort to learning these techniques can easily perform an *in vivo* MRS/MRSI experiment. However, implementation of MRS on a broad clinical scale, or in multi-center studies is often far more challenging. There are many factors that should be considered before a spectrum of reasonable quality can be observed. Particularly, the one issue that is most often missed by reviewers is the need for training and education of the novice MRS users. Facilities, such as Massachusetts General Hospital's (MGH) Neuroradiology department, have started to employ dedicated clinical spectroscopists, on duty to maintain the MRS systems for all clinical scanners, monitor spectral analysis and quality, develop and implement new MRS protocols, and train neuroradiology residents, fellows, and all MR technicians in the acquisition of accurate and reliable MR spectra. The majority of technicians and clinicians are unfamiliar with MR spectra, and require education to differentiate a spectrum containing quality data from one of mostly noise. Training topics should include the effects of poor voxel placement, sources of artifacts such as motion and susceptibility [276, 277], lipid inclusion, and the status of magnet shimming. Post-processing of spectra, with consideration of phasing and scaling, should also be addressed in training. The establishment of websites at MGH for MR technicians with "quick reference" guides to voxel placement has also helped to improve the quality of ^{1}H MRS/MRSI.

Little guidance currently exists in the clinician's education that promotes a physician in determining when an MRS examination should be prescribed, and how should the result of the study be interpreted and incorporated in clinical decision making [278]. If MRS is to become a widely used clinical tool, further training and education may be necessary for clinicians to understand applications and limitations of MRS in following the progression or treatment of various diseases. Another issue that clinicians must be aware of is the complexity involved in translating MRS research results to patients cares [278]. Direct translation of statistically significant MRS research results typically found in large cohorts to an individual patient can often be difficult due to the inherent biologic variability among patients.

Localization

Many techniques have been developed for the purpose of localization in both single-voxel MRS and multivoxel MRSI. Early localization techniques revolved around the use of surface coils and ^{31}P MRS, but the most utilized techniques

today in single-voxel ^{1}H spectroscopy are PRESS and STEAM techniques. Both techniques excite only the VOI with frequency selective rf pulses. The flip angles, sequence timing and placement of gradient pulses are different for each technique. The nature of the echo signal is the major difference between the two techniques. Refocusing the complete net echo signal forms the echo in PRESS. STEAM, on the other hand only preserves part of the magnetization to produce the stimulated echo. This causes the SNR of PRESS to be greater than that for STEAM (theoretically by a factor of 2). Advantages and disadvantages for the use of each technique can be found in many publications [279-284]. MRSI uses either of these techniques, but is modified to obtain spectra from multiple smaller voxels placed within the VOI.

Water Suppression

The large concentration of water compared to the miniscule amount of metabolites that exists in tissues present a great challenge to performing ^{1}H MRS/MRSI. In clinical ^{1}H MRS, measurement sequences must include ways to suppress the predominant water signal. Water suppression does not have to be complete, and a method that allows for 50-100-fold reduction in the water peaks amplitude may be sufficient. A small water peak can be used for frequency and phase corrections before being subtracted from the MR signal. This technique reduces baseline distortions that can resulted from water suppression. The most commonly used water suppression method is achieved by eliminating the water signal prior to exciting and observing the FID. This is achieved through the use of a chemical shift selective saturation (CHESS) pulse, which is followed by a dephasing gradient pulse [12]. Effective water suppression can also be achieved with other techniques such as water suppression enhanced through T1 effects (WET) [285], and with the use of multiple repetitions of selective pulse and dephasing gradient. Drastic reduction of water signal in spectroscopy with the stimulated echo acquisition mode, or DRYSTEAM, uses this multiple pulse technique [286].

Multi-center Studies

The translation of meaningful research observations into clinically applicable examinations for any disease or condition need verification both with sufficient numbers of subjects and from different clinical centers. When considering the application of MRS/MRSI on a multi-center scale, the chances for errors increase exponentially. Multiple cites, having people with various levels of training, who have varying ideas of what parameters ensure a high quality spectrum, each with different hardware specifications (coils, magnets, etc.), all increase the chance of injecting serious error into the results. An effective means of avoiding error is declaring one site the principal site, which will design the necessary protocol and disseminate it to the other sites. Metabolite phantoms, all created from the same solution at the same time, should be shipped to all centers, and routine spectroscopy quality control analyses should be performed on the phantom in order to assess inter-site reliability and instrument stability of each site at all time. The data from both the phantom and the enrolled patients should be analyzed by a designated site for spectral quantification to

ensure that the same fitting parameters are used in analyzing the data [47].

3.2. Challenges to MRS and MRSI as Clinical Evaluation Tools

Narrow Chemical Shift Imaging Range

Most metabolites of interest found in a ^{1}H MRS spectrum occur in a small chemical shift range of 10-15 ppm. Quantification of ^{1}H spectra obtained using a high field instrument is easier than *in vivo* due to the increased resolution in the spectrum. However, most clinical MRS occurs on magnets with lower field strengths (1.5 T or less), which results in a spectrum with overlapping peaks for metabolites, thereby causing quantification difficulties. The impact of this issue may be reduced by different approaches. The selective editing or suppression of specific resonances can allow for easier and more accurate assessment of metabolites. Spectral editing can be achieved by designing pulse sequences which exploit T1 and T2 relaxation differences of metabolites, spin coupling, quantum coherence [287, 288], and resonance frequencies [289]. For instance, these techniques allow drug-induced variations in GABA to be monitored and detected in the human brain, giving insights into the effects of therapy on patients with epilepsy [290]. *In vivo* [1]H 2D MR correlation spectroscopy was found to facilitate separation of metabolite and macromolecule peaks overlapping with GABA and creatine in the 1D spectrum [291, 292]. This technique was successfully used to follow epilepsy patients treated with a ketogenic diet [291].

As MR technology and application in radiology departments progress, the use of higher field magnets (3.0 T and above) will become more prevalent. For instance, the use of a 4 T scanner has made it is possible to improve Cho quantification in breast cancer [117]. However, with higher fields, the use of higher order shims must be considered to achieve increased spectral, spatial and temporal resolution [293, 294]. Transitions to higher field will also benefit MRS studies involving nuclei with low gyromagnetic ratios such as ^{13}C and [31]P [295-297]. Although difficulties arise with the use of high field magnets, several studies have demonstrated that these limitations can be overcome with time and effort [294, 298].

Methods for Archiving Data

Picture archiving and communication system (PACS) is crucial for the daily clinical image operations of a clinical radiologist. While radiologists have used this method for years as a practical way to work in different physical locations at once, the archiving of spectroscopic data, especially the large volumes of MRSI data, has been difficult and is usually a problem left to each site. It is often achieved by having the MR technicians post-process the data, and through the use of software to generate images of the spectrum, they can be posted on the web and viewed from other sites. Working towards this goal, a web archival and interface system was created and implemented in the Department of Radiology at University of California, Los Angeles [299] that allowed for retrieval of MRSI data by radiologists via any PC from internet. This system allows the users to specify the voxel location that they wish to observe, to view both the spectra and all corresponding images, and to

provide integral and ratio data of the metabolites measured from spectra. It permits MRSI data to be viewed world wide, but requires security measures to ensure patient confidentiality. However, this system does not allow a user to reprocess the raw data, since what the user actually views are pictures of the processed raw data. This technique obviously has many limitations and a better solution is necessary for clinicians to be able to post-process the data themselves after they have been trained to perform the task.

Quality Assurance of Spectral Data

Little has been published on the issues of quality assurance or even to define the spectral quality that must be obtained to ensure accurate results [300-303]. It is admittedly true that when experts in the field of MRS are asked to define the qualities which make up a "good" spectrum, the reply is that it depends on a multitude of factors such as use of short or long echo time (TE), use of *in vivo* MRS or MRSI, and even which organs/tissue types are being examined. An excellent review was recently published with the hope of beginning a much needed dialogue between these experts to form a general consensus of parameters and quality factors needed for clinical MRS use [276]. This review not only discusses causes of artifacts and problems in automated fitting models, but also delineates criteria for quality assurance and rejection of data.

Diagnosis using Automated Pattern Recognition Techniques

Radiologists quite often rely on visual examination to interpret a spectrum, which is a biased approach that lacks quantification and is based solely on the training of the individual. Automated pattern recognition techniques for diseases, such as brain tumor classification, have been proposed [304], but have relied on manual prepossessing of the phasing or measuring peak areas [305]. Reports exist for the INTERPRET project, which has developed a system for the classification of brain tumors based on comparing an unknown spectrum of a tumor to a database of tumor spectra each with a known pathology classification [106, 306]. In one report, brain tumors were classified as either meningioma, or astrocytomas, based on the automated pattern recognition. The system relied on the use of a training data set that consisted of 94 spectra gathered from 3 different sites. When 50 other cases were used to test the recognition system, linear discriminate analysis successfully classified 48/50 in the test set, as proven by histopathology, and the remaining two were considered to be atypical cases. Testing spectra obtained from multiple sites indicated that the differences in spectral patterns are greater between tumor types than for acquisition parameters [106].

Quantification and Interpretation of Spectra

Clinicians and scientists who have a more intimate understanding of MRS utilize many methods for quantification of *in vivo* MR spectra [117, 307-314]. A relative calculation can be performed in which metabolite peaks of interest are integrated and are normalized to a metabolite that is assumed to be unchanged by the disease. Cr is typically the metabolite of choice for normalization because it is believed that its concentration does not vary with age. The results of a recent 3D ^{1}H MRS study, however,

indicate that Cr may not be a reliable denominator because its concentration varies among normal volunteers [315].

Another means of spectral quantification is the use of absolute units. An example of this is to express the metabolite contents as a percentage based on the area of the unsuppressed water signal, without further corrections or conversions. Many prefer absolute concentration measurements instead, but this approach also has complications due to overlapping resonances found within spectra, inherit propogation of errors due to correction factors used, and unpredictable forms of both line shape and baseline.

Several fitting routines have been developed such as linear combination LCModel [89, 90] and the PROBE package from GE [316]. Before spectral fitting occurs, it is imperative to pay attention to the quality of spectra, or else the likelihood of inaccurate results within a study increases. Spectral features that may influence accurate fitting include distortions due to motion [277, 317, 318], artifacts [276], poor signal to noise ratio, broad peak linewidths, and lipid contamination from the scalp. The macromolecule signal contribution in a spectrum should also be considered when quantifying and interpreting a spectrum [319, 320], as it has been found to change with certain diseases.

An alternative means of quantifying metabolites and statistically significant finding differences between optimally obtained spectra is to perform principal component analysis. Some groups have begun using this method [321, 322]. The primary benefit is that it introduces the least amount of error in the interpretation of the spectra because it relies on all the data set, not just individual, user-selected metabolites to account for the amount of variation among the peaks in a set of spectra. While this still does not overcome the problem of improperly obtaining and processing spectra, it does address the issue of quantification. Full disclosure of processing parameters, in addition to acquisition parameters is also vital.

Patient Issues

Even with all the scientific and technological difficulties solved, there is still an issue of primary importance for the patient, which must be resolved before MRS can be used routinely in clinic, at least in the United States. The principal difficulty is due to the lack of reimbursement by many insurance policies for MRS studies, which ultimately places the financial burden on the patient [278]. This issue, although will determine the ultimate success of MRS and MRSI in medical practices, is indeed beyond our expertise.

ACKNOWLEDGMENTS

ABBREVIATIONS

AD   =   Alzheimer disease

ADC	=	Apparent diffusion coefficient
ALS	=	Amyotrophic lateral sclerosis
B_o	=	Externally applied magnetic field
Cho	=	Choline (*in vivo* including phosphocholine and glycerophosphocholine)
Cit	=	Citrate
CNI	=	Choline-to-NAA index
CNS	=	Central nervous system
Cr	=	Creatine (*in vivo* including phosphocreatine)
CSI	=	Chemical shift imaging
DCE	=	Dynamic contrast-enhanced
DWI	=	Diffusion-weighted imaging
EDSS	=	The expanded disability status scale
EPSI	=	Echo planar spectroscopic imaging
FID	=	Free induction decay
FNAB	=	Fine-needle aspiration biopsy
FT	=	Fourier transform
GABA	=	-aminobutyric acid
GBM	=	Glioblastoma multiforme (WHO IV)
Glx	=	Glutamate and/or glutamine (*in vivo*)
GM	=	Gray matter
HPLC	=	High-pressure liquid chromatography
HRMAS	=	High resolution magic angle spinning
IGE	=	Idiopathic generalized epilepsy
Lac	=	Lactate
LCModel	=	Linear combination model
MET	=	Metastasis
MGH	=	Massachusetts general hospital
MI	=	Myo-inositol
MNG	=	Meningioma
MRS	=	Magnetic resonance spectroscopy
MRSI	=	Magnetic resonance spectroscopic imaging
MS	=	Multiple sclerosis
mTLE	=	Mesial temporal lobe epilepsy
NAA	=	N-acetyl aspartate
NAWM	=	Normal appearing white matter
NMR	=	Nuclear magnetic resonance
PA	=	Polyamines
PC	=	Principal component
PCA	=	Principal component analysis
PD	=	Parkinson disease
Phe	=	Phenylalanine

PPMS	=	Primary progressive multiple sclerosis
PRESS	=	Point-resolved spectroscopy
PSA	=	Prostate specific antigen
rCBF	=	Regional cerebral blood flow
rf	=	Radiofrequency
RRMS	=	Relapsing-remitting multiple sclerosis
SNR	=	Signal to noise ratio
SPMS	=	Secondary progressive multiple sclerosis
STEAM	=	Stimulated echo ecquisition eode
T1	=	Longitudinal relaxation time
T2	=	Transverse relaxation time
T	=	Tesla, the unit for magnetic field strength
TE	=	Echo time
TLE	=	Temporal lobe epilepsy
TM	=	Mixing time
TR	=	Recycle time
VOI	=	Volume of interest
WHO	=	World health organization
WM	=	White matter

REFERENCES

[1] Damadian R. Tumor detection by nuclear magnetic resonance. Science 1971; 171(976): 1151-1153.

[2] Callaghan PT. Principles of Nuclear Magnetic Resonance Microscopy. New York: Oxford University Press Inc.; 2003. 1-492 p.

[3] Haacke EM, Brown RW, Thompson MR, Venkatesan R. Magnetic Resonance Imaging: Physical Principles and Sequence Design. New York, NY: John Wiley & Sons, Inc.; 1999. 1-914 p.

[4] Salibi N, Brown MA. Clinical MR Spectroscopy: First Principles. New York: John Wiley & Sons, Inc.; 1998. 1-220 p.

[5] Ernst RR, Bodenhausen G, Wokaun A. Principles of Nuclear Magnetic Resonance in One and Two Dimension. New York: Clarendon Press; 1988. 1-610 p.

[6] Slichter CP. Principles of Magnetic Resonance. Cardona M, Fulde P, von Klitzing K, Queisser HJ, editors. New York: Springer-Verlag New York Berlin Heidelberg; 1990. 1-655 p.

[7] Pykett IL, Rosen BR. Nuclear magnetic resonance: *in vivo* proton chemical shift imaging. Work in progress. Radiology 1983; 149(1): 197-201.

[8] Maudsley AA, Hilal SK, Simon HE, Wittekoek S. *In vivo* MR spectroscopic imaging with P-31. Work in progress. Radiology 1984; 153(3): 745-750.

[9] Gordon RE. Topical magnetic resonance. Biosci Rep 1982; 2(9): 701-706.

[10] Gordon RE, Hanley PE, Shaw D, Gadian DG, Radda GK, Styles P, Bore PJ, Chan L. Localization of metabolites in animals using 31P topical magnetic resonance. Nature 1980; 287(5784): 736-738.

[11] Cox SJ, Styles P. Toward biochemical imaging. J Magn Reson 1980; 40: 209-212.

[12] Haase A, Frahm J, Hanicke W, Matthaei D. 1H NMR chemical shift selective (CHESS) imaging. Phys Med Biol 1985; 30(4): 341-344.

[13] Bottomley PA; General Electric Company, assignee. Selective volume method for performing localized NMR spectroscopy. United States patent 4480228. 1984 October 30, 1984.

[14] Frahm J, Merboldt KD, Hanicke W, al. e. Stimulated echo imaging. J Magn Reson 1985; 64: 81-95.

[15] Maudsley AA, Oppelt A, Ganssen A. Rapid measurement of magnetic field distribtions using nuclear magnetic resonance. Forsch u Entwickl - Ber Bd 1979; 8(6): 326-331.

[16]   Maudsley AA, Hilal SK, Simon HE; Philips Medical Systems, Inc., assignee. NMR Imaging Methods. United States patent 4585992. 1986 April 29, 1986.

[17]   Brown TR, Kincaid BM, Ugurbil K. NMR chemical shift imaging in three dimensions. Proc Natl Acad Sci U S A 1982; 79(11): 3523-3526.

[18]   Gonen O, Viswanathan AK, Catalaa I, Babb J, Udupa J, Grossman RI. Total brain N-acetylaspartate concentration in normal, age-grouped females: quantitation with non-echo proton NMR spectroscopy. Magn Reson Med 1998; 40(5): 684-689.

[19]   Bonneville F, Moriarty DM, Li BS, Babb JS, Grossman RI, Gonen O. Whole-brain N-acetylaspartate concentration: correlation with T2-weighted lesion volume and expanded disability status scale score in cases of relapsing-remitting multiple sclerosis. AJNR Am J Neuroradiol 2002; 23(3): 371-375.

[20]   Bottomley PA. Spatial localization in NMR spectroscopy *in vivo*. Ann N Y Acad Sci 1987; 508: 333-348.

[21]   Matthaei D, Frahm J, Haase A, Merboldt KD, Hanicke W. Multipurpose NMR imaging using stimulated echoes. Magn Reson Med 1986; 3(4): 554-561.

[22]   Cheng LL, Ma MJ, Becerra L, Ptak T, Tracey I, Lackner A, Gonzalez RG. Quantitative neuropathology by high resolution magic angle spinning proton magnetic resonance spectroscopy. Proc Natl Acad Sci U S A 1997; 94(12): 6408-6413.

[23]   Urenjak J, Williams SR, Gadian DG, Noble M. Specific expression of N-acetylaspartate in neurons, oligodendrocyte-type-2 astrocyte progenitors, and immature oligodendrocytes *in vitro*. J Neurochem 1992; 59(1): 55-61.

[24]   Urenjak J, Williams SR, Gadian DG, Noble M. Proton nuclear magnetic resonance spectroscopy unambiguously identifies different neural cell types. J Neurosci 1993; 13(3): 981-989.

[25]   Galanaud D, Nicoli F, Le Fur Y, Guye M, Ranjeva JP, Confort-Gouny S, Viout P, Soulier E, Cozzone PJ. Multimodal magnetic resonance imaging of the central nervous system. Biochimie 2003; 85(9): 905-914.

[26]   Heerschap A, Kok RD, van den Berg PP. Antenatal proton MR spectroscopy of the human brain *in vivo*. Childs Nerv Syst 2003; 19(7-8): 418-421.

[27]   Kok RD, van den Bergh AJ, Heerschap A, Nijland R, van den Berg PP. Metabolic information from the human fetal brain obtained with proton magnetic resonance spectroscopy. Am J Obstet Gynecol 2001; 185(5): 1011-1015.

[28]   Kok RD, van den Berg PP, van den Bergh AJ, Nijland R, Heerschap A. Maturation of the human fetal brain as observed by 1H MR spectroscopy. Magn Reson Med 2002; 48(4): 611-616.

[29]   Kreis R, Hofmann L, Kuhlmann B, Boesch C, Bossi E, Huppi PS. Brain metabolite composition during early human brain development as measured by quantitative *in vivo* 1H magnetic resonance spectroscopy. Magn Reson Med 2002; 48(6): 949-958.

[30]   Valenzuela MJ, Sachdev PS, Wen W, Shnier R, Brodaty H, Gillies D. Dual voxel proton magnetic resonance spectroscopy in the healthy elderly: subcortical-frontal axonal N-acetylaspartate levels are correlated with fluid cognitive abilities independent of structural brain changes. Neuroimage 2000; 12(6): 747-756.

[31]   Cooke FJ, Blamire AM, Manners DN, Styles P, Rajagopalan B. Quantitative proton magnetic resonance spectroscopy of the cervical spinal cord. Magn Reson Med 2004; 51(6): 1122-1128.

[32]   Graham GD, Hwang JH, Rothman DL, Prichard JW. Spectroscopic assessment of alterations in macromolecule and small-molecule metabolites in human brain after stroke. Stroke 2001; 32(12): 2797-2802.

[33]   Graham GD, Barker PB, Brooks WM, Morris DC, Ahmed W, Bryniarski E, Hearshen DO, Sanders JA, Holshouser BA, Turkel CC. MR spectroscopy study of dichloroacetate treatment after ischemic stroke. Neurology 2000; 55(9): 1376-1378.

[34]   Parsons MW, Li T, Barber PA, Yang Q, Darby DG, Desmond PM, Gerraty RP, Tress BM, Davis SM. Combined (1)H MR spectroscopy and diffusion-weighted MRI improves the prediction of stroke outcome. Neurology 2000; 55(4): 498-505.

[35]   Rumpel H, Lim WE, Chang HM, Chan LL, Ho GL, Wong MC, Tan KP. Is myo-inositol a measure of glial swelling after stroke? A magnetic resonance study. J Magn Reson Imaging 2003; 17(1): 11-19.

[36]   Ashwal S, Holshouser BA, Shu SK, Simmons PL, Perkin RM, Tomasi LG, Knierim DS, Sheridan C, Craig K, Andrews GH, Hinshaw DB. Predictive value of proton magnetic resonance

[37]   Barkovich AJ, Westmark KD, Bedi HS, Partridge JC, Ferriero DM, Vigneron DB. Proton spectroscopy and diffusion imaging on the first day of life after perinatal asphyxia: preliminary report. AJNR Am J Neuroradiol 2001; 22(9): 1786-1794.

[38]   Kadri M, Shu S, Holshouser B, Deming D, Hopper A, Peverini R, Ashwal S. Proton magnetic resonance spectroscopy improves outcome prediction in perinatal CNS insults. J Perinatol 2003; 23(3): 181-185.

[39]   Malik GK, Pandey M, Kumar R, Chawla S, Rathi B, Gupta RK. MR imaging and *in vivo* proton spectroscopy of the brain in neonates with hypoxic ischemic encephalopathy. Eur J Radiol 2002; 43(1): 6-13.

[40]   Maneru C, Junque C, Bargallo N, Olondo M, Botet F, Tallada M, Guardia J, Mercader JM. (1)H-MR spectroscopy is sensitive to subtle effects of perinatal asphyxia. Neurology 2001; 57(6): 1115-1118.

[41]   Brooks WM, Stidley CA, Petropoulos H, Jung RE, Weers DC, Friedman SD, Barlow MA, Sibbitt WL, Jr., Yeo RA. Metabolic and cognitive response to human traumatic brain injury: a quantitative proton magnetic resonance study. J Neurotrauma 2000; 17(8): 629-640.

[42]   Garnett MR, Blamire AM, Corkill RG, Cadoux-Hudson TA, Rajagopalan B, Styles P. Early proton magnetic resonance spectroscopy in normal-appearing brain correlates with outcome in patients following traumatic brain injury. Brain 2000; 123 (Pt 10): 2046-2054.

[43]   Garnett MR, Blamire AM, Rajagopalan B, Styles P, Cadoux-Hudson TA. Evidence for cellular damage in normal-appearing white matter correlates with injury severity in patients following traumatic brain injury: A magnetic resonance spectroscopy study. Brain 2000; 123 (Pt 7): 1403-1409.

[44]   Garnett MR, Corkill RG, Blamire AM, Rajagopalan B, Manners DN, Young JD, Styles P, Cadoux-Hudson TA. Altered cellular metabolism following traumatic brain injury: a magnetic resonance spectroscopy study. J Neurotrauma 2001; 18(3): 231-240.

[45]   Son BC, Park CK, Choi BG, Kim EN, Choe BY, Lee KS, Kim MC, Kang JK. Metabolic changes in pericontusional oedematous areas in mild head injury evaluated by 1H MRS. Acta Neurochir Suppl 2000; 76: 13-16.

[46]   Chang L, Ernst T, Witt MD, Ames N, Gaiefsky M, Miller E. Relationships among brain metabolites, cognitive function, and viral loads in antiretroviral-naive HIV patients. Neuroimage 2002; 17(3): 1638-1648.

[47]   Lee PL, Yiannoutsos CT, Ernst T, Chang L, Marra CM, Jarvik JG, Richards TL, Kwok EW, Kolson DL, Simpson D, Tang CY, Schifitto G, Ketonen LM, Meyerhoff DJ, Lenkinski RE, Gonzalez RG, Navia BA. A multi-center 1H MRS study of the AIDS dementia complex: validation and preliminary analysis. J Magn Reson Imaging 2003; 17(6): 625-633.

[48]   Samann PG, Schlegel J, Muller G, Prantl F, Emminger C, Auer DP. Serial proton MR spectroscopy and diffusion imaging findings in HIV-related herpes simplex encephalitis. AJNR Am J Neuroradiol 2003; 24(10): 2015-2019.

[49]   Gupta RK, Vatsal DK, Husain N, Chawla S, Prasad KN, Roy R, Kumar R, Jha D, Husain M. Differentiation of tuberculous from pyogenic brain abscesses with *in vivo* proton MR spectroscopy and magnetization transfer MR imaging. AJNR Am J Neuroradiol 2001; 22(8): 1503-1509.

[50]   Garg M, Gupta RK, Husain M, Chawla S, Chawla J, Kumar R, Rao SB, Misra MK, Prasad KN. Brain abscesses: etiologic categorization with *in vivo* proton MR spectroscopy. Radiology 2004; 230(2): 519-527.

[51]   Cucurella MG, Rovira A, Rio J, Pedraza S, Tintore MM, Montalban X, Alonso J. Proton magnetic resonance spectroscopy in primary and secondary progressive multiple sclerosis. NMR Biomed 2000; 13(2): 57-63.

[52]   Garbern JY, Yool DA, Moore GJ, Wilds IB, Faulk MW, Klugmann M, Nave KA, Sistermans EA, van der Knaap MS, Bird TD, Shy ME, Kamholz JA, Griffiths IR. Patients lacking the major CNS myelin protein, proteolipid protein 1, develop length-dependent axonal degeneration in the absence of demyelination and inflammation. Brain 2002; 125(Pt 3): 551-561.

[53]   Antuono PG, Jones JL, Wang Y, Li SJ. Decreased glutamate + glutamine in Alzheimer's disease detected *in vivo* with (1)H-MRS at 0.5 T. Neurology 2001; 56(6): 737-742.

[54]   Block W, Traber F, Flacke S, Jessen F, Pohl C, Schild H. In-vivo proton MR-spectroscopy of the human brain: assessment of N-acetylaspartate (NAA) reduction as a marker for neurodegeneration. Amino Acids 2002; 23(1-3): 317-323.

[55]   Catani M, Mecocci P, Tarducci R, Howard R, Pelliccioli GP, Mariani E, Metastasio A, Benedetti C, Senin U, Cherubini A. Proton magnetic resonance spectroscopy reveals similar white matter biochemical changes in patients with chronic hypertension and early Alzheimer's disease. J Am Geriatr Soc 2002; 50(10): 1707-1710.

[56]   Dixon RM, Bradley KM, Budge MM, Styles P, Smith AD. Longitudinal quantitative proton magnetic resonance spectroscopy of the hippocampus in Alzheimer's disease. Brain 2002; 125(Pt 10): 2332-2341.

[57]   Kantarci K, Jack CR, Jr., Xu YC, Campeau NG, O'Brien PC, Smith GE, Ivnik RJ, Boeve BF, Kokmen E, Tangalos EG, Petersen RC. Regional metabolic patterns in mild cognitive impairment and Alzheimer's disease: A 1H MRS study. Neurology 2000; 55(2): 210-217.

[58]   Waldman AD, Rai GS. The relationship between cognitive impairment and *in vivo* metabolite ratios in patients with clinical Alzheimer's disease and vascular dementia: a proton magnetic resonance spectroscopy study. Neuroradiology 2003; 45(8): 507-512.

[59]   Baik HM, Choe BY, Son BC, Jeun SS, Kim MC, Lee KS, Kim BS, Lee JM, Lee HK, Suh TS. Proton MR spectroscopic changes in Parkinson's diseases after thalamotomy. Eur J Radiol 2003; 47(3): 179-187.

[60]   Summerfield C, Gomez-Anson B, Tolosa E, Mercader JM, Marti MJ, Pastor P, Junque C. Dementia in Parkinson disease: a proton magnetic resonance spectroscopy study. Arch Neurol 2002; 59(9): 1415-1420.

[61]   Bowen BC, Pattany PM, Bradley WG, Murdoch JB, Rotta F, Younis AA, Duncan RC, Quencer RM. MR imaging and localized proton spectroscopy of the precentral gyrus in amyotrophic lateral sclerosis. AJNR Am J Neuroradiol 2000; 21(4): 647-658.

[62]   Ellis CM, Simmons A, Glover A, Dawson JM, Williams SC, Leigh PN. Quantitative proton magnetic resonance spectroscopy of the subcortical white matter in motor neuron disease. Amyotroph Lateral Scler Other Motor Neuron Disord 2000; 1(2): 123-129.

[63]   Abe K, Takanashi M, Watanabe Y, Tanaka H, Fujita N, Hirabuki N, Yanagihara T. Decrease in N-acetylaspartate/creatine ratio in the motor area and the frontal lobe in amyotrophic lateral sclerosis. Neuroradiology 2001; 43(7): 537-541.

[64]   Sarchielli P, Pelliccioli GP, Tarducci R, Chiarini P, Presciutti O, Gobbi G, Gallai V. Magnetic resonance imaging and 1H-magnetic resonance spectroscopy in amyotrophic lateral sclerosis. Neuroradiology 2001; 43(3): 189-197.

[65]   Kenn W, Ochs G, Pabst TA, Hahn D. 1H spectroscopy in patients with amyotrophic lateral sclerosis. J Neuroimaging 2001; 11(3): 293-297.

[66]   Pohl C, Block W, Karitzky J, Traber F, Schmidt S, Grothe C, Lamerichs R, Schild H, Klockgether T. Proton magnetic resonance spectroscopy of the motor cortex in 70 patients with amyotrophic lateral sclerosis. Arch Neurol 2001; 58(5): 729-735.

[67]   Cheng LL, Newell K, Mallory AE, Hyman BT, Gonzalez RG. Quantification of neurons in Alzheimer and control brains with ex vivo high resolution magic angle spinning proton magnetic resonance spectroscopy and stereology. Magn Reson Imaging 2002; 20(7): 527-533.

[68]   Garseth M, Sonnewald U, White LR, Rod M, Zwart JA, Nygaard O, Aasly J. Proton magnetic resonance spectroscopy of cerebrospinal fluid in neurodegenerative disease: indication of glial energy impairment in Huntington chorea, but not Parkinson disease. J Neurosci Res 2000; 60(6): 779-782.

[69]   Wilken B, Dechent P, Brockmann K, Finsterbusch J, Baumann M, Ebell W, Korenke GC, Pouwels PJ, Hanefeld FA, Frahm J. Quantitative proton magnetic resonance spectroscopy of children with adrenoleukodystrophy before and after hematopoietic stem cell transplantation. Neuropediatrics 2003; 34(5): 237-246.

[70]   De Stefano N, Dotti MT, Mortilla M, Federico A. Magnetic resonance imaging and spectroscopic changes in brains of patients with cerebrotendinous xanthomatosis. Brain 2001; 124(Pt 1): 121-131.

[71]   Geissler A, Frund R, Scholmerich J, Feuerbach S, Zietz B. Alterations of cerebral metabolism in patients with diabetes mellitus studied by proton magnetic resonance spectroscopy. Exp Clin Endocrinol Diabetes 2003; 111(7): 421-427.

[72]   Leuzzi V, Bianchi MC, Tosetti M, Carducci CL, Carducci CA, Antonozzi I. Clinical significance of brain phenylalanine concentration assessed by *in vivo* proton magnetic resonance spectroscopy in phenylketonuria. J Inherit Metab Dis 2000; 23(6): 563-570.

[73]   Mortilla M, Ermini M, Nistri M, Dal Pozzo G, Falcini F. Brain study using magnetic resonance imaging and proton MR spectroscopy in pediatric onset systemic lupus erythematosus. Clin Exp Rheumatol 2003; 21(1): 129-135.

[74]   Axford JS, Howe FA, Heron C, Griffiths JR. Sensitivity of quantitative (1)H magnetic resonance spectroscopy of the brain in detecting early neuronal damage in systemic lupus erythematosus. Ann Rheum Dis 2001; 60(2): 106-111.

[75]   Grachev ID, Fredrickson BE, Apkarian AV. Abnormal brain chemistry in chronic back pain: an *in vivo* proton magnetic resonance spectroscopy study. Pain 2000; 89(1): 7-18.

[76]   Puri BK, Counsell SJ, Zaman R, Main J, Collins AG, Hajnal JV, Davey NJ. Relative increase in choline in the occipital cortex in chronic fatigue syndrome. Acta Psychiatr Scand 2002; 106(3): 224-226.

[77]   Shim TS, Lee JH, Kim SY, Lim TH, Kim SJ, Kim DS, Kim WD. Cerebral metabolic abnormalities in COPD patients detected by localized proton magnetic resonance spectroscopy. Chest 2001; 120(5): 1506-1513.

[78]   Tarasow E, Panasiuk A, Siergiejczyk L, Orzechowska-Bobkiewicz A, Lewszuk A, Walecki J, Prokopowicz D. MR and 1H MR spectroscopy of the brain in patients with liver cirrhosis and early stages of hepatic encephalopathy. Hepatogastroenterology 2003; 50(54): 2149-2153.

[79]   Rovira A, Grive E, Pedraza S, Alonso J. Magnetization transfer ratio values and proton MR spectroscopy of normal-appearing cerebral white matter in patients with liver cirrhosis. AJNR Am J Neuroradiol 2001; 22(6): 1137-1142.

[80]   Spahr L, Vingerhoets F, Lazeyras F, Delavelle J, DuPasquier R, Giostra E, Mentha G, Terrier F, Hadengue A. Magnetic resonance imaging and proton spectroscopic alterations correlate with parkinsonian signs in patients with cirrhosis. Gastroenterology 2000; 119(3): 774-781.

[81]   Walecki J, Michalak MJ, Michalak E, Bilinska ZT, Ruzyllo W. Usefulness of 1H MR spectroscopy in the evaluation of myocardial metabolism in patients with dilated idiopathic cardiomyopathy: pilot study. Acad Radiol 2003; 10(10): 1187-1192.

[82]   Goddard AW, Mason GF, Almai A, Rothman DL, Behar KL, Petroff OA, Charney DS, Krystal JH. Reductions in occipital cortex GABA levels in panic disorder detected with 1h-magnetic resonance spectroscopy. Arch Gen Psychiatry 2001; 58(6): 556-561.

[83]   Massana G, Gasto C, Junque C, Mercader JM, Gomez B, Massana J, Torres X, Salamero M. Reduced levels of creatine in the right medial temporal lobe region of panic disorder patients detected with (1)H magnetic resonance spectroscopy. Neuroimage 2002; 16(3 Pt 1): 836-842.

[84]   Jung RE, Yeo RA, Love TM, Petropoulos H, Sibbitt WL, Jr., Brooks WM. Biochemical markers of mood: a proton magnetic resonance spectroscopy study of normal human brain. Biol Psychiatry 2002; 51(3): 224-229.

[85]   Mullins PG, Rowland L, Bustillo J, Bedrick EJ, Lauriello J, Brooks WM. Reproducibility of 1H-MRS measurements in schizophrenic patients. Magn Reson Med 2003; 50(4): 704-707.

[86]   Yeo RA, Hill DE, Campbell RA, Vigil J, Petropoulos H, Hart B, Zamora L, Brooks WM. Proton magnetic resonance spectroscopy investigation of the right frontal lobe in children with attention-deficit/hyperactivity disorder. J Am Acad Child Adolesc Psychiatry 2003; 42(3): 303-310.

[87]   Kantarci K, Shin C, Britton JW, So EL, Cascino GD, Jack CR, Jr. Comparative diagnostic utility of 1H MRS and DWI in evaluation of temporal lobe epilepsy. Neurology 2002; 58(12): 1745-1753.

[88]   Park SW, Chang KH, Kim HD, Song IC, Lee DS, Lee SK, Chung CK, Yu IK, Han MH, Park YH. Lateralizing ability of single-voxel proton mr spectroscopy in hippocampal sclerosis: comparison with

mr imaging and positron emission tomography. AJNR Am J Neuroradiol 2001; 22(4): 625-631.

[89] Provencher SW. Estimation of metabolite concentrations from localized *in vivo* proton NMR spectra. Magn Reson Med 1993; 30(6): 672-679.

[90] Provencher SW. Automatic quantitation of localized *in vivo* 1H spectra with LCModel. NMR Biomed 2001; 14(4): 260-264.

[91] Govindaraju V, Young K, Maudsley AA. Proton NMR chemical shifts and coupling constants for brain metabolites. NMR Biomed 2000; 13(3): 129-153.

[92] Alkan A, Sarac K, Kutlu R, Yakinci C, Sigirci A, Aslan M, Ozcan H, Yologlu S. Proton MR spectroscopy features of normal appearing white matter in neurofibromatosis type 1. Magn Reson Imaging 2003; 21(9): 1049-1053.

[93] Freeman JL, Coleman LT, Wellard RM, Kean MJ, Rosenfeld JV, Jackson GD, Berkovic SF, Harvey AS. MR imaging and spectroscopic study of epileptogenic hypothalamic hamartomas: analysis of 72 cases. AJNR Am J Neuroradiol 2004; 25(3): 450-462.

[94] Gajewicz W, Papierz W, Szymczak W, Goraj B. The use of proton MRS in the differential diagnosis of brain tumors and tumor-like processes. Med Sci Monit 2003; 9(9): MT97-105.

[95] Hayashi T, Kumabe T, Jokura H, Fujihara K, Shiga Y, Watanabe M, Higano S, Shirane R. Inflammatory demyelinating disease mimicking malignant glioma. J Nucl Med 2003; 44(4): 565-569.

[96] Harada M, Uno M, Hong F, Hisaoka S, Nishitani H, Matsuda T. Diffusion-weighted *in vivo* localized proton MR spectroscopy of human cerebral ischemia and tumor. NMR Biomed 2002; 15(1): 69-74.

[97] Wilken B, Dechent P, Herms J, Maxton C, Markakis E, Hanefeld F, Frahm J. Quantitative proton magnetic resonance spectroscopy of focal brain lesions. Pediatr Neurol 2000; 23(1): 22-31.

[98] Murphy M, Loosemore A, Clifton AG, Howe FA, Tate AR, Cudlip SA, Wilkins PR, Griffiths JR, Bell BA. The contribution of proton magnetic resonance spectroscopy (1HMRS) to clinical brain tumour diagnosis. Br J Neurosurg 2002; 16(4): 329-334.

[99] Majos C, Alonso J, Aguilera C, Serrallonga M, Perez-Martin J, Acebes JJ, Arus C, Gili J. Proton magnetic resonance spectroscopy ((1)H MRS) of human brain tumours: assessment of differences between tumour types and its applicability in brain tumour categorization. Eur Radiol 2003; 13(3): 582-591.

[100] Moller-Hartmann W, Herminghaus S, Krings T, Marquardt G, Lanfermann H, Pilatus U, Zanella FE. Clinical application of proton magnetic resonance spectroscopy in the diagnosis of intracranial mass lesions. Neuroradiology 2002; 44(5): 371-381.

[101] Howe FA, Barton SJ, Cudlip SA, Stubbs M, Saunders DE, Murphy M, Wilkins P, Opstad KS, Doyle VL, McLean MA, Bell BA, Griffiths JR. Metabolic profiles of human brain tumors using quantitative *in vivo* 1H magnetic resonance spectroscopy. Magn Reson Med 2003; 49(2): 223-232.

[102] Murphy PS, Rowland IJ, Viviers L, Brada M, Leach MO, Dzik-Jurasz AS. Could assessment of glioma methylene lipid resonance by *in vivo* (1)H-MRS be of clinical value? Br J Radiol 2003; 76(907): 459-463.

[103] Kuesel AC, Briere KM, Halliday WC, Sutherland GR, Donnelly SM, Smith ICP. Mobile lipid accumulation in necrotic tissue of high grade astrocytomas. Anticancer Res 1996; 16: 1485-1490.

[104] Cheng LL, Chang IW, Louis DN, Gonzalez RG. Correlation of high-resolution magic angle spinning proton magnetic resonance spectroscopy with histopathology of intact human brain tumor specimens. Cancer Res 1998; 58(9): 1825-1832.

[105] Cheng LL, Anthony DC, Comite AR, Black PM, Tzika AA, Gonzalez RG. Quantification of microheterogeneity in glioblastoma multiforme with ex vivo high-resolution magic-angle spinning (HRMAS) proton magnetic resonance spectroscopy. Neuro-oncol 2000; 2(2): 87-95.

[106] Tate AR, Majos C, Moreno A, Howe FA, Griffiths JR, Arus C. Automated classification of short echo time in *in vivo* 1H brain tumor spectra: a multicenter study. Magn Reson Med 2003; 49(1): 29-36.

[107] Herminghaus S, Pilatus U, Moller-Hartmann W, Raab P, Lanfermann H, Schlote W, Zanella FE. Increased choline levels coincide with enhanced proliferative activity of human neuroepithelial brain tumors. NMR Biomed 2002; 15(6): 385-392.

[108] Shimizu H, Kumabe T, Shirane R, Yoshimoto T. Correlation between choline level measured by proton MR spectroscopy and

Ki-67 labeling index in gliomas. AJNR Am J Neuroradiol 2000; 21(4): 659-665.

[109] Opstad KS, Provencher SW, Bell BA, Griffiths JR, Howe FA. Detection of elevated glutathione in meningiomas by quantitative *in vivo* 1H MRS. Magn Reson Med 2003; 49(4): 632-637.

[110] Isobe T, Matsumura A, Anno I, Yoshizawa T, Nagatomo Y, Itai Y, Nose T. Quantification of cerebral metabolites in glioma patients with proton MR spectroscopy using T2 relaxation time correction. Magn Reson Imaging 2002; 20(4): 343-349.

[111] Murphy PS, Dzik-Jurasz AS, Leach MO, Rowland IJ. The effect of Gd-DTPA on T(1)-weighted choline signal in human brain tumours. Magn Reson Imaging 2002; 20(1): 127-130.

[112] Davidson A, Payne G, Leach MO, McVicar D, Britton JM, Watson M, Tait DM. Proton magnetic resonance spectroscopy ((1)H-MRS) of the brain following high-dose methotrexate treatment for childhood cancer. Med Pediatr Oncol 2000; 35(1): 28-34.

[113] Rock JP, Scarpace L, Hearshen D, Gutierrez J, Fisher JL, Rosenblum M, Mikkelsen T. Associations among magnetic resonance spectroscopy, apparent diffusion coefficients, and image-guided histopathology with special attention to radiation necrosis. Neurosurgery 2004; 54(5): 1111-1117; discussion 1117-1119.

[114] Schlemmer HP, Bachert P, Herfarth KK, Zuna I, Debus J, van Kaick G. Proton MR spectroscopic evaluation of suspicious brain lesions after stereotactic radiotherapy. AJNR Am J Neuroradiol 2001; 22(7): 1316-1324.

[115] Kallen K, Burtscher IM, Holtas S, Ryding E, Rosen I. 201Thallium SPECT and 1H-MRS compared with MRI in chemotherapy monitoring of high-grade malignant astrocytomas. J Neurooncol 2000; 46(2): 173-185.

[116] Murphy PS, Viviers L, Abson C, Rowland IJ, Brada M, Leach MO, Dzik-Jurasz AS. Monitoring temozolomide treatment of low-grade glioma with proton magnetic resonance spectroscopy. Br J Cancer 2004; 90(4): 781-786.

[117] Bolan PJ, Meisamy S, Baker EH, Lin J, Emory T, Nelson M, Everson LI, Yee D, Garwood M. *In vivo* quantification of choline compounds in the breast with 1H MR spectroscopy. Magn Reson Med 2003; 50(6): 1134-1143.

[118] Cecil KM, Schnall MD, Siegelman ES, Lenkinski RE. The evaluation of human breast lesions with magnetic resonance imaging and proton magnetic resonance spectroscopy. Breast Cancer Res Treat 2001; 68(1): 45-54.

[119] Yeung DK, Yang WT, Tse GM. Breast cancer: *in vivo* proton MR spectroscopy in the characterization of histopathologic subtypes and preliminary observations in axillary node metastases. Radiology 2002; 225(1): 190-197.

[120] Bolan PJ, DelaBarre L, Baker EH, Merkle H, Everson LI, Yee D, Garwood M. Eliminating spurious lipid sidebands in 1H MRS of breast lesions. Magn Reson Med 2002; 48(2): 215-222.

[121] Mountford CE, Somorjai RL, Malycha P, Gluch L, Lean C, Russell P, Barraclough B, Gillett D, Himmelreich U, Dolenko B, Nikulin AE, Smith IC. Diagnosis and prognosis of breast cancer by magnetic resonance spectroscopy of fine-needle aspirates analysed using a statistical classification strategy. Br J Surg 2001; 88(9): 1234-1240.

[122] Cheng LL, Chang IW, Smith BL, Gonzalez RG. Evaluating human breast ductal carcinomas with high-resolution magic-angle spinning proton magnetic resonance spectroscopy. J Magn Reson 1998; 135(1): 194-202.

[123] Sitter B, Sonnewald U, Spraul M, Fjosne HE, Gribbestad IS. High-resolution magic angle spinning MRS of breast cancer tissue. NMR Biomed 2002; 15(5): 327-337.

[124] Allen JR, Prost RW, Griffith OW, Erickson SJ, Erickson BA. *In vivo* proton (H1) magnetic resonance spectroscopy for cervical carcinoma. Am J Clin Oncol 2001; 24(5): 522-529.

[125] Mahon MM, Cox IJ, Dina R, Soutter WP, McIndoe GA, Williams AD, deSouza NM. (1)H magnetic resonance spectroscopy of preinvasive and invasive cervical cancer: *in vivo*-ex vivo profiles and effect of tumor load. J Magn Reson Imaging 2004; 19(3): 356-364.

[126] Mahon MM, Williams AD, Soutter WP, Cox IJ, McIndoe GA, Coutts GA, Dina R, deSouza NM. 1H magnetic resonance spectroscopy of invasive cervical cancer: an *in vivo* study with ex vivo corroboration. NMR Biomed 2004; 17(1): 1-9.

[127] Oya N, Aoki J, Shinozaki T, Watanabe H, Takagishi K, Endo K. Preliminary study of proton magnetic resonance spectroscopy in bone and soft tissue tumors: an unassigned signal at 2.0-2.1 ppm

may be a possible indicator of malignant neuroectodermal tumor. Radiat Med 2000; 18(3): 193-198.

[128] Schwarz AJ, Maisey NR, Collins DJ, Cunningham D, Huddart R, Leach MO. Early *in vivo* detection of metabolic response: a pilot study of 1H MR spectroscopy in extracranial lymphoma and germ cell tumours. Br J Radiol 2002; 75(900): 959-966.

[129] Star-Lack JM, Adalsteinsson E, Adam MF, Terris DJ, Pinto HA, Brown JM, Spielman DM. *In vivo* 1H MR spectroscopy of human head and neck lymph node metastasis and comparison with oxygen tension measurements. AJNR Am J Neuroradiol 2000; 21(1): 183-193.

[130] Okada T, Harada M, Matsuzaki K, Nishitani H, Aono T. Evaluation of female intrapelvic tumors by clinical proton MR spectroscopy. J Magn Reson Imaging 2001; 13(6): 912-917.

[131] Dzik-Jurasz AS, Murphy PS, George M, Prock T, Collins DJ, Swift I, Leach MO, Rowland IJ. Human rectal adenocarcinoma: demonstration of 1H-MR spectra *in vivo* at 1.5 T. Magn Reson Med 2002; 47(4): 809-811.

[132] Katz-Brull R, Rofsky NM, Lenkinski RE. Breathhold abdominal and thoracic proton MR spectroscopy at 3T. Magn Reson Med 2003; 50(3): 461-467.

[133] Mountford CE, Delikatny EJ, Dyne M, Holmes KT, Mackinnon WB, Ford R, Hunter JC, Truskett ID, Russell P. Uterine cervical punch biopsy specimens can be analyzed by 1H MRS. Magn Reson Med 1990; 13(2): 324-331.

[134] Delikatny E, Russell P, Hunter J, Hancock R, Atkinson K, van Haaften-Day C, Mountford C. Proton MR and human cervical neoplasia. I. Ex vivo spectroscopy allows distinction of invasive carcinoma of the cervix from carcinoma in situ and other preinvasive lesions. Radiology 1993; 188: 791-796.

[135] Sitter B, Bathen T, Hagen B, Arentz C, Skjeldestad FE, Gribbestad IS. Cervical cancer tissue characterized by high-resolution magic angle spinning MR spectroscopy. MAGMA 2004; 16(4): 174-181.

[136] Mahon MM, deSouza NM, Dina R, Soutter WP, McIndoe GA, Williams AD, Cox IJ. Preinvasive and invasive cervical cancer: an ex vivo proton magic angle spinning magnetic resonance spectroscopy study. NMR Biomed 2004; 17(3): 144-153.

[137] Kamba M, Meshitsuka S, Iriguchi N, Koda M, Kimura K, Ogawa T. Measurement of relative fat content by proton magnetic resonance spectroscopy using a clinical imager. J Magn Reson Imaging 2000; 11(3): 330-335.

[138] Kamba M, Kimura K, Koda M, Ogawa T. Proton magnetic resonance spectroscopy for assessment of human body composition. Am J Clin Nutr 2001; 73(2): 172-176.

[139] Sinha R, Dufour S, Petersen KF, LeBon V, Enoksson S, Ma YZ, Savoye M, Rothman DL, Shulman GI, Caprio S. Assessment of skeletal muscle triglyceride content by (1)H nuclear magnetic resonance spectroscopy in lean and obese adolescents: relationships to insulin sensitivity, total body fat, and central adiposity. Diabetes 2002; 51(4): 1022-1027.

[140] Renema WK, Klomp DW, Philippens ME, van den Bergh AJ, Wieringa B, Heerschap A. Magnetization transfer effect on the creatine methyl resonance studied by CW off-resonance irradiation in human skeletal muscle on a clinical MR system. Magn Reson Med 2003; 50(3): 468-473.

[141] Rico-Sanz J, Moosavi M, Thomas EL, McCarthy J, Coutts GA, Saeed N, Bell JD. *In vivo* evaluation of the effects of continuous exercise on skeletal muscle triglycerides in trained humans. Lipids 2000; 35(12): 1313-1318.

[142] Prescot AP, Collins DJ, Leach MO, Dzik-Jurasz AS. Human gallbladder bile: noninvasive investigation *in vivo* with single-voxel 1H MR spectroscopy. Radiology 2003; 229(2): 587-592.

[143] Dzik-Jurasz AS, Prescot AP, Leach MO, Collins DJ. Non-invasive study of human gall bladder bile *in vivo* using (1)H-MR spectroscopy. Br J Radiol 2003; 76(907): 483-486.

[144] Jacobs MA, Horska A, van Zijl PC, Barker PB. Quantitative proton MR spectroscopic imaging of normal human cerebellum and brain stem. Magn Reson Med 2001; 46(4): 699-705.

[145] Wiedermann D, Schuff N, Matson GB, Soher BJ, Du AT, Maudsley AA, Weiner MW. Short echo time multislice proton magnetic resonance spectroscopic imaging in human brain: metabolite distributions and reliability. Magn Reson Imaging 2001; 19(8): 1073-1080.

[146] McLean MA, Woermann FG, Simister RJ, Barker GJ, Duncan JS. *In vivo* short echo time 1H-magnetic resonance spectroscopic

[147] Vigneron D, Bollen A, McDermott M, Wald L, Day M, Moyher-Noworolski S, Henry R, Chang S, Berger M, Dillon W, Nelson S. Three-dimensional magnetic resonance spectroscopic imaging of histologically confirmed brain tumors. Magn Reson Imaging 2001; 19(1): 89-101.

[148] Kadota T, Horinouchi T, Kuroda C. Development and aging of the cerebrum: assessment with proton MR spectroscopy. AJNR Am J Neuroradiol 2001; 22(1): 128-135.

[149] Horska A, Kaufmann WE, Brant LJ, Naidu S, Harris JC, Barker PB. *In vivo* quantitative proton MRSI study of brain development from childhood to adolescence. J Magn Reson Imaging 2002; 15(2): 137-143.

[150] Rotondo E, Bruschetta G, Sacca A, Bramanti P, Di Pasquale MR. Straightforward relative quantitation and age-related human standards of N-acetylaspartate at the centrum semiovale level by CSI (1)H-MRS. Magn Reson Imaging 2003; 21(9): 1055-1060.

[151] Schuff N, Ezekiel F, Gamst AC, Amend DL, Capizzano AA, Maudsley AA, Weiner MW. Region and tissue differences of metabolites in normally aged brain using multislice 1H magnetic resonance spectroscopic imaging. Magn Reson Med 2001; 45(5): 899-907.

[152] Carhuapoma JR, Wang PY, Beauchamp NJ, Keyl PM, Hanley DF, Barker PB. Diffusion-weighted MRI and proton MR spectroscopic imaging in the study of secondary neuronal injury after intracerebral hemorrhage. Stroke 2000; 31(3): 726-732.

[153] Mihara F, Kuwabara Y, Yoshida T, Yoshiura T, Sasaki M, Masuda K, Matsushima T, Fukui M. Correlation between proton magnetic resonance spectroscopic lactate measurements and vascular reactivity in chronic occlusive cerebrovascular disease: a comparison with positron emission tomography. Magn Reson Imaging 2000; 18(9): 1167-1174.

[154] Chu WJ, Mason GF, Pan JW, Hetherington HP, Liu HG, San Pedro EC, Mountz JM. Regional cerebral blood flow and magnetic resonance spectroscopic imaging findings in diaschisis from stroke. Stroke 2002; 33(5): 1243-1248.

[155] Govindaraju V, Gauger GE, Manley GT, Ebel A, Meeker M, Maudsley AA. Volumetric proton spectroscopic imaging of mild traumatic brain injury. AJNR Am J Neuroradiol 2004; 25(5): 730-737.

[156] Miller SP, McQuillen PS, Vigneron DB, Glidden DV, Barkovich AJ, Ferriero DM, Hamrick SE, Azakie A, Karl TR. Preoperative brain injury in newborns with transposition of the great arteries. Ann Thorac Surg 2004; 77(5): 1698-1706.

[157] Pelletier D, Nelson SJ, Oh J, Antel JP, Kita M, Zamvil SS, Goodkin DE. MRI lesion volume heterogeneity in primary progressive MS in relation with axonal damage and brain atrophy. J Neurol Neurosurg Psychiatry 2003; 74(7): 950-952.

[158] Suhy J, Rooney WD, Goodkin DE, Capizzano AA, Soher BJ, Maudsley AA, Waubant E, Andersson PB, Weiner MW. 1H MRSI comparison of white matter and lesions in primary progressive and relapsing-remitting MS. Mult Scler 2000; 6(3): 148-155.

[159] Kapeller P, McLean MA, Griffin CM, Chard D, Parker GJ, Barker GJ, Thompson AJ, Miller DH. Preliminary evidence for neuronal damage in cortical grey matter and normal appearing white matter in short duration relapsing-remitting multiple sclerosis: a quantitative MR spectroscopic imaging study. J Neurol 2001; 248(2): 131-138.

[160] Inglese M, Li BS, Rusinek H, Babb JS, Grossman RI, Gonen O. Diffusely elevated cerebral choline and creatine in relapsing-remitting multiple sclerosis. Magn Reson Med 2003; 50(1): 190-195.

[161] Chard DT, Griffin CM, McLean MA, Kapeller P, Kapoor R, Thompson AJ, Miller DH. Brain metabolite changes in cortical grey and normal-appearing white matter in clinically early relapsing-remitting multiple sclerosis. Brain 2002; 125(Pt 10): 2342-2352.

[162] Sharma R, Narayana PA, Wolinsky JS. Grey matter abnormalities in multiple sclerosis: proton magnetic resonance spectroscopic imaging. Mult Scler 2001; 7(4): 221-226.

[163] Schocke MF, Berger T, Felber SR, Wolf C, Deisenhammer F, Kremser C, Seppi K, Aichner FT. Serial contrast-enhanced magnetic resonance imaging and spectroscopic imaging of acute multiple sclerosis lesions under high-dose methylprednisolone therapy. Neuroimage 2003; 20(2): 1253-1263.

[164]   Tedeschi G, Bonavita S, McFarland HF, Richert N, Duyn JH, Frank JA. Proton MR spectroscopic imaging in multiple sclerosis. Neuroradiology 2002; 44(1): 37-42.

[165]   De Stefano N, Narayanan S, Francis GS, Arnaoutelis R, Tartaglia MC, Antel JP, Matthews PM, Arnold DL. Evidence of axonal damage in the early stages of multiple sclerosis and its relevance to disability. Arch Neurol 2001; 58(1): 65-70.

[166]   Reddy H, Narayanan S, Arnoutelis R, Jenkinson M, Antel J, Matthews PM, Arnold DL. Evidence for adaptive functional changes in the cerebral cortex with axonal injury from multiple sclerosis. Brain 2000; 123 (Pt 11): 2314-2320.

[167]   Tartaglia MC, Narayanan S, De Stefano N, Arnaoutelis R, Antel SB, Francis SJ, Santos AC, Lapierre Y, Arnold DL. Choline is increased in pre-lesional normal appearing white matter in multiple sclerosis. J Neurol 2002; 249(10): 1382-1390.

[168]   Oh J, Pelletier D, Nelson SJ. Corpus callosum axonal injury in multiple sclerosis measured by proton magnetic resonance spectroscopic imaging. Arch Neurol 2004; 61(7): 1081-1086.

[169]   Schuff N, Capizzano AA, Du AT, Amend DL, O'Neill J, Norman D, Kramer J, Jagust W, Miller B, Wolkowitz OM, Yaffe K, Weiner MW. Selective reduction of N-acetylaspartate in medial temporal and parietal lobes in AD. Neurology 2002; 58(6): 928-935.

[170]   Colla M, Ende G, Bohrer M, Deuschle M, Kronenberg G, Henn F, Heuser I. MR spectroscopy in Alzheimer's disease: gender differences in probabilistic learning capacity. Neurobiol Aging 2003; 24(4): 545-552.

[171]   Frederick B, Satlin A, Wald LL, Hennen J, Bodick N, Renshaw PF. Brain proton magnetic resonance spectroscopy in Alzheimer disease: changes after treatment with xanomeline. Am J Geriatr Psychiatry 2002; 10(1): 81-88.

[172]   Mielke R, Schopphoff HH, Kugel H, Pietrzyk U, Heindel W, Kessler J, Heiss WD. Relation between 1H MR spectroscopic imaging and regional cerebral glucose metabolism in Alzheimer's disease. Int J Neurosci 2001; 107(3-4): 233-245.

[173]   Schuff N, Rooney WD, Miller R, Gelinas DF, Amend DL, Maudsley AA, Weiner MW. Reanalysis of multislice (1)H MRSI in amyotrophic lateral sclerosis. Magn Reson Med 2001; 45(3): 513-516.

[174]   Suhy J, Miller RG, Rule R, Schuff N, Licht J, Dronsky V, Gelinas D, Maudsley AA, Weiner MW. Early detection and longitudinal changes in amyotrophic lateral sclerosis by (1)H MRSI. Neurology 2002; 58(5): 773-779.

[175]   Kalra S, Genge A, Arnold DL. A prospective, randomized, placebo-controlled evaluation of corticoneuronal response to intrathecal BDNF therapy in ALS using magnetic resonance spectroscopy: feasibility and results. Amyotroph Lateral Scler Other Motor Neuron Disord 2003; 4(1): 22-26.

[176]   Kalra S, Cashman NR, Caramanos Z, Genge A, Arnold DL. Gabapentin therapy for amyotrophic lateral sclerosis: lack of improvement in neuronal integrity shown by MR spectroscopy. AJNR Am J Neuroradiol 2003; 24(3): 476-480.

[177]   Fatemi A, Barker PB, Ulug AM, Nagae-Poetscher LM, Beauchamp NJ, Moser AB, Raymond GV, Moser HW, Naidu S. MRI and proton MRSI in women heterozygous for X-linked adrenoleukodystrophy. Neurology 2003; 60(8): 1301-1307.

[178]   Eichler FS, Barker PB, Cox C, Edwin D, Ulug AM, Moser HW, Raymond GV. Proton MR spectroscopic imaging predicts lesion progression on MRI in X-linked adrenoleukodystrophy. Neurology 2002; 58(6): 901-907.

[179]   Izquierdo M, Adamsbaum C, Benosman A, Aubourg P, Bittoun J. MR spectroscopic imaging of normal-appearing white matter in adrenoleukodystrophy. Pediatr Radiol 2000; 30(9): 621-629.

[180]   Sijens PE, Oudkerk M, Reijngoud DJ, Leenders KL, De Valk HW, Van Spronsen FJ. 1H MR chemical shift imaging detection of phenylalanine in patients suffering from phenylketonuria (PKU). Eur Radiol 2004; 14(10): 1895-1900.

[181]   Ende G, Braus DF, Walter S, Weber-Fahr W, Henn FA. Multiregional 1H-MRSI of the hippocampus, thalamus, and basal ganglia in schizophrenia. Eur Arch Psychiatry Clin Neurosci 2003; 253(1): 9-15.

[182]   O'Neill J, Levitt J, Caplan R, Asarnow R, McCracken JT, Toga AW, Alger JR. 1H MRSI evidence of metabolic abnormalities in childhood-onset schizophrenia. Neuroimage 2004; 21(4): 1781-1789.

[183]   Bertolino A, Callicott JH, Mattay VS, Weidenhammer KM, Rakow R, Egan MF, Weinberger DR. The effect of treatment with antipsychotic drugs on brain N-acetylaspartate measures in patients with schizophrenia. Biol Psychiatry 2001; 49(1): 39-46.

[184]   Braus DF, Ende G, Weber-Fahr W, Demirakca T, Henn FA. Favorable effect on neuronal viability in the anterior cingulate gyrus due to long-term treatment with atypical antipsychotics: an MRSI study. Pharmacopsychiatry 2001; 34(6): 251-253.

[185]   Layton ME, Friedman SD, Dager SR. Brain metabolic changes during lactate-induced panic: effects of gabapentin treatment. Depress Anxiety 2001; 14(4): 251-254.

[186]   Levitt JG, O'Neill J, Blanton RE, Smalley S, Fadale D, McCracken JT, Guthrie D, Toga AW, Alger JR. Proton magnetic resonance spectroscopic imaging of the brain in childhood autism. Biol Psychiatry 2003; 54(12): 1355-1366.

[187]   Smith EA, Russell A, Lorch E, Banerjee SP, Rose M, Ivey J, Bhandari R, Moore GJ, Rosenberg DR. Increased medial thalamic choline found in pediatric patients with obsessive-compulsive disorder versus major depression or healthy control subjects: a magnetic resonance spectroscopy study. Biol Psychiatry 2003; 54(12): 1399-1405.

[188]   Vythilingam M, Charles HC, Tupler LA, Blitchington T, Kelly L, Krishnan KR. Focal and lateralized subcortical abnormalities in unipolar major depressive disorder: an automated multivoxel proton magnetic resonance spectroscopy study. Biol Psychiatry 2003; 54(7): 744-750.

[189]   Bertolino A, Frye M, Callicott JH, Mattay VS, Rakow R, Shelton-Repella J, Post R, Weinberger DR. Neuronal pathology in the hippocampal area of patients with bipolar disorder: a study with proton magnetic resonance spectroscopic imaging. Biol Psychiatry 2003; 53(10): 906-913.

[190]   Moore CM, Breeze JL, Gruber SA, Babb SM, Frederick BB, Villafuerte RA, Stoll AL, Hennen J, Yurgelun-Todd DA, Cohen BM, Renshaw PF. Choline, myo-inositol and mood in bipolar disorder: a proton magnetic resonance spectroscopic imaging study of the anterior cingulate cortex. Bipolar Disord 2000; 2(3 Pt 2): 207-216.

[191]   Castillo M, Kwock L, Courvoisie H, Hooper SR. Proton MR spectroscopy in children with bipolar affective disorder: preliminary observations. AJNR Am J Neuroradiol 2000; 21(5): 832-838.

[192]   Obergriesser T, Ende G, Braus DF, Henn FA. Hippocampal 1H-MRSI in ecstasy users. Eur Arch Psychiatry Clin Neurosci 2001; 251(3): 114-116.

[193]   Bernasconi A, Tasch E, Cendes F, Li LM, Arnold DL. Proton magnetic resonance spectroscopic imaging suggests progressive neuronal damage in human temporal lobe epilepsy. Prog Brain Res 2002; 135: 297-304.

[194]   Bernasconi A, Bernasconi N, Natsume J, Antel SB, Andermann F, Arnold DL. Magnetic resonance spectroscopy and imaging of the thalamus in idiopathic generalized epilepsy. Brain 2003; 126(Pt 11): 2447-2454.

[195]   Li LM, Dubeau F, Andermann F, Arnold DL. Proton magnetic resonance spectroscopic imaging studies in patients with newly diagnosed partial epilepsy. Epilepsia 2000; 41(7): 825-831.

[196]   Simister RJ, Woermann FG, McLean MA, Bartlett PA, Barker GJ, Duncan JS. A short-echo-time proton magnetic resonance spectroscopic imaging study of temporal lobe epilepsy. Epilepsia 2002; 43(9): 1021-1031.

[197]   Woermann FG, McLean MA, Bartlett PA, Barker GJ, Duncan JS. Quantitative short echo time proton magnetic resonance spectroscopic imaging study of malformations of cortical development causing epilepsy. Brain 2001; 124(Pt 2): 427-436.

[198]   Capizzano AA, Vermathen P, Laxer KD, Matson GB, Maudsley AA, Soher BJ, Schuff NW, Weiner MW. Multisection proton MR spectroscopy for mesial temporal lobe epilepsy. AJNR Am J Neuroradiol 2002; 23(8): 1359-1368.

[199]   Pauli E, Eberhardt KW, Schafer I, Tomandl B, Huk WJ, Stefan H. Chemical shift imaging spectroscopy and memory function in temporal lobe epilepsy. Epilepsia 2000; 41(3): 282-289.

[200]   Vikhoff-Baaz B, Malmgren K, Jonsson L, Starck G, Ljungberg M, Forssell-Aronsson E, Uvebrant P, Ekholm S. Lateralisation with magnetic resonance spectroscopic imaging in temporal lobe epilepsy: an evaluation of visual and region-of-interest analysis of metabolite concentration images. Neuroradiology 2001; 43(9): 721-727.

[201]   Li LM, Cendes F, Andermann F, Dubeau F, Arnold DL. Spatial extent of neuronal metabolic dysfunction measured by proton MR

spectroscopic imaging in patients with localization-related epilepsy. Epilepsia 2000; 41(6): 666-674.

[202] Maton B, Gilliam F, Sawrie S, Faught E, Hugg J, Kuzniecky R. Correlation of scalp EEG and 1H-MRS metabolic abnormalities in temporal lobe epilepsy. Epilepsia 2001; 42(3): 417-422.

[203] Antel SB, Li LM, Cendes F, Collins DL, Kearney RE, Shinghal R, Arnold DL. Predicting surgical outcome in temporal lobe epilepsy patients using MRI and MRSI. Neurology 2002; 58(10): 1505-1512.

[204] Li LM, Cendes F, Antel SB, Andermann F, Serles W, Dubeau F, Olivier A, Arnold DL. Prognostic value of proton magnetic resonance spectroscopic imaging for surgical outcome in patients with intractable temporal lobe epilepsy and bilateral hippocampal atrophy. Ann Neurol 2000; 47(2): 195-200.

[205] Serles W, Li LM, Antel SB, Cendes F, Gotman J, Olivier A, Andermann F, Dubeau F, Arnold DL. Time course of postoperative recovery of N-acetyl-aspartate in temporal lobe epilepsy. Epilepsia 2001; 42(2): 190-197.

[206] Suhy J, Laxer KD, Capizzano AA, Vermathen P, Matson GB, Barbaro NM, Weiner MW. 1H MRSI predicts surgical outcome in MRI-negative temporal lobe epilepsy. Neurology 2002; 58(5): 821-823.

[207] Hajek M, Dezortova M, Liscak R, Vymazal J, Vladyka V. 1H MR spectroscopy of mesial temporal lobe epilepsies treated with Gamma knife. Eur Radiol 2003; 13(5): 994-1000.

[208] Jemal A, Tiwari RC, Murray T, Ghafoor A, Samuels A, Ward E, Feuer EJ, Thun MJ. Cancer statistics, 2004. CA Cancer J Clin 2004; 54(1): 8-29.

[209] Cirak B, Horska A, Barker PB, Burger PC, Carson BS, Avellino AM. Proton magnetic resonance spectroscopic imaging in pediatric pilomyxoid astrocytoma. Childs Nerv Syst 2004.

[210] Rijpkema M, Schuuring J, van der Meulen Y, van der Graaf M, Bernsen H, Boerman R, van der Kogel A, Heerschap A. Characterization of oligodendrogliomas using short echo time 1H MR spectroscopic imaging. NMR Biomed 2003; 16(1): 12-18.

[211] Galanaud D, Chinot O, Nicoli F, Confort-Gouny S, Le Fur Y, Barrie-Attarian M, Ranjeva JP, Fuentes S, Viout P, Figarella-Branger D, Cozzone PJ. Use of proton magnetic resonance spectroscopy of the brain to differentiate gliomatosis cerebri from low-grade glioma. J Neurosurg 2003; 98(2): 269-276.

[212] Son BC, Kim MC, Choi BG, Kim EN, Baik HM, Choe BY, Naruse S, Kang JK. Proton magnetic resonance chemical shift imaging (1H CSI)-directed stereotactic biopsy. Acta Neurochir (Wien) 2001; 143(1): 45-49; discussion 49-50.

[213] Burtscher IM, Skagerberg G, Geijer B, Englund E, Stahlberg F, Holtas S. Proton MR spectroscopy and preoperative diagnostic accuracy: an evaluation of intracranial mass lesions characterized by stereotactic biopsy findings. AJNR Am J Neuroradiol 2000; 21(1): 84-93.

[214] Dowling C, Bollen AW, Noworolski SM, McDermott MW, Barbaro NM, Day MR, Henry RG, Chang SM, Dillon WP, Nelson SJ, Vigneron DB. Preoperative proton MR spectroscopic imaging of brain tumors: correlation with histopathologic analysis of resection specimens. AJNR Am J Neuroradiol 2001; 22(4): 604-612.

[215] Li X, Lu Y, Pirzkall A, McKnight T, Nelson SJ. Analysis of the spatial characteristics of metabolic abnormalities in newly diagnosed glioma patients. J Magn Reson Imaging 2002; 16(3): 229-237.

[216] McKnight TR, von dem Bussche MH, Vigneron DB, Lu Y, Berger MS, McDermott MW, Dillon WP, Graves EE, Pirzkall A, Nelson SJ. Histopathological validation of a three-dimensional magnetic resonance spectroscopy index as a predictor of tumor presence. J Neurosurg 2002; 97(4): 794-802.

[217] McKnight TR, Noworolski SM, Vigneron DB, Nelson SJ. An automated technique for the quantitative assessment of 3D-MRSI data from patients with glioma. J Magn Reson Imaging 2001; 13(2): 167-177.

[218] Gupta RK, Cloughesy TF, Sinha U, Garakian J, Lazareff J, Rubino G, Rubino L, Becker DP, Vinters HV, Alger JR. Relationships between choline magnetic resonance spectroscopy, apparent diffusion coefficient and quantitative histopathology in human glioma. J Neurooncol 2000; 50(3): 215-226.

[219] Croteau D, Scarpace L, Hearshen D, Gutierrez J, Fisher JL, Rock JP, Mikkelsen T. Correlation between magnetic resonance spectroscopy imaging and image-guided biopsies: semiquantitative

and qualitative histopathological analyses of patients with untreated glioma. Neurosurgery 2001; 49(4): 823-829.

[220] Kamada K, Moller M, Saguer M, Ganslandt O, Kaltenhauser M, Kober H, Vieth J. A combined study of tumor-related brain lesions using MEG and proton MR spectroscopic imaging. J Neurol Sci 2001; 186(1-2): 13-21.

[221] Pirzkall A, McKnight TR, Graves EE, Carol MP, Sneed PK, Wara WW, Nelson SJ, Verhey LJ, Larson DA. MR-spectroscopy guided target delineation for high-grade gliomas. Int J Radiat Oncol Biol Phys 2001; 50(4): 915-928.

[222] Law M, Yang S, Wang H, Babb JS, Johnson G, Cha S, Knopp EA, Zagzag D. Glioma grading: sensitivity, specificity, and predictive values of perfusion MR imaging and proton MR spectroscopic imaging compared with conventional MR imaging. AJNR Am J Neuroradiol 2003; 24(10): 1989-1998.

[223] Pirzkall A, Li X, Oh J, Chang S, Berger MS, Larson DA, Verhey LJ, Dillon WP, Nelson SJ. 3D MRSI for resected high-grade gliomas before RT: tumor extent according to metabolic activity in relation to MRI. Int J Radiat Oncol Biol Phys 2004; 59(1): 126-137.

[224] Pirzkall A, Nelson SJ, McKnight TR, Takahashi MM, Li X, Graves EE, Verhey LJ, Wara WW, Larson DA, Sneed PK. Metabolic imaging of low-grade gliomas with three-dimensional magnetic resonance spectroscopy. Int J Radiat Oncol Biol Phys 2002; 53(5): 1254-1264.

[225] Chan AA, Lau A, Pirzkall A, Chang SM, Verhey LJ, Larson D, McDermott MW, Dillon WP, Nelson SJ. Proton magnetic resonance spectroscopy imaging in the evaluation of patients undergoing gamma knife surgery for Grade IV glioma. J Neurosurg 2004; 101(3): 467-475.

[226] Li X, Jin H, Lu Y, Oh J, Chang S, Nelson SJ. Identification of MRI and 1H MRSI parameters that may predict survival for patients with malignant gliomas. NMR Biomed 2004; 17(1): 10-20.

[227] Oh J, Henry RG, Pirzkall A, Lu Y, Li X, Catalaa I, Chang S, Dillon WP, Nelson SJ. Survival analysis in patients with glioblastoma multiforme: predictive value of choline-to-N-acetylaspartate index, apparent diffusion coefficient, and relative cerebral blood volume. J Magn Reson Imaging 2004; 19(5): 546-554.

[228] Kuznetsov YE, Caramanos Z, Antel SB, Preul MC, Leblanc R, Villemure JG, Pokrupa R, Olivier A, Sadikot A, Arnold DL. Proton magnetic resonance spectroscopic imaging can predict length of survival in patients with supratentorial gliomas. Neurosurgery 2003; 53(3): 565-574; discussion 574-566.

[229] Lee MC, Pirzkall A, McKnight TR, Nelson SJ. 1H-MRSI of radiation effects in normal-appearing white matter: dose-dependence and impact on automated spectral classification. J Magn Reson Imaging 2004; 19(4): 379-388.

[230] Rock JP, Hearshen D, Scarpace L, Croteau D, Gutierrez J, Fisher JL, Rosenblum ML, Mikkelsen T. Correlations between magnetic resonance spectroscopy and image-guided histopathology, with special attention to radiation necrosis. Neurosurgery 2002; 51(4): 912-919; discussion 919-920.

[231] Virta A, Patronas N, Raman R, Dwyer A, Barnett A, Bonavita S, Tedeschi G, Lundbom N. Spectroscopic imaging of radiation-induced effects in the white matter of glioma patients. Magn Reson Imaging 2000; 18(7): 851-857.

[232] Weybright P, Maly P, Gomez-Hassan D, Blaesing C, Sundgren PC. MR spectroscopy in the evaluation of recurrent contrast-enhancing lesions in the posterior fossa after tumor treatment. Neuroradiology 2004; 46(7): 541-549.

[233] Preul MC, Caramanos Z, Villemure JG, Shenouda G, LeBlanc R, Langleben A, Arnold DL. Using proton magnetic resonance spectroscopic imaging to predict *in vivo* the response of recurrent malignant gliomas to tamoxifen chemotherapy. Neurosurgery 2000; 46(2): 306-318.

[234] Tzika AA, Zarifi MK, Goumnerova L, Astrakas LG, Zurakowski D, Young-Poussaint T, Anthony DC, Scott RM, Black PM. Neuroimaging in pediatric brain tumors: Gd-DTPA-enhanced, hemodynamic, and diffusion MR imaging compared with MR spectroscopic imaging. AJNR Am J Neuroradiol 2002; 23(2): 322-333.

[235] Tzika AA, Astrakas LG, Zarifi MK, Petridou N, Young-Poussaint T, Goumnerova L, Zurakowski D, Anthony DC, Black PM. Multiparametric MR assessment of pediatric brain tumors. Neuroradiology 2003; 45(1): 1-10.

[236] Tzika AA, Astrakas LG, Zarifi MK, Zurakowski D, Poussaint TY, Goumnerova L, Tarbell NJ, Black PM. Spectroscopic and perfusion

magnetic resonance imaging predictors of progression in pediatric brain tumors. Cancer 2004; 100(6): 1246-1256.

[237]   Tzika AA, Zurakowski D, Poussaint TY, Goumnerova L, Astrakas LG, Barnes PD, Anthony DC, Billett AL, Tarbell NJ, Scott RM, Black PM. Proton magnetic spectroscopic imaging of the child's brain: the response of tumors to treatment. Neuroradiology 2001; 43(2): 169-177.

[238]   Warren KE, Frank JA, Black JL, Hill RS, Duyn JH, Aikin AA, Lewis BK, Adamson PC, Balis FM. Proton magnetic resonance spectroscopic imaging in children with recurrent primary brain tumors. J Clin Oncol 2000; 18(5): 1020-1026.

[239]   van der Graaf M, Schipper RG, Oosterhof GO, Schalken JA, Verhofstad AA, Heerschap A. Proton MR spectroscopy of prostatic tissue focused on the detection of spermine, a possible biomarker of malignant behavior in prostate cancer. Magma 2000; 10(3): 153-159.

[240]   Swindle P, McCredie S, Russell P, Himmelreich U, Khadra M, Lean C, Mountford C. Pathologic characterization of human prostate tissue with proton MR spectroscopy. Radiology 2003; 228(1): 144-151.

[241]   Tomlins A, Foxall P, Lindon J, Lynch M, Spraul M, Everett J, Nicholson J. High resolution magic angle spinning 1H nuclear magnetic resonance analysis of intact prostatic hyperplastic and tumor tissue. Analy Common 1998; 35: 113-115.

[242]   Cheng LL, Wu C, Smith MR, Gonzalez RG. Non-destructive quantitation of spermine in human prostate tissue samples using HRMAS 1H NMR spectroscopy at 9.4 T. FEBS Lett 2001; 494(1-2): 112-116.

[243]   Swanson MG, Vigneron DB, Tabatabai ZL, Males RG, Schmitt L, Carroll PR, James JK, Hurd RE, Kurhanewicz J. Proton HR-MAS spectroscopy and quantitative pathologic analysis of MRI/3D-MRSI-targeted postsurgical prostate tissues. Magn Reson Med 2003; 50(5): 944-954.

[244]   Schricker AA, Pauly JM, Kurhanewicz J, Swanson MG, Vigneron DB. Dualband spectral-spatial RF pulses for prostate MR spectroscopic imaging. Magn Reson Med 2001; 46(6): 1079-1087.

[245]   Males RG, Vigneron DB, Star-Lack J, Falbo SC, Nelson SJ, Hricak H, Kurhanewicz J. Clinical application of BASING and spectral/spatial water and lipid suppression pulses for prostate cancer staging and localization by *in vivo* 3D 1H magnetic resonance spectroscopic imaging. Magn Reson Med 2000; 43(1): 17-22.

[246]   Dhingsa R, Qayyum A, Coakley FV, Lu Y, Jones KD, Swanson MG, Carroll PR, Hricak H, Kurhanewicz J. Prostate cancer localization with endorectal MR imaging and MR spectroscopic imaging: effect of clinical data on reader accuracy. Radiology 2004; 230(1): 215-220.

[247]   Kaji Y, Wada A, Imaoka I, Matsuo M, Terachi T, Kobashi Y, Sugimura K, Fujii M, Maruyama K, Takizawa O. Proton two-dimensional chemical shift imaging for evaluation of prostate cancer: external surface coil vs. endorectal surface coil. J Magn Reson Imaging 2002; 16(6): 697-706.

[248]   van Dorsten FA, van der Graaf M, Engelbrecht MR, van Leenders GJ, Verhofstad A, Rijpkema M, de la Rosette JJ, Barentsz JO, Heerschap A. Combined quantitative dynamic contrast-enhanced MR imaging and (1)H MR spectroscopic imaging of human prostate cancer. J Magn Reson Imaging 2004; 20(2): 279-287.

[249]   Yuen JS, Thng CH, Tan PH, Khin LW, Phee SJ, Xiao D, Lau WK, Ng WS, Cheng CW. Endorectal magnetic resonance imaging and spectroscopy for the detection of tumor foci in men with prior negative transrectal ultrasound prostate biopsy. J Urol 2004; 171(4): 1482-1486.

[250]   Zaider M, Zelefsky MJ, Lee EK, Zakian KL, Amols HI, Dyke J, Cohen G, Hu Y, Endi AK, Chui C, Koutcher JA. Treatment planning for prostate implants using magnetic-resonance spectroscopy imaging. Int J Radiat Oncol Biol Phys 2000; 47(4): 1085-1096.

[251]   Mizowaki T, Cohen GN, Fung AY, Zaider M. Towards integrating functional imaging in the treatment of prostate cancer with radiation: the registration of the MR spectroscopy imaging to ultrasound/CT images and its implementation in treatment planning. Int J Radiat Oncol Biol Phys 2002; 54(5): 1558-1564.

[252]   Zelefsky MJ, Cohen G, Zakian KL, Dyke J, Koutcher JA, Hricak H, Schwartz L, Zaider M. Intraoperative conformal optimization for transperineal prostate implantation using magnetic resonance spectroscopic imaging. Cancer J 2000; 6(4): 249-255.

[253]   DiBiase SJ, Hosseinzadeh K, Gullapalli RP, Jacobs SC, Naslund MJ, Sklar GN, Alexander RB, Yu C. Magnetic resonance spectroscopic imaging-guided brachytherapy for localized prostate cancer. Int J Radiat Oncol Biol Phys 2002; 52(2): 429-438.

[254]   Coakley FV, Teh HS, Qayyum A, Swanson MG, Lu Y, Iii MR, Pickett B, Shinohara K, Vigneron DB, Kurhanewicz J. Endorectal MR Imaging and MR Spectroscopic Imaging for Locally Recurrent Prostate Cancer after External Beam Radiation Therapy: Preliminary Experience. Radiology 2004.

[255]   Pickett B, Ten Haken RK, Kurhanewicz J, Qayyum A, Shinohara K, Fein B, Roach M, 3rd. Time to metabolic atrophy after permanent prostate seed implantation based on magnetic resonance spectroscopic imaging. Int J Radiat Oncol Biol Phys 2004; 59(3): 665-673.

[256]   Mueller-Lisse UG, Swanson MG, Vigneron DB, Hricak H, Bessette A, Males RG, Wood PJ, Noworolski S, Nelson SJ, Barken I, Carroll PR, Kurhanewicz J. Time-dependent effects of hormone-deprivation therapy on prostate metabolism as detected by combined magnetic resonance imaging and 3D magnetic resonance spectroscopic imaging. Magn Reson Med 2001; 46(1): 49-57.

[257]   Jacobs MA, Barker PB, Bottomley PA, Bhujwalla Z, Bluemke DA. Proton magnetic resonance spectroscopic imaging of human breast cancer: a preliminary study. J Magn Reson Imaging 2004; 19(1): 68-75.

[258]   Bredella MA, Losasso C, Moelleken SC, Huegli RW, Genant HK, Tirman PF. Three-point Dixon chemical-shift imaging for evaluating articular cartilage defects in the knee joint on a low-field-strength open magnet. AJR Am J Roentgenol 2001; 177(6): 1371-1375.

[259]   Hilaire L, Wehrli FW, Song HK. High-speed spectroscopic imaging for cancellous bone marrow R(2)* mapping and lipid quantification. Magn Reson Imaging 2000; 18(7): 777-786.

[260]   Lin CS, Fertikh D, Davis B, Lauerman WC, Henderson F, Schellinger D. 2D CSI proton MR spectroscopy of human spinal vertebra: feasibility studies. J Magn Reson Imaging 2000; 11(3): 287-293.

[261]   Hu J, Xia Y, Shen Y, Li J, Zuo CS, Xuan Y, Jiang Q. Significant differences in proton trimethyl ammonium signals between human gastrocnemius and soleus muscle. J Magn Reson Imaging 2004; 19(5): 617-622.

[262]   Vermathen P, Boesch C, Kreis R. Mapping fiber orientation in human muscle by proton MR spectroscopic imaging. Magn Reson Med 2003; 49(3): 424-432.

[263]   Vermathen P, Kreis R, Boesch C. Distribution of intramyocellular lipids in human calf muscles as determined by MR spectroscopic imaging. Magn Reson Med 2004; 51(2): 253-262.

[264]   Hu J, Jiang Q, Xia Y, Zuo C. High spatial resolution *in vivo* 2D (1)H magnetic resonance spectroscopic imaging of human muscles with a band-selective technique. Magn Reson Imaging 2001; 19(8): 1091-1096.

[265]   Shen W, Mao X, Wang Z, Punyanitya M, Heymsfield SB, Shungu DC. Measurement of intramyocellular lipid levels with 2-D magnetic resonance spectroscopic imaging at 1.5 T. Acta Diabetol 2003; 40 Suppl 1: S51-54.

[266]   Mansfield P. Spatial mapping of the chemical shift in NMR. J Phys D: Appl Phys 1983; 16: L235-L238.

[267]   Du W, Du YP, Fan X, Zamora MA, Karczmar GS. Reduction of spectral ghost artifacts in high-resolution echo-planar spectroscopic imaging of water and fat resonances. Magn Reson Med 2003; 49(6): 1113-1120.

[268]   Oshio K, Kyriakos W, Mulkern RV. Line scan echo planar spectroscopic imaging. Magn Reson Med 2000; 44(4): 521-524.

[269]   Ebel A, Soher BJ, Maudsley AA. Assessment of 3D proton MR echo-planar spectroscopic imaging using automated spectral analysis. Magn Reson Med 2001; 46(6): 1072-1078.

[270]   Ebel A, Maudsley AA. Improved spectral quality for 3D MR spectroscopic imaging using a high spatial resolution acquisition strategy. Magn Reson Imaging 2003; 21(2): 113-120.

[271]   Ebel A, Maudsley AA. Comparison of methods for reduction of lipid contamination for *in vivo* proton MR spectroscopic imaging of the brain. Magn Reson Med 2001; 46(4): 706-712.

[272]   Pelletier D, Nelson SJ, Grenier D, Lu Y, Genain C, Goodkin DE. 3-D echo planar (1)HMRS imaging in MS: metabolite comparison from supratentorial vs. central brain. Magn Reson Imaging 2002; 20(8): 599-606.

[273]   Medved M, Du W, Zamora MA, Fan X, Olopade OI, MacEneaney PM, Newstead G, Karczmar GS. The effect of varying spectral resolution on the quality of high spectral and spatial resolution magnetic resonance images of the breast. J Magn Reson Imaging 2003; 18(4): 442-448.

[274]   Du W, Du YP, Bick U, Fan X, MacEneaney PM, Zamora MA, Medved M, Karczmar GS. Breast MR imaging with high spectral and spatial resolutions: preliminary experience. Radiology 2002; 224(2): 577-585.

[275]   Medved M, Newstead GM, Fan X, Du W, Du YP, MacEneaney PM, Culp RM, Kelcz F, Olopade OI, Zamora MA, Karczmar GS. Fourier components of inhomogeneously broadened water resonances in breast: a new source of MRI contrast. Magn Reson Med 2004; 52(1): 193-196.

[276]   Kreis R. Issues of spectral quality in clinical 1H-magnetic resonance spectroscopy and a gallery of artifacts. NMR Biomed 2004; 17(6): 361-381.

[277]   Doyle VL, Howet FA, Griffiths JR. The effect of respiratory motion on CSI localized MRS. Cooperative Group on MR Applications to Cancer. Phys Med Biol 2000; 45(8): 2093-2104.

[278]   Alger JR. Regulatory, financial and ethical aspects of routine clinical magnetic resonance spectroscopy. NMR Biomed 2000; 13(5): III-V.

[279]   Katz-Brull R, Lenkinski RE. Frame-by-frame PRESS 1H-MRS of the brain at 3 T: the effects of physiological motion. Magn Reson Med 2004; 51(1): 184-187.

[280]   Longo R, Vidimari R. *In vivo* localized 1H NMR spectroscopy: an experimental characterization of the PRESS technique. Phys Med Biol 1994; 39(1): 207-215.

[281]   Ernst T, Hennig J. Coupling effects in volume selective 1H spectroscopy of major brain metabolites. Magn Reson Med 1991; 21(1): 82-96.

[282]   Moonen CT, von Kienlin M, van Zijl PC, Cohen J, Gillen J, Daly P, Wolf G. Comparison of single-shot localization methods (STEAM and PRESS) for *in vivo* proton NMR spectroscopy. NMR Biomed 1989; 2(5-6): 201-208.

[283]   Yongbi NM, Payne GS, Collins DJ, Leach MO. Quantification of signal selection efficiency, extra volume suppression and contamination for ISIS, STEAM and PRESS localized 1H NMR spectroscopy using an EEC localization test object. Phys Med Biol 1995; 40(7): 1293-1303.

[284]   Kwock L, Brown MA, Castillo M. Extraneous lipid contamination in single-volume proton MR spectroscopy: phantom and human studies. AJNR Am J Neuroradiol 1997; 18(7): 1349-1357.

[285]   Ogg RJ, Kingsley PB, Taylor JS. WET, a T1- and B1-insensitive water-suppression method for *in vivo* localized 1H NMR spectroscopy. J Magn Reson B 1994; 104(1): 1-10.

[286]   Moonen CTW, van Zijl PCM. Highly effective water suppression for *in vivo* proton NMR spectroscopy (DRYSTEAM). J Magn Reson 1990; 88: 28-41.

[287]   Lei H, Peeling J. Off-resonance effects of the radiofrequency pulses used in spectral editing with double-quantum coherence transfer. J Magn Reson 2000; 144(1): 89-95.

[288]   McLean MA, Busza AL, Wald LL, Simister RJ, Barker GJ, Williams SR. *In vivo* GABA+ measurement at 1.5T using a PRESS-localized double quantum filter. Magn Reson Med 2002; 48(2): 233-241.

[289]   Sotak CH. Multiple quantum NMR spectroscopy methods for measuring the apparent self-diffusion coefficient of *in vivo* lactic acid. NMR Biomed 1991; 4(2): 70-72.

[290]   Ranjeva JP, Confort-Gouny S, Le Fur Y, Cozzone PJ. Magnetic resonance spectroscopy of brain in epilepsy. Childs Nerv Syst 2000; 16(4): 235-241.

[291]   Wang ZJ, Bergqvist C, Hunter JV, Jin D, Wang DJ, Wehrli S, Zimmerman RA. *In vivo* measurement of brain metabolites using two-dimensional double-quantum MR spectroscopy--exploration of GABA levels in a ketogenic diet. Magn Reson Med 2003; 49(4): 615-619.

[292]   Hu J, Xu Y, Jiang Q, Sehgal V, Shen Y, Xuan Y, Xia Y. Spectral pattern of total creatine and trimethyl ammonium in multiple sclerosis. Magn Reson Imaging 2004; 22(3): 427-429.

[293]   Marzola P, Osculati F, Sbarbati A. High field MRI in preclinical research. Eur J Radiol 2003; 48(2): 165-170.

[294]   Di Costanzo A, Trojsi F, Tosetti M, Giannatempo GM, Nemore F, Piccirillo M, Bonavita S, Tedeschi G, Scarabino T. High-field proton MRS of human brain. Eur J Radiol 2003; 48(2): 146-153.

[295]   Oz G, Henry PG, Seaquist ER, Gruetter R. Direct, noninvasive measurement of brain glycogen metabolism in humans. Neurochem Int 2003; 43(4-5): 323-329.

[296]   Gruetter R, Seaquist ER, Kim S, Ugurbil K. Localized *in vivo* 13C-NMR of glutamate metabolism in the human brain: initial results at 4 tesla. Dev Neurosci 1998; 20(4-5): 380-388.

[297]   Lei H, Zhu XH, Zhang XL, Ugurbil K, Chen W. *In vivo* 31P magnetic resonance spectroscopy of human brain at 7 T: an initial experience. Magn Reson Med 2003; 49(2): 199-205.

[298]   Bartha R, Drost DJ, Menon RS, Williamson PC. Comparison of the quantification precision of human short echo time (1)H spectroscopy at 1.5 and 4.0 Tesla. Magn Reson Med 2000; 44(2): 185-192.

[299]   Alger JR, Frew AJ, Cloughesy TF, Del Vecchio W, Villablanca JP, Curran JG. Novel methodology for the archiving and interactive reading of clinical magnetic resonance spectroscopic imaging. Magn Reson Med 2002; 48(3): 411-418.

[300]   Podo F, Henriksen O, Bovee WM, Leach MO, Leibfritz D, de Certaines JD. Absolute metabolite quantification by *in vivo* NMR spectroscopy: I. Introduction, objectives and activities of a concerted action in biomedical research. Magn Reson Imaging 1998; 16(9): 1085-1092.

[301]   Hajek M, Burian M, Dezortova M. Application of LCModel for quality control and quantitative *in vivo* 1H MR spectroscopy by short echo time STEAM sequence. Magma 2000; 10(1): 6-17.

[302]   Griffiths JR, Tate AR, Howe FA, Stubbs M. Magnetic Resonance Spectroscopy of cancer-practicalities of multi-centre trials and early results in non-Hodgkin's lymphoma. Eur J Cancer 2002; 38(16): 2085-2093.

[303]   de Certaines JD, Cathelineau G. Safety aspects and quality assessment in MRI and MRS: a challenge for health care systems in Europe. J Magn Reson Imaging 2001; 13(4): 632-638.

[304]   Mader I, Roser W, Hagberg G, Schneider M, Sauter R, Seelig J, Radue EW, Steinbrich W. Proton chemical shift imaging, metabolic maps, and single voxel spectroscopy of glial brain tumors. Magma 1996; 4(2): 139-150.

[305]   Preul MC, Caramanos Z, Collins DL, Villemure JG, Leblanc R, Olivier A, Pokrupa R, Arnold DL. Accurate, noninvasive diagnosis of human brain tumors by using proton magnetic resonance spectroscopy. Nat Med 1996; 2(3): 323-325.

[306]   Devos A, Lukas L, Suykens JA, Vanhamme L, Tate AR, Howe FA, Majos C, Moreno-Torres A, van der Graaf M, Arus C, Van Huffel S. Classification of brain tumours using short echo time 1H MR spectra. J Magn Reson 2004; 170(1): 164-175.

[307]   Tong Z, Yamaki T, Harada K, Houkin K. *In vivo* quantification of the metabolites in normal brain and brain tumors by proton MR spectroscopy using water as an internal standard. Magn Reson Imaging 2004; 22(7): 1017-1024.

[308]   Beer M. Cardiac spectroscopy: techniques, indications and clinical results. Eur Radiol 2004; 14(6): 1034-1047.

[309]   Kanowski M, Kaufmann J, Braun J, Bernarding J, Tempelmann C. Quantitation of simulated short echo time 1H human brain spectra by LCModel and AMARES. Magn Reson Med 2004; 51(5): 904-912.

[310]   Geurts JJ, Barkhof F, Castelijns JA, Uitdehaag BM, Polman CH, Pouwels PJ. Quantitative 1H-MRS of healthy human cortex, hippocampus, and thalamus: metabolite concentrations, quantification precision, and reproducibility. J Magn Reson Imaging 2004; 20(3): 366-371.

[311]   Schirmer T, Auer DP. On the reliability of quantitative clinical magnetic resonance spectroscopy of the human brain. NMR Biomed 2000; 13(1): 28-36.

[312]   Duc CO, Trabesinger AH, Weber OM, Meier D, Walder M, Wieser HG, Boesiger P. Quantitative 1H MRS in the evaluation of mesial temporal lobe epilepsy *in vivo*. Magn Reson Imaging 1998; 16(8): 969-979.

[313]   De Beer R, Barbiroli B, Gobbi G, Knijn A, Kugel H, Langenberger KW, Tkac I, Topp S. Absolute metabolite quantification by *in vivo* NMR spectroscopy: III. Multicentre 1H MRS of the human brain addressed by one and the same data-analysis protocol. Magn Reson Imaging 1998; 16(9): 1107-1111.

[314]   Chard DT, McLean MA, Parker GJ, MacManus DG, Miller DH. Reproducibility of *in vivo* metabolite quantification with proton magnetic resonance spectroscopic imaging. J Magn Reson Imaging 2002; 15(2): 219-225.

[315] Li BS, Wang H, Gonen O. Metabolite ratios to assumed stable creatine level may confound the quantification of proton brain MR spectroscopy. Magn Reson Imaging 2003; 21(8): 923-928.

[316] Moats RA, Watson L, Shonk T, Tokuyama S, Braslau D, Eto R, Mandigo JC, Ross BD. Added value of automated clinical proton MR spectroscopy of the brain. J Comput Assist Tomogr 1995; 19(3): 480-491.

[317] Felblinger J, Kreis R, Boesch C. Effects of physiologic motion of the human brain upon quantitative 1H-MRS: analysis and correction by retro-gating. NMR Biomed 1998; 11(3): 107-114.

[318] Schwarz AJ, Leach MO. Implications of respiratory motion for the quantification of 2D MR spectroscopic imaging data in the abdomen. Phys Med Biol 2000; 45(8): 2105-2116.

[319] Hofmann L, Slotboom J, Boesch C, Kreis R. Characterization of the macromolecule baseline in localized (1)H-MR spectra of human brain. Magn Reson Med 2001; 46(5): 855-863.

[320] Hofmann L, Slotboom J, Jung B, Maloca P, Boesch C, Kreis R. Quantitative 1H-magnetic resonance spectroscopy of human brain: Influence of composition and parameterization of the basis set in linear combination model-fitting. Magn Reson Med 2002; 48(3): 440-453.

[321] Stoyanova R, Brown TR. NMR spectral quantitation by principal component analysis. III. A generalized procedure for determination of lineshape variations. J Magn Reson 2002; 154(2): 163-175.

[322] Griffin JL, Bollard M, Nicholson JK, Bhakoo K. Spectral profiles of cultured neuronal and glial cells derived from HRMAS (1)H NMR spectroscopy. NMR Biomed 2002; 15(6): 375-384.

Chapter 13

Disease Studies – Cancer*

L. L. Cheng

Departments of Radiology and Pathology

Massachusetts General Hospital

Harvard Medical School

Boston, Massachusetts, U. S. A.

&

U. Pohl

Department of Histopathology

Addenbrooke's Hospital

Cambridge, U. K.

Content:

In the era of "-omics"

Biological science in the 21st century has been marked by the amending of well-recognized scientific branches into newly created disciplines with the suffix of "-omics." As you may have already noticed, in less then half a decade such popularized disciplines as genomics and proteomics have been embraced by the scientific community, as well as the mass media, although the exact scopes and dimensions of these disciplines are still in the process of development. Not surprisingly, the topic of this book, metabolomics - a junior member of the "-omics" family- and the connection of metabolomics with the aspect of this chapter, human oncology, are even less concretely defined. To facilitate our discussions in this chapter we wish to define current cancer metabolomics as: a study of the global variations of metabolites, and a measurement of global profiles of

metabolites from various known metabolic pathways under the influence of oncological

developments and progressions. We wish to emphasize the keyword in this definition is

"global", which is clearly different from other adjectives, such as "individual".

This seemingly simple definition may not be obvious when you try translating it

into clinical research. In fact, if you proposed to search for cancer metabolite profiles

before the turn of the 21st century you would probably be branded as conducting "fishing

expeditions." Fortunately, the expedition phrase has gradually faded away from today's

scientific colloquy and the disengagement between perceptions of common sense and the

rules in scientific pursuits have been somewhat lessened in regard to metabolomics. As

evidence, if you browse the website of the National Institute of Health (NIH) of the

U.S.A., you will find the word "metabolomics" in the title of Requests for Applications

(RFAs) published by the agency[1]; in addition, at the same time as this chapter is being

prepared in October, 2005, a workshop titled "Frontiers in Metabolomics for Cancer

Research" is being organized by the National Cancer Institute at NIH.

This change of heart regarding the "-omics" came as a direct result of the birth of

genomics. The technological inventions, such as those accompanying the human genome

project, have created this new scientific branch that captures the front pages of mass

media news as well the covers of scientific journals. After the completion of the human

genome project, the innovative use of the suffix "-omics" was created to reflect the

processes of searching for correlations between the large arrays of genome data measured

---

[1] "Metabolomics Technology Development" http://grants.nih.gov/grants/guide/rfa-files/RFA-RM-04-002.html and "Genomic, Proteomic, and Metabolomic Fingerprints as Alcohol Biomarkers" http://grants.nih.gov/grants/guide/rfa-files/RFA-AA-06-001.html.

by these new technologies, with physiological and pathological conditions. Genomics, rather than genetics, has granted "licenses" to many pursuits of clinical importance that would otherwise be rejected by scientific communities because of their exploratory nature and the lack of hypotheses that could be clearly delineated. In other words, the introduction of these new "-omics" branches has ratified formerly inconceivable concepts, allowing scientists a greater breadth of exploration in areas into which they have only vague insight; these explorations do not come at the expense of good science, however, and the "-omics" studies still rely on sound data collection and valid, measurable parameters.

There are many genomics examples of gene expression studies for oncology that can be found in literatures in the past five years. For instance, in a seminal paper published in Nature in 2000, C. M. Perou et. al. reported results of DNA microarrays of 8,102 human genes analyzed using breast tissue samples from 42 individuals[1]. Among the measured genes they analyzed 1,753 (22% of 8,102) of them in an effort to establish "molecular portraits of human breast tumours," as shown in **Figure 1**. In this cluster analysis map each row represents a single gene, while each column came from a measured sample. Without getting into details it may be appreciated that, with the appearance of clustered red and green dots, the map seems to indicate the existence of certain patterns that are not completely random. In hindsight, considering research development experiences since the publication of the paper, one can ponder a number of issues regarding the published study that may have direct implications to the topic of this chapter. Firstly, considering biological variations among individuals, how representative the "portraits" could be if a number of tumors were only collected from a single case?

Secondly, how valuable would the gene profiles be without knowing the pathological details from which the profiles were derived? These issues arise because of the existence of heterogeneity, a major characteristic of human malignancy, i.e. the pathological features and the amount of these features vary among different regions in the same tumor, and the study was conducted on homogenized tissue blocks[2]. Later studies have indicated that these problems could be resolved to satisfactory degrees. The first issue is administrative and somewhat easy to solve as long as multiple clinical cases are available to the study. To solve the second issue, a colleague of ours, D. C. Sgroi, has demonstrated the need for and the feasibility of sample preparation via a special protocol. With the assistance of laser capture microdissection techniques, Sgroi and his colleagues removed pathologically identified specific cell types from 36 breast cancer patients (**Figure 2**), and subjected these removed cells to 12,000-gene cDNA microarray analyses[3]. By analyzing the most varied 1,940 genes (16% of 12,000), they were able to propose genomic profiles for tumors of different grades, as shown in **Figure 3**. Although there are many other studies that may be discussed, these two reports contain some common features that may be appreciated for our subsequent discussion. First, more than 80% of measured parameters did not reach the final analyses, and second, at least, more than half of the genes that composed the final cluster maps were of unknown functions, according to the most conservative estimation.

This seemingly "new" concept for research designs (deviating from the dominated and accepted structure of hypothesis-driven research approaches) has in fact always been employed in medical science and medicinal practice during the progression of modern medicine. For instance, considering histopathology and patient prognostication, and even

equipped with the most up-to-date knowledge of anatomic pathology, it is almost

impossible for us to imagine how one would propose any intelligent hypothesis that could

relate cellular morphological changes with disease processes at the dawn of the discovery

of optical microscopes, or even today. Nevertheless, that did not prevent observation

based anatomic pathology from becoming a discipline that dictates almost every aspect of

oncological practice to this day (as will be discussed later in this chapter). Thus, we can

appreciate the emphasis on the criteria of hypothesis-driven research as the philosophical

practices accompanying the blooming of sciences in the 20th century. In addition we

should also realize the vital value of scientific explorations and derivations from these

observations both in the history and at present. And finally, as hypothesis driven research

was a valuable tool of the past, so can we appreciate the transition in the 21st century to

this new era of "-omics" and the immense scientific potential this era holds.

The current metabolomics

Examining the active field of current metabolomics from the same perspective

that you may use to scrutinize the status of genomics, you may realize that the state of

current metabolomic activities is fundamentally different from contemporary genomics or

proteomics. To fully appreciate the status and utilize the capability of current

metabolomics, we need to dwell a bit on the still young history of genomics.

The development of genomics relied almost entirely on innovations in the

technologies of molecular biology. One such innovation which is now widely used was

the creation of gene microarrays, as exemplified in the previously discussed human breast

cancer studies. The fundamental characteristic of these new array paradigms is their

ability to measure a very large number of parameters at the same time. These parameters can either be the investigation of thousands of genes from one sample, or the simultaneous comparison of the expression of one gene for hundreds of tissue samples. These investigations produce massive amounts of data in a magnitude that was never before witnessed in the human pursuits of biological science. In the context of human pathology, this situation may resemble the overwhelming sensation that our predecessors might have experienced when optical microscopes were first introduced into gross anatomy. The rules of engagement were changed. Thus, the transition to morphological examination more than a century ago required digestion and evaluation efforts of many generations, in many decades, to present us with the current prominent status of anatomic pathology. While optical microscopes allowed pathological evaluations to intrude into smaller physical spaces, genomics expanded our ability to evaluate a vast amount of genetic parameters, for many of which our current genetic knowledge cannot provide insight. Hence, we may expect that the efforts of the coming generations may be necessary to fully comprehend the functional importance of these genes; although hopefully the ever-increasing pace of developments in science and technology may facilitate these digestion and evaluation efforts. For example, at the time this chapter is being prepared, we notice a current publication on *interactome* and *transcriptome* in Nature (11 August, 2005)[4]. In this work M. Vidal and colleagues expanded the previous concept of interactome for studies of protein-protein interactions, a. k. a. *interactomics*, into evaluations of relationships of gene expression profiles, now known as *integrative interactomics,* to identify the functions of genes in *Caenorhabditis elegans*.

Fortunately, the current status of metabolomics is less complicated than the those of genomics and proteomics, which mostly present either dots of individual genes or proteins with *unknown* linkages among them, or genes/proteins with indiscernible functions that require interactomics to reveal them. As already stated in the beginning of this chapter, our interpretation of and emphasis for the current metabolomics is focused on evaluations of global variations and global profiles of metabolites from various *known* metabolic pathways in relationship with physiological and pathological processes. This "known" vs. "unknown" difference, in our opinion, is the unique characterization of metabolomics that philosophically differentiates it from the current concepts of genomics and proteomics.

This "known" status is due solely to the fact that, up till now, there have not been fundamental technological breakthroughs in the innovation of metabolite analysis. This situation is very unlike the fields of genomics and proteomics where breakthrough technical innovations have been witnessed in the past years. Methodologies used in current metabolite analyses were well-established in past decades. Because of this the metabolic knowledge currently studied by the methodologies of analytic chemistry are known, at least individually, for each metabolite based on characterization through many tests and proven metabolic pathways. These methodologies currently include nuclear magnetic spectroscopy (NMR), mass spectroscopy, and gas chromatography.

You may agree with the concept that the words "genomics" and "proteomics" first serve to capture the images of scientific frontiers whose constitutes and significance are still unclear. Second these terms emphasize the need to consider all the measurable parameters simultaneously. If you concur with these statements then from our above

discussion you may realize that the same concept cannot be applied to the parallel expression – metabolomics – without alterations. At the present, conducted with the above-mentioned well-tested methodologies for metabolite analyses, the chance for the discovery of new metabolites in vast quantities as witnessed in the other "-omics" fields is relatively slim. However, this should not discourage the development of metabolomics from the philosophical aspect of the "-omics" concept on global interpretations of the organization of the current knowledge on the overall metabolite pathways. The task of primary importance in current metabolomics is to interpret the global metabolite alterations collectively in the context of their overall changes in relation to human physiological and pathological conditions. For the purpose of this chapter, it is to better understand the global inter-connectivity of metabolites from various known metabolic pathways during the development and progression of human malignancies. Such a concept reflects and agrees well with the somewhat ancient idea that the human body is a united organic entity within which all the biological processes are inter-connected and balanced to produce measurable metabolite profiles. It is this overall profile, likely not a single metabolite, that may alter cell chemistry and be informative as indicative of disease. We also wish to emphasize that our statement regarding the slim chance for discovering new metabolites with the current analytic methods merely reflects our assessment of the limitations of the existing analytic methodologies. It by no means indicates we should stop expanding our knowledge on human metabolism. On the contrary, given the numbers of new genes and proteins being discovered, we believe the numbers of metabolites unknown to us may be too large to estimate.

A metabolite, according to Oxford English Dictionary, is "a substance that is a substrate or product of a metabolic reaction, or that is necessary to a metabolic reaction; *esp.* an intermediate or end product of a metabolic pathway (Draft Revision Dec. 2001)." The pictorial interpretations of this simple definition can be very complicated for many of us to grasp. Demonstrations of the current knowledge on human metabolism can be found in various maps and charts of metabolic pathways; charts such as the one comprehensively generated by Dr. Donald E. Nicholson of Leeds, England, in collaboration with the International Union of Biochemistry & Molecular Biology and with Sigma-Aldrich (**Figure 4**). Since any substance registered in such a chart, and possibly millions of the others that are still unknown to us, can potentially be the fair targets and subjects of metabolomics, the complex future of metabolomics seems impossible to comprehend at this moment. On the other hand, if we again consider that under normal conditions all of these pathways in a human body are initialized by dietary intakes, then such a puzzling chart may be simplified greatly to carbohydrates, lipids, proteins, amino acids, etc. Thus, it seems that any measurement of these substances, using any modality taught in college classes of analytical chemistry, can be potential subjects of and tools for metabolomics. In reality, we need to point out that, presently in 2005, the bulk of the so-called metabolomics data associated with human oncology is supplied by NMR analyses. We attribute this observation to the fact that there has been an established NMR community actively pursuing identification of cancer related metabolites far prior to the era of "-omics." We hope that by now you have noticed that whenever we mention metabolomics we define it as "the current metabolomics" or "metabolomics of today." This is due particularly to the above-mentioned fact of the

prior existence of analytic technologies in metabolite chemistry. Many parts of our

discussion should be viewed as applicable only to the present status of metabolomics.

Although it is hard to predict the era to come, we are certain that technical developments

will change the face as well as the contents of metabolomics in the near future. The

situation of current and future metabolomics is concisely summarized by the previously

mentioned NIH RFA: "Technologies currently in use for metabolomic analysis include

NMR, chromatography and mass spectrometry, each of which has significant limitations

in quantification, scope, and/or throughput. No one technology can effectively measure,

identify and quantify, with sufficient sensitivity and precision, the diverse range of

metabolites and their dynamic fluctuations in cells. An integrated set of technologies is

needed to address the entire spectrum of challenges for metabolomics. Ideally, new

technologies should yield quantitative, comprehensive data and be applicable to

achieving anatomical resolution at the cellular and subcellular level"[2].

The current oncology

Any clinical procedure in modern medicine, including oncology, can be

characterized into one of the following categories for disease management: screening,

diagnosis, or therapy. Developments in modern medicine, therefore, have been spinning

around advancements in these areas. Surveying the current status of oncology, the

impacts of new scientific knowledge and technology innovations are evident.

Unfortunately the consequence of new knowledge and its impact on the life or the quality

---

[2] "Metabolomics Technology Development" http://grants.nih.gov/grants/guide/rfa-files/RFA-RM-04-

002.html

of life for patients may not always be as pleasant as expected. For instance, with the realization of the relationship between certain genetic mutations and breast cancer development, prophylactic mastectomy (preventive removal of breasts) has been offered to women who are considered to be at high risk. However, harboring certain genetic mutations does not mean that cancer is present, or will always occur. Hence, it may be argued that prophylactic mastectomy might not be necessary for all women in whom these mutations are detected. Therefore, it can be best argued that in such a case new and more accurate disease markers are urgently needed; specifically markers that are particularly sensitive in early detection of cancer and preferably pre-cancerous lesions. The pursuit of how best to incorporate scientific developments into oncological practices to serve patients and not merely to treat diseases presents not only as a medical or technological topic, but a medical philosophical and ethical issue as well.

Examining the effects of emerging disciplines on disease management, we find that histopathology (the current "gold standard" in cancer diagnosis) is no longer viewed as an optimal diagnostic tool. Histopathology provides accurate, literal pictures of the existing state of specimens under evaluation. However, its ability is limited when it comes to providing information that may delineate the preceding condition of the individual patient prior to the particular histopathological presentation or to suggesting the possible or probable disease course for an individual condition, partly due to the limited nature of morphological appearances that may mask the actual character of the disease. Histopathology works statistically well in providing disease interpretations for a class of conditions or a group of patients. Particularly, the histopathological approach to cancer diagnosis has served oncology sufficiently in the past, when the oncological

needs for decision-makings on therapies were a direct result of symptoms that had displayed clinical significance. However, these past successes have been challenged in the current era of cancer screening, when patient presentations are asymptomatic and the diseases are early enough to defy the statistical efficiency of the morphological pathology. With the creation of new testing protocols there is now a societal demand for early diagnosis and individual disease management. For this reason, if you immerse yourself in oncological discussion in these days, often what you will hear is not how to treat this group of patients, but rather what is the best treatment plan for this *individual*. This situation can best be illustrated by some examples.

Prostate Cancer

When discussing the impact of the new screening era on oncology, no other type of cancer is more divisive than prostate cancer. The status of prostate cancer as a common, controversial malignancy has not changed since the second half of the 1980s when the blood test of prostate specific antigen (PSA) for cancer screening was introduced. In the United States alone in 2005, it is estimated that more than 635 men are diagnosed with the disease daily, and another 83 lose their lives to the disease[5]. Meanwhile, considerable concerns have been expressed regarding the adverse effects of surgical intervention for tumors that may never likely become life threatening, as the >150 radical prostatectomies performed each day in the U.S. result in impotence for >90 men, and/or incontinence of urine for >45 men.

Facing this complicated situation involving a common disease, instead of posting clinical questions that intrigue us, we encourage you to ponder simultaneously a number of factors related to prostate cancer: the increased incidence rate achieved with PSA

screening led to the increase of "indolent" cancers in PSA screening populations; the seemingly steady death rate over the history (**Figure 5**); the adverse effects experienced by considerable numbers of patients as results of therapies; and the large body of autopsy evidence that shows about 20-30% of men before the PSA testing era harbored indolent prostate cancer in their gland in non-prostate-cancer related deaths. How should all these facts play into decision making in the prostate cancer clinic, both in terms of providing the most appropriate care for an individual patient and for the interests of healthcare costs of the society?

These issues were realized by the National Institute of Cancer (NCI) in the U.S. in the 1990s. At the request of the then NCI director, Dr. Richard Klausner, the NCI Prostate Cancer Progress Review Group (PRG) was formed in 1997 with more than twenty prominent scientists and patient advocates on prostate cancer. After more than one year of work, the PRG published a report titled, "Defeating Prostate Cancer: Crucial Directions for Research"[3]. In the PRG Report the panel notes that "[b]ased on autopsy studies it is estimated that as many as 1 in 4 men 30 years of age may harbor a small focus of PCa in their glands." Furthermore, "[t]he basic problem … is that while about 11 percent of all men will contract clinically significant PCa in their lifetime, only 3.6 percent will die of it. The challenge is to determine which of the 7 to 8 percent can safely go untreated." The Report cites "our inability to distinguish 'indolent' from 'aggressive' carcinomas," concluding that this can "lead to the adverse consequences of over-treatment" if "[the] tumor is one that will remain 'quiescent,' or clinically insignificant throughout [the patient's] natural life span."

---

[3] http://prg.nci.nih.gov/pdfprgreports/1998prostate.pdf

The utility of PSA testing in detecting clinically significant prostate tumors has been clinically proven. However, in the PSA screening era, most newly diagnosed prostate cancer (more than 70% at conservative estimations) belong to a similar group according to Gleason histological grading, which current histopathology cannot further sub-categorize without additional surgical intervention. Furthermore, tumors of clinical significance may be neither lethal to their hosts, nor indicative for "definitive therapies" that may increase "morbidity, particularly incontinence and/or impotence," as being noted by the PRG report. In fact, the PGR report estimates that currently in the U.S. >30% of prostate cancer patients are over-treated. The urgent task set forth by the PRG report is to discover "new and better markers than PSA for the early diagnosis of patients who harbor fast-progressing and virulent forms of prostate cancer." These markers are expected to "refine" early detection with PSA testing by identifying cancers able to kill their hosts if left untreated, double-checking for overlooked virulent cancers, and in doing so furnishing "prognostic markers that can guide the therapy of patients in an individualized fashion". To realize this goal, the PRG advised the development and validation of molecular assays with the comments that "[e]valuation of limited disease in the prostate is prone to extensive sampling error caused by heterogeneity. The availability of micro-dissection techniques and/or aspiration biopsy, coupled with molecular analyses (i.e. RT-PCR) or array analysis), could provide new approaches to conventional tissue analysis." If these words from the 1990s are translated into today's vernacular, they likely indicate the future advances in prostate cancer clinic will be discovered through "-omics".

Breast Cancer

The numbers of NCI Progress Report Groups (PRG) have grown to 12 that cover almost all types of human malignancies[4]. However, before the turn of the 21st century, there were only two issued in 1998. One of them was the previously discussed prostate cancer PRG, and the other, commissioned in the same period and published at the same time, was titled: "Charting the Course: Priorities for Breast Cancer Research"[5].

The status of breast cancer in women is very similar to that of prostate cancer in men. In the U.S., breast cancer has always been the most frequently diagnosed cancer in women, and was only reduced to the second leading cause of cancer death in 1980s after the increase of lung cancer incidence[6].

In this era of public awareness and improved screening technologies breast cancer, similar to prostate cancer, presents its own controversial issues. Controversies in the care of breast cancer patients can be visualized and understood, step-by-step, by following the practices in a comprehensive breast health clinic:

Very often one to several suspicious lesions are identified by self-examination, annual physical examination, and/or a mammography. Since no non-invasive diagnostic modality is now available, everyone agrees that a biopsy, whether a fine-needle aspiration (FNA) or more often a core needle biopsy (both possible in a doctors' office), is necessary.

Unfortunately, this may be the last universal agreement among caregivers, breast cancer patients, and their physicians regarding treatment options. Disagreements arise immediately at the interpretation of the observation of many FNA and core needle biopsy

---

[4] http://planning.cancer.gov/disease/plans.shtml#prg.

[5] http://prg.nci.nih.gov/pdfprgreports/1998breastcancer.pdf

specimens. Discrepancies in these observations often result in open biopsies (operating room procedures) for these FNA and/or core needle inconclusive patients, who represent a very large population. Focused on the histopathology issues of breast cancer, the breast cancer PRG report recognized that light-microscope based diagnostic and prognostic "criteria are suboptimal," and recommended that "markers should be sought that will signal the presence and identity of specific types of lesions, indicate their prognosis if left untreated, and predict the likelihood that they will respond to particular types of therapy. Clinically useful markers will most likely be identified and characterized first in tissue samples obtained during biopsy or surgical procedures."

Another controversy in today's breast cancer clinic deals with the uncertainty of how to deal with the greatly increased number of ductal carcinoma in situ (DCIS) patients in the mammographic screening era. Twenty years ago DCIS represented only <1-5% of detected breast malignancies. The introduction and widespread availability of mammographic screening, which has greatly improved our ability to detect non-palpable and asymptomatic breast cancer, has increased the reported incidence of DCIS detection to >50% of all malignancies discovered by mammogram-directed biopsies. This increase has generated a spectrum of challenges to current surgical pathology, ranging from evaluation of breast biopsy specimens to direction of post-surgery therapy. For instance, it is known that frozen section intra-operative evaluation, while generally reliable in diagnosing palpable breast masses, is of limited use in the diagnosis of non-palpable DCIS. The vast number of cases itself has also indicated that DCIS, rather than a simple breast cancer subtype, represents a collection of lesions with varied malignant potential and morphological heterogeneity. Thus, the interobserver reproducibility of

histopathological diagnosis for DCIS is poor. Mastectomy is considered a curative treatment for DCIS, but its radical nature has recently been criticized as unnecessary overtreatment for many women with mammogram-detected, early stage DCIS. Ideally, all women diagnosed with non- or less aggressive DCIS could successfully be treated with breast-conserving treatment (BCT), but this course may not be successful for highly aggressive lesions. Commonly histopathology cannot classify variations in DCIS morphology, assess tumor aggressiveness, nor direct adjuvant systematic therapies (AST) for individual patients, particularly when the objectives for intervention emphasize consideration of a patient's comfort and quality of life. Regarding DCIS, the PRG summarized that "[t]hese women will have near normal survival but may experience short and long-term morbidity from treatment. DCIS is seriously understudied from a disease- and patient-focused outcomes perspective." The PRG further recommends research to integrate patient-focused data "with biological prognostic information to make the best treatment decisions" for these DCIS patients.

The increased number of tumors detected at early stages have also generated another controversy. Currently treatments for tumors at early stages (such as DCIS, and low grades) occupy an entirely different arena from they did two decades ago in the era predominated by total mastectomy. Breast-conserving treatment is considered to be a major aim of breast cancer treatment in the 21st century. The new BCT approach is clinically and scientifically sound, since it has been shown that patients with a grade I tumor have an 85% chance of surviving for 10 years after diagnosis; however, a grade III tumor reduces the chance of 10-year survival to 45%. An 85% likelihood for survival at 10 years following diagnosis can be considered a great achievement in our battle against

breast cancer in light of cancer epidemiology. However, in reality clinicians and patients

are more interested to know, not cancer statistics, but if THIS patient will survive for 10

years. Each patient represents 100% of her own statistics, and unfortunately, due to the

extreme heterogeneity of the disease, the current pathology cannot differentiate the 85%

survival from the 15% mortality group. Uncertainty as to the nature and aggressiveness

of an individual woman's cancer, and the need to rely on historical statistical data, can

result in undertreatment or overtreatment of the *individual* woman. For example,

chemotherapy is routinely given to women with breast tumors over 1 cm and negative

lymph nodes even though only 3-5% of those treated are expected to benefit.

Conversely, chemotherapy is routinely withheld from women with tumors under 1 cm

and negative lymph nodes, even though some will ultimately develop metastatic disease.

New approaches to characterize tumors that better reflect their biological behavior are

sorely needed. These needs were concisely summarized by the PRG as the opportunities

in breast cancer research to: "Develop new methods to diagnose clinically significant

breast disease and predict clinical outcome better than conventional histologic

examination and the few available biomarker assays ;" and to discover "biomarkers that

predict the clinical outcome of precancerous and cancerous breast lesions if left untreated

(i.e., prognostic factors) with a high degree of certainty."

This list of controversies related to the breast cancer clinic goes on, but we will

stop after the next one concerning post-surgery adjuvant systemic therapy (AST).

Current pathology, developed from observations over the last 100 years, has identified

many prognostic factors for invasive breast cancer, such as tumor size, differentiation

status, lymph node stage, vascular invasion, etc. However, these factors have proven to

be too generalized in that they fail to consider the biochemical characteristic of an individual tumor. Since almost all the AST currently used in breast cancer clinic — chemo- and radiotherapy — are known to have association with morbidity, personalized therapeutic protocols based on tumor biomolecular signatures are clearly the hope of future breast cancer clinics, especially in the age of BCT. In addition, although there are a number of oncological drugs available, the current AST chemotherapies are still generally conducted on a trial-and-error basis for an individual patient. If one agent fails, valuable time in the window of treatment is lost. Clinicians thus face an urgent need to measure and understand the biological nature of a specific tumor in order to predict the potential efficacy of a particular agent for an individual patient. Again, the breast cancer PRG urges researchers to "learn more about the biology of breast cancer for the purpose of predicting clinical course and predicting response to therapy;" and to discover "biomarkers that predict the response of precancerous and cancerous breast lesions to specific types of therapy (i.e., predictive factors) with a high degree of certainty."

The arguments for and discussions of the need for new and better disease markers for every step of oncological clinics can be made for every type of cancer. Biomarkers that are urgently needed include those that are particularly sensitive in early detection of cancer and precancerous lesions, as well as biomarkers that may test the current oncological hypothesis that cancers may be controlled as chronic disorders, rather than being intervened as acute diseases.

From histological to molecular pathology

The discovery and invention of cancer screening protocols were the fruits of intensive cancer research efforts in the 1970s and 1980s that resulted in the advancements of knowledge in cancer biology and developments in biomedical technologies. The contributions of these screening practices in the identification of malignancies at their early stages, and in the improvement of disease control and patients' survival, were evident. For instance, at present, the percentage of women diagnosed with breast cancer is 1.5 times higher then it was 25 years ago, while the percentage of women who die of the disease has been reduced by about 15% from its value a quarter of a century ago. Similarly, as previously discussed, with the assistance of blood PSA tests, the detection of incidences of prostate cancer at relatively early stages has increased greatly. Thus, if we look narrowly at the ratio between the greatly increased incidences over the seemingly almost unaltered death numbers due to the disease it may be argued that the invention of PSA testing has guided many asymptomatic prostate cancer patients to seek early treatments, and the "cure rate" of the disease has improved. However, as already discussed, there are some troubling facts related to these early diagnoses that should lead us to pause and evaluate the current status of the clinic and the clinical impacts of early diagnoses. This data illustrates the fact that morphology-based histological pathology served oncological practice sufficiently to the end of 1980s, or even the beginning of 1990s, prior to the establishment of the current concepts and practices of cancer screening. In those days, oncological clinics received patients either with palpable masses, or internal masses which had grown to become functionally destructive. In other words, before the start of the cancer-screening era, oncological clinics dealt with relatively later stage diseases. From these cases, pathological evidences and experiences

were also accumulated from the corresponding stages of the diseases. Therefore, the criteria for cancer diagnoses that matured in those days are based heavily on later stage histological pathologies and need to be up-dated to include new observations of vast amounts of tumors diagnosed at early stages.

Fortunately, crises and opportunities often come hand-in-hand. Developments in molecular biology, particularly in cancer biology, coincide with the progression of cancer screening evolution. These developments have greatly enlarged our breadth of knowledge, or, more conservatively, have begun to unveil mysteries surrounding the biological mechanism behind these morphological alterations. Applications for these developments in clinical practices have created new pathological branches that form current molecular pathology. A number of these new biological markers have been utilized in clinical evaluations. For instance, many common names, such as estrogen receptor (ER), P53, etc., have been integrated into comprehensive pathological evaluations for their empirical values in the patient prognostications of certain malignancies.

To systematically analyze the potential utility of cancer biological information - bioinformatics- obtained from genomics, proteomics, and/or metabolomics in assisting histopathology in oncological clinics, it may be helpful to analyze the relationship among these scientific branches. To begin these analyses, we need to assume that the metabolic activities in malignant cells are different from those in normal cells. We consider this hypothesis to be scientifically sound, reasonable and self-evident.

Based on this hypothesis, we wish to consider the sequence of events in cancer development and the roles metabolites play. Changes in metabolic profiles are the results

of certain active metabolic pathways. For these pathways to be active, active enzymes are needed. To have enzyme activities, enzymes need to be synthesized. Furthermore, to synthesize enzyme proteins requires the existence of messenger RNAs (mRNAs), and forth the correct DNAs. On the other hand, with mutated DNA the required mRNA may not be available for the synthesis of the enzymatic proteins; thus as a result of the DNA mutation, certain metabolic pathways are blocked. We can only present this basic molecular biology concept as a chain of events, however, we wish to emphasize that by presenting in this way we do not suggest that there are measurable temporal sequences and delays in association with genes, proteins, and metabolites. Viewing the human body as a united entity, without the exact knowledge regarding the dynamic rates of these molecular (genomic, proteomic, and metabolomic) transformations, we can speculate that the entire process may occur simultaneously and be coupled with feed-back loops and parallel processes. This means that a logically clean chain of events is not always discernable; although we suspect that there must be a time window during which the presentation of malignancy transformations may be detectable by molecular biology means, while the revelation in cellular morphology is still uncertain. Thus, quantitative evaluations (proteomics, metabolomics) of the biological activities of an individual lesion may provide more sensitive and predictive parameters that may be able to subcategorize histomorphology results.

From this above reasoning, we can likely conclude that in order to observe certain metabolic profiles during or after malignant transformations, their corresponding gene players need to be in the right time and place, i.e. these genomic factors may be the necessary condition for the formation of the related metabolomic results. Hence, the

processes of malignancy formations and progressions will require every player involved in all these "-omics," and every interfering factor in the entire duration, to be in harmonic association. Factors from all these disciplines reflect the same biological process from different angles, and at different points in the malignancy formation. In the larger picture of genomics, proteomics, and metabolomics, genomics has a stronger predictive capability than proteomics or metabolomics, while the latter two are viewed more as studies of the *current state* of the malignancy (although this may change as our understanding of complex gene relationships develops). A complete assessment of the strengths and weaknesses of parameters measured from each discipline, and their correlations with histopathological observations and oncological realities, presents great potential for the improvement of cancer characterization to meet the needs of the current screening era.

Having discussed the general connections between all these disciplines and their relationship with human oncology, we would like to clearly state the importance of histopathology and its predominant role in the present practice of oncology. We are compelled to do so because one of us, as a clinical pathologist, reads pathology slides under microscopes everyday; more importantly we believe new disciplines should complement, not directly contradict, histopathology. Current histopathology, as previously explained, is the gold standard for the diagnosis of malignancy and the prognostication of a patient. The knowledge of this field is based on the collective and continuous contributions of human efforts over the past centuries. The very basic "do no harm" principle of modern medicine requires us to practice oncology exclusively based on the recommendations of histopathological conclusions until there is convincing

clinical proof that other modalities can bring more benefit to the patients.

Acknowledging that histopathology is a very subjective tool that leads to a lot of gray

area, we conclude that histopathology is an excellent point from which to launch

research in the areas of the "-omics" and, with time, new quantitative forms of

measurements will be developed.

Chemical detection of cancer

To be trained as a board certified pathologist requires one's earnest efforts for

more than a decade. However, after a few minutes with an effective pathologist anyone

with genuine interest may be able to appreciate the unique cellular pattern presentation of

cancer observable under a microscope. A nice depiction of the disease can be found on

the cover of the first issue of Nature Review Cancer (**Figure 6**), where leg-like arrays of

diseased cells spreading into the surrounding of the lesion pictorially exemplifies why

"cancer" gets its name from the Greek word for "crab." Seeing cancer cells and the

"crab" formation under a microscope irrefutably displays the presence of the condition.

In contrast to visual presentations of the disease, the idea of diagnosis based on molecular

biology or chemistry requires more imagination. Nevertheless, evidence of associations

between the presence of certain proteins/metabolites and clinical conditions of cancers

has been broadly studied and reported. For instance, in 1993 C. E. Mountford and

colleagues reported an interesting study involving magnetic resonance spectroscopy

analysis of lymph node metastasis in a rat model. From their study they found the

sensitivity of MRS in suggesting the existence of malignant cells in lymph nodes, what

they termed "micrometastases," that were not apparent even when the entire node was

serially sectioned and examined by histology. However, the MR conclusions were confirmed with the development of malignancy by xenografting nodal tissue into nude mice[7]. Studies such as this are extremely clinically relevant. In 1990, a retrospective study in Lancet revealed that: "Serial sectioning of lymph nodes judged to be disease-free after routine examination revealed micro-metastases in an additional 83 (9%) of 921 breast cancer subjects"[8].

The utility of biological markers in human cancer classification for the purpose of predicting patient outcomes have also been demonstrated in human clinical studies. An example of such evaluations in human brain tumors was published by one of us with D. N. Louis and colleagues in 2003. The study investigated the use of gene expression profiling of a 12,000 gene microarray in classifying a set of 50 high-grade gliomas (28 glioblastomas and 22 anaplastic oligodendrogliomas). By developing a prediction model, results of the study indicated that the inclusion of genomic profiles could produce brain tumor classification criteria that were more objective, explicit, and consistent with patient clinical outcomes than assessments made from standard pathology alone[9].

Chemical and molecular biological detections of cancer have also evolved in more clearly "seeing" tumours with the development of various molecular imaging methodologies, including infrared, mass spectroscopy, and magnetic resonance. The advantage of these imaging approaches is that they preserve the concept of recognizing the anatomic structures central to pathology evaluations by expanding the visible wavelength used in histopathology into the invisible domains of human vision. However, at present, there are still many limiting trade-off aspects regarding these attempts. Commonly, a better spatial resolution (or anatomic details) comes at the expense of a

limited spectral resolution (differentiating different chemicals) for any imaging modality because of the intrinsic competition between signals and noises.

Discussions on applications for genomics and proteomics in human malignancy, as rapidly emerging fields, are beyond the scope of the current monograph on metabolomics. However, we wish to point out that the differences between proteomics and metabolomics, in our opinion, are not as fundamental as the differences between them and genomics. To simplify the difference between proteomics and metabolomics, if metabolomics concentrates on the understanding of molecules that are considered to be monomers (for instance, amino acids), then proteomics focuses on the research of some kind of polymers of these monomers (i.e. proteins). Therefore, any method developed in analytic chemistry, or found in an instrumental analysis textbook, can have its potential applications in both proteomics and metabolomics studies. However, there are exceptions.

One exception, a method that may only be used for metabolomics but not for proteomics analysese , happens to be the major topic that we will discuss in the rest of this chapter, i.e. cancer pathology measured with intact tissue high resolution magnetic resonance spectroscopy. In general, this approach is capable of analyzing cellular metabolites and tissue histopathology from the same sample. This methodology eliminates the confounding factor of tumour heterogeneity seeing in a correspondence between molecular profiles and histopathological patterns created with separate samples from the same clinical case. We select this chemical methodology to illustrate applications for metabolomics on human cancer for several reasons. First, since the methodology was proposed by one of us in mid 1990s, it has been rapidly utilized by

many research laboratories around the world on a variety of human diseases including many types of malignancies. Second, we have not yet seen any other metabolic approach (mass spectroscopy, liquid chromatography, or infrared, etc) that can demonstrate the same degree of relevance to clinical oncology in terms of the potential to establish one-to-one correlations between metabolite profiles and tissue pathologies, for almost all of the other approaches require procedures of chemical extractions of tissue samples that have not yet been characterized by histopathology.

Magnetic resonance spectroscopy and cancer

Before we engage in the discussion of intact tissue high resolution magnetic resonance spectroscopy on identification and utilization of cancer metabolomics, we wish to overview briefly the field of magnetic resonance spectroscopy in cancer prior to the discovery of this methodology.

Magnetic resonance (MR) spectroscopy has also been known as NMR (nuclear magnetic resonance) to chemists and physicists decades before the medical use of magnetic resonance imaging (MRI). NMR signals are extremely sensitive to changes in chemical environments and have been widely applied in physical and chemical analyses before the invention of MRI. For the topic of this chapter we will confine ourselves to discussion of ex vivo tissue magnetic resonance spectroscopy and will not traverse the enormous field of medical imaging.,

Prior to the "-omics" era magnetic resonance spectroscopy had shown the ability to quantify metabolites of different cell types and detect relatively small populations of abnormal cells. Diagnostic in vivo proton magnetic resonance spectroscopy studies of

human malignancies have aimed at characterization of lesions and assessment of tumor grades and stages. However, these attempts have not yet reached the critical status where clinical decisions can be based solely on these measurements.

It has long been considered that fundamental in vivo improvements rely on the more accurate characterization and quantification of tumor metabolites measurable ex vivo at high magnetic field strength with high spectroscopic resolution. Ex vivo studies started more than two decades ago aimed to: correlate cancer pathologies with spectroscopically measurable metabolite alterations; elucidate the details of cancer metabolites so as to better to understand tumor biology; and improve designs of in vivo methodologies. The ex vivo studies conducted prior to the introduction of intact tissue high resolution magnetic resonance spectroscopy utilized the conventional NMR methodology designed to analyze aqueous homogeneous solutions. Unfortunately, such an approach rests on the false assumption that fundamental physical differences between aqueous solutions and non-liquid tissues are relatively insignificant. In reality, substantial differences exist between aqueous solutions and intact tissues. As an unavoidable result, low spectral resolution data observed with non-liquid tissues preclude measurement of individual metabolites.

The invalidity of the above assumption (i.e. intact biological tissues and aqueous solutions may be treated similarly) did not go unrecognized before the discovery of intact tissue high resolution methodology. To overcome the issue of low resolution observed with intact tissue samples, and to achieve measurement of individual metabolites at high spectral resolution, tissue metabolites were analyzed in solutions of chemical extractions. Unfortunately there were other difficulties or uncertainties associated with extraction

approaches. First, understandably, the measured spectral results depend on the applied

extraction procedures and their completeness. Since the assurance of completeness may

not be tested by any experimental design that involves the procedure itself, it may be

accurate to state that extractions may alter measurable metabolites to an unknown degree.

Second, and more importantly, as previously discussed, heterogeneity of human

malignancies limits the usefulness of extraction approaches because the procedure

prevents histopathological evaluation of the same specimen. Hence, even equipped with

perfectly resolved spectra and precisely quantified metabolite concentrations, no one

could rationalize the pathology compositions that generated this data. Regrettably, an

extremely large body of extract studies on human malignancies, which could be

misleading to various degrees, exists in the literature. In short, we will never know the

exact pathological details corresponding with various chemical and biological profiles

obtained for many types of human malignancies in hundreds, maybe thousands, of

publications. Applications of conventional NMR on studies of animal models may not be

assessed with equal alarm, as tumour heterogeneity often does not play a critical role in

those models, sometimes referred to as "living Petri dishes."

Development of intact tissue MR spectroscopy

During his post-doctoral studies at the Massachusetts General Hospital and

Harvard Medical School, one of us discovered that spectral resolution of proton (1H)

NMR of intact tissue could be greatly enhanced by subjecting the unaltered intact tissue

sample to a NMR technique known as magic angle spinning (MAS), which was

previously developed for chemical studies of solids. This line-narrowing technique by

mechanical sample rotation can generate spectral resolution sufficient for the identification and quantification of individual metabolites in *intact* biological tissue without needing to produce solutions of tissue extractions. In a later study, with a critical observation made by D. C. Anthony, a neuropathologist and the then acting Chief of Pathology at Boston's Children Hospital, it was found that under a moderate rotation (for instance below 3 kHz for brain tumor tissues) tissue pathological structures did not undergo severe alterations[10]. This meant routine histopathology could be conducted with samples after spectroscopy analyses, if the pathologist is aware of certain possible artifacts introduced by the mechanical spinning. Only after this additional discovery was the HRMAS methodology established as a capable choice for recording sample metabolite concentrations and quantitative pathology from the same specimens in order to correlatespectroscopic data with quantitative pathology . This methodology has since been termed high resolution magic angle spinning proton magnetic resonance spectroscopy (a. k. a. HRMAS 1HMRS). For readers who wish to know more about the methodology, its physical description and experimental design, we suggest you consult Chapter 4 in this monograph, titled "Analytical Methods – MAS NMR," by D. Cory and colleagues.

HRMAS 1HMR spectroscopy has multifold advantages. For instance, histopathology evaluations are the impressions of pattern recognitions by a trained observer, whereas spectroscopy examinations can express a medical condition by numerical values once the links between data of spectroscopy and known pathologies are established. Therefore, a computer can readily assume further analyses of spectroscopy results, while computerization of histopathological evaluations is still difficult for us to

envision. Furthermore, the above-mentioned numerical nature of spectroscopic

evaluation of tissue status may be more objective and repeatable than the "artistic" nature

of histopathological evaluations. Even more importantly, HRMAS 1HMRS will likely

constitute biological parameters for patient prognostication that will be complimentary to

or more sensitive/accurate than those in current clinical practice based on cellular

morphology.

It also needs to be realized that, although drastic improvements in tissue

metabolic analyses have been fostered by the introduction of this method, the discussed

tissue magnetic resonance spectroscopy is not the "silver bullet" that can solve all the

remaining issues with cancer diagnosis. There are still many intrinsic limitations

associated with intact tissue spectroscopy analyses. For example, utilizing this analytic

approach alone will not solve the widely recognized "sampling error" problem associated

with histopathology, i.e. histopathology results can only be as good as a measure of

features that present themselves on the evaluated tissue slides. Due to the heterogeneous

nature of human malignancies, false negative conclusions may be reached if the sampled

tissue specimens contain no cancer cells, particularly during biopsies. This clinical issue

clearly cannot be overcome by utilizing a different analytic protocol. In fact, we suspect

that similarly as histopathology, any molecular pathology evaluation will also encounter

sampling errors of its own kind. Similarly, as we previously reported that different

regions possess different metabolite profiles that correlate with differences in tissue

pathologies observed in a case of human brain tumor[10], we suspect that heterogeneities in

genomic and proteomic profiles may also exist, hence susceptible to sampling errors.

Interesting questions to consider are how much overlap exists among these

heterogeneities, which one is less heterogeneous throughout the lesion, and which one may have the largest field effect that extending the malignant information beyond the perimeters of the optical or human vision visible lesions. We will discuss and illustrate this concept of field effects with examples in the following sections.

From tissue MR spectra to cancer metabolomics

The status of cancer metabolite studies can best be presented by reviewing current publications of research using intact tissue MR spectroscopy. First of all, these studies have covered many types of human cancers including: brain, prostate, cervix, breast, kidney, and sarcomas. Next, we notice the gradual shift in the nature of studies away from "proof-of-concept" examinations, with small numbers of subjects, toward evaluations of clinical populations with cases number ranging from 50+. We also observe a gradual change in the overall perception of the MR spectroscopy methodology. This MR spectroscopy methodology is now recognized for its unique advantage in establishing correlations between cellular metabolites and tissue pathologies measured from the same sample. Finally, a trend in the research design of extreme metabolomics importance is also emerging: the traditional NMR approach of attempting to relate changes in single metabolites with the disease conditions has been substituted by the concept of analyzing the *global* metabolite profiles and seeking to reveal the changes in these *overall* profiles that are associated with the physiological and pathological conditions of interest. It is precisely this last trend, which agrees with our definition of metabolomics, that has convinced us metabolomics has reached the status where it can claim membership in the "-omics" family. These methodological evolutions in the

studies of human malignancies illustrate the maturation process through which a technical discovery may ultimately deliver important health advances.

There is a two-fold motivation for investigations of NMR-visible metabolites in biological tissues. The original inspiration responded to the conviction that these metabolites might be of pathological importance and useful to improving the accuracy of disease diagnoses. Research endeavors towards this direction started in the late 1970s and early 1980s. Subsequently, in the 1990s, rapid technical innovations in MR imaging motivated researchers to try and understand the spectroscopic features observed in the newly developed localized in vivo MR spectroscopy, and attempt to design new in vivo strategies for spectroscopy measurement of targeted specific metabolites. Both motivating factors consider human malignant conditions the most suitable systems to test hypotheses and develop techniques because samples from the identifiable lesions associated with the diseases can be either removed for ex vivo analysis or localized from MR images for in vivo evaluations. Furthermore, imaging visible sites of lesions also allows the identification and selection of "normals," or disease-free sites from the same subject, such as the contralateral site in the cases of brain tumors, to be used as paired controls to reveal disease related metabolite alterations. For these reasons, and also due to the relative cardiac/respiratory motion stability and tissue homogeneity of the brain compared to other organs, human brains and brain tumors have been the main spectroscopy research targets, although brain tumors represent only about 1% of all malignancies.

Since studies of the brain have dominated the development of in vivo MRS both in concept and technology, it was logical that a number of initial intact tissue HRMAS

MR spectroscopy studies of human oncology were devoted to analyses of human brain tumors. Another advantage of studies with brain tissue that makes measurement of cellular metabolites less challenging is the lack of adipose tissue, which can mask spectral regions of interest in tissue such as breast tissue. Therefore, without extensive masking of cellular metabolite signals by the presence of fatty acid peaks, the net effect of signal peak narrowing produced by the application of the HRMAS technique was evident and easy to visualize, which contributed to the general acceptance of the approach as a valid innovation for analyses of intact human pathological tissues (**Figure 7**). Later, with the acceptance of the concept, it was proven that using HRMAS even in breast tissues the peak widths from fat signals could be reduced to result in spectral windows where metabolite signals were visible and quantifiable.

The benefit and rational of studying brain tumors encountered one critical logistic issue that was somewhat unique to this particular malignancy: tissue availability. Unlike treatment of any other malignant conditions, neurosurgeons, or more precisely patients, cannot afford to remove additional brain tissue just to create a clean surgical margin of malignancy. Hence, instead of using scalpels, the neurosurgeons often resort to the assistance of suction tips to remove minimal but absolutely necessary amounts of cancerous tissue. Hence, excess tumor material after pathological diagnosis is often very limited and not readily available for research. This perhaps also explains our observation of literature on HRMAS tissue spectroscopy studies of human brain tumors. Most studies evaluate different aspects of the feasibility of methodology with small patient numbers (e.g. for each type and grade), such as the validity of measuring spectral and pathological data from the same specimens and the correlations between in vivo and ex vivo

spectroscopic observations. We have not yet seen a report of an ex vivo tissue study with significantly large patient numbers that can address the issue of biological variations. Technical developments and feasibility studies addressing issues encountered during studies of a particular malignancy have also been seen in reports on other more common types of cancers, for instance, the effects of tissue degradation on the measured cellular metabolite profiles, and the developments of slow rate HRMAS methodology during human prostate cancer studies.

The effect and function of HRMAS can be visualized as "squeezing" a broad resonance peak into a center band surrounded by a number of side bands distanced by the sample rotation rate, as illustrated in **Figure 8**. These side bands can severely hinder the interpretation of observations if they fall into regions where metabolite signals of interest reside. Therefore, in common practice, sample rotation rates are chosen such that they are fast enough to "push" the first pair of side bands at each side of the center band outside the spectral regions of interest, which means the utilization of rotation rates between 3~5 kHz for proton spectra depending the used magnetic field strength. At these rotation rates pathological identification of cancer cells is possible, but some tissue types display evidence of the centrifugal stress related artifactual alterations on the samples. For instance, in prostate tissue the glandular structures, particularly the glandular spaces, were significantly altered. These pathological structures are extremely important for the establishment of correlations with tissue metabolic profiles. Therefore, maximal preservation and accurate histopathological quantification is sought. To achieve this, following the basic principles of physics, one needs to consider reducing the structural damage from the centrifugal stress of sample rotation by using reduced rotation rates.

Without involving too much detail on the physics of HRMAS, experimental results have shown that for many types of human tissue a reduction in rotation rates to less than 1 kHz does not decrease the ability of HRMAS to produce spectra of narrow peaks, while the details of tissue pathological structures are largely preserved. Several studies on the development of slow HRMAS methodologies have been reported, and these methodologies have been utilized in evaluations of large patient populations.

It should be realized that results of these technical developments and feasibility evaluations are likely to be tissue type specific, hence the applicability to different types of tissue samples needs to be tested individually. For example, results published by one of us on techniques of slow HRMAS developed for human prostate cancer analyses also worked well with brain tissues for both tissue types are characterized by lack of adipose components[11, 12]. The proposed scheme is rendered ineffective, however, with the reported slow rotation rates, on samples rich in adipose tissue, such as those of breast or skin. On the other hand, samples of mostly connective tissue nature may be more durable to mechanical stresses, hence their pathological structures are less vulnerable to higher rates of HRMAS sample rotation.

The above discussion directly addresses an important issue related to evaluation of tissue metabolite profiles and pathological quantities from the same sample. We have rationalized the tremendous significance of such a sequential analytic protocol in the evaluations of human cancers due to the heterogeneous characteristics of malignant diseases. While we have emphasized the capability of the HRMAS MRS approach in addressing this fundamental need, we are also aware that among the several dozens of research articles of HRMAS MRS on human cancers, only a handful of them were

conducted according to this protocol. The rest of them followed the "classical" approach where results of metabolites and pathologies are obtained from adjacent samples, as in studies involving tissue chemical extractions. Although our previous arguments on utilizing the same samples are still vital valid, many reports did show correlations between the measured tissue metabolite concentrations and patient cancer status so clearly and convincingly with adjacent samples we would be hard pressed to discount them. To reconcile the seeming conflict between the concept and reality one must consider, these observations might suggest a "field effect", i.e. the malignancy related tissue metabolite profiles, or cancer metabolomics, are delocalized from cancer cells and extend to their surrounding histopathologically benign tissues. Although the suggestion of the existence of "field effects" in cancer metabolomics can only be considered a hypothesis, it is certainly not a foreign concept, particularly regarding the widely accepted and studied cancer-stroma effects in today's molecular oncology.

An additional troubling issue in current literature is a deviation from our "global" concept of metabolomics. In many studies a number of individual metabolites were measured in an attempt to associate them with the malignant condition. Although these studies may not represent the perfect approach for metabolomics, they contain valid observations. These results likely reflect the fact that many metabolites previously linked to malignancy could indeed be the major contributors to the characteristic metabolite profiles of a particular condition. This is verified by the following example, which we hope illustrates our suggested approach for studies of human cancer metabolomics:

Recently, one of us published a report on the study of human prostate cancer with intact tissue HRMAS MR spectroscopy[13]. In short, this study included 199 prostate

tissue samples obtained from 82 prostate cancer patients after prostatectomy. The study was conducted by first analyzing samples with HRMAS MR spectroscopy, and then with quantitative pathology. Metabolite concentrations were calculated from the spectroscopy data and their profiles were generated by statistics with principle component analysis (PCA). Quantitative pathological evaluations of these tissue samples indicated that 20 samples of the total 199 samples from prostate cancer patients contained cancerous glands, while the rest (n=179) represented histologically benign tissue obtained from cancerous prostates. This was not surprising as it agrees with the frequency seen in biopsy in prostate cancer clinic and reflects the infiltrative, heterogeneous nature of prostate cancer. Following spectroscopy and pathology analyses, tissue metabolite profiles were correlated with quantitative pathology findings using linear regression analysis, and evaluated against patient pathological statuses by using analysis of variance (ANOVA). Paired-t-tests were then used to show the ability of tissue metabolite profiles to differentiate malignant from benign samples obtained from the same patient (**Figure 9**), and correlated with patient serum PSA levels. Finally, metabolite profiles obtained from histologically benign tissue samples were used to delineate a subset of less aggressive tumors and predict tumor perineural invasion within the subset.

Reflecting on the discussions in this section, we wish to emphasize a number of points within this example that directly address our concept of cancer metabolomics.

Firstly, it is feasible and clinically important to conduct intact tissue studies of a large patient population, from which results may be revealed that potentially revolutionize oncological treatment.

Second, histomorphological evaluations of the same samples are critical for the correct interpretation of spectroscopic data and to define cancer metabolomic profiles.

Third, correct data statistical analysis is crucial to generate tissue metabolomic profiles. There are many bio-statistical approaches that one can use to achieve this purpose, in the example, principle component analysis (PCA) was used. The selection of PCA for the analyses of spectroscopy data in the example was based on the aim of the work: to correlate spectral metabolite profiles with tissue pathologies and patient clinical statuses. Based on our definition of cancer metabolomics, malignant pathological processes manifest simultaneous changes in multiple measurable metabolites, and a change in a single metabolite may not represent the underlying process. To test this hypothesis, PCA attempts to identify combinations (principal components or PCs) of the measured concentrations that may reflect distinct pathological processes if they exist in the set of the samples. Positive contributions of certain metabolites indicate the elevations of these metabolites within the component (process), and negative contributions suggest suppressions. For instance, the study has shown that the cancer-related principle components 13 and 14 both had metabolites phosphocholine (PChol) and choline (Chol) as their major positive contributors in agreement with current in vivo and ex vivo MRS literature's descriptions of the relationship of these metabolites with malignancy.

Finally, the reported capability of certain metabolite profiles (represented as principle components) to differentiate various pathological tumor stages, measured with histopathologically benign samples from cancerous prostates, seems to support the

hypothesis of the existence of "field effects". However, the scale and the extent of these effects are still largely undefined.

Future directions and implications

In summary, we organized this chapter in light of the potential metabolomics applications to malignancy diagnosis with tissue samples. We consider intact tissue HRMAS MR spectroscopy is still the best, and the only known, method that can provide both metabolite and pathology data from the same samples. Because our aims are orientated around this specific aspect of extreme oncological importance, we did not include discussions on chemical measurements of body fluids or other liquid samples, and their potential usages in clinic.

Within this specific scope of the chapter, with the apparently sufficient developments of the spectroscopy methodology, the emphasis of cancer metabolomics in the near future will be focused on answering four key issues:

In connection with evaluations of current histopathology and within the parameters thus defined, the first task of cancer metabolomics is to test the sensitivities of metabolite profiles in subcategorizing tumor conditions for patient outcomes in the same histopathological groups. Secondly, research in this field will attempt to identify metabolomic profiles reflecting the status of tumor biology that can be used to indicate the tumor's sensitivity to a particular treatment protocol. The third task will likely concentrate on the identification of metabolomic profiles that may be more sensitive than histopathology evaluations in indicating pre-cancerous conditions. Finally, we envision that in order to gain more comprehensive understanding on cancer biology in terms of disease mechanisms and treatment strategies, increasing research efforts will focus on

aspects that connect metabolomics with genomics and proteomics, particularly in clinical

and pre-clinical areas where the concepts of non-invasive diagnoses of human

malignancies with molecular imaging have been forcefully pursued. With the future of

metabolomics now at hand it is reasonable to assume that cancer metabonomics will have

major contributions to the history of medical science.

References

1.   Perou CM, Sorlie T, Eisen MB, van de Rijn M, Jeffrey SS, Rees CA, Pollack JR,
        Ross DT, Johnsen H, Akslen LA, Fluge O, Pergamenschikov A, Williams C, Zhu
        SX, Lonning PE, Borresen-Dale AL, Brown PO, Botstein D. Molecular portraits
        of human breast tumours. Nature 2000;406(6797):747-752.

2.   Perou CM, Jeffrey SS, van de Rijn M, Rees CA, Eisen MB, Ross DT,
        Pergamenschikov A, Williams CF, Zhu SX, Lee JC, Lashkari D, Shalon D,
        Brown PO, Botstein D. Distinctive gene expression patterns in human mammary
        epithelial cells and breast cancers. Proc Natl Acad Sci U S A 1999;96(16):9212-
        9217.

3.   Ma XJ, Salunga R, Tuggle JT, Gaudet J, Enright E, McQuary P, Payette T,
        Pistone M, Stecker K, Zhang BM, Zhou YX, Varnholt H, Smith B, Gadd M,
        Chatfield E, Kessler J, Baer TM, Erlander MG, Sgroi DC. Gene expression
        profiles of human breast cancer progression. Proc Natl Acad Sci U S A
        2003;100(10):5974-5979.

4.   Gunsalus KC, Ge H, Schetter AJ, Goldberg DS, Han JD, Hao T, Berriz GF,
        Bertin N, Huang J, Chuang LS, Li N, Mani R, Hyman AA, Sonnichsen B,

Echeverri CJ, Roth FP, Vidal M, Piano F. Predictive models of molecular machines involved in Caenorhabditis elegans early embryogenesis. Nature 2005;436(7052):861-865.

5.   Jemal A, Tiwari RC, Murray T, Ghafoor A, Samuels A, Ward E, Feuer EJ, Thun MJ. Cancer statistics, 2004. CA Cancer J Clin 2004;54(1):8-29.

6.   Jemal A, Murray T, Ward E, Samuels A, Tiwari RC, Ghafoor A, Feuer EJ, Thun MJ. Cancer statistics, 2005. CA Cancer J Clin 2005;55(1):10-30.

7.   Mountford C, Lean C, Hancock R, Dowd S, Mackinnon W, Tattersall M, Russell P. Magnetic resonance spectroscopy detects cancer in draining lymph nodes. Invasion & Metastasis 1993;13:57-71.

8.   Bettelheim R, Price K, Gelber R, Davis B, Castiglione M, Goldhirsch A, Neville A. the International (Ludwig) Breast Cancer Study Group, Prognostic importance of occult axillary lymph node micrometastases from breast cancer. Lancet 1990;335:1565-1568.

9.   Nutt CL, Mani DR, Betensky RA, Tamayo P, Cairncross JG, Ladd C, Pohl U, Hartmann C, McLaughlin ME, Batchelor TT, Black PM, von Deimling A, Pomeroy SL, Golub TR, Louis DN. Gene expression-based classification of malignant gliomas correlates better with survival than histological classification. Cancer Res 2003;63(7):1602-1607.

10.   Cheng LL, Anthony DC, Comite AR, Black PM, Tzika AA, Gonzalez RG. Quantification of microheterogeneity in glioblastoma multiforme with ex vivo high-resolution magic-angle spinning (HRMAS) proton magnetic resonance spectroscopy. Neuro-oncol 2000;2(2):87-95.

11.   Taylor JL, Wu CL, Cory D, Gonzalez RG, Bielecki A, Cheng LL. High-resolution magic angle spinning proton NMR analysis of human prostate tissue with slow spinning rates. Magn Reson Med 2003;50(3):627-632.

12.   Burns MA, Taylor JL, Wu CL, Zepeda AG, Bielecki A, Cory DG, Cheng LL. Reduction of Spinning Sidebands in Proton NMR of Human Prostate Tissue With Slow High-Resolution Magic Angle Spinning. Magnetic Resonance in Medicine 2005;53:In Press.

13.   Cheng LL, Burns MA, Taylor JL, He W, Halpern EF, McDougal WS, Wu CL. Metabolic characterization of human prostate cancer with tissue magnetic resonance spectroscopy. Cancer Res 2005;65(8):3030-3034.

14.   Cheng LL, Ma MJ, Becerra L, Ptak T, Tracey I, Lackner A, Gonzalez RG. Quantitative neuropathology by high resolution magic angle spinning proton magnetic resonance spectroscopy. Proc Natl Acad Sci U S A 1997;94(12):6408-6413.

15.   Zheng L. Solid state NMR studies of proton diffusion [PhD]. Waltham: Brandeis University; 1993.

Figure Legends

Figure 1. The 1,753-gene cluster diagram revealing gene expression in 84 experimental

   samples of breast cancer reported by C. M. Perou et.al. Each row represents a

   single gene, and each column an experimental sample. The colored bars on the

   right identified the gene clusters corresponding to (from the top): endothelial,

   stromal/fibroblast, basal epithelial, B-cells, adipose-enriched/normal breast,

   macrophage, T-cells, and luminal epithelial cells (From Figure 1b)[1].

Figure 2. Laser capture microdissection identified normal breast epithelium (white

   arrows) and abnormal epithelium (black arrows) from ADH, DCIS, and IDC from

   a single breast specimen. Images of precapture (lane a), postcapture (lane b), and

   the captured epithelial compartments (lane c) are shown (From Figure 1)[3].

Figure 3. Two-dimensional clustering of 61 samples and the top 200 genes correlating

   with tumor grade (From Figure 3)[3].

Figure 4. A metabolic pathway chart produced by Dr. Donald E. Nicholson of Leeds,

   England, in collaboration with the International Union of Biochemistry &

   Molecular Biology and with Sigma-Aldrich.

Figure 5. Statistical data on human prostate cancer in the U. S. (Based on the data kindly

   provided by A. Jemal, also see[6]).

Figure 6. The cover of the first issue of Nature Review Cancer (October 2001).

Figure 7. A comparison of brain tissue MR spectra obtained with a sample a) static; and

   b) with 2.5 kHz rotation at the magic angle (54º44' away from the direction of the

   magnet field.) (From Figure 1)[14].

Figure 8. An illustration of the effects of magic angle spinning on the appearance of

 spectral patterns measured with crystalline powder samples of barium chlorate

 monohydrate at room temperature with sample spinning rate from 0 to 10 kHz

 (From Figure 2-5)[15].

Figure 9. (**a.**) High-Resolution Magic Angle Spinning (HRMAS) 1H MR spectrum of

 intact tissue obtained from the removed prostate of a 61 y.o. patient with Gleason

 score 6, T2b tumors. Histopathology analysis of the tissue sample (insert) after its

 spectroscopy measurement revealed that the sample contained 40%

 histopathologically defined benign epithelium and 60% stromal structures, with

 no identifiable cancerous glands. Cellular metabolites mentioned in the text are

 labeled on the spectrum. The 36 most intense resonance peaks or metabolite

 groups above the horizontal bars were selected for analyses, while the other

 regions were excluded from calculation, partly due to surgery-related alcohol

 contamination. (**b**) 3D plot of Principal Component 13 (PC13 correlates linearly

 with vol% of cancer cells in tissue samples) vs. phosphocholine (Pchol) vs.

 choline (Chol). Cancerous and histologically benign (histo-benign) tissue

 samples from 13 patients can be visually separated in observation plane. The

 paired Student's t-test (cancer vs. histo-benign from the same patients) results for

 PC13, PChol and Chol are: 0.012, 0.004, and 0.001. Only results from these 13

 patients could be evaluated with paired tests, for other cancer positive samples

 were collected from patients with whom no histo-benign samples were analyzed.

 (**c**) The canonical plot resulting from discriminant analysis of the three variables

 in Fig. 1b. presents the maximum separation between the two groups. (**d**) The

resulting receiver operating characteristic (ROC) curves indicates the accuracy of

using the three variables in Fig. 1b. to positively identify cancer samples (From
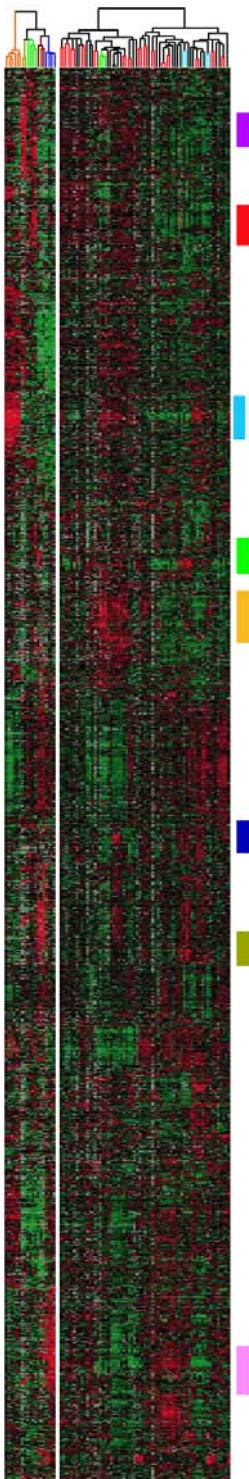
Figure 1)[13].

Figure 1.

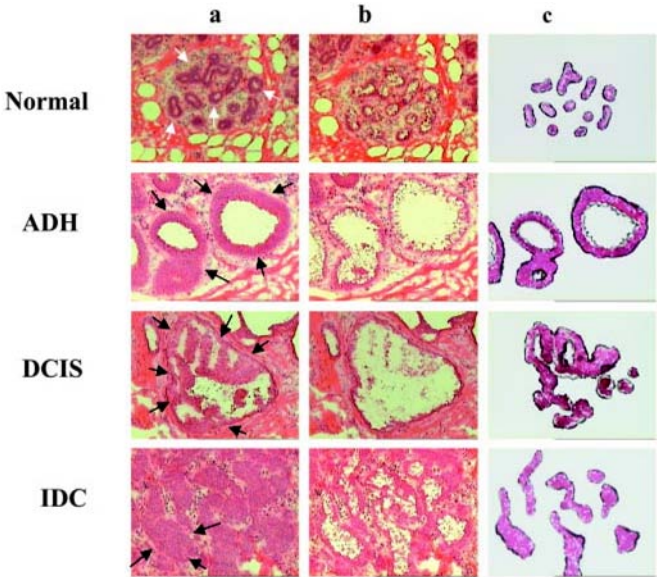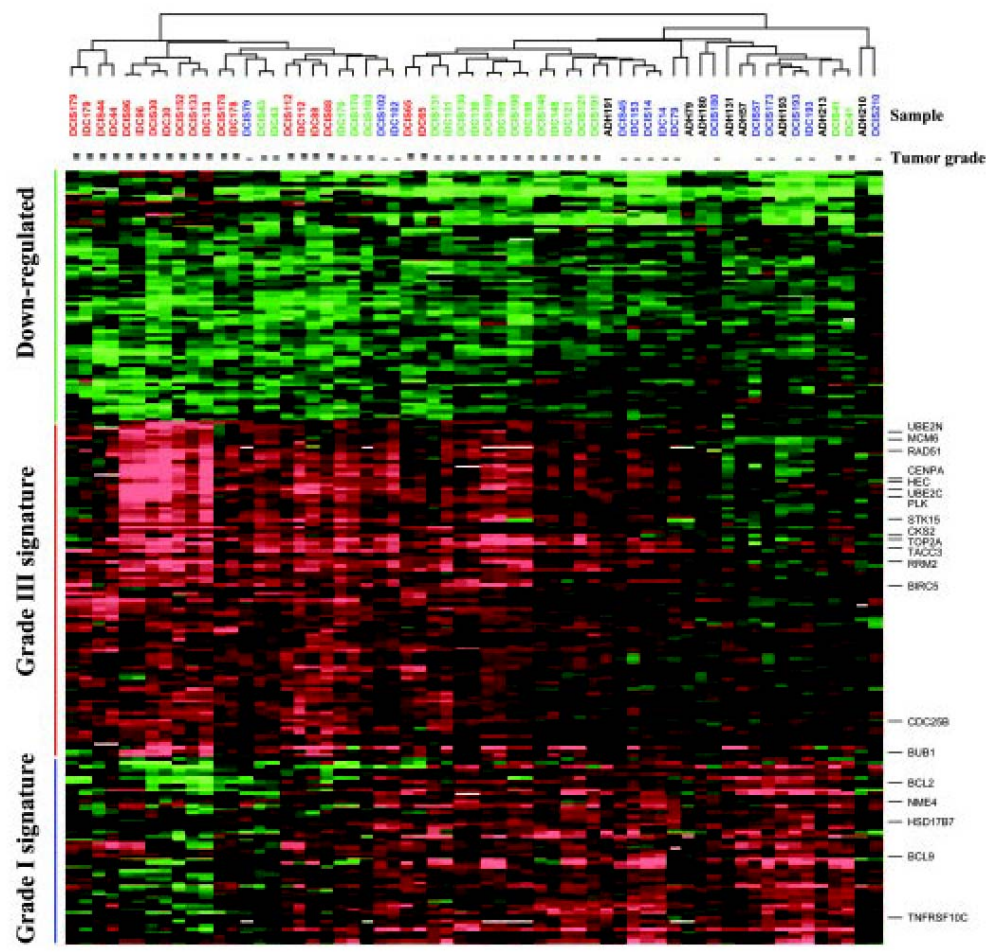**Figure 2.**

Figure 3.

Figure 4.

Figure 5.

Figure 6.

Figure 7.
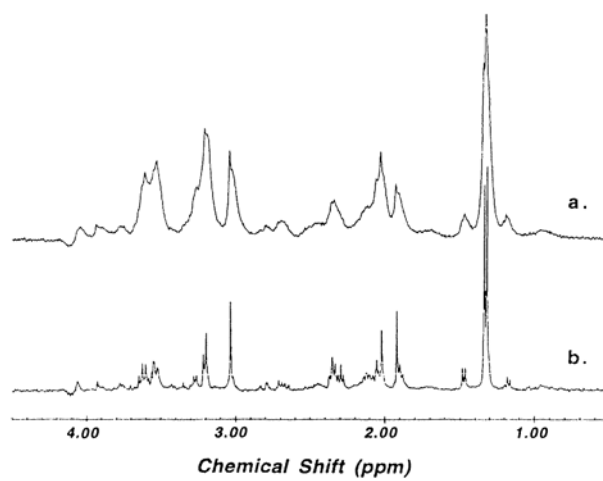

Chemical Shift (ppm)
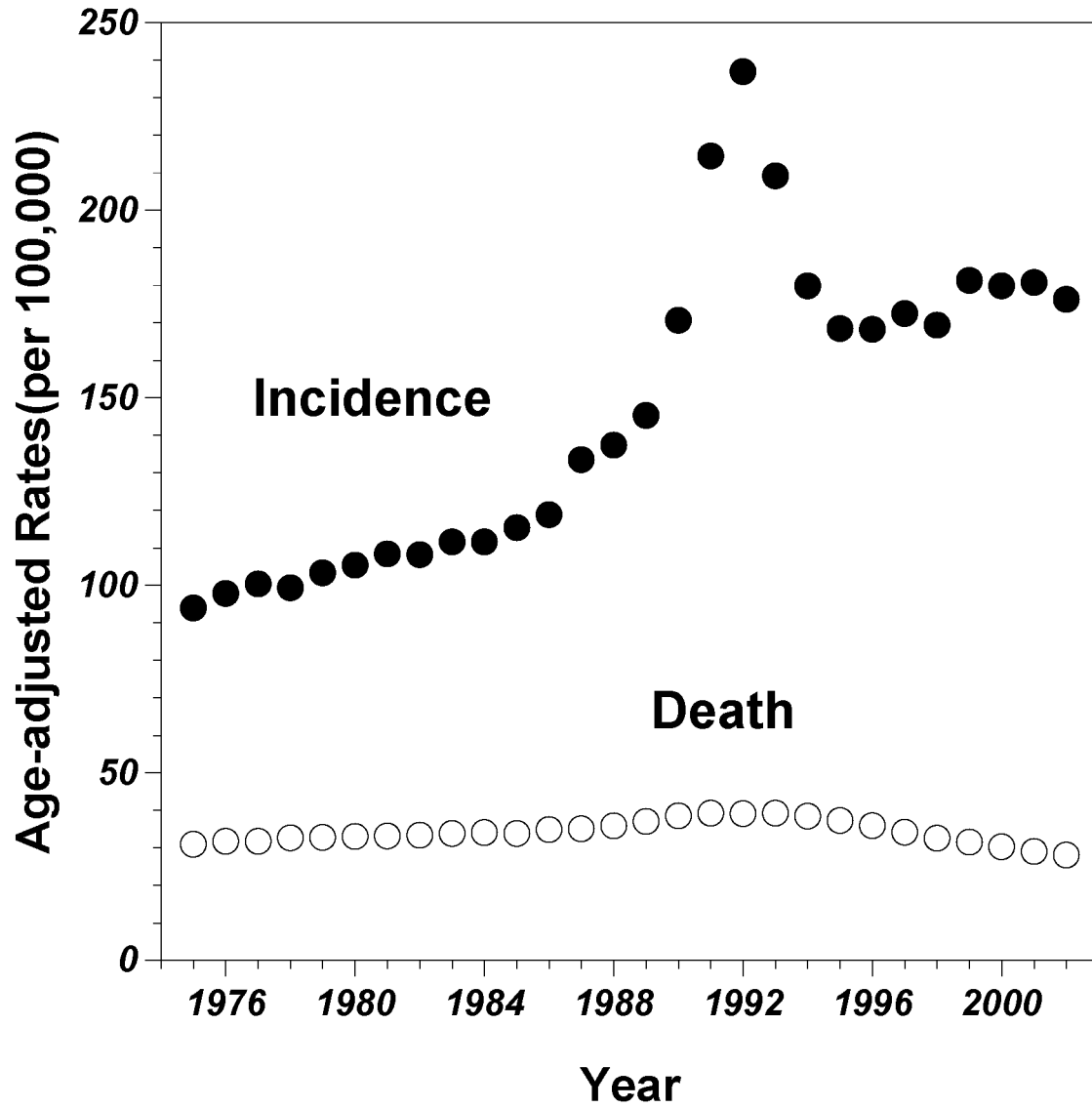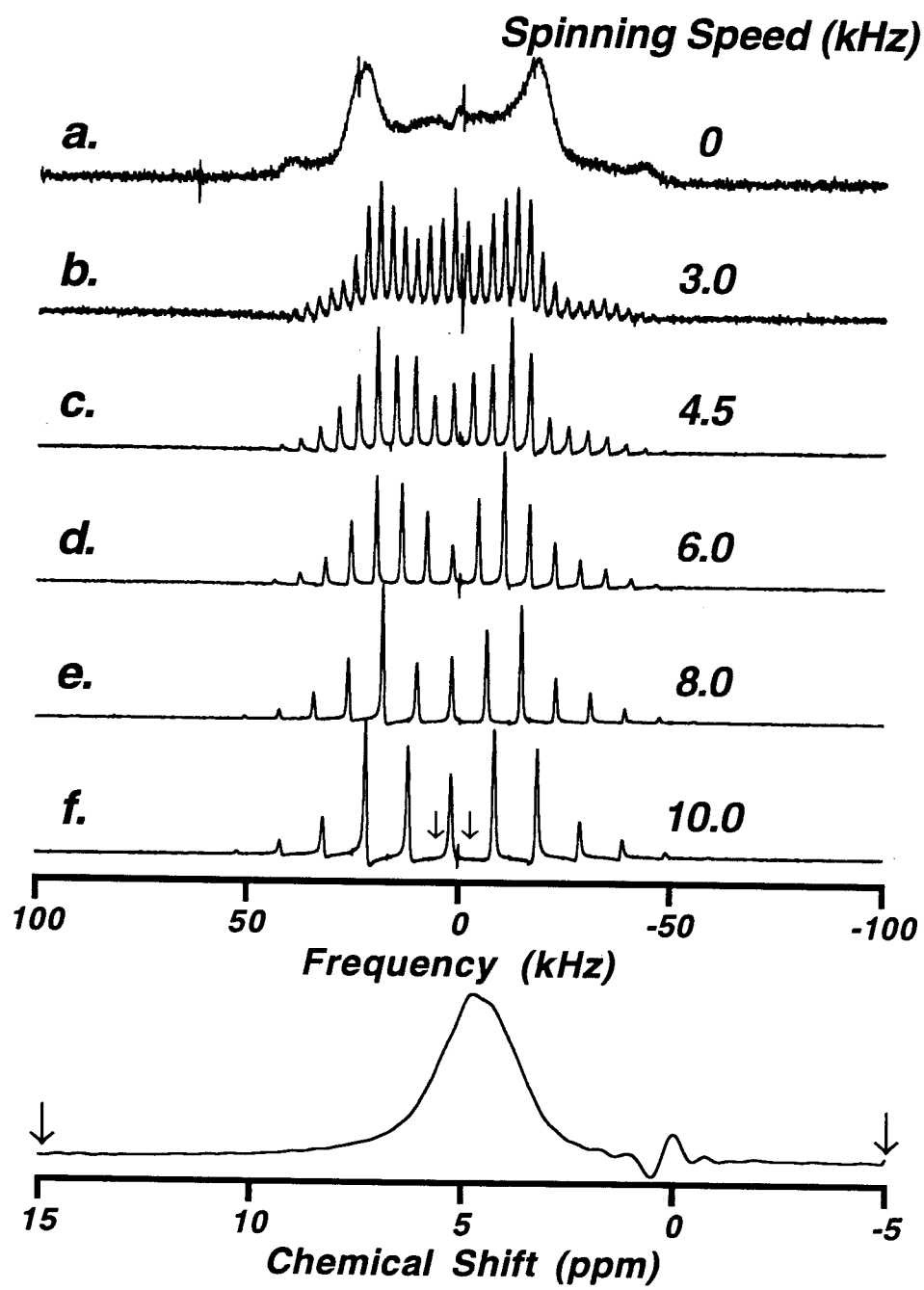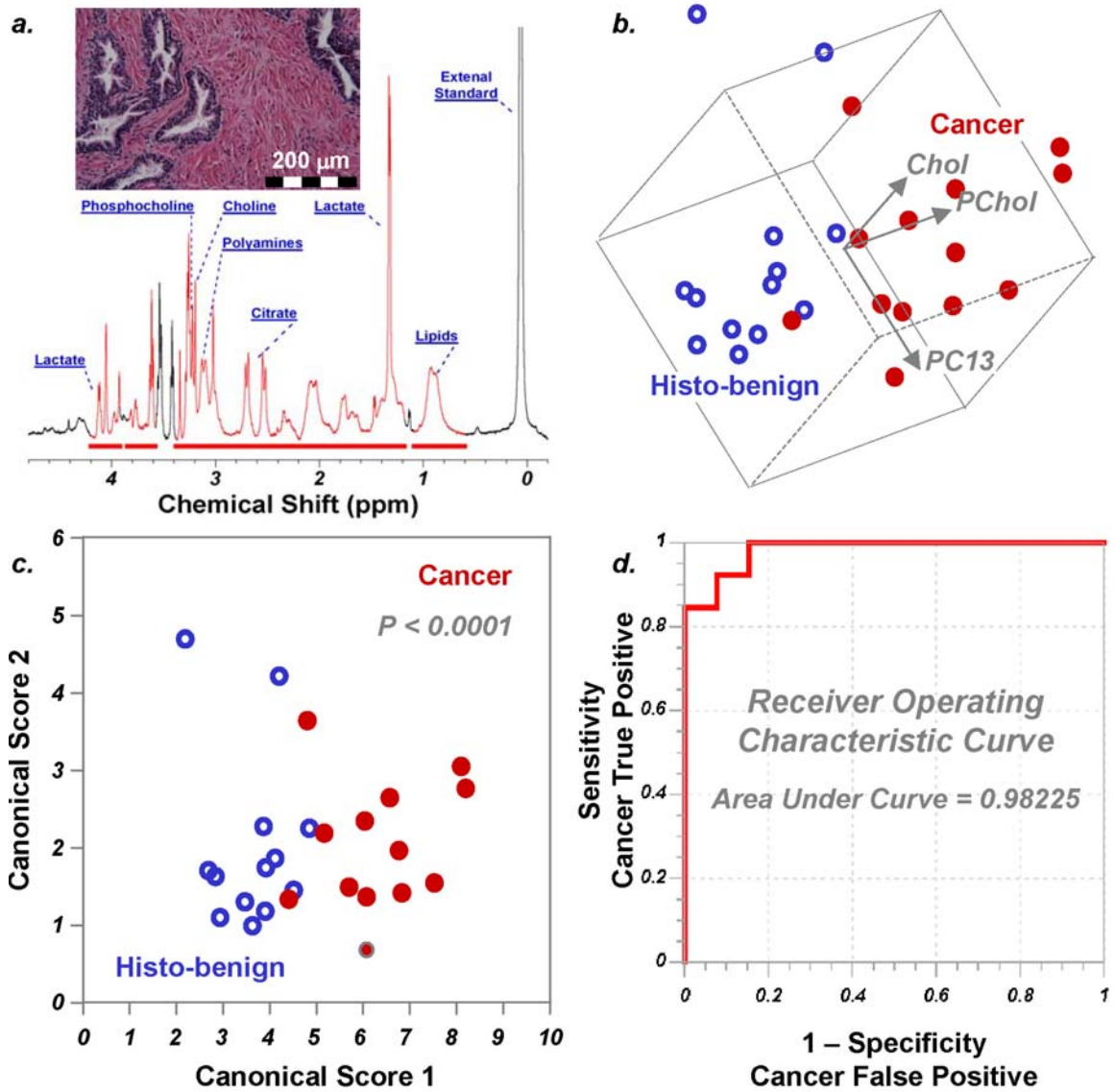
Figure 8.

Figure 9.

View Message

To: kcrocker@nmr.mgh.harvard.edu
From: ISMRM2006@mirasmart.com
Subject: Abstract 2880 Confirmation
Date: 11/15/2005 11:14:16 AM

Congratulations on the successful submission of your Abstract to the ISMRM 2006 Submission Website. For your records, please print a copy of this email.

Abstract ID: 2880

Login Name: kwjordan

Abstract Title: 'Evaluation of Human Prostate Tissue Metabolites with HRMAS 1HNMR After Three-Year Storage at -80°C'

Abstract Review Category: 904 MRS of Cells, Body Fluids & Others

Please use the Abstract ID in all communications about your Abstract.

This email is being automatically sent to you from the ISMRM 2006 Submission Website.

Evaluation of Human Prostate Tissue Metabolites with HRMAS 1HNMR After Three-Year Storage at -80ºC

Kate W. Jordan[1] and Leo L. Cheng[1,2]

Departments of [1]Pathology and [2]Radiology, Massachusetts General Hospital, Harvard Medical School, Boston, Massachusetts

Introduction: The assumption that tissue sample storage in the –80ºC condition prevents metabolite degradation or alteration is widely accepted, but has never been tested. Considering the up and coming prominence of metabolite studies for biomedical utilities, and taking into consideration that many of the samples for these studies come from tissue banks where long term storage is implicit, we felt the effect on metabolite concentrations, if any, of extended storage time should be examined. In this study human prostate tissues, removed from various zones of five prosatectomy patients, that had been stored at –80ºC for 32 months were analyzed with high resolution magic angle spinning (HRMAS) MR spectroscopy, and compared to the original measurements of the same specimens from 2002 when snap frozen for less than 24 hours.

Materials and Methods: In 2002 we conducted a study that evaluated the tissue freeze-thawing process in the presentation of HRMAS spectroscopy measured metabolite concentrations. The 11 excess tissue samples from the 2002 study were maintained at -80ºC for three years. In 2005 four samples with extra material were duplicated and a total of 15 samples were run via the same experimental protocol as the 2002 study. Briefly, samples were carried out on a Bruker (Billerica, MA) ADVANCE spectrometer operating at 600 MHz (14.1T); spectra were collected at 3ºC for optimal tissue preservation with spinning speeds of 600 and 700 Hz with or without rotor synchronized DANTE sequence of 1000 DANTE pulses of 1.5 µs (8.4º flip angle). Spectra measured at 600 Hz spinning without DANTE were used to quantify the total metabolite signal intensities. Spectroscopic data were processed with Nuts software (Acorn NMR Inc. Livermore, CA). Following spectroscopic analyses all samples were formalin fixed, paraffin embedded, cut at 5µm, and H&E stained. Serial sections at 100 µm apart were read by a pathologist and volume percentages of histological benign epithelia and stromal cells were quantified.

Results and Discussion: Figure 1 compares two proton HRMAS spectra acquired from the same prostate specimen from (a) the 2005 and (b) the 2002 study, illustrating that metabolic alterations after storage at –80ºC are as minimal as visual evaluation can dissimilate. While other samples in the study produced visually dissimilar spectra, histopathology revealed that dissimilarities in spectra are more critically influenced by tissue heterogeneity then freeze storage effects. To confirm this hypothesis we examined the paired t-tests for 21 common metabolite resonance peaks measured from HRMAS spectra; significant metabolite differences exist (after Bonferroni corrections) between the 2002 and 2005 samples *only* if the vol% epithelial difference is greater that 20%. When rigorous controls on pathological compositions are applied we found that no statistically significant metabolic differences exist when absolute epithelial differences are less than 10% or relative differences are less than 20% (**Table 1**).
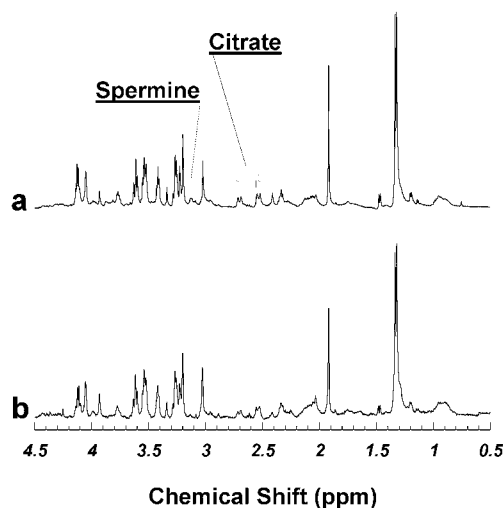

Figure 1: Human prostate tissue HRMAS proton spectra from the same surgical specimen of a cancerous prostate measured (a) in 2005 after stored at –80ºC for 32 months, and (b) in 2002 after snap freezing.

Table 1: The concentration (mM) of 21 prostate metabolites for seven sample pairs with relative differences of epithelial volume percentages less than 20% within each pair; mean, standard deviation, and paired t-tests are compared.

	2005		2002		Paired t-Test
	Mean	**SD**	**Mean**	**SD**	
Lac(4.10-4.14) [a]	14.29	3.98	12.87	6.68	0.38
MI(4.05)	10.30	2.77	12.57	5.39	0.31
3.60-3.63 [b]	16.98	6.78	20.17	13.57	0.56
3.34	5.18	2.08	5.49	1.95	0.82
3.29	1.11	0.63	2.53	2.13	0.13
3.27	8.79	2.38	11.17	5.60	0.30
3.25-3.26	12.22	3.32	13.95	5.85	0.26
Pch(3.22)	1.05	0.28	1.44	1.05	0.38
Chol(3.20)	1.53	0.22	1.70	0.91	0.64
Spm(3.05-3.14)	1.75	2.69	2.21	1.72	0.52
Cr(3.03)	2.66	0.92	5.19	3.69	0.08
Cit(2.70-2.73)	4.87	1.86	3.44	1.66	0.19
2.31-2.37	5.60	2.13	10.17	3.32	0.06
2.01-2.14	29.67	14.92	42.51	6.99	0.13
Acet(1.92)	1.36	3.02	1.19	2.54	0.44
1.68-1.78	10.89	7.11	10.98	7.34	0.98
Ala(1.47-1.49)	1.00	0.42	1.52	1.13	0.18
Lac(1.32-1.34)	17.45	4.18	20.53	9.80	0.37
1.19-1.20	2.70	2.30	2.13	2.67	0.35
1.04-1.05	0.51	0.32	1.59	2.21	0.25
Lipid(0.90) [c]	22.87	5.11	14.65	6.55	0.03

Conclusion: Analyzing samples that have been preserved at –80ºC for 32 months, and comparing their spectroscopic results to those from the same specimens after they were snap frozen for less than 24 hours, led us to conclude that the effect of freeze storage on metabolite concentration is negligible. Such alterations, even if in existence, are much less critical to the interpretation of tissue HRMAS spectroscopy for disease management purposes than the influence of tissue heterogeneities. These results are prostate tissue specific, however, and cannot be directly extended to other tissue types without further study.

ISMRM abstract
mod.doc

--------------------------- Original Message ---------------------------
Subject: RE: Evaluation of Human Prostate Tissue Metabolites with HRMAS
1HNMR After Three-Year Storage at -80XC From: "ISMRM2006"
<ISMRM2006@mirasmart.com>
Date: Tue, January 31, 2006 6:37 pm
To: kcrocker@nmr.mgh.harvard.edu

Dear Colleague:

Thank you for submitting an abstract to be considered for presentation at
the scientific sessions of the ISMRM 14th Scientific Meeting in Seattle,
Washington, USA.

We are pleased to inform you that your abstract (title above), has been
selected for presentation as a poster at this year's Scientific Meeting.
To maximize opportunities for discussion, one quarter of the posters will
be formally represented by authors at each of four poster sessions. Your
poster is assigned to be presented during the following traditional poster
session :

DAY/DATE: Tuesday, 9 May
TIME: 1:30:00 PM - 3:30:00 PM

You will be informed of your program number before the meeting. When you
arrive at the convention center, please verify your program number in the
Program Book in case there have been last minute changes. While every
effort was made to honor authors' choices of traditional or e-poster
formats, because of thematic or space considerations, some abstracts were
not assigned the preferred format.

Although we try to control for possible conflicts, it may happen that some
authors will be asked to present more than one poster at a session. If
this happens to you, we suggest that you request a co-author to stand at
one of the posters. However, submission of this abstract constituted a
commitment by the author(s) to present if accepted. Failure to present
may jeopardize acceptance of future submissions

Each presenter is assigned a space which measures 1.2m/4ft high and
1.2m/4ft. wide. For your convenience, helpful information regarding
poster presentations can be found at the following link:

http://www.ismrm.org/06/guidelines.htm

Please note that posters must be mounted before noon on Monday, 8 May, and
must remain available for viewing until 12:30 on 12 May. Authors who
submitted more than one paper will receive a separate letter indicating
the disposition of each.

The meeting Proceedings will be published on CD-Rom only, with the full text of all accepted abstracts available to advance registrants online on 21 April.

On behalf of the Annual Meeting Program Committee, I thank you in advance for your participation in this year's meeting.

Sincerely,
David G. Norris, Chair
2006 Annual Meeting Program Committee

Dr. L. L. Cheng

--------------------------- Original Message ---------------------------
Subject: 2006 AACR Annual Meeting - Abstract Number #5948
From: "AACR" <AACR@DBPUB.COM>
Date: Tue, January 17, 2006 2:10 pm
To: "virnacr@nmr.mgh.harvard.edu" <virnacr@nmr.mgh.harvard.edu>

January 2006

Re: 2006 AACR Annual Meeting in Washington, DC

Temporary Abstract Number #5948
Title: Clinical Research 18

Dear Dr. Cortez Retamozo:

Your above-referenced abstract has been scheduled for presentation in a
Poster Session at the 2006 AACR Annual Meeting in Washington, DC and will
be published in the 2006 Proceedings of the American Association for
Cancer Research. Presentation information pertaining to your abstract is
below:

Session ID: Clinical Research 18
Session Date and Start Time: Wednesday, April 5, 2006 8:00 AM
Permanent Abstract Number: 5301

Please refer to the printed Final Program (distributed onsite) or the
online Annual Meeting Itinerary Planner [available in early March through
the AACR Website at http://www.aacr.org] for the exact location of your
presentation.

Instructions for Presenters in Poster Sessions can be found on the 2006
AACR Annual Meeting home page:
http://www.aacr.org/page5395.aspx

Poster Session presenters at the AACR Annual Meeting must register for the
full meeting at the rate appropriate to their membership status and obtain
their own hotel accommodations. Registration and housing information are
included below:

Advance Registration Deadline: February 24, 2006
Online Registration System:
https://www2.compusystems.com/servlet/AttendeeRegLoginServlet?evt_uid=170

Housing Deadline: March 8, 2006
Online Housing System:
http://www.aacr.org/page5289.aspx

Online Airline Reservation System:
http://www.aacr.org/page5141.aspx

For more information, visit the 2006 AACR Annual Meeting home page at

http://www.aacr.org/page5295.aspx.

Thank you for your participation in the 2006 AACR Annual Meeting.

Sincerely,

Daniel A. Haber, M.D., Ph.D.
Program Committee Chairperson

PLEASE NOTE: This document is your official notice of acceptance. No
separate letter of acceptance will be mailed.

From:	Virna Fatima Cortez Retamozo [virnacr@nmr.mgh.harvard.edu]
Sent:	Tuesday, February 07, 2006 10:48 AM
To:	cheng@nmr.mgh.harvard.edu
Subject:	[Fwd: 2006 AACR Annual Meeting: Abstract Number 5948 -- Second Confirmation]

AACRabstratVirnaC
ortez.doc

--------------------------- Original Message ---------------------------
Subject: 2006 AACR Annual Meeting: Abstract Number 5948 -- Second
Confirmation From: "AACR" <AACR@DBPUB.COM>
Date: Mon, January 23, 2006 5:41 pm
To: "virnacr@nmr.mgh.harvard.edu" <virnacr@nmr.mgh.harvard.edu>

Dear Author: Due to a data error, the previous notification letter that
was sent to you on January 17 listed the session category in place of your
abstract title. This second confirmation notice lists the correct abstract
title for your reference; please be assured that your abstract will
display correctly in the Program and Proceedings of the AACR. The
scheduling information provided in your initial notice has NOT changed,
but it is repeated below for your reference.

January 2006

Re: 2006 AACR Annual Meeting in Washington, DC

Temporary Abstract Number #5948
Title: Evaluating human prostate cancer growth with ornithine
decarboxylase

Dear Dr. Cortez Retamozo:

Your above-referenced abstract has been scheduled for presentation in a
Poster Session at the 2006 AACR Annual Meeting in Washington, DC and will
be published in the 2006 Proceedings of the American Association for
Cancer Research. Presentation information pertaining to your abstract is
below:

Session ID: Clinical Research 18
Session Date and Start Time: Wednesday, April 5, 2006 8:00 AM
Permanent Abstract Number: 5301

Please refer to the printed Final Program (distributed onsite) or the
online Annual Meeting Itinerary Planner [available in early March through
the AACR Website at http://www.aacr.org] for the exact location of your
presentation.

Instructions for Presenters in Poster Sessions can be found on the 2006
AACR Annual Meeting home page:
http://www.aacr.org/page5395.aspx

Poster Session presenters at the AACR Annual Meeting must register for the
full meeting at the rate appropriate to their membership status and obtain
their own hotel accommodations. Registration and housing information are

included below:

Advance Registration Deadline: February 24, 2006
Online Registration System:
https://www2.compusystems.com/servlet/AttendeeRegLoginServlet?evt_uid=170

Housing Deadline: March 8, 2006
Online Housing System:
http://www.aacr.org/page5289.aspx

Online Airline Reservation System:
http://www.aacr.org/page5141.aspx

For more information, visit the 2006 AACR Annual Meeting home page at
http://www.aacr.org/page5295.aspx.

Thank you for your participation in the 2006 AACR Annual Meeting.

Sincerely,

Daniel A. Haber, M.D., Ph.D.
Program Committee Chairperson

PLEASE NOTE: This document is your official notice of acceptance. No
separate letter of acceptance will be mailed.

Evaluating Human Prostate Cancer Growth with Ornithine Decarboxylase

Virna Cortez-Retamozo[1], Kate Jordan[1], Wenlie He[1], Chin-Lee Wu[1], Leo L. Cheng[1,2]

Department of [1]Pathology and [2]Radiology, Massachusetts General Hospital, Harvard Medical School, Boston, Massachusetts

The widespread use of serum prostate-specific antigen (PSA) screening for prostate cancer (PCa) has resulted in a dramatic increase in early-stage prostate cancer detection. However, how to most effectively treat PCa patients is often a topic of much debate. The information obtained from serial PSA levels (known as PSA velocity) has been found to be a more powerful tool than a single PSA test result, as PSA velocity has shown significant association with tumor stage, grade, time to PSA failure, and time to PCa-specific mortality following prostatectomy. Unfortunately, to obtain a value for PSA velocity, multiple PSA tests are needed over a period of a clinical window, which in reality may not always be in the patient's best interest. Furthermore, clinical data indicates that primary PCa grows at a relatively slow rate, but growth rates of PCa at distant metastatic sites are comparable to more aggressive cancers. During the course of this study, high levels of spermine in the prostate have been suggested as a PCa inhibitor according to *in vitro* cell-line measurements. Our previous *ex vivo* MR spectroscopy analyses of human prostate tissues identified a positive correlation between the level of spermine and the amount of benign prostate epithelia; however, no relationship between the level of spermine and PCa growth rate, determined by PSA velocity, was found. We thus hypothesized the existence of a relationship between the level of ornithine decarboxylase (ODC), the first rate-limiting enzyme of the spermine pathway, and tumor growth rate. In this study we used semi-quantitative One Step RT-PCR to analyze ODC levels of various epithelial specimens of prostate pathologies obtained with Laser Captured Microdissection (LCM) from prostate cancer biopsies. Transcripts encoding ODC from epithelial LCMs were significantly higher than those of the endogenous control 18S rRNA. We found ODC over-expression levels linearly correlated to patient's PSA velocity results as shown by regression analysis ($R^2 = 0.861$; $P < 0.023$). Hence, our results demonstrate a direct correlation of ODC gene expression level and PSA velocity, and thus ODC levels could be used to assess PCa tumor growth.

Keywords: Prostate, Ornithine Decarboxylase, Gene Expression Analysis, PSA velocity

Dr. L. L. Cheng

To: Dr. L. L. Cheng
Subject: RE: Corrected DoD PCRP requests use of your article Dr. Cheng

-----Original Message-----
From: Whitehead, Gail Ms Azimuth, Inc. [mailto:gail.whitehead@us.army.mil]
Sent: Saturday, October 29, 2005 10:58 AM
To: cheng@nmr.mgh.harvard.edu
Subject: Corrected DoD PCRP requests use of your article Dr. Cheng

Hello Dr. Leo Cheng,

The Department of Defense, United States Army Medical Research and Materiel Command, Congressionally Directed Medical Research Programs (CDMRP) is currently preparing its Annual Report for the CDMRP fiscal year 2005. CDMRP scientists have reviewed our funded awards and selected your work in prostate cancer research as an example of identifying the most appropriate treatments for men with prostate cancer. We are requesting your approval to use the following article about your research by using the April 15, 2005, *Cancer Research* article reprinted in the CDMRP Annual Report.

PCRP RESEARCH IN THE NEWS

April 15, 2005 - Boston, Massachusetts
MR spectroscopy may be superior for determining prostate cancer prognosis

Detailed analysis of tissue chemistry could identify most appropriate treatment; more study needed.

A new way of evaluating prostate tumors may help physicians and patients choose the best treatment strategy. Using magnetic resonance (MR) spectroscopy, which provides detailed information on the chemical composition of tissue samples, researchers from Massachusetts General Hospital (MGH) have shown that chemical profiles of prostate tissue can determine a tumor's prognosis better than standard pathological studies do. The report appears in the April 15 issue of Cancer Research.

"Our study indicates that analyzing prostate tissue's metabolic profile may give clinicians additional information about the biologic status of the disease that could allow them, in consultation with their patients, to make better-informed decisions on the next steps to take," says Leo L. Cheng, Ph.D., of the MGH Radiology and Pathology Departments, the report's lead author.

Since the prostate-specific antigen (PSA) test became widely used to screen for prostate cancer, tumor detection rates have increased dramatically, particularly among those at early stages of the disease. But increased detection has led to a clinical dilemma, since standard histologic evaluation, based on a biopsy sample's appearance under a microscope, often cannot distinguish which tumors are going to spread and which are not. Many men live for years with slow-growing prostate tumors before they die of unrelated causes, and treating such patients could cause more harm than benefit, Cheng notes. So finding a better way to determine which patients need aggressive treatment and which can try watchful waiting has been a major challenge.

Another problem is that a biopsy sample from one area of the prostate may miss malignant cells elsewhere in the gland. Removal of the entire prostate can give a more definitive diagnosis, but if the tumor is a slow-growing one, the patient would have undergone unnecessary surgery. Surgery also is not appropriate when cancer has already spread beyond the prostate, since that situation requires other therapeutic approaches such as chemotherapy or drugs that block testosterone's action.

Although MR spectroscopy has been used for many years to measure the chemical composition of materials, including biological samples, it has not been useful for analyzing tumor specimens. In recent years, Cheng and his colleagues have been developing a spectroscopic technique called high-resolution magic angle spinning that provides detailed analysis of a sample's components without destroying its cellular structure. The current study was designed to evaluate the technique's potential for providing information useful for clinical decision-making in prostate cancer.

The researchers used MR spectroscopy to analyze tissue samples from 82 patients in whom prostate cancer had been confirmed by prostatectomy. Almost 200 separate samples were studied, including many that appeared benign to standard histological examination. They then compared the spectroscopy results—detailed profiles of each sample's chemical components—with the information gathered from pathological analyses of the removed glands and the patients' clinical outcomes.

Several chemical components of the tissue samples were found to correlate with the tumors' invasiveness and aggressiveness, supporting the potential of these metabolic profiles to provide valuable clinical information. Perhaps most significantly, even samples of apparently benign tissue had components that could successfully identify more and less aggressive tumors elsewhere in the prostate.

"Not only are the spectroscopy studies as good as histopathology in differentiating cancer cells from benign cells, they may be even better if they can find these metabolic differences in tissues that look benign," says Cheng. "We need to do a larger scale, more systematic study of this technique before it can be applied to clinical practice. And we hope to collaborate with other institutions to identify different metabolic profiles that could provide additional information." Cheng is an assistant professor of Radiology and Pathology at Harvard Medical School.

The study's co-authors are Melissa Burns, Jennifer Taylor, Chin-Lee Wu, M.D., Ph.D., and Wenlei He, M.D., Ph.D., of MGH Pathology; Elkan Halpern, Ph.D., MGH Radiology; and Scott McDougal, M.D., chief of MGH Urology. The study was supported by grants from the National Institutes of Health and the U.S. Department of Defense.

Please respond by Friday, November 4, 2005 using a reply e-mail indicating your approval to use the article in the CDMRP Annual Report.

The CDMRP Annual Report is provided to various United States military and government officials including those in the Office of the Surgeon General. It is also used to provide information to the American public and to respond to requests for information about CDMRP funded research.

CDMRP staff send their encouragement for your efforts in prostate cancer research and wish you and your team success.

Gail Whitehead
Public Affairs Coordinator, Azimuth, Inc.
for the USAMRMC, CDMRP
Fort Detrick, MD 21702-5024
301-619-7783
gail.whitehead@det.amedd.army.mil

2/3/2006